

AD-A122 859

CUMULATIVE DAMAGE MODEL FOR ADVANCED COMPOSITE
MATERIALS(U) DYNA EAST CORP WYNNWOOD PA
P C CHOU ET AL SEP 82 AFWAL-RR-82-4083

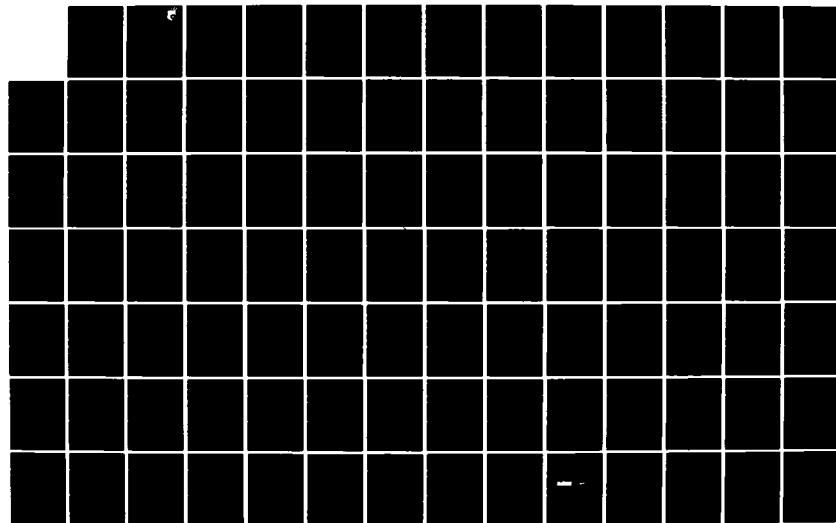
1/3

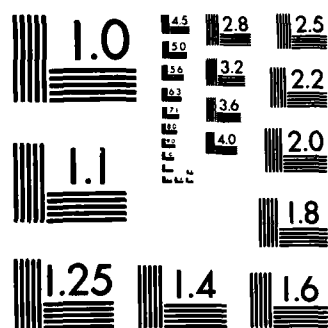
UNCLASSIFIED

F33655-80-C-5039

F/G 11/4

NL





MICROCOPY RESOLUTION TEST CHART
NATIONAL BUREAU OF STANDARDS-1963-A

AFWAL-TR-82-4083

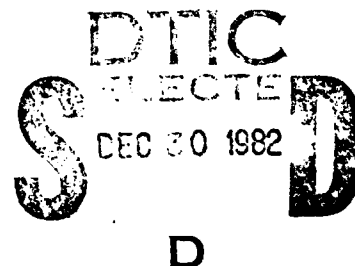


CUMULATIVE DAMAGE MODEL FOR ADVANCED COMPOSITE MATERIALS

Dyna East Corporation
227 Hemlock Road
Wynnewood, PA 19096

September 1982

Final Report for period February 1981 - April 1982



Approved for public release; distribution unlimited.

MATERIALS LABORATORY
AIR FORCE WRIGHT AERONAUTICAL LABORATORIES
AIR FORCE SYSTEMS COMMAND
WRIGHT-PATTERSON AIR FORCE BASE, OHIO 45433

AD A122859

DTIC FULL COPY

NOTICE

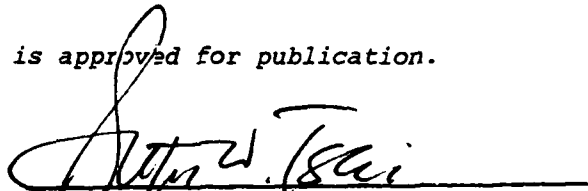
When Government drawings, specifications, or other data are used for any purpose other than in connection with a definitely related Government procurement operation, the United States Government thereby incurs no responsibility nor any obligation whatsoever; and the fact that the government may have formulated, furnished, or in any way supplied the said drawings, specifications, or other data, is not to be regarded by implication or otherwise as in any manner licensing the holder or any other person or corporation, or conveying any rights or permission to manufacture use, or sell any patented invention that may in any way be related thereto.

This report has been reviewed by the Office of Public Affairs (ASD/PA) and is releasable to the National Technical Information Service (NTIS). At NTIS, it will be available to the general public, including foreign nations.

This technical report has been reviewed and is approved for publication.



MARVIN KNIGHT
Materials Research Engineer
Mechanics & Surface Interactions Branch



STEPHEN W. TSAI, Chief
Mechanics & Surface Interactions Branch
Nonmetallic Materials Division

FOR THE COMMANDER



FRANKLIN D. CHERRY, Chief
Nonmetallic Materials Division

"If your address has changed, if you wish to be removed from our mailing list, or if the addressee is no longer employed by your organization please notify AFWAL/MLBM, W-PAFB, OH 45433 to help us maintain a current mailing list".

Copies of this report should not be returned unless return is required by security considerations, contractual obligations, or notice on a specific document.

REPORT DOCUMENTATION PAGE		READ INSTRUCTIONS BEFORE COMPLETING FORM
1. REPORT NUMBER AFWAL-TR-82-4083	2. GOVT ACCESSION NO. <i>A122 859</i>	3. RECIPIENT'S CATALOG NUMBER
4. TITLE (and Subtitle) CUMULATIVE DAMAGE MODEL FOR ADVANCED COMPOSITE MATERIALS		5. TYPE OF REPORT & PERIOD COVERED FINAL REPORT FEB 1981 - APR 1982
		6. PERFORMING ORG. REPORT NUMBER
7. AUTHOR(s) PEI CHI CHOU A. S. D. WANG HARRY MILLER		8. CONTRACT OR GRANT NUMBER(s) F33615-80-C-5039
9. PERFORMING ORGANIZATION NAME AND ADDRESS DYNA EAST CORPORATION 227 HEMLOCK ROAD WYNNEWOOD, PA 19096		10. PROGRAM ELEMENT, PROJECT, TASK AREA & WORK UNIT NUMBERS 24190320
11. CONTROLLING OFFICE NAME AND ADDRESS MATERIALS LABORATORY (AFWAL/MLBM) AIR FORCE WRIGHT AERONAUTICAL LABORATORIES WRIGHT-PATTERSON AFB, OH 45433		12. REPORT DATE SEPTEMBER 1982
		13. NUMBER OF PAGES 227 pages
14. MONITORING AGENCY NAME & ADDRESS (if different from Controlling Office)		15. SECURITY CLASS. (of this report) UNCLASSIFIED
		15a. DECLASSIFICATION/DOWNGRADING SCHEDULE
16. DISTRIBUTION STATEMENT (of this Report) APPROVED FOR PUBLIC RELEASE; DISTRIBUTION UNLIMITED		
17. DISTRIBUTION STATEMENT (of the abstract entered in Block 20, if different from Report)		
18. SUPPLEMENTARY NOTES		
19. KEY WORDS (Continue on reverse side if necessary and identify by block number) COMPOSITES, CUMULATIVE DAMAGE, DELAMINATION, ENERGY RELEASE RATE, FATIGUE, FRACTURE, GRAPHITE/EPOXY, TRANSVERSE CRACKING		
20. ABSTRACT (Continue on reverse side if necessary and identify by block number) The objective of this research program is to develop a cumulative damage model for polymer-based, fiber reinforced composite laminates. To this end, four major damage modes are identified for concentrated study in this program. These include matrix-dominant transverse cracking and interlaminar delamination, fiber microbuckling under compressive stress, and fiber breaking and splitting under axial tension in the fiber direction. Generally, one or more of these damage modes are observed in the process of laminate failure. Analytical studies have been made in the past to describe the mechanics of each of		

these damage modes under conditions of static loads. The approach taken in this program is to adopt some of the existing mechanistically augmented damage models and extend them to describe the four types of damage modes under conditions of arbitrary cyclic loads.

This report details the development of a cumulative damage model during the first phase of the program. Here, only the failure modes of transverse cracking and delamination are studied. The development of the model is based on the axioms of the classical fracture mechanics. The existing model for transverse cracking initiation under static load is extended to the multiple crack case, and this model and the static delamination model are then used as a basis for a constant amplitude fatigue damage model. Cumulative damage is obtained through a cycle by cycle application of the constant amplitude model and through the concept of constant damage states.

Results from a comprehensive experimental program have been correlated with the analytical model providing both initial values for the model parameters and initial verification of the approach to cumulative damage.

Accession For	
NTIS GRA&I	<input checked="" type="checkbox"/>
DTIC TAB	<input type="checkbox"/>
Unannounced	<input type="checkbox"/>
Justification	
By	
Distribution/	
Availability Codes	
Dist	Avail and/or Special
A	



TABLE OF CONTENTS

	<u>Page</u>
I. Introduction	1
II. Background Review	3
III. Development of a Cumulative Damage Model	12
A. Static Criterion for Damage Initiation and Growth	12
1. Model for Transverse Crack Initiation	18
2. Model for Multiple Crack Formation	21
3. Model for Edge Delamination Initiation and Growth	24
B. Fatigue Growth Model Based on Energy Release Rate	27
1. Model for Multiple Transverse Cracks	29
2. Model for Edge Delamination	30
C. A Cumulative Damage Model	31
IV. Experimental Program	50
A. Introduction	50
B. Material and Laminate Characterization	52
C. Static Load-Damage Tests	52
D. Constant Amplitude Fatigue Tests	54
E. Cumulative Damage Tests	57
V. Correlation of Data with Model	108
A. Introduction	108
B. Static Fracture Model	108
C. Constant Amplitude Fatigue Model	119
D. Cumulative Damage	127
VI. Summary and Recommendations	183
References	188

Appendices	A-1
A. Review of Fracture Mechanics	A-1
B. The Finite Element Scheme	B-1
C. Tables of Experimental Data	C-1

LIST OF FIGURES

<u>Number</u>	<u>Title</u>	<u>Page</u>
3.1	Griffith's Crack Problem. $L \gg a, W \gg a$.	33
3.2	Griffith Hypothesis for the Strength of Unnotched Plate.	34
3.3	Schematics of Multiple Transverse Cracks in [0/90] _s Laminates.	35
3.4	Cracking Geometry and Finite Element Representation of a Transverse Crack.	36
3.4(a)	Single Transverse Crack Geometry.	36
3.4(b)	Single Transverse Crack Finite Element Model.	36
3.5	Typical $C(a)$ and $C_T(a)$ Curve for Transverse Crack	37
3.6	Graphical ^e Representation for the Onset of a Transverse Crack.	38
3.7(a)	Strain Energy Release Rates for (1) The Griffith Plate; (2) Bounded Plate With $b > a_c$; (3) Bounded Plate With $b < a_c$.	39
3.7(b)	Onset Stress Curves ^c for (1) The Griffith Plate; (2) Bounded Plate With $b > a_c$; (3) Bounded Plate With $b < a_c$.	39
3.8	Interlaminar Shear Stress on -25/90 Interface.	40
3.9	Transverse Crack Density vs. Applied Load.	41
3.10(a)	Schematic Relation Between $f(\sigma_{cr})$ and $f(a_c)$ Through Energy Release Rate Criterion.	42
3.10(b)	Crack Density Distribution as Function of Load σ_{cr} .	42
3.11	Cracking Geometry and Finite Element Representation of Mid-plane Edge Delamination.	43
3.12	Cracking Geometry and Finite Element Representation of an Off-mid-plane Interface Delamination.	44
3.13	Typical $G(a)$ for Edge Delamination.	45
3.14	The Schematic Definition of the Damage Growth Function in the Transverse Cracking Process.	46
3.14(a)	Static Loading.	46
3.14(b)	Fatigue Loading, Constant σ_f .	46
3.15	The Schematic Definition of the Damage Growth Function in the Edge Delamination Process.	47
3.15(a)	Static Loading.	47
3.15(b)	Fatigue Loading, Constant σ_f .	47
3.16	Schematics for the Concept of Constant Damage Curves.	48
3.17	Schematics for the Concept of a Cumulative Damage Model.	49
3.17(a)	Schematic of a Spectrum Loading History.	49
3.17(b)	Damage Growth Path in the Load-Life Plane.	49
4.1	Typical Specimen Dimensions	65
4.1(a)	Typical Tension Specimen.	65
4.1(b)	Typical Compression Specimen.	65
4.2	Tensile Stress-Strain Diagram: Unidirectional Material	66

LIST OF FIGURES (cont'd)

<u>Number</u>	<u>Title</u>	<u>Page</u>
4.3	Compressive Stress-Strain Diagram: Unidirectional Material.	67
4.4	Tensile Stress-Strain Diagram: $[\pm 45]_{2s}$ Laminate.	68
4.5	Compressive Stress-Strain Diagram: $[\pm 45]_{2s}$ Laminate.	69
4.6	Photomicrograph of Cross Section of Unidirectional Material, 500x.	70
4.7	Two Parameter Weibull Cumulative Distribution for Ultimate Tensile Strength of Unidirectional Material	71
4.8	Two-Parameter Weibull Cumulative Distribution of Ultimate Compressive Strength of Unidirectional Material.	72
4.9	Typical Tensile Stress-Strain Diagram for $[0_2/90_2]_s$ Laminates.	73
4.10	Typical Stress-Strain Diagram for $[0_2/90_3]_s$ Laminates	74
4.11	Typical Tensile Stress-Strain Diagram for $[\pm 25/90]_s$ Laminates.	75
4.12	Typical Tensile Stress-Strain Diagram for $[\pm 25/90_2]_s$ Laminates.	76
4.13	Typical Tensile Stress-Strain Diagram for $[\pm 25/90_3]_s$ Laminates.	77
4.14	Series of X-Radiographs Showing Damage Progression In a $[0_2/90_2]_s$ Specimen.	78
4.14	Continued.	79
4.14	Continued.	80
4.15	Series of X-Radiographs Showing Damage Progression In a $[0_2/90_3]_s$ Specimen.	81
4.15	Continued.	82
4.15	Continued.	83
4.16	Series of X-Radiographs Showing Damage Progression In a $[\pm 25/90]_s$ Specimen.	84
4.16	Continued.	85
4.17	Load-Damage Relation for $[\pm 25/90]_s$ Laminate.	86
4.18	Load-Damage Relation for $[\pm 25/90_2]_s$ Laminate.	87
4.19	Load-Damage Relation for $[\pm 25/90_3]_s$ Laminate.	88
4.20	Load-Damage Relation for $[0_2/90_2]_s$ Laminate.	89
4.21	Load-Damage Relation for $[0_2/90_3]_s$ Laminate.	90
4.22(a)	X-Radiograph of Damage in a $[\pm 25/90]_s$ Specimen.	91
4.22(b)	Photomicrograph of Damage Region Showing Typical Transverse Crack.	91
4.22a(a)	X-Radiograph of Damage in a $[\pm 25/90_2]_s$ Specimen.	92
4.22a(b)	Photomicrograph of Damage Region.	93
4.23	Cycles vs. Number of Transverse Cracks for $(0_2/90_2)_s$	94
4.24	Cycles vs. Number of Transverse Cracks for $(0_2/90_3)_s$	95
4.25	Cycles vs. Percent Delamination for $(\pm 25/90)_s$	96
4.26(a)	Cycles vs. Number of Transverse Cracks for $(\pm 25/90_2)_s$	97
4.26(b)	Cycles vs. Percent Delamination for $(\pm 25/90_2)_s$	98

LIST OF FIGURES (cont'd)

<u>Number</u>	<u>Title</u>	<u>Page</u>
4.27(a)	Cycles vs. Number of Transverse Cracks for $(\pm 25/90_3)_s$	99
4.27(b)	Cycles vs. Percent Delamination for $(\pm 25/90_3)_s$.	100
4.28	Schematics for the Concept of Constant Damage Curves.	101
4.29	Constant Damage Curves for $(0_2/90_2)_s$.	102
4.30	Constant Damage Curves for $(0_2/90_3)_s$.	103
4.31	Constant Damage Curves for $(\pm 25/90)_s$.	104
4.32	Constant Damage Curves for $(\pm 25/90_2)_s$.	105
4.33	Constant Damage Curves for $(\pm 25/90_3)_s$.	106
4.34	Cumulative Damage Based on the Concept of Constant Damage State.	107
4.34(a)	Schematic of a Spectrum Loading History.	107
4.34(b)	Damage Growth Path in the Load-Life Plane.	107
5.1(a)	Mechanical Load Shape Functions vs. Relative Crack Length for $[0_2/90_2]$ and $[0_2/90_3]$ Laminates.	133
5.1(b)	Thermal Load Shape Functions vs. Relative Crack Length for $[0_2/90_2]$ Laminates.	134
5.2(a)	Mechanical Load Shape Functions for Transverse Cracking in $(\pm 25/90)_s$ Laminates.	135
5.2(b)	Thermal Load Shape Functions for Transverse Cracking in $(\pm 25/90)_s$.	136
5.3(a)	Mechanical Load Shape Functions for Mid-Plane Delamination of $(\pm 25/90)_s$ Laminates.	137
5.3(b)	Thermal Load Shape Functions for Mid-Plane Delamination of $(\pm 25/90)_s$ Laminates.	138
5.4(a)	Mechanical Load Shape Functions for Mixed Mode Delamination of $(\pm 25/90)_s$ Laminates.	139
5.4(b)	Thermal Load Shape Functions for Mixed Mode Delamination of $(\pm 25/90)_s$ Laminates.	140
5.5	Schematics of Two Different Cracking Actions in Unidirectional Laminate.	141
5.5(a)	$0^\circ/0^\circ$ Delamination Action.	141
5.5(b)	Transverse Cracking Action.	141
5.6	Transverse Crack Initiation Strain vs. Relative Critical Crack Length; $(0_2/90_2)_s$ and $(0_2/90_3)_s$.	142
5.7	Histogram Representation of Load-Damage Results for $[0_2/90_2]$ Laminate.	143
5.8	Histogram Representation of Load-Damage Results for $[0_2/90_3]$ Laminate.	144
5.9	Distributions of Initial Flaws Per Unit Length for $[0_2/90_2]$ and $[0_2/90_3]$ Laminates.	145
5.10	Two Segment Approximation to the σ - a_c Relation.	146
5.11	Load-Damage Relation for $[0_2/90_2]$ Laminate.	147
5.12	Crack Density vs. Static Load for $(0_2/90_3)_s$ Laminate.	148
5.13	Interlaminar Shear Stress on $-25/90$ Interface.	149
5.14	Ratio of Energy Release Rates for a Crack Placed a Distance, s , From a Previously Formed Crack.	150
5.15	Load-Damage Relation for $[0_2/90_2]_s$ Laminate.	151

LIST OF FIGURES (cont'd)

<u>Number</u>	<u>Title</u>	<u>Page</u>
5.16	Distribution of N^* for $(0_2/90_2)_s$ Laminate for Three Maximum Fatigue Loads Under Constant Amplitude Fatigue.	152
5.17	Distributions of N^* for $(0_2/90_3)_s$ Laminate for Three Maximum Fatigue Loads Under Constant Amplitude Fatigue.	153
5.18	Cycles vs. Damage Growth Rate for $(0_2/90_2)_s$.	154
5.19	Cycles vs. Damage Growth Rate for $(0_2/90_3)_s$.	155
5.20	Cycles vs. Number of Transverse Cracks for $(0_2/90_2)_s$.	156
5.21	Cycles vs. Number of Transverse Cracks for $(0_2/90_3)_s$.	157
5.22(a)	Number of Cracks vs. Cycles for $(0_2/90_2)_s$.	158
5.22(b)	Number of Cracks vs. Cycles for $(0_2/90_3)_s$.	159
5.22(c)	Number of Cracks vs. Cycles for $(0_2/90_2)_s$.	160
5.23(a)	Number of Cracks vs. Cycles for $(0_2/90_3)_s$.	161
5.23(b)	Number of Cracks vs. Cycles for $(0_2/90_3)_s$.	162
5.23(c)	Number of Cracks vs. Cycles for $(0_2/90_3)_s$.	163
5.24	Cycles vs. Damage Growth Rate for $(\pm 25/90)_s$.	164
5.25	Cycles vs. Percent Delamination for $(\pm 25/90)_s$.	165
5.26	Damage Rate vs. Cycles for Transverse Cracking in $(\pm 25/90_2)_s$ Laminate.	166
5.27	Damage Rate vs. Cycles for Transverse Cracks in $(\pm 25/90_2)_s$ Laminate.	167
5.28	Damage Rate vs. Cycles for Delamination in $(\pm 25/90_2)_s$ Laminate.	168
5.29	Damage Rate vs. Cycles for Delamination in $(\pm 25/90_3)_s$ Laminate.	169
5.30	Number of Transverse Cracks vs. Cycles for $(\pm 25/90_2)_s$ Laminate.	170
5.31	Number of Transverse Cracks vs. Cycles for $(\pm 25/90_3)_s$ Laminate.	171
5.32	% Delamination vs. Cycles for $(\pm 25/90_2)_s$ Laminate.	172
5.33	% Delamination vs. Cycles for $(\pm 25/90_3)_s$ Laminate.	173
5.34	Cumulative Damage Tests: $(0_2/90_2)_s$.	174
5.35	Cumulative Damage Tests: $(0_2/90_2)_s$.	175
5.36	Cumulative Damage Tests: $(0_2/90_3)_s$.	176
5.37	Cumulative Damage Tests: $(0_2/90_3)_s$.	177
5.38	Cumulative Damage Tests: $(\pm 25/90)_s$.	178
5.39	Cumulative Damage Tests: $(\pm 25/90)_s$.	179
5.40	Cumulative Damage Tests: $(\pm 25/90)_s$.	180
5.41	Comparison of Predicted and Observed Transverse Crack Density at Completion of Cumulative Damage Tests.	181
5.42	Comparison of Predicted and Observed % Delamination at Completion of Cumulative Damage Tests of $(\pm 25/90)_s$ Laminate.	182

LIST OF FIGURES (cont'd)

<u>Number</u>	<u>Title</u>	<u>Page</u>
6.1	Schematic of Damage Progression Leading to Final Failure.	187
A.1	Schematic Diagram of a Cracked Body Under Uni-axial Load.	A-7
A.2	Typical Load-Displacement Diagram for Cracked Body.	A-7
B.1	Schematic of Crack Closure Technique.	B-10
B.2	The Three Crack Extension Modes.	B-11
B.3	Finite Element Mesh at a Crack Tip Illustrating the Crack Closure Technique.	B-12
B.4	Stress Intensity Factor Approach Reference Solution.	B-13
B.5	Comparison of Energy Release Rate Calculated From Stress Intensity Factor and From Finite Element Code.	B-14
B.6	Comparison of G Calculated By FEM to Exact Value of G for Transversely Isotropic Laminate.	B-15

LIST OF TABLES

<u>Number</u>	<u>Title</u>	<u>Page</u>
4.1	Design of Test Program.	59
4.2	Material Properties.	60
4.3	Laminate Properties.	61
4.4	Onset Loads for Damage.	62
4.5	Maximum Stress Levels for Fatigue Tests.	63
4.6	Cumulative Damage Tests.	64
5.1	Summary of Test Results for G_{Ic} and $G_{(I,II)c}$	130
5.2	Some Results Based on the Fracture Models.	131
5.3	Damage Rate Equation Constants Determined by Linear Regression.	132
C.1	Cycle-Damage Data for $(0_2/90_2)_s$.	C-2
C.2	Cycle-Damage Data for $(0_2/90_2)_s$.	C-3
C.3	Cycle-Damage Data for $(\pm 25/90)_s$.	C-4
C.4	Cycle-Damage Data for $(\pm 25/90_2)_s$.	C-5
C.4	Continued.	C-6
C.5	Cycle-Damage Data for $(\pm 25/90_3)_s$.	C-7
C.5	Continued.	C-8
C.6	Cumulative Damage Test Data.	C-9
C.6	Continued.	C-10
C.6	Continued.	C-11
C.6	Continued.	C-12
C.6	Continued.	C-13
C.6	Continued.	C-14

I. INTRODUCTION

The objective of this research program is to develop a cumulative damage model for polymer-based, fiber reinforced composite laminates. The ideal model would contain the effects of loading history, character of the applied stress (tension, compression, etc.) and ply properties on the effective laminate responses--strength, modulus and life--of an arbitrary symmetric laminate with known unidirectional ply properties. To this end, four major damage modes are identified for concentrated study in this program. These include matrix-dominant transverse cracking and interlaminar delamination, fiber micro-buckling under compressive stress, and fiber breaking and splitting under axial tension in the fiber direction. Generally, one or more of these damage modes are observed in the process of laminate failure. Analytical studies have been made in the past to describe the mechanics of each of these damage modes under conditions of static loads; various theories have been advanced to predict the onset and progress of these individual damage events.

The approach taken in this program is to adopt some of the existing mechanistically augmented damage models and extend them to describe the four types of damage modes under conditions of arbitrary cyclic loads.

This report details the development of a cumulative damage model during the first phase of the program. Here, only the failure modes of transverse cracking and delamination are studied. The development of the model is based on the axioms of the classical fracture mechanics and a comprehensive analytical and experimental correlation effort.

Section II of this report presents a brief survey of literature and background review on failure modes, growth mechanisms and modeling approaches for strength and/or life predictions of polymer-based fibrous composites.

The formulation of the cumulative damage model is presented in Section III. The static fracture analysis of transverse cracking and edge delamination mechanisms, and the criteria for their initiation and growth under sustained loading are presented first. The fundamental element of the fracture analysis is the classical concept of energy release rate. This concept is then extended to describe the initiation and growth processes under constant amplitude cyclic loads. A damage growth rate equation is proposed which relates the intricate load-cycle-damage relationship. Finally, a cumulative damage model is constructed based on the growth rate equation and the concept of constant damage states.

Section IV details the experimental study. Four groups of test results are presented and discussed, including the basic material characterization data; static load-damage relations; fatigue load-cycle-damage relations and damage accumulation under simple spectrum loading conditions. Test specimens are designed so as to reveal separate mechanisms for transverse cracking and for delamination. Consequently, the most influential physical, geometrical and loading parameters in each of the damage modes can be identified from the test data.

A preliminary correlation between the proposed model and the experiments is conducted on all the aspects of the development. Important results are presented in Section V. It will be shown that the basic concepts adopted in the model are physically consistent. The specific form for the proposed damage growth rate equation remains to be adjusted when more experimental data are obtained in the next phase of the study.

Section VI gives a brief summary of the progress made during the first phase of this program, and an outline of future directions for the second and the third phases of the program.

II. BACKGROUND REVIEW

In the strength analysis of fiber reinforced composite laminates, one common approach is the well-known "first ply failure" theory (see e.g. Tsai and Hahn [1]). The basic assumption in the theory is that failure occurs in the individual plies as an independent event, and it is governed solely by the inherent ply strength property. When the first ply fails, the load is carried by the remaining plies, and so forth. Hence, by means of a laminate stress analysis and some suitable ply failure criteria, a progressive ply-by-ply failure process is constructed, and the final strength of the laminate estimated.

This approach does not take into account the actual failure modes in the plies or between the plies, or the growth nature of any of the failure modes. But, experimental evidences have shown that failure in laminates involves complicated intra-layer and inter-layer crackings and their progression. Depending on the nature of the applied load, a multitude of failure modes have been found in composite laminates. For polymer-based graphite fibrous system, for instance, at least four major failure modes have been found as the most prevalent. These include the matrix-dominant transverse cracking; interlaminar delamination; and fiber-dominant microbuckling under compression; fiber breaking/splitting under tension. In order to effectively use the material, a deeper understanding in the intricate mechanisms of these failure modes is necessary.

Experiments on graphite-epoxy laminates under tension have shown that fiber-matrix interface cracking and/or interlaminar cracking generally occur before either fiber breakage or the ultimate laminate failure. Interlaminar cracking occurs frequently in the form of free edge delamination. The driving

force in the delamination growth is associated with the interlaminar stresses that exist near the free edge region of the laminate, such as the straight edge of a tension coupon [2-6], or the free-edge surface at a through hole [7-8]. These stresses are highly concentrated near the point where layer interface meets the laminate free edge. The sign and magnitude of these interlaminar stresses depend on the stacking sequence and lay-up angles of the laminates. Hence, some laminates are more prone to delamination than others, depending on their lamination structure; it also influences the ultimate strength of the laminates [9-12].

The knowledge of the free edge interlaminar stresses provides a physical explanation of the edge delamination phenomenon; a suitable theory defining the conditions for its initiation and propagation remains a subject of recent research. In a series of tests by Rodini and Eisenmann [13] on graphite-epoxy laminates in the form $[\pm 45_n / 0_n / 90_n]_s$, $n = 1, 2, 3$, it is reported that the critical applied tensile stress at the onset of edge delamination varied with the thickness of the material layer. That is, the critical stress decreased with the increase of n . The dependence of the critical stress on the material layer thickness could not be explained by the magnitude of the inter-laminar stresses alone.

Studies of the transverse cracking mechanisms in laminates have been equally extensive in recent years [14-16]. Transverse cracks are caused by the in-plane tensile stress which is normal to the fibers in a given unidirectional material layer. For example, consider a $[0/90]_s$ type of laminate under uniaxial tension; transverse cracks may occur in the 90° -layer once the applied stress reaches some critical value. Thus, a failure criterion based on ply stress, such as the first ply failure theory, would predict that the onset

stress for transverse cracking is determined by the tensile strength of the 90°-layer. Contrary to the prediction, experiments have shown that the critical tensile stress, in-situ in the 90°-layer, varies greatly with the thickness of the 90°-layer itself. The general trend is that it increases with the decrease of the 90°-layer thickness. This layer-thickness effect on the critical onset stress was first documented by Bader, et. al. [16], who attributed the effect to the constraining actions from the adjacent 0°-layers. The presence of the 0°-layers not only arrests the transverse crack, but also restrains or delays it from forming in the first place. They explained that the physical quantity which controls the transverse cracking mechanisms is associated with the amount of strain energy stored in the 90°-layer, thus the thickness dependent effect.

The thickness effect on crack initiation observed both in edge delamination and transverse cracking has been explained from a probabilistic point of view [13, 17]. In this view, it is assumed that in each material layer there is a distribution of microdefects and that a similar distribution of defects may also exist on the layer interfaces. Hence, increasing the thickness (or volume) of the material layer increases the probability of crack formation and growth. This reasoning can certainly explain, albeit only qualitatively, the observed layer-thickness effect. But, any vigorous analysis based on this approach must address the interrelationships in the stress field, the defects, coalescence of defects, etc. at the microscopic level. Owing to the extremely complex microstructure of the composite such an approach is practically unattainable.

An alternative to the micromechanics approach is to perform a fracture analysis at a much larger dimensional level, where cracks of size much larger than the fiber diameter are recognized. It is thought that, within the frame-

work of ply elasticity* [1] and the classical fracture mechanics [18], the initiation and growth processes of transverse cracking and edge delamination can be modeled.

In a series of recent studies [19-26], Wang, Crossman and co-workers have taken such an approach and presented a unified energy method to study delamination and transverse cracks in graphite-epoxy laminates. The method is based on the energy release rate concept [18], that a crack-like flaw can be propagated when the strain energy release rate near the crack tip is sufficient to overcome the material's fracture resistance. Thus, the central elements in this method are (1) measurement of the material's fracture resistance, and (2) the calculation of the crack-tip strain energy release rate, the driving force for crack extension.

As in any analytical model construction, idealization and simplification have to be made in order to reduce mathematical complications. In modeling the free edge delamination, for instance, Wang and Crossman assumed that the crack growth is self-similar, or co-planar, whose path is contained in the interface between two layers. Thus, the growth path is one-dimensional and the crack front is represented by a point. Similarly, transverse cracks are also assumed self-similar, with their paths parallel to the fiber-matrix interface of the 90° -layer. This idealization makes it possible for a two-dimensional stress analysis with a crack growth simulation by some suitable finite element technique. The computational routine developed by Wang and Crossman is based on an earlier work of Rybicki and Kanninen [27], who applied Irwin's crack-closure method [18] to compute the crack-tip stress intensity factor. Later, Rybicki, et. al. used the finite element technique to model a free edge

*Each of the plies is considered elastic and homogeneous.

delamination problem [28].

It is noted that the self-similar crack path assumption involves a considerable approximation. For example, the observed crack surfaces of transverse cracks or delamination in graphite-epoxy composites are generally ragged, and the crack path zig-zag, even when viewed macroscopically. Hence, the self-similar approximation can be tolerated only in the overall modeling, if the material property (the material fracture resistance) is measured as a bulk quantity over a relatively large crack extension area. In this manner, the physical nature of the crack path can be included in the measurement [26].

More specifically, although transverse cracking and edge delamination are both matrix-dominant cracks, their individual resistance against crack growth when measured as a bulk quantity can differ considerably. In a recent experimental study, Cullen [29] and Williams [30] measured the material fracture resistance G_{IC} for respectively, the $0^\circ/0^\circ$ interface delamination and the $90^\circ/90^\circ$ interface delamination. They reported that G_{IC} for $0^\circ/0^\circ$ delamination is much higher than that for $90^\circ/90^\circ$ delamination. They attributed the difference to the different microscopic crack surface details in these two cases.

Another related problem in the measured material resistance is the possible matrix yielding that occurs near the crack-tip, especially under some shearing modes. Vanderkley [31] showed that the total energy release rate measured under mixed mode ($G_{I,II}$) crack action is several times larger than that measured under a pure mode-I action in a unidirectional graphite-epoxy composite. Similar findings have been reported by Wilkins [32] and Jurf and Pipes [33]. Wang, Kishore and Feng [34] showed that $G_{(I,II)C}$ is monotonically increasing with the ratio G_{II}/G_I .

After these physical questions have been taken into account, the energy

release rate method developed by Wang and Crossman [26] was tested recently in an extensive experimental case study. The method is proved to be a viable alternative also for investigating several other types of sub-laminate failure modes, such as fiber splitting in notched unidirectional laminate under tension [34].

Laminates under compressive loading general exhibit three levels of failure development: local instability of the fibers known as microbuckling, delamination of plies leading to ply buckling, and the overall global instability of the laminate. Aside from the global instability consideration which is structural rather than material in nature, the other two types of local instability mechanisms are closely associated with the matrix-dominant properties of the material system. Microbuckling in unidirectional laminates under compression has been studied by Rosen [35], Davis [36], Wang [37] and others. The analytical model by Wang [37] considers a section of the fiber as a bending element on elastic foundation. Microbuckling of the element depends on the initial fiber deflection (from being straight) and the in-plane shear modulus G_{LT} of the unidirectional system. Inclusion of fiber deflection enables the computational model to incorporate the non-linear shear behavior of the composite. The non-linear shear behavior (G_{LT}) reflects not only the properties of the fiber, the matrix and the fiber-matrix interface, but also the effect of environmental factors on these properties.

For general laminates of multi-directional plies, local ply buckling has been observed [36]. Wang and Slomiana [38] examined recently the instability failure in quasi-isotropic graphite-epoxy laminates, and found that delamination cracking generally proceeds ply instability. They applied the energy release rate method discussed earlier to predict the onset of delamination under compressive loading. Apparently, the energy method proves to be appli-

cable again in this case.

For laminates containing a large amount of 0° plies, fiber breakage is usually the predominant failure mode. Recent work by Tirosh [39] showed that the methods of classical fracture mechanics, especially the energy release rate concept, may be applied to predict the onset of fiber breakage. This approach has also been taken to study crack growth in unidirectional laminates containing some initial notches [40-42].

Apparently, fiber breakage mechanisms in unidirectional composite exhibit a considerable random character. Several statistical models have been formulated to obtain the strength distribution using a bundle theory with known strength properties of a single fiber. Rosen [35], Zweben [43], Harlow [44] and Phoenix [45] are among the notable contributors in the field. However, a linkage between the statistical models and the fracture mechanics model has not so far been available.

While a considerable gain has been made in understanding the modes and mechanisms of damage in composite laminate under static loading, damage modes under dynamical and/or cyclic loading remain far more perplexing. Generally, it is believed that static loading and fatigue loading cause similar damages, although additional effects of cyclic loading must be accounted for, such as hysteretic heating and load frequency effects, etc. [46]. A review of fatigue damage mechanisms has been given by Stinchcomb and Reifsnider [47].

In a series of laminate damage experiments, Reifsnider, et. al. [48] showed that, given a type of laminate, there seems to exist a particular damage state which is characteristic to that laminate, regardless whether the load is statically applied or cyclically applied. The stress threshold or fatigue cycle threshold for a particular damage state to occur seem to be rather deterministic. Similar observations are reported by Wang and Slomiana [38] with

laminates under compression.

These experimental observations suggest that a deterministic relationship may be found which links the load amplitude-damage-cyclic time, given the laminate with known unidirectional ply properties and the nature of loading. Assuming that the mode of damage in a laminate is the same under static and fatigue loads, then the load-damage-life relation may be established through a fracture analysis.

The classical crack growth relation for metals, for example, models the crack-like damage growth rate under cyclic load in the form:

$$\frac{da}{dN} = \alpha (\Delta K)^\beta$$

where a = crack size, N = cycles, ΔK = stress intensity factor ratio, and α and β are empirical constants.

A similar form has been suggested by Owen and Bishops [49] based on their experimental data on glass-epoxy materials. Wilkins, et. al. [50] suggested the rate equation:

$$\frac{da}{dN} = BG^n$$

where a is crack size, G is energy release rate, N is cycles and B and n are constants, for growth edge delamination in graphite-epoxy laminate. G is the energy release rate associated with the maximum fatigue load.

for growth edge delamination in graphite-epoxy laminate. G is the energy release rate associated with the maximum fatigue load.

Other similar fatigue growth rate equations have been suggested by Ratwani and Kan [51], Howe and Owen [52], Carswell [53], etc. All stemmed from the classical concept for metal fatigue studies.

Recently, a more specific growth rate relation has been proposed by Wang and Slomiana [38] for edge delamination under both tension--tension and compression--compression fatigue:

$$\frac{da}{dN} = \alpha \left(\frac{G_c - G}{G_c} \right)^{\beta \ln N}$$

This equation, however, was only exploratory since there was not enough experimental data to verify it more definitely. But the essential feature of this equation is that the load and geometrical effects are implicitly expressed in the quantity G , while α , G_c and β are pure material constants. Cumulative damage estimation for spectrum loadings can also be derived from the classical cumulative rule for metals. Wilkins [50], et. al. suggested the equation:

$$a = a_o + \sum_{i=1}^N \left(B_i G_i^n \right)$$

where i sums over the differing levels of the applied load.

A cumulative rule based on the concept of constant damage lines in the load-life domain has been suggested by Wang and Slomiana [38] for delamination growth under spectrum loads. But, again, the concept remains to be developed, pending more experimental data.

The field for fatigue damage growth study remains wide open; there is not an established analytical model that is applicable to damage development in composites as widely accepted as those developed for metals.

III. DEVELOPMENT OF A CUMULATIVE DAMAGE MODEL

In Section 1, it was pointed out that the main objective of the first phase of the research program is to develop a cumulative damage model for two of the four major sub-laminate failure modes. Namely, the initiation and growth processes of transverse cracking and edge delamination under both static and fatigue loads will be investigated. As has been discussed in the preceding section, these two types of failures cannot be described adequately from the standpoint of the concept of ply strength; rather, the method of fracture mechanics should be applied in order to simulate the growth development of these crack-like failures.

Accordingly, this section will begin with a unified presentation of the fracture model formulated by Wang and Crossman [26] which models the initiation of transverse cracks and edge delamination under static loads.

By introducing a random distribution of material property, the model is then extended for multiple transverse cracks under a statically ascending load.

The assumption that the crack-like growth mechanisms are the same in static and in (constant amplitude) cyclic fatigue loads is used to formulate a fatigue damage rate equation. This equation provides a deterministic relationship between damage size and cyclic time under a given fatigue load. The growth rate equation is then used to generate "constant damage" lines in the S-N domain. It will be shown that this latter concept of constant damage lines forms the basis of a cumulative damage model for laminates subjected to arbitrary spectrum loading conditions.

A. STATIC CRITERION FOR DAMAGE INITIATION AND GROWTH

The fracture model of Wang and Crossman [26] is based directly on the original concept of Griffith [54], who considered a thin, brittle plate under

uniform tension as shown in Figure 3.1. The plate has a through-crack of length $2a$ which is orientated perpendicular to the direction of the applied stress σ . The length of the crack is assumed small compared to the dimension of the plate; $a \ll L$; $a \ll W$. Griffith introduced the surface energy of the brittle material and formulated the criterion according to which the existing crack begins to propagate unstable. He postulated that an increase in the crack size causes a decrease in the stored strain energy near the crack-tip; and the loss of the strain energy is converted entirely into surface energy. The result is an increase in the free surface area due to the crack extension.

Let U and U_0 be the total strain energy of the plate with and without the crack, respectively. And, let $\Delta U = U_0 - U$ be the loss of strain energy of the plate due to the presence of the crack. Then, for the existing crack of size $2a$, the Griffith criterion states that the crack begins to propagate when:

$$\frac{\partial}{\partial a} (\Delta U) da \geq (4\gamma) da \quad (3.1)$$

where γ is the material surface energy of a unit of free surface.

For the Griffith problem (plane stress), ΔU is given by:

$$\Delta U = \frac{\pi}{2} \frac{a^2 \sigma^2}{E} \quad (3.2)$$

Upon substitution into 3.1, the following dependence of the critical stress on crack size is obtained:

$$\sigma_{cr} = \left(\frac{2E\gamma}{\pi a} \right)^{1/2} \quad (3.3)$$

According to the equation 3.3, the crack of original length $2a$ remains unchanged until the applied stress σ reaches the value given by 3.3; at this instant a dynamic process of growth begins.

The Griffith equation 3.3 brings upon two important practical questions. The first is that, using 3.3, σ_{cr} becomes infinite as $a \rightarrow 0$. Of course, no real material can sustain an infinite stress. In fact, given a plate having no crack at all, one finds only a finite strength for the plate. This contradiction is circumvented by introducing the concept of inherent material flaws, which are assumed to exist naturally within the plate. The real physical identity of the flaws is lost, however, within the framework of the "continuum assumption" from which stresses, strain energy, etc. are calculated. In reality, the flaws exist, perhaps, at the dimensional level of the grain-boundary, or the molecular structure of the material. The macroscopic effect of these microflaws is then represented by assuming the existence of a macroscopic crack distribution $f(a_c)$ in the plate. The no-crack ultimate strength σ_u of the plate is calculated from 3.3 using the worst flaw of size $2a_c$ in the $f(a_c)$ distribution; see figure 3.2. Clearly, the existence of $f(a_c)$ at the macroscopic level can only be viewed as a necessary postulation.

Another practical question is related to the definition of γ , the free surface energy. Actually, it represents the irreversible work required to create a unit free surface area. For brittle material such as glass, crack growth as defined by 3.3 has been shown to be quite valid. For most other structural materials, the crack-tip region usually exhibits some degree of ductile deformation. Early studies by Irwin [55], Orowan [56] and others led to the concept of the so-called "quasi-brittle fracture." According to this concept, equation 3.3 is also correct for most materials if the quantity γ is replaced by the irreversible energy dissipated in the surface region of the

crack per unit area of free surface. This last quantity depends on the ductility or elasticity of the material near the crack-tip; and it is usually found to be orders of magnitude larger than the theoretically calculated value of the material's free surface energy γ .

The foregoing discussions become more relevant when crack-like failures in composite materials are considered. The fundamental assumptions in the Griffith theory must also be properly interpreted for composites whose inhomogeneity is much larger than that in metals.

As has been discussed earlier, stress analysis for multi-layer laminates can be performed only at the level of layer-elasticity. That is the individual layer is idealized as a homogeneous medium in much the same manner as the "continuum" assumption in the theory of elasticity. Consequently, when a crack-like failure in this idealized material is analyzed, the same concern arises in identifying properly the quantity a_c and the quantity γ if the Griffith theory is to be employed. As before, these quantities must be considered a material property and are measured at the dimensional level where the stress analysis is performed. As far as composite materials are concerned, the size of a_c can be very large, being the worst in the distribution of the microflaws $f(a_c)$. Similarly, the quantity γ has to be the gross value over a sufficiently larger crack surface area, depending on the size of inhomogeneity and the microscopic details of the crack path.

In this sense, the Griffith equation 3.3 can be generalized to treat most of the major types of crack growth problems that are found in layered composites.

Now, consider the quantity ΔU in 3.1. Since U_0 does not depend on a , the Griffith criterion may be rewritten as:

$$\frac{\partial U}{\partial a} > \frac{\partial S}{\partial a} \quad (3.4)$$

where S is the total surface energy of the solid in the context of the aforementioned "quasi-brittle" fracture.

The quantity $\partial U/\partial a$ depends on the stress field near the crack-tip, which in turn depends on the geometry of the crack. It represents the driving force in propagating the crack and is commonly referred to as the available strain release rate, $G(a)$, a function of crack size a . The quantity $\partial S/\partial a$ depends on the microstructure of the crack surface and it represents the resistance of the material against the crack propagation. For material of uniform property, $\partial S/\partial a$ is independent of a . It is commonly called the critical energy release rate G_c , which is equal to 2γ in ideally brittle materials.

Thus, the Griffith criterion 3.4 becomes:

$$G(a) \geq G_c \quad (3.5)$$

Accordingly, the development of the classical fracture mechanics rests upon the calculation of $G(a)$ analytically, and the measurement of G_c physically. Within the framework of the theory of elasticity, $G(a)$ may be calculated by a number of techniques (detail discussions on these techniques are included in Appendixes A and B); and G_c may be measured using several experimental methods.

For the two types of sub-laminate failure, namely the 90°-layer cracking (transverse cracking) and edge delamination, it is assumed that microflaws exist along the fiber-matrix interface, and the ply-to-ply interfaces. These flaws are generally of a size in the order of the fiber diameter, whose crack propagation mechanisms is in the realm of micro-mechanics. Here, it is postulated only that these microflaws propagate and coalesce into a macroscopic proportion under a certain critical far field loading condition. The size of

the cracks at the macroscale depends on the micro-structure of the material (perhaps also on a host of other material processing factors, such as the curing process, post-cure handling, etc.). These initial microcracks are described by an assumed "flaw" distribution, denoted by $f(a_c)$. The exact form of $f(a_c)$ is generally unknown and is random in nature. It is regarded here, however, as a known macroscopic material property, along with other properties such as the stiffness constant, G_c , etc. of the basic material.

Since both the transverse cracking and free edge delamination processes are modeled as one-dimensional self-similar crack propagation, the energy release rate $G(a)$ in each case can then be calculated by a numerical finite element technique (see Appendix B) as a function of crack size a and the applied load.

The Griffith criterion of 3.5, when applied to predict the initiation of the sub-laminate cracks, is replaced by the general statement:

$$G(a_c) \geq G_c \quad (3.7)$$

where a_c is the worst in $f(a_c)$.

The stability of crack growth following initiation is governed by the conditions:

$$G(a + \Delta a) < G_c \quad ; \text{ stable growth} \quad (3.8)$$

$$G(a + \Delta a) > G_c \quad ; \text{ unstable growth} \quad (3.9)$$

$$G(a + \Delta a) \sim G_c \quad ; \text{ neutral growth} \quad (3.10)$$

where a ($>a_c$) is the size of the extending crack for which the growth stability is to be determined.

The foregoing conditions form the general criterion for a crack to initiate and to propagate, pending the determination of $G(a)$ and definition of G_c . In the following, the models specializing transverse cracking and edge delamination are discussed in more detail.

(1) Model for Transverse Crack Initiation

Transverse cracks are generally formed in multiples such as illustrated in figure 3.3. The crack growth geometry for a single transverse crack is shown in Figure 3.4. The first crack is assumed to have an initial size $2a_c$, the worst flaw in $f(a_c)$ for the unbounded 90° -layer. It is further assumed that this flaw is situated in the middle of the 90° -layer. The growth kinematics is then represented by the finite element model as shown in figure 3.4(b). Thus, the solution domain is the two-dimensional x - z plane, resulting in a generalized plane strain deformation field [5]. Let the laminate be subjected to a uniaxial tension represented by a far field uniform laminate strain $\bar{\epsilon}_x$, the energy release rate function $G(a)$ is then calculated and expressed by:

$$G(a) = [C_e(a)\bar{\epsilon}_x^2]t \quad (3.11)$$

where t is a characteristic length (e. g., thickness of a ply). The coefficient function $C_e(a)$ is calculated by imposing $\bar{\epsilon}_x = 1$, so that $C_e(a)$ is independent of the loading.

Figure 3.5 shows the general behavior of $C_e(a)$ for a transverse crack in the laminate whose 90° -layer thickness is larger than $2a_c$. Note that the crack size $2a$ is ultimately limited by the thickness of the 90° -layer, $2b$. The strain energy release rate is seen to increase initially with the increase of cracking

size. As the crack approaches the ply interface, the energy release rate begins to decrease; the rate of decrease depends on the relative rigidity of the outside layer. Generally, the maximum of $G(a)$ is located at $a_m < b$.

Similarly, if the laminate is subjected to a uniform temperature drop of ΔT , causing a tensile stress in the 90° -layer, then the calculated energy release rate function for the transverse crack is expressed by:

$$G(a) = [C_T(a)\Delta T^2]t. \quad (3.12)$$

Typical behavior of $C_T(a)$ for a transverse crack is similar to that of $C_e(a)$ shown in figure 3.5. Also, $C_T(a)$ has a maximum value at the same $a_m < b$. The entire $C_T(a)$ curve is generated numerically by imposing $\Delta T = 1$, so that it does not depend on ΔT .

In practice, all epoxy-based laminates are subjected to some thermal residual loading when cured. The effects of the residual stresses on transverse cracking can be evaluated by simply assuming a uniform temperature change:

$$\Delta T = T - T_0 \quad (3.13)$$

where T_0 is usually the curing temperature, or the temperature at which the laminate is free of residual stresses; T is the temperature for which the stress is computed.

Thus, when the laminate is loaded by uniaxial tension, denoted by the far-field strain $\bar{\epsilon}_x$, a combined loading condition must be considered. In this case, the total energy release rate $G(a)$ is expressed in the form:

$$G(a) = [C_e(a)\bar{e}_x^2 + C_{eT}(a)\bar{e}_x\Delta T + C_T(a)\Delta T^2]t \quad (3.14)$$

where

$$C_{eT}(a) = 2[C_e(a) \cdot C_T(a)]^{1/2} \quad (3.15)$$

The growth of transverse cracking is primarily in mode-I, or the opening mode. Accordingly, onset of a transverse crack in the 90°-layer whose 90°-layer thickness is larger than $2a_c$ is defined when:

$$G(a_c) = G_{Ic}, \quad \text{if } b > a_c \quad (3.16)$$

With the definition 3.16 for crack initiation, equation 3.14 becomes a quadratic equation in \bar{e}_x , if ΔT is given. The positive root of \bar{e}_x defines the critical applied laminate stress at onset of the crack:

$$(\bar{\sigma}_x)_{cr} = \bar{E}_x(\bar{e}_x)_{cr} \quad (3.17)$$

where \bar{E}_x is the laminate stiffness in the loading direction.

Figure 3.6 illustrates the criterion for the onset of transverse crack graphically. It is seen that $G(a_c)$ at the applied laminate stress given by 3.17 must have a value equal to G_{Ic} . Once the crack is formed, the available $G(a) > G_{Ic}$ for all $a > a_c$. Hence, the growth is unstable, or is dynamical. The crack is, of course, eventually arrested by the outside constraining layers. During this unstable crack growth, excess energy is released, represented by the shaded area in figure 3.6. The effect of the excess energy on the laminate will not be discussed in this report, however.

In cases where the thickness of the 90° -layer is small, such as the $[0/90/0]$ laminate, then, b (= one-half the 90° -ply thickness) is very small. And, in fact, it may be much smaller than a_c , which is a property found in unbounded 90° -layer. In this case, the original assumed flaw distribution $f(a_c)$ will be truncated by the thickness of the 90° -layer. Then, for all possible flaws of size less than $2b$, the maximum available energy release rate $G(a)$ occurs at $a = a_m < b$; see figure 3.5. Hence, the onset stress is then determined by the criterion:

$$G(a_m) > G_{IC} \quad \text{if } b < a_c \quad (3.18)$$

Figure 3.7 summarizes graphically the onset criterion for transverse cracking in thick 90° -layer laminate and thin 90° -layer laminate. It is seen that the formation of the crack is unstable in the former, while stable in the latter. The onset load determined by 3.18 represents, therefore, the smallest possible load for the first transverse crack to initiate.

(2) Model for Multiple Crack Formation

The foregoing discussions concerned only the critical condition under which the first transverse crack is formed. If the 90° -layer has an ideally uniform property, then multiple cracks would occur simultaneously at some regular spacing [15]. This spacing is said to be determined by a shear-lag zone [14]. This shear-lag zone is simply the shear stress transfer zone surrounding a transverse crack. Figure 3.8 illustrates the shear transfer zone for some $[\pm 25/90]_n$ laminate [26]. It is seen that the shear stress along the $25^\circ/90^\circ$ interface is highly concentrated near the root of the transverse crack and it decays rapidly at a distance away from the crack root.

Based on the results shown in figure 3.8 and more generated by Wang and Crossman [57], the size of the shear-lag zone depends only on the thickness of the 90°-layer. That is the ideal multiple crack spacing is given by:

$$S = kb \quad (3.19)$$

where k is some multiplier suitable to describe the size of the shear-lag zone.

In practice, the definition of the shear-lag zone cannot be precise, since the shear stress decays exponentially, see figure 3.8. Thus, some empirical definition for k is necessary. Specific values for k will be discussed in Section V.

Moreover, the idealized multiple cracking process does not actually occur in reality. Rather, if the first crack forms at some critical far-field load, $\bar{\sigma}_{cr}$, then the second crack would form at a different location (not necessarily at the characteristic spacing) at a slightly higher load. Hence, the density of the cracks is rising with the applied load, such as illustrated in figure 3.9. Generally, there is no characteristic crack density can be defined by the concept of shear-lag. And, often, the event of multiple crack formation is interrupted by other sub-laminate cracking event at higher load, such as edge delamination, or other interface crackings.

Assuming the formation of each transverse crack is the result of an existing flaw in the 90°-layer, the size and location distributions of the flaws can then determine the load-crack density relation such as shown in figure 3.9. But such an approach may require a special probabilistic search method, such as the Monte Carlo procedure.

To model the development of multiple transverse cracks under increasing load, it is assumed here that a saturated crack density n_m exists for some

unit length of the laminate. This saturation crack density, n_m , is believed to depend in some manner on the shear-lag distance $S = kb$. But their exact relation could not be determined. It is said that in a unit length of the laminate, there are n_m initial flaws that eventually become transverse cracks. The flaw cumulative distribution function $F(a_c)$ takes the form, say, of a Weibull function:

$$F(a_c) = 1 - \exp\left[-\left(\frac{a_c}{\beta}\right)^\alpha\right] \quad (3.20)$$

Since from the single crack model, for any given a_c there is an onset stress $\bar{\sigma}_{cr}$ determined from the energy release rate criterion 3.16:

$$G(a_c) = G_{IC} \quad (3.21)$$

Then for the distribution of a_c in 3.20, a corresponding distribution of the onset stresses $F(\bar{\sigma}_{cr})$ may be obtained by a numerical procedure.

Upon determining the distribution function $F(\bar{\sigma}_{cr})$, the load-crack density relationship is then given by:

$$n = n_m F(\bar{\sigma}_{cr}) \quad (3.22)$$

where n is the crack-density function under ascending load and n_m is saturation crack density. Figure 3.10 illustrates this computational process graphically.

The parameters in the $F(a_c)$ function must be determined by fitting some experimental results, while n_m may be determined either by experiment or some empirical rule such as:

$$n_m = 1/kb$$

(3.23)

where k takes some appropriately chosen value.

(3) Model for Edge Delamination Initiation and Growth

The cracking geometry of free edge delamination in a symmetrical laminate is illustrated in figures 3.11 and 3.12. Figure 3.11 shows a mid-plane delamination and the corresponding finite element modeling scheme; figure 3.12 shows a delamination along an interface other than the mid-plane of the laminate. Owing to the symmetry of the laminate, the cracking action in the former case is essentially of mode I, while in the latter case the crack action is generally mixed, including modes I, II, and III.

In both cases, the crack is assumed to form along the prescribed interface, and to propagate in self-similar manner toward the interior of the laminate. Hence, the solution domain is the two-dimensional y - z plane, being a generalized plane strain deformation field.

In order to determine the critical condition for initiation, the energy release rate curve $G(a)$ is first generated numerically by the finite element procedure. Since the laminate has more than one interface, it is not generally possible to decide a priori which interface is going to delaminate under the applied load. Normally, a free edge interlaminar stress analysis is conducted first, before any edge delamination calculation. The details of the interlaminar stress field then provide some indication as to which one of the interfaces an edge crack is likely to occur. Then, a calculation of $G(a)$ for crack propagation along this selected interface is performed next. Sometimes, there are more than one possible interfaces which are likely to delaminate; then, $G(a)$ curves for each of these possible crack locations have to be generated. Furthermore, a mid-plane delamination is of mode I, or opening mode, in a symmetric laminate; while an off-mid-plane delamination is of a mixed-mode

case. For the two different modes of delamination, the material resistance in each case may also be different. Depending on the microscopic details of the cracking surfaces, the critical energy release rates G_c for mid-plane cracking and for off-mid-plane cracking have been shown experimentally to differ considerably for some unidirectional graphite-epoxy [31-34]. Hence, a trial calculation is usually required to determine just which interface is the most energetically possible for an edge delamination.

Figure 3.13 shows a typical $G(a)$ curve for a delamination growth along either the mid-plane, or an interface other than the mid-plane. The general behavior of $G(a)$ is that it increases rapidly to reach a maximum value at $a = a_m$. After this point, the value of G becomes essentially a constant, independent of the crack size a (assuming the width of the laminate is large compared to the crack size a). The value of a_m at which G attains its maximum, depends on a number of factors. The most notable factor is the layer thickness of the two adjacent layers on whose interface the delamination propagates. For example, if $G(a)$ represents the total energy release rate curve for a mid-plane delamination for the laminates $[\pm 45_n / 0_n / 90_n]_s$, $n = 1, 2, 3$, then the maximum of G would occur at about $a_m = nt$, t being the thickness of one ply. Hence, the available maximum G in the case of $n = 1$, for instance, is much smaller than the available maximum G in the case of $n = 2$.

This thickness dependence nature of G_{max} on layer thickness is not exactly the same as the previously discussed transverse cracking problems. The reason for the existence of G_{max} is also due to the constraining effect of the layer structure of the laminate.

As in the transverse cracking problems, $G(a)$ curve of an edge delamination growth can also be expressed in terms of the applied thermal and mechanical loads:

$$G(a) = [C_e(a)\bar{e}_x^2 + C_{eT}\bar{e}_x \Delta T + C_T(a)\Delta T^2]t \quad (3.24)$$

where the coefficient functions C_e , C_T and C_{eT} are defined identically as those expressed in equations 3.11, 3.12 and 3.15, respectively.

If the computed $G(a)$ is for a mid-plane delamination growth, then the onset of delamination is defined when

$$G(a_c) = G_{Ic}, \quad \text{if } a_c < a_m \quad (3.25)$$

or

$$G(a_m) = G_{Ic}, \quad \text{if } a_c > a_m. \quad (3.26)$$

The physical reason for the difference between 3.25 and 3.26 is the same as in the transverse cracking problems discussed earlier.

If the computed $G(a)$ is for an off-mid-plane delamination growth, then $G(a)$ so computed would consist three modal parts; the criterion for the onset of such a mixed-mode crack can thus be similarly given as:

$$G(a_c) = G_{(I, II, III)c}, \quad \text{if } a_c < a_m \quad (3.27)$$

or

$$G(a_m) = G_{(I, II, III)c}, \quad \text{if } a_c > a_m \quad (3.28)$$

Experiments are required to decide the value of G_{Ic} and the value of $G_{(I, II, III)c}$.

Whichever final growth criterion is used, the growth stability of delamination is theoretically unstable if $a_c < a_m$; and it is a neutral growth if $a_c > a_m$. Actually, the delamination growth is generally stable. This is because the interface flaw size a_c is not uniform along the specimen; it is always the weakest location where delamination starts first. Thus, load must be increased in order to extend the delamination further. As the delamination grows larger, the structural stiffness of the specimen is further reduced; and so is the available energy release rate G under the same load.

Onset of edge delamination in most laminates has been observed to occur very late in the loading process; sometimes the onset load is close to 95% the laminate ultimate load. Thus, relatively speaking, the edge delamination growth process is short, compared to the growth development of transverse cracks.

B. Fatigue Growth Model Based on Energy Release Rate

In this sub-section, an effort is made to extend the energy release rate concept of fracture growth in order to model the crack growth process in laminates under constant amplitude cyclic fatigue load. The objective is to predict the state of damage in terms of the fatigue load and fatigue cycle.

As far as transverse cracking and delamination are concerned, experimental observations have shown that the mode of damage remains unaltered whether the laminate is under static or fatigue loads. The influence of the fatigue load level merely shifts the damage event with time (fatigue cycle). Figure 3.14 illustrates schematically the development of transverse cracks (in terms of crack density) under static and fatigue loads. In figure 3.14(a), the crack-density (n) versus applied load (σ) plot is displayed; the one-to-one curve between $n - \sigma$ can be predicted by the multiple cracking model discussed previously. In particular, the model identifies explicitly the onset load σ_{TC}

for the first transverse crack in the $n - \sigma$ curve.

Now, in Figure 3.14(b), similar damage growth curves are shown in the $n - N$ plane, N being the number of cycles for which the laminate has been loaded under the constant amplitude fatigue load σ_f . Here, it is assumed that $\sigma_f < \sigma_{TC}$, so that under σ_f some cycles are needed to initiate the first crack at N_{TC} . Clearly, the effect of the fatigue load is manifested by the shifting of the damage curves along the N -axis.

Similarly, figure 3.15 illustrates the growth development for edge delamination. The behavior of crack growth under static and fatigue loads are identical to the transverse crack case, except in this case the delamination size a is used as a measure of damage.

Thus, the objective here is to define the "damage growth" functions $F_{TC}(\sigma_f, n, N)$ and $F_{DL}(\sigma_f, a, N)$, which map the one-to-one damage-load curve onto the damage-cycle plane.

In order to formulate the "damage growth" functions F_{TC} and F_{DL} , it will be assumed that damage growth is driven by the maximum energy release rate G each time the fatigue load reaches the maximum amplitude σ_f . The material resistance against the crack growth is the quantity G_c . The effect of cycling is expressed by a general growth rate equation of the form:

$$\frac{da}{dN} \sim \alpha (G/G_c)^p \quad (3.29)$$

where α and p are some constants.

Since the quantity G includes implicitly the fatigue load σ_f , the size of crack a , and other geometrical and structural factors of the laminate (stacking sequence, etc.), the constants α and p in the rate equation 3.29

are essentially material dependent only. The exact value of the constants, however, must be determined from experiments.

Integration of the growth rate equation yields the damage state as a function of the fatigue load σ_f (in G) and the fatigue cycle N.

(1) Model for Multiple Transverse Cracks

In the case of transverse cracking, it was assumed earlier that the 90°-layer of the laminate possesses a flaw distribution $F(a_c)$. Under statically increasing load, each of the a_c in the distribution becomes eventually a transverse crack. The total number of such cracks is denoted by n_m .

Under fatigue load σ_f , and σ_f is assumed less than the onset load σ_{TC} , the flaw of size a_c becomes a full crack in a total of N_{TC} cycles. Thus, from equation 3.29:

$$\int_{a_c}^{\text{full crack}} da = \int_0^{N_{TC}} \alpha (G/G_c)^p dN \quad (3.30)$$

Since, from fracture mechanics calculation, G is defined for $a_c \leq a \leq$ full crack, and since a_c is actually a distribution, equation 3.30 provides the needed vehical to calculate the distribution function $F(N_{TC})$ from the given function $F(a_c)$.

Consequently, the distribution function for the crack density n in the n - N domain is finally given by

$$n(N) = n_m F(N_{TC}) \quad (3.31)$$

The onset cycle for the first crack is defined by setting $n = 1$.

An alternative transverse crack growth model may be formulated by proposing a rate equation in terms of the crack density n directly:

$$\frac{dn}{dN} \sim \alpha (G/G_c)^p \quad (3.32)$$

Note that the crack density n is eventually bounded by the number n_m ; hence, the expression 3.32 may depend on N ; that is, the constant p may be a function of N . Some specific details in this development are discussed in Section V of this report.

(2) Model for Edge Delamination

The initiation of edge delamination is assumed to be caused by the worst flaw a_c on the free edge of the laminate. Under load this flaw of size a_c becomes a recognizable delamination crack a^* ; then, a^* continues growth into a large delamination.

Under fatigue load σ_f (assumed σ_f is smaller than the static onset load of delamination), the cycles necessary to initiate a free edge delamination is defined by integrating the growth rate equation 3.29:

$$\int_{a_c}^{a^*} da = \int_0^{N_{DL}} \alpha (G/G_c)^p dN \quad (3.33)$$

Equation 3.33 defines N_{DL} under a given σ_f and some appropriate definition of a^* . The constants α and p are associated with the material property during the initiation process, which involves some unknown microscopic processes such as flaw coalescence mechanisms. This, clearly, makes the determination of α and p entirely empirical.

Once the delamination starts at the macro-level, a similar growth equation may again be formulated:

$$\int_{a^*}^a da = \int_{N_{DL}}^N \alpha (G/G_c)^p dN \quad (3.34)$$

In the above expression, it is conceivable that the constants α and p may actually be different from those appeared in 3.33, due to the possible differences in the initiation processes which is microscopic, and the growth process which is macroscopically modeled. In particular, for a small size test specimen, some structural effects emerge as the delamination crack becomes larger (such as end-lab constraint, structural stiffness loss, etc.). It is then conceivable also that the constant may depend on the parameter N . These points are further discussed in Section V.

Basically, equations 3.30 and 3.31 form the basis for determining the damage growth function F_{TC} for transverse cracking, and equations 3.33 and 3.34 form the basis for F_{DL} for delamination. All these are carried out numerically, of course.

C. A Cumulative Damage Model

Cumulative damage under spectrum load is here described by a model which is based on the concept of "constant" damage state. Take, for instance, the fatigue damage growth function $F_{DL}(\sigma_f, a, N)$ discussed in the preceding subsection. It is assumed that a given state of damage, which is expressed by the delamination size a , can be induced by some constant amplitude fatigue load σ_f in N cycles; and it can also be induced by some static load σ without cycling. Thus, a $\sigma - N$ relation exists for a given state of damage. And, this relationship is found through the function of $F_{DL}(\sigma_f, a, N)$.

Figure 3.16 illustrates this concept by a family of plots in the $\sigma - N$ domain. The constant damage curves are generated from the damage growth function F_{DL} . These curves can be compared with experimentally generated ones to verify the validity of the constant damage concept, and the correctness of the proposed growth rate equation.

From the constant damage curves in the $\sigma - N$ domain, the cumulative damage model is constructed as follows:

Consider the spectrum load history such as shown in figure 3.17(a). The laminate is subjected to a constant amplitude fatigue load σ_1 for a period of N_1 cycles. The damage at the end of N_1 cycles is found at point A in the $\sigma - N$ domain, figure 3.17(b). The constant damage curve passing point A is devoted by a_1 . Now, the amplitude of the fatigue load is increased to σ_2 for a period of $(N_2 - N_1)$ cycles, see figure 3.17(a). Since the damage in the laminate at the onset of σ_2 is still a_1 , the location of this damage state is at the intersect of σ_2 and the curve a_1 , point B. Then for a period of $(N_2 - N_1)$ cycles, the damage state in the laminate advances to C, where the constant damage line a_2 passes through. At the end of N_2 cycles, the fatigue amplitude is lower to σ_1 again for a period of $(N_3 - N_2)$ cycles. During this period, the damage state advances from point D on curve a_2 to point E on curve a_3 .

Since at each level of the fatigue load, the initial damage state is known, and the number of cycles specified, the damage state at the end of the cycling can thus be found from the damage growth function F_{DL} . The final damage is given by:

$$a = \sum_{i=1}^3 \int_{N_{i-1}}^{N_i} \alpha (G_i / G_c)^P dN \quad (3.35)$$

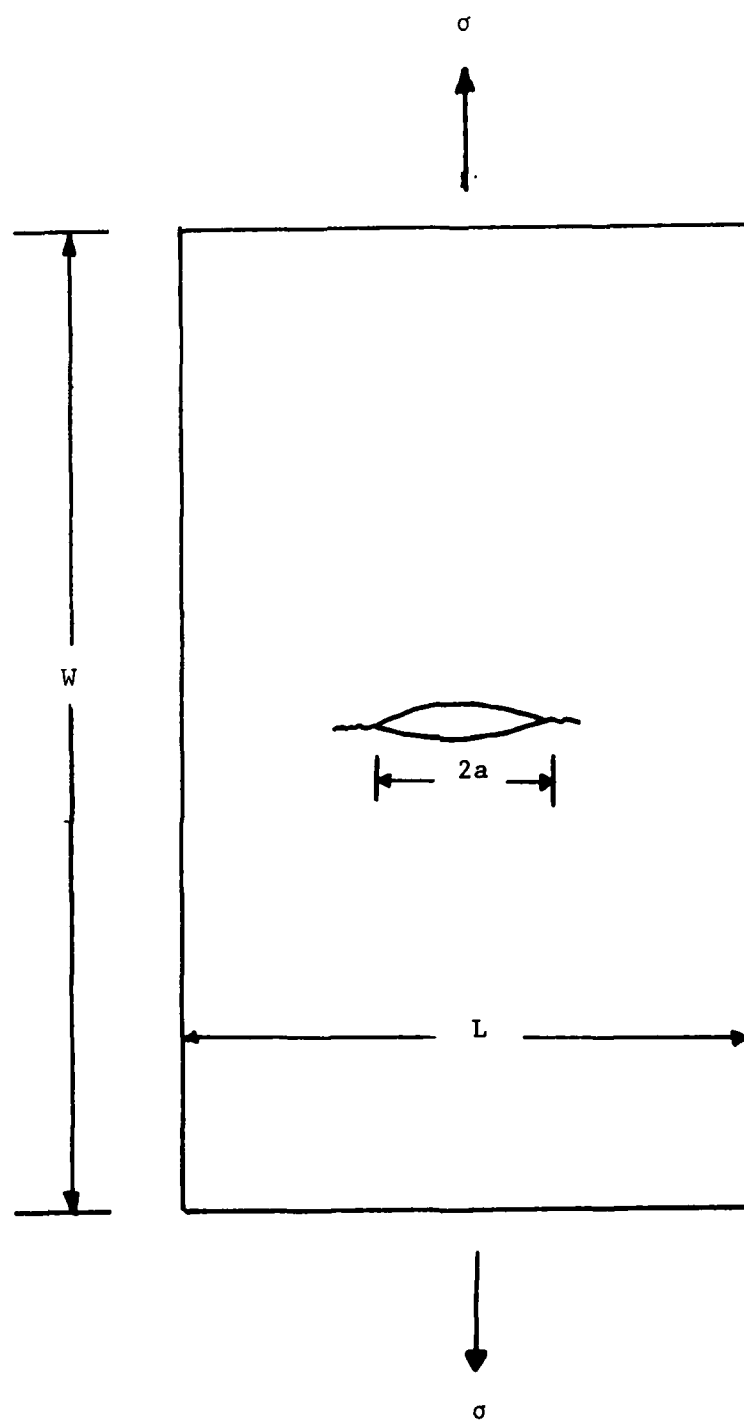


Figure 3.1, Griffith's Crack Problem. $L \gg a$, $W \gg a$.

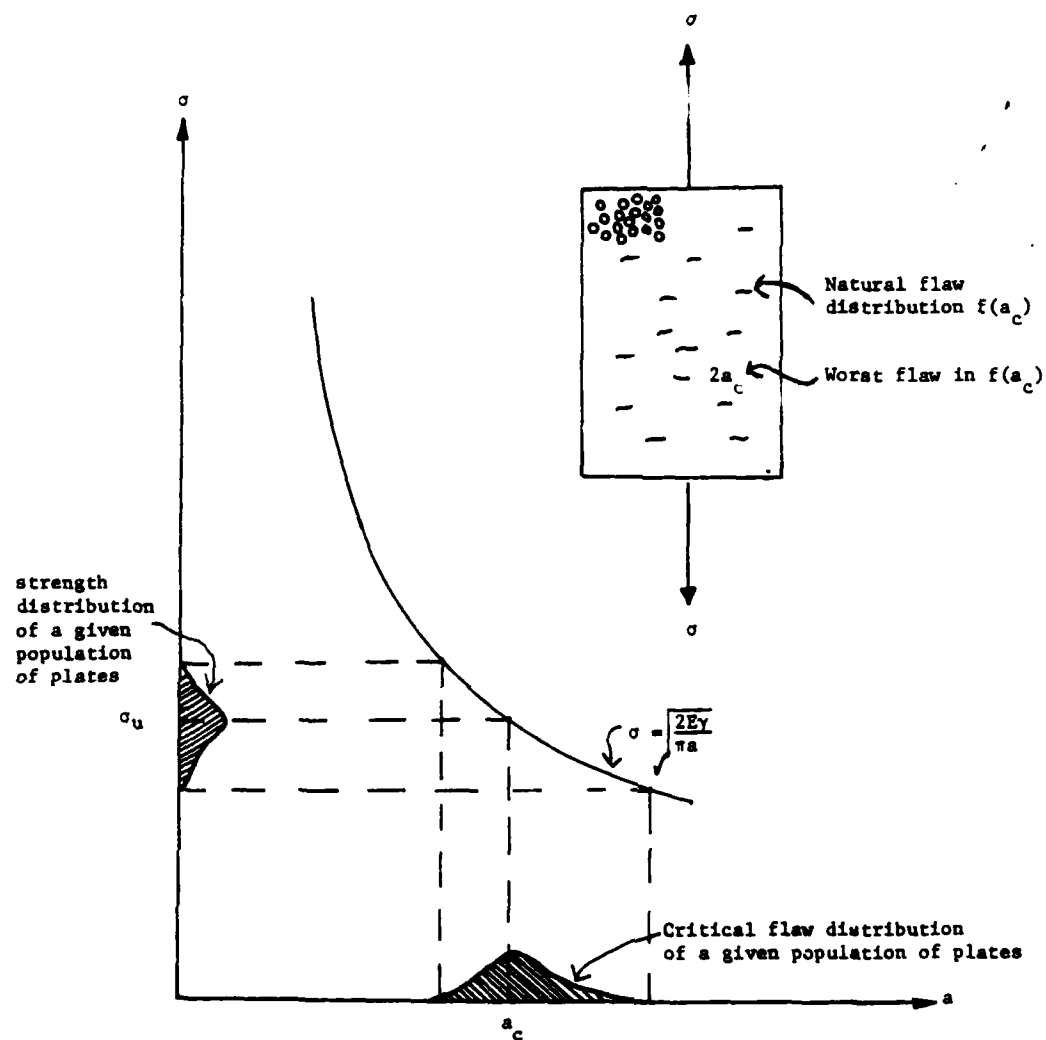


Figure 3.2: Griffith Hypothesis for the Strength of Unnotched Plate.

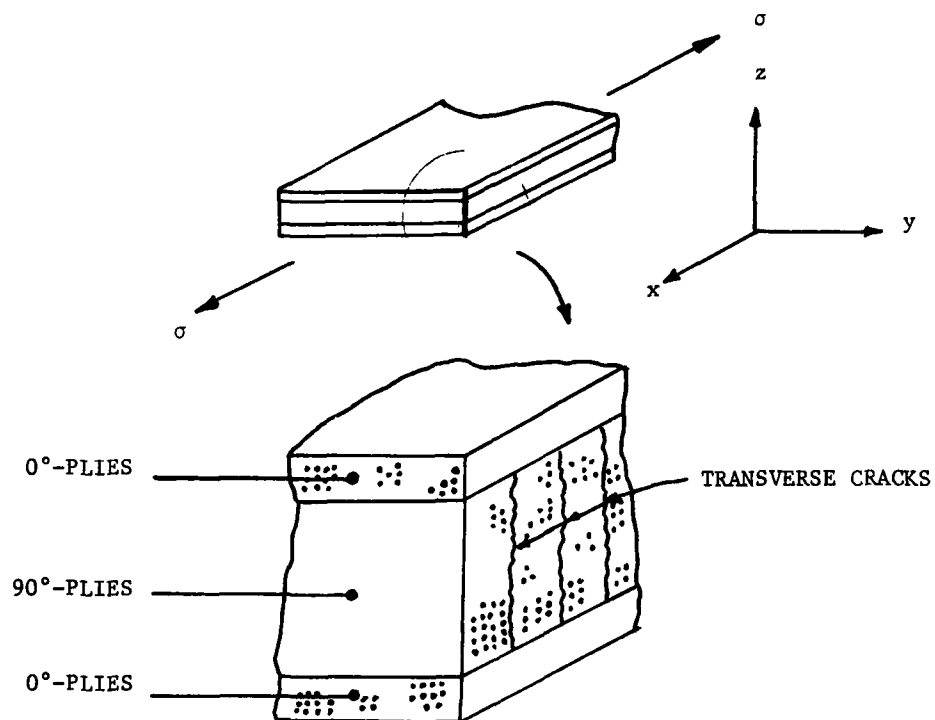
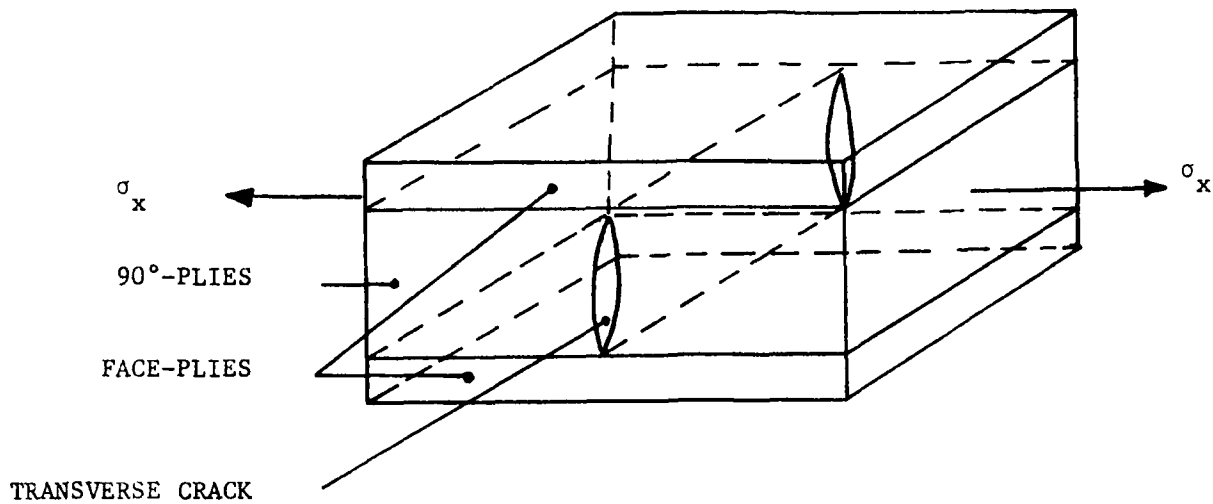
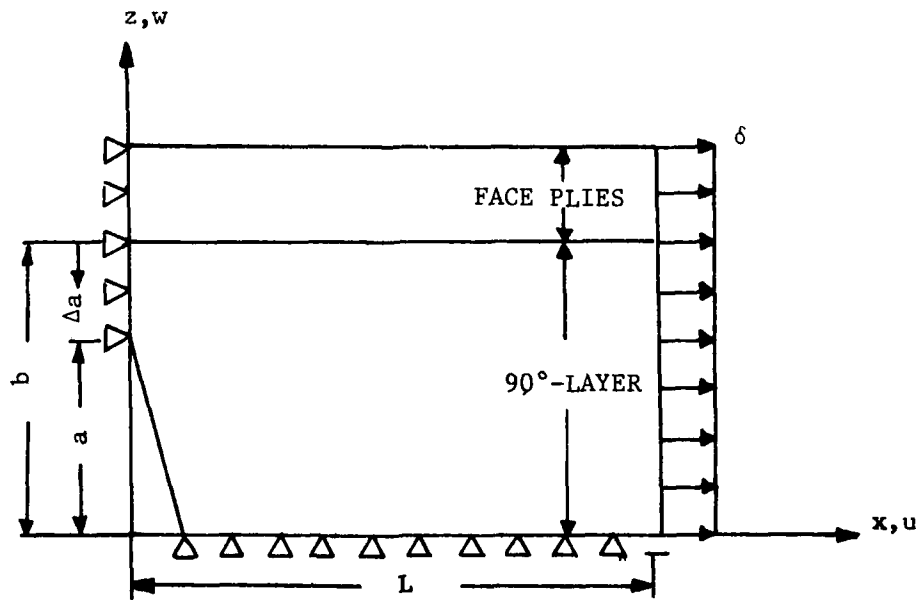


Figure 3.3. Schematics of Multiple Transverse Cracks in $[0/90]_s$ Laminates.



(a) Single Transverse Crack Geometry



(b) Single Transverse Crack Finite Element Model

Figure 3.4. Cracking Geometry and Finite Element Representation of a Transverse Crack.

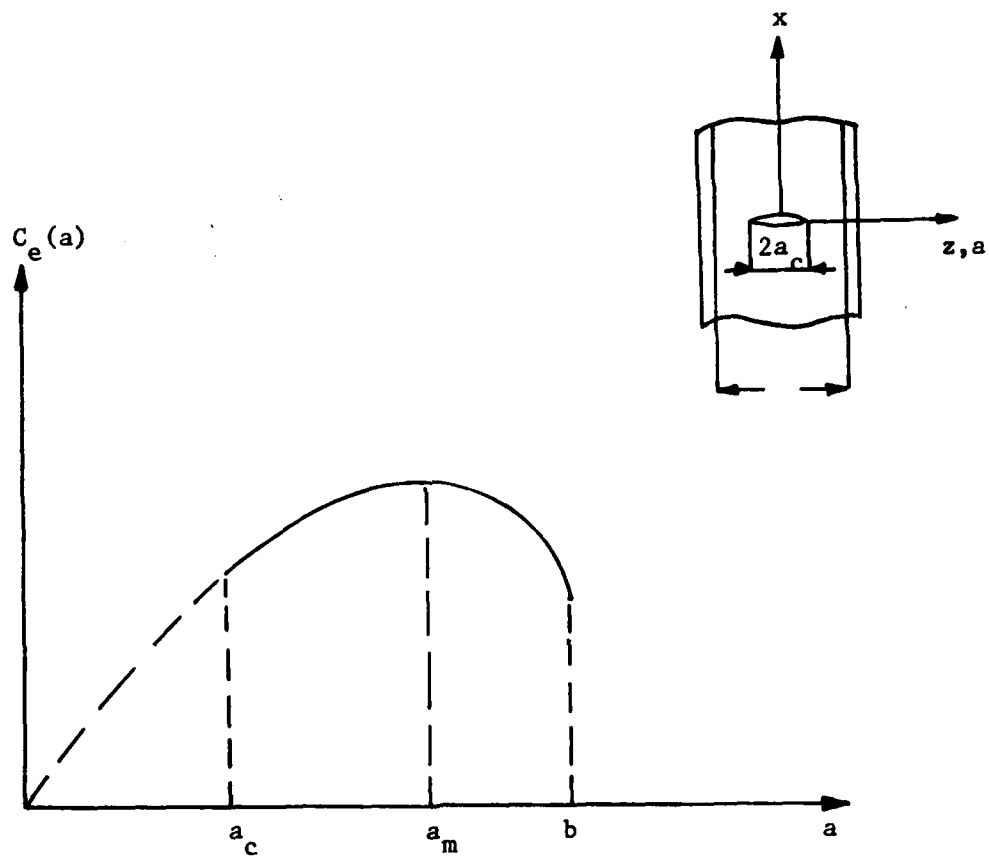


Figure 3.5. Typical $C_e(a)$ and $C_T(a)$ Curve for Transverse Crack

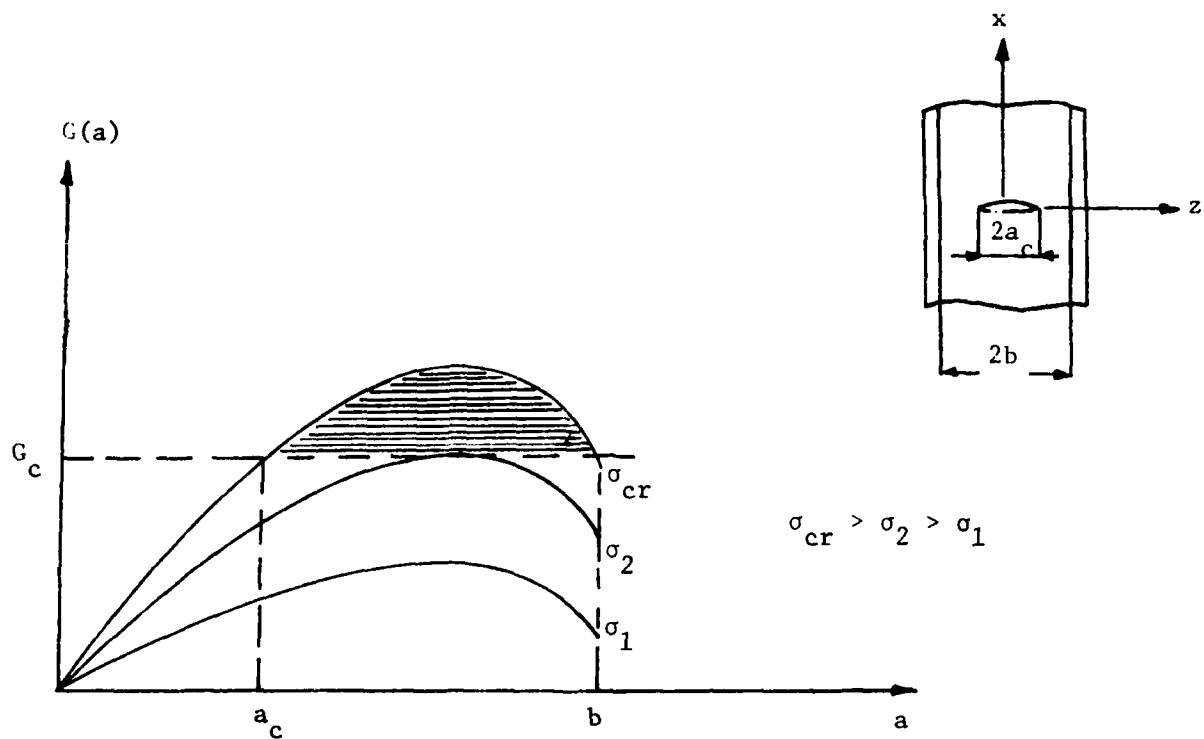


Figure 3.6. Graphical Representation for the Onset of a Transverse Crack.

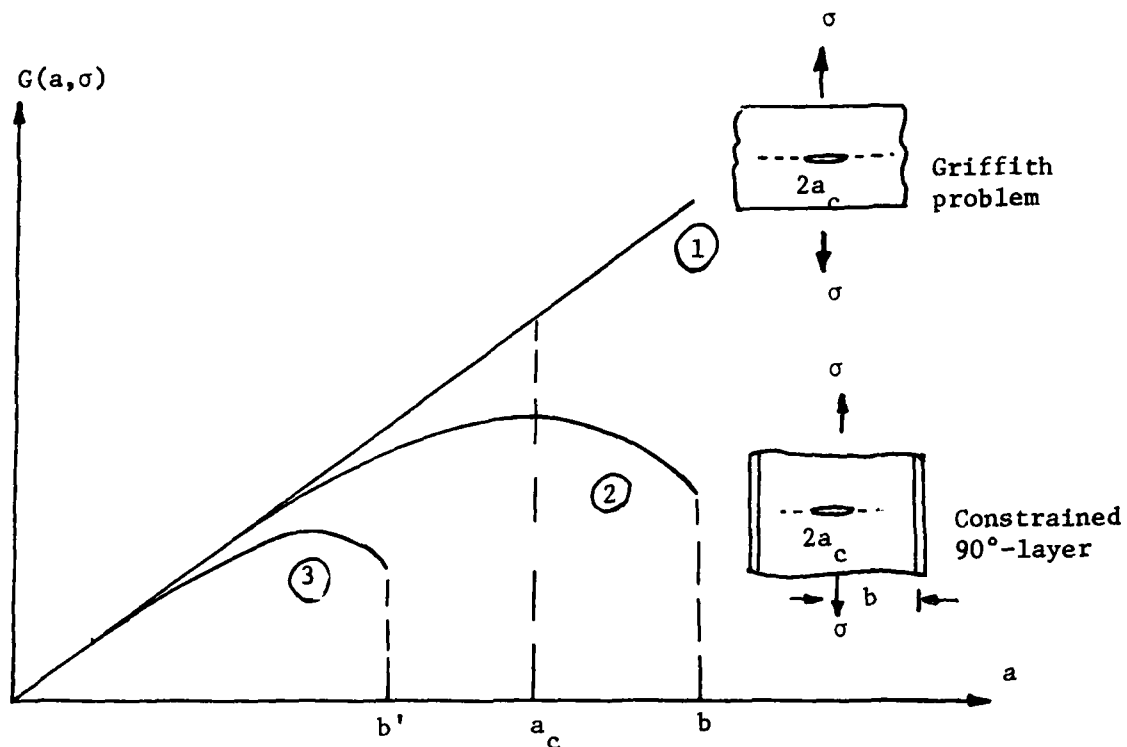


Figure 3.7(a). Strain Energy Release Rates for (1) the Griffith Plate; (2) Bounded Plate with $b > a_c$; (3) Bounded Plate with $b < a_c$.

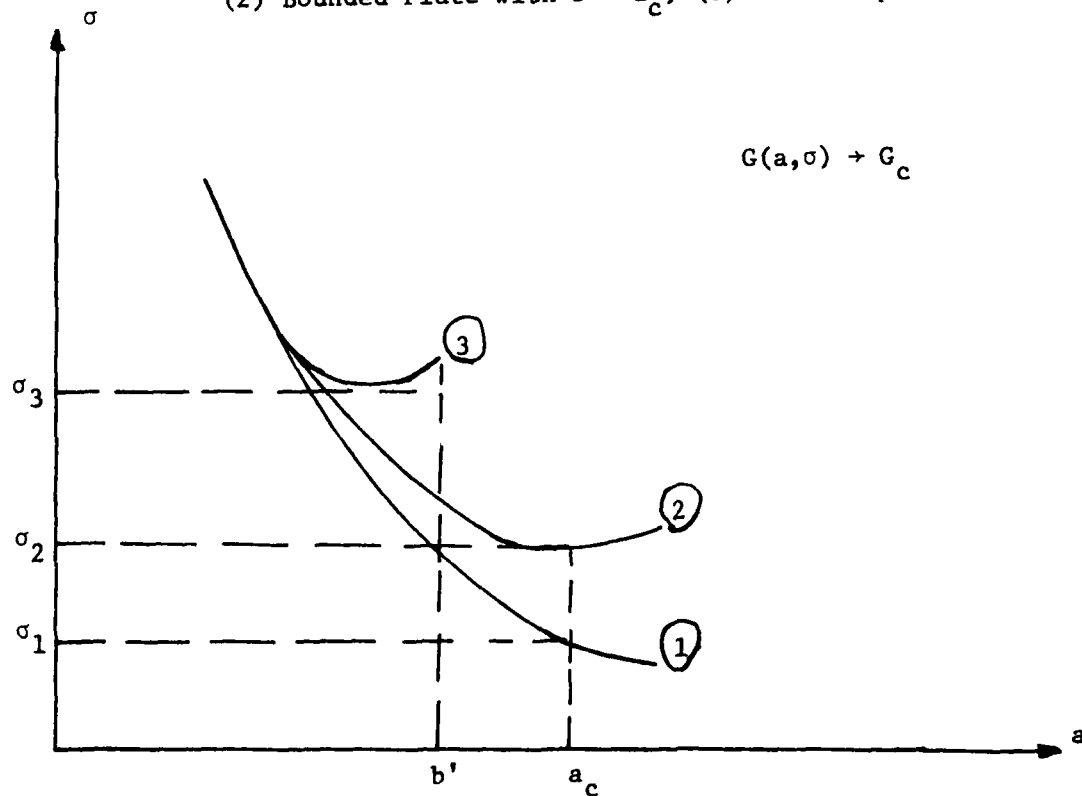


Figure 3.7(b). Onset Stress Curves for (1) the Griffith Plate; (2) bounded Plate with $b > a_c$; (3) Bounded Plate with $b < a_c$.

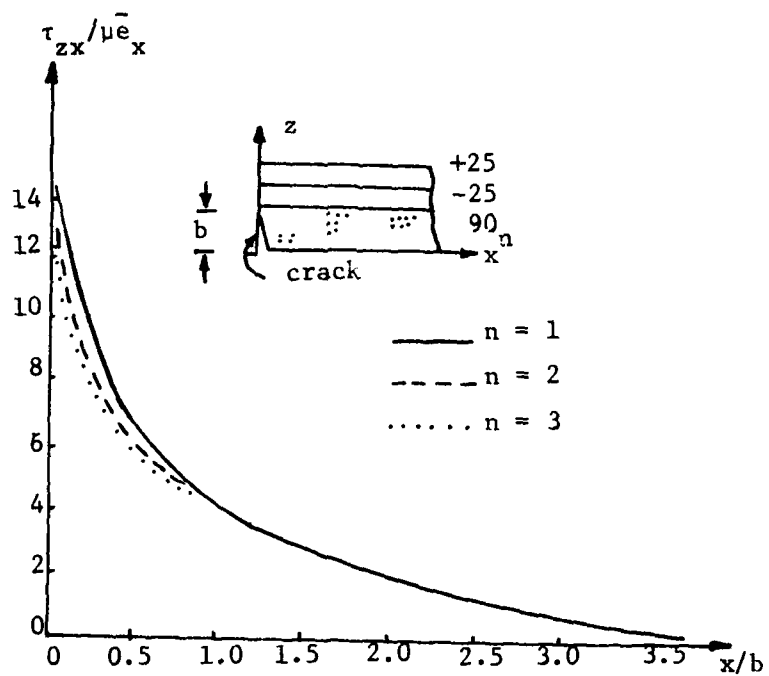


Figure 3.8. Interlaminar Shear Stress on -25/90 Interface.
 x is measured from the root of the crack.

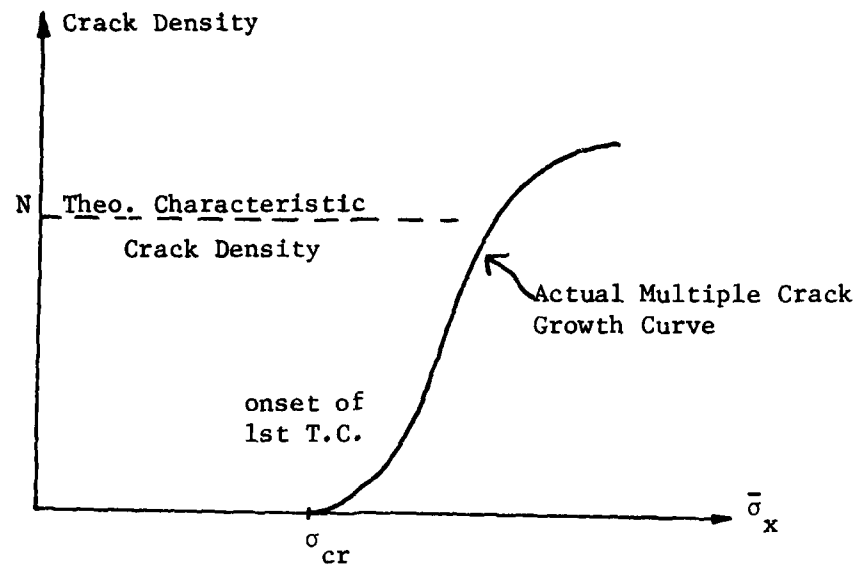


Figure 3.9. Transverse Crack Density vs. Applied Load.
N is the Theoretical Characteristic Density.

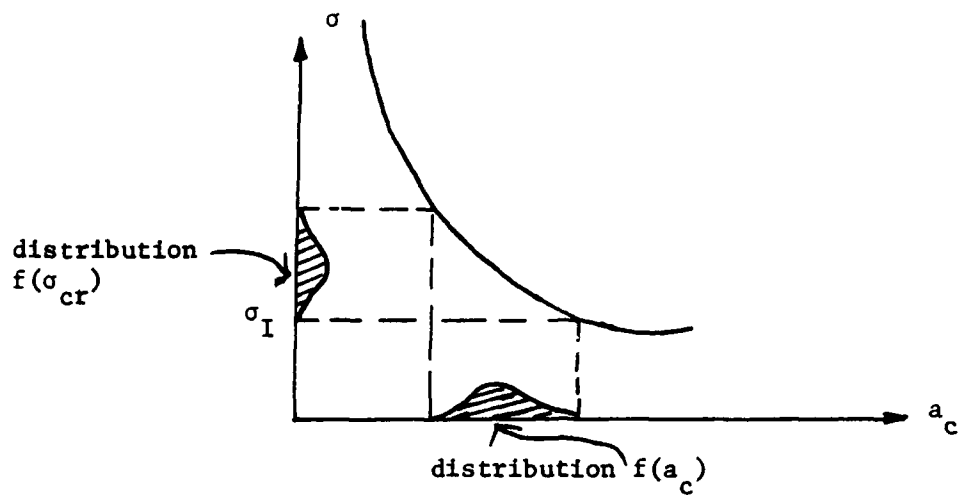


Figure 3.10(a). Schematic Relation Between $f(\sigma_{cr})$ and $f(a_c)$ Through Energy Release Rate Criterion.

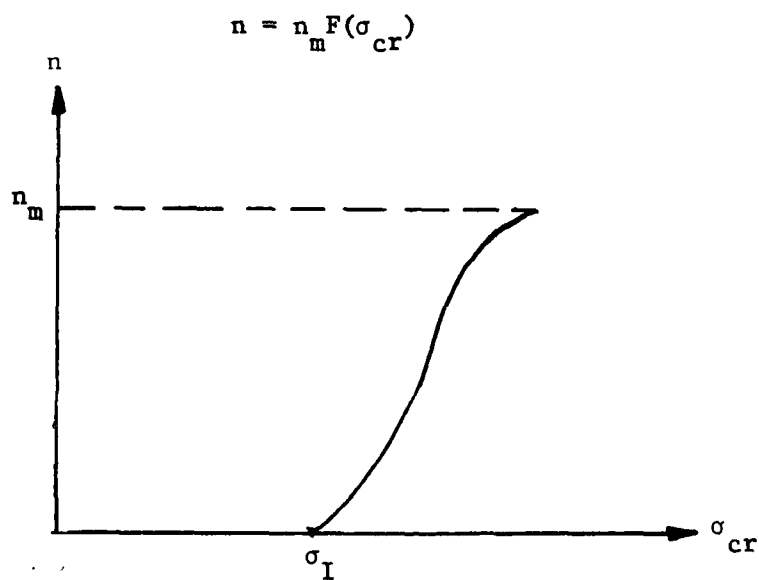


Figure 3.10(b). Crack Density Distribution as Function of Load σ_{cr} . σ_I is Determined by Onset of the First Crack.

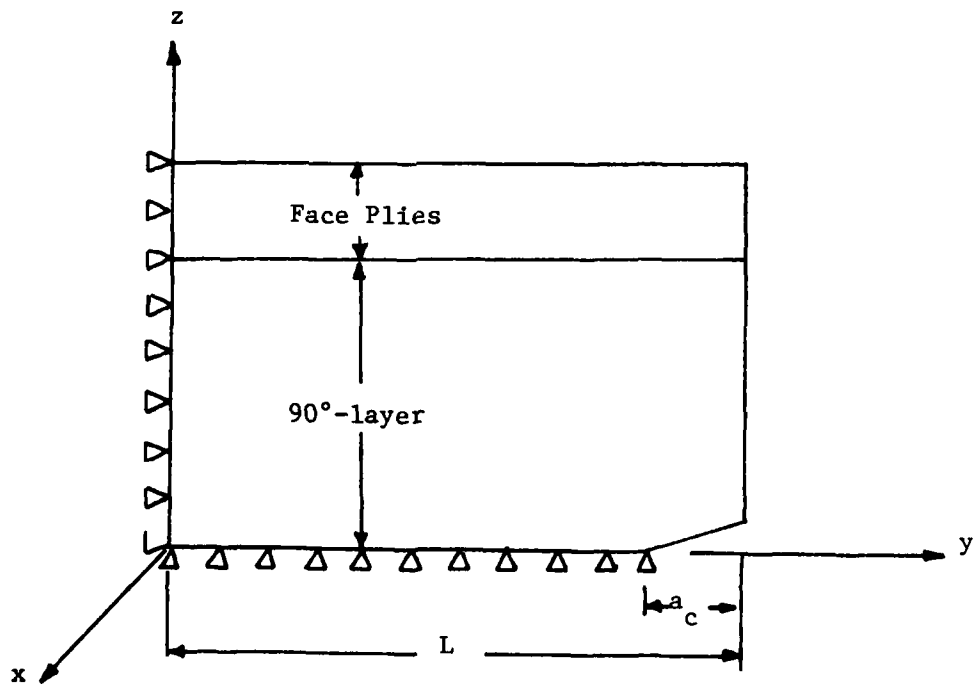
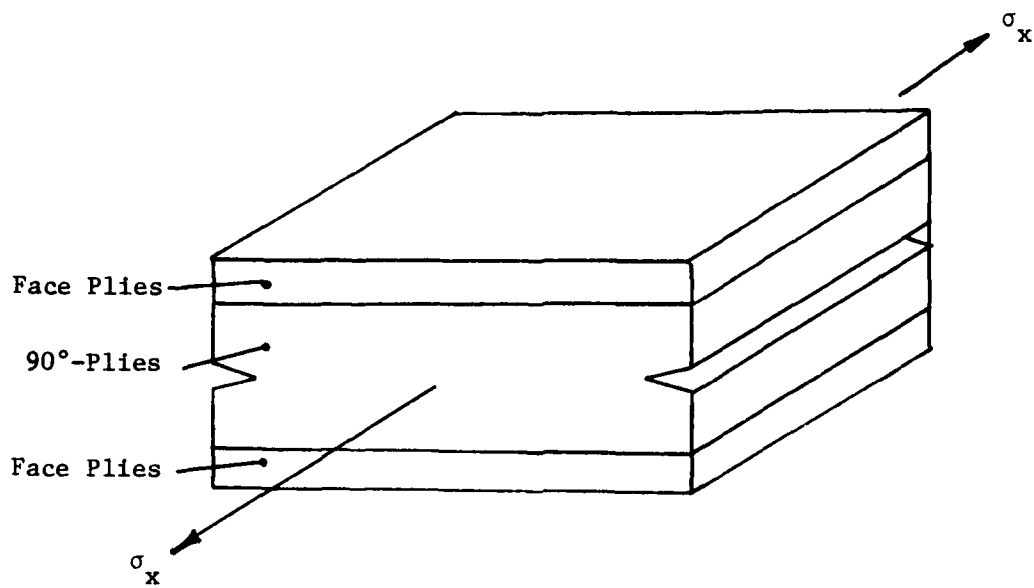


Figure 3.11. Cracking Geometry and Finite Element Representation of Mid-plane Edge Delamination.

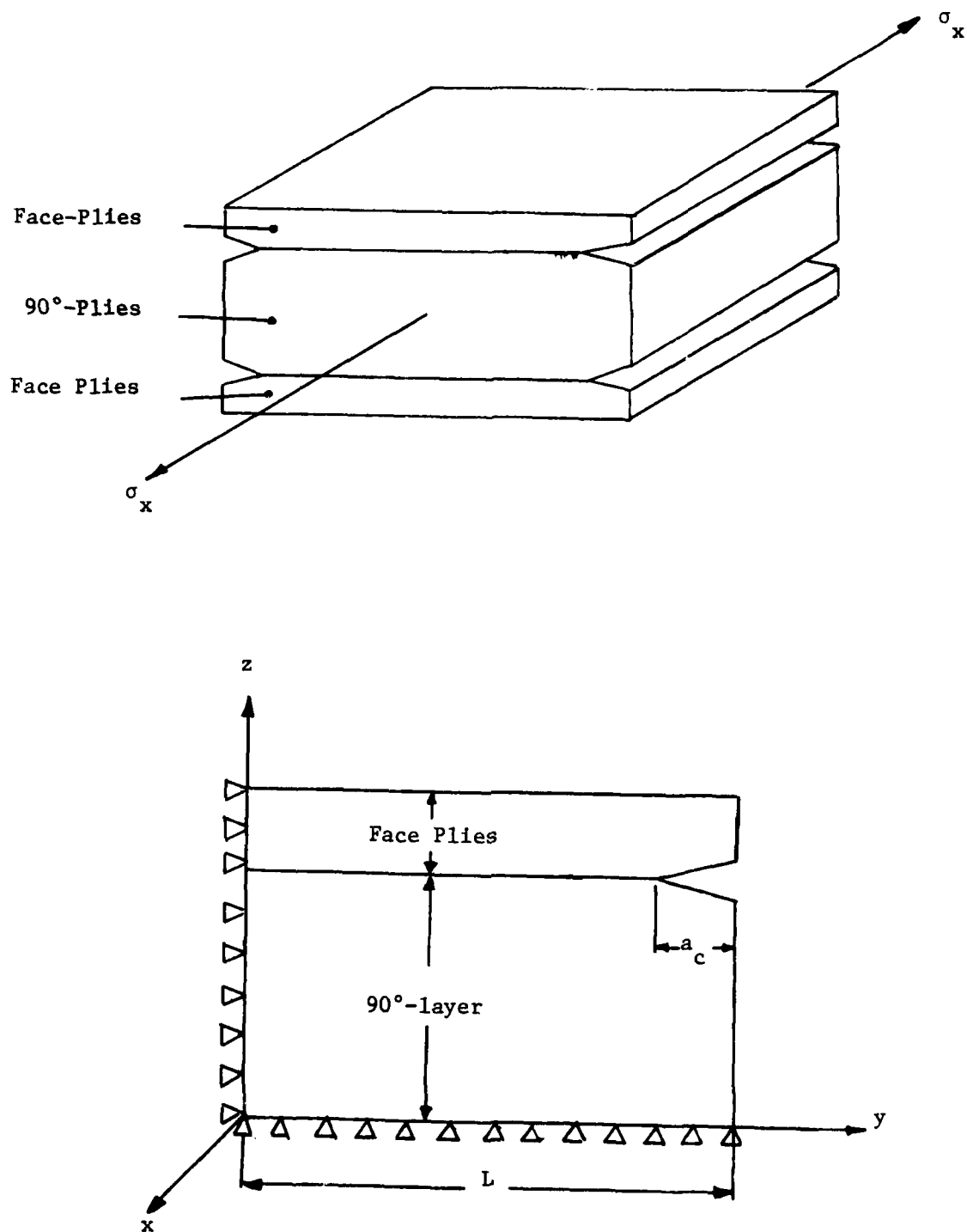


Figure 3.12. Cracking Geometry and Finite Element Representation of an Off-mid-plane Interface Delamination.

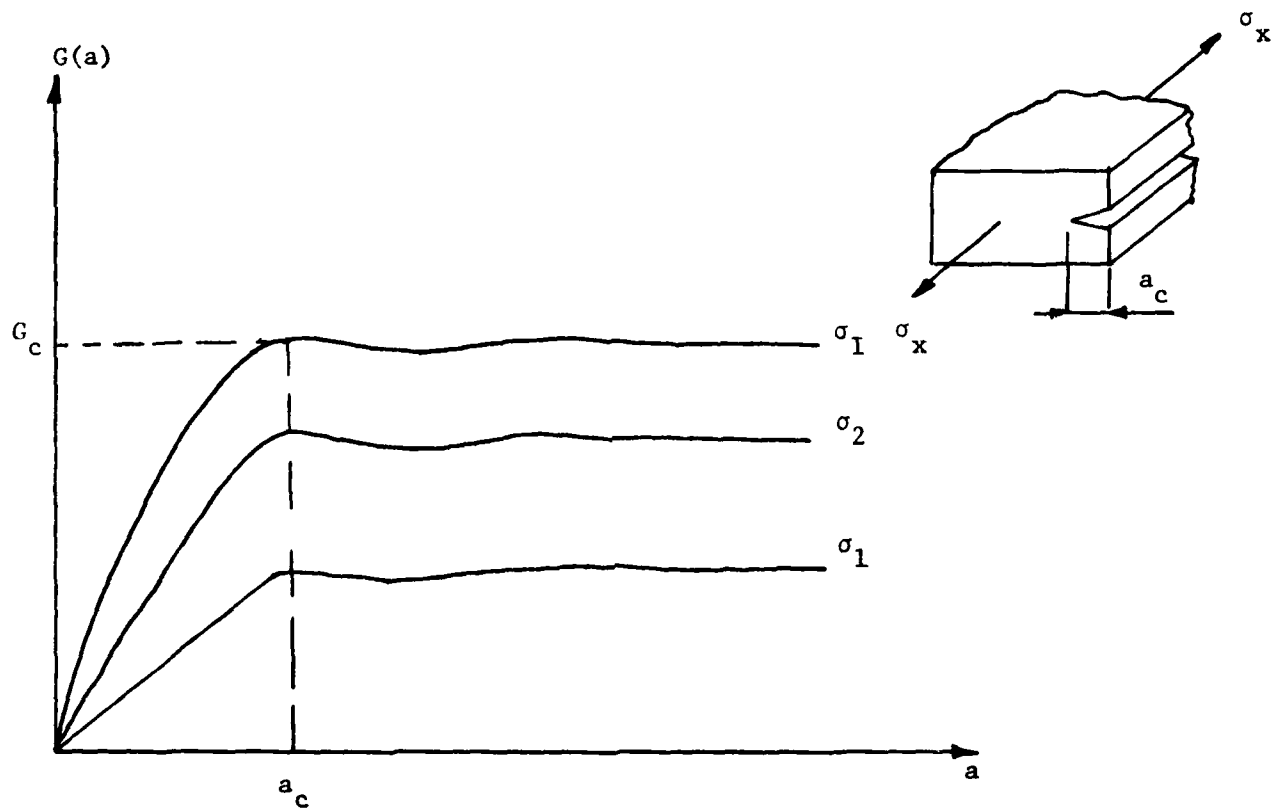


Figure 3.13. Typical $G(a)$ for Edge Delamination.

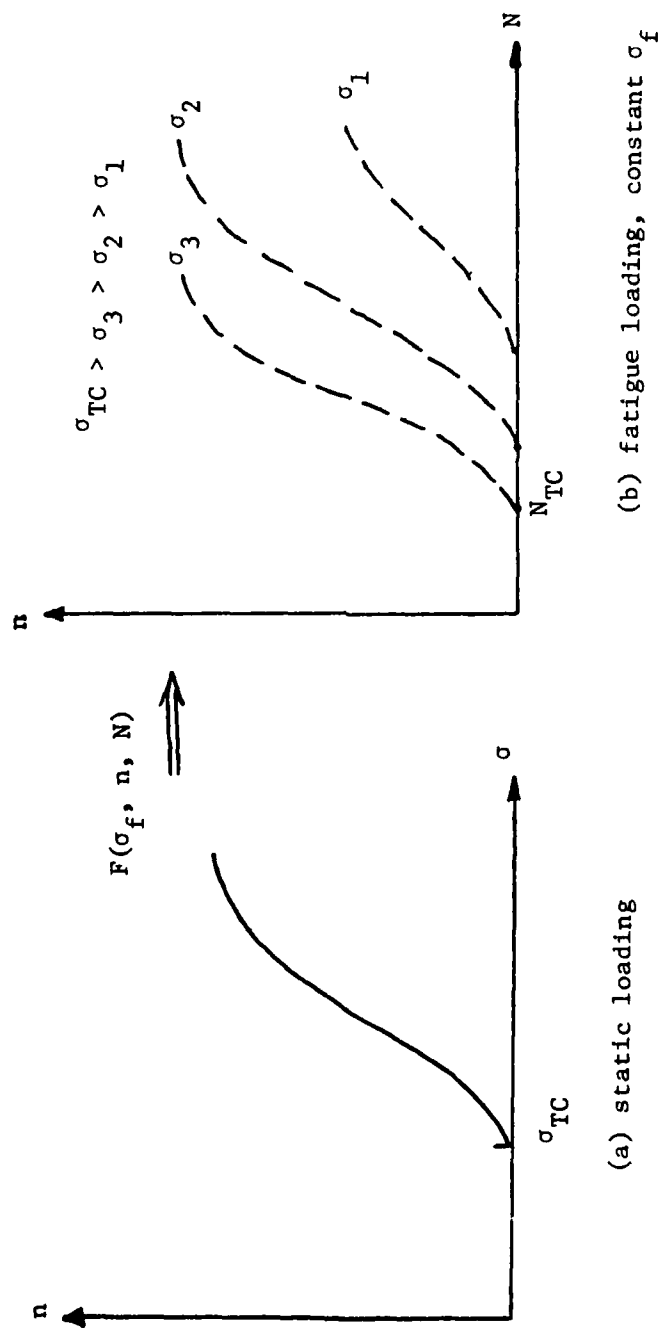


Figure 3.14. The Schematic Definition of the Damage Growth Function in the Transverse Cracking Process.

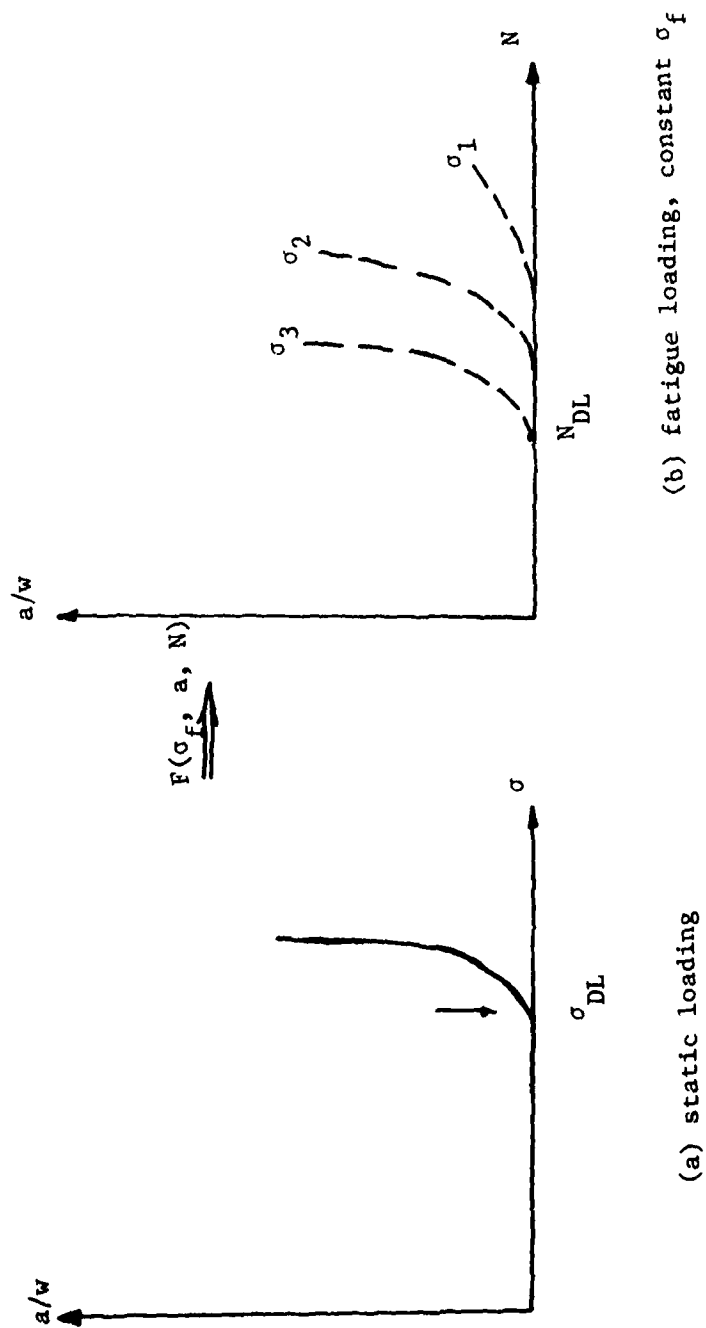


Figure 3.15. The Schematic Definition of the Damage Growth Function in the Edge Delamination Process.

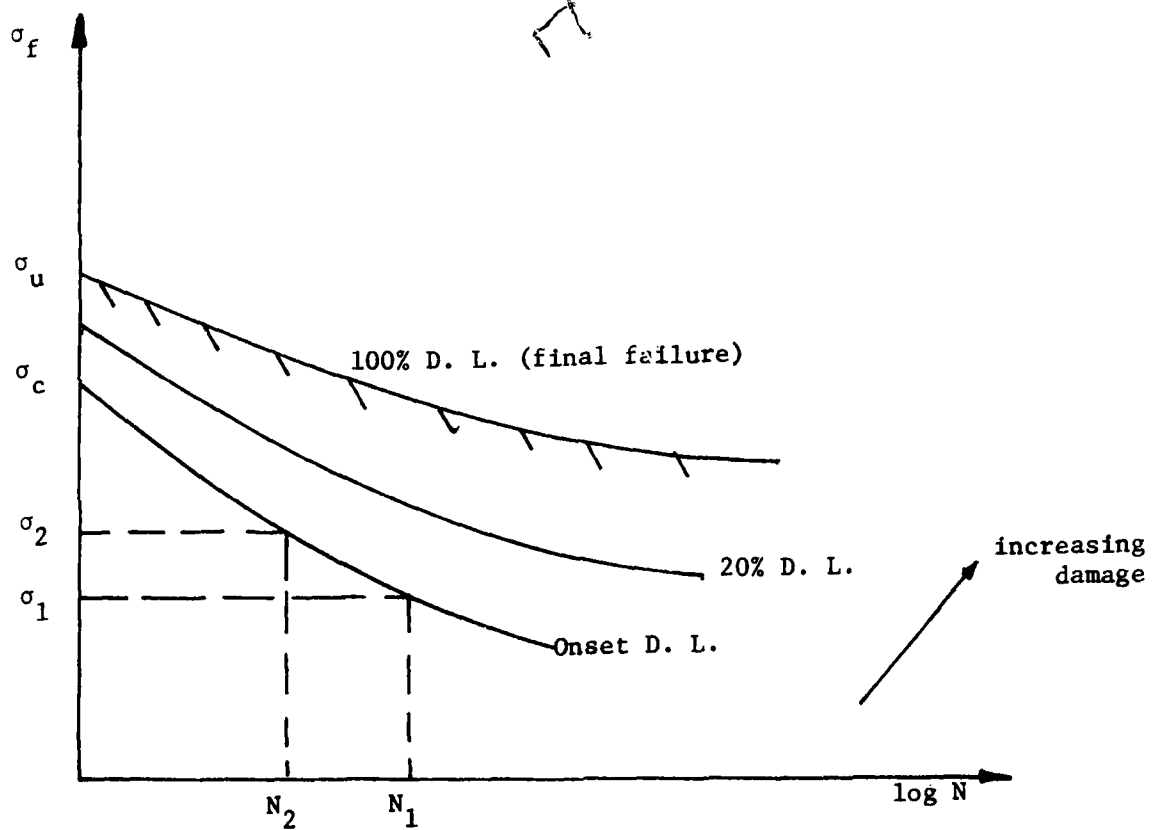
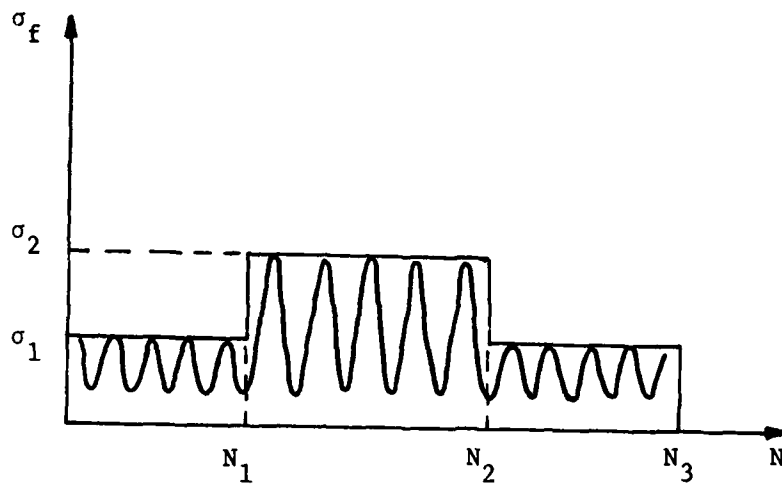
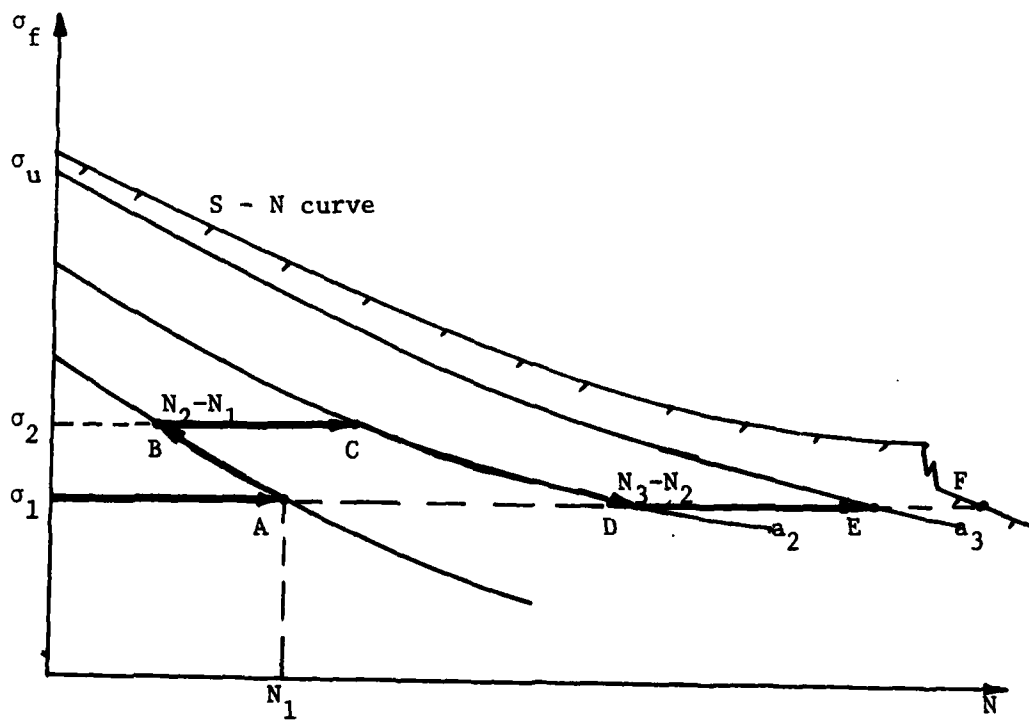


Figure 3.16. Schematics for the Concept of Constant Damage Curves



(a) Schematic of a Spectrum Loading History



(b) Damage Growth Path in the Load-Life Plane

Figure 3.17. Schematics for the Concept of a Cumulative Damage Model.

IV. EXPERIMENTAL PROGRAM

A. Introduction

Our cumulative damage model is based on four major modes of laminate damage. The overall objectives of the experimental program will be to obtain values of the parameters essential to the theoretical model and to provide a means for refinement and verification of the model for each of the four modes of major damage.

The basic approach involves studying specially selected laminates to gain a basic understanding of the specifics of each mode of major damage. This also includes a study of the same modes in different laminates and the effects of mode interactions. An important step in the present work is to determine the static damage modes and the order of their occurrence. Next, it must be verified that the same modes and trends occur under cyclic loading conditions. Finally, the individual pieces of the model can then be tied together for more general laminates under complex loading conditions.

In the present work, the AS3501-6 material system has been chosen for study. The following laminates have been chosen for detailed examination:

- 1) Unidirectional
- 2) $(\pm 45)_{2s}$
- 3) $(0_2/90_2)_s$
- 4) $(0_2/90_3)_s$
- 5) $(\pm 25/90)_s$
- 6) $(\pm 25/90_2)_s$
- 7) $(\pm 25/90_3)_s$

The goals of the experimental program during this phase of the project are:

- a) characterize the material;
- b) determine the required relationships and parameters for incorporation into the model; and
- c) provide initial verification of the energy release rate model as applied to the transverse cracking and delamination modes of major damage.

A series of both static and fatigue tests has been designed using the above laminates to achieve these goals. Table 4-1 shows the overall design of the test program. In general, the static tests serve the purposes of material characterization (including the determination of the material critical energy release rate $G_{I,IIc}$ and critical flaw size a_c) and development of load-damage (S-a) relations. The fatigue tests serve the purposes of determining parameters of the cumulative damage models and of developing both the load-life (S-N) and load-damage (N-a) relations. All tests in the phase were conducted at room temperature and humidity level, and all fatigue tests were tension-tension using three maximum amplitudes and a constant $R = 0.1$. In addition to the static and constant amplitude fatigue tests, a brief series of cumulative damage tests were performed using the $(0_2/90_2)_s$, $(0_2/90_3)_s$ and $(\pm 25/90)_s$ laminates.

Panels of all laminates were prepared in-house and cured using the facilities of the Naval Air Development Center according to procedures detailed in an approved quality assurance plan. Specimens were obtained from the panels by using a diamond saw. Typical specimen dimensions are shown in figure 4-1.

In the following sections, details and results of the experiments will be presented. Tables of raw experimental data are included in Appendix C.

B. Material and Laminate Characterization

A series of tests were performed on the unidirectional and $(\pm 45)_{2s}$ laminates for the purpose of determining the elastic constants of the material. A $(0)_8$ laminate was used for static tensile tests and a $(0)_{12}$ laminate for compressive tests. All tests were conducted on an Instron Universal Tester under room conditions. Load was applied at a displacement control rate of 0.01" per minute. Typical stress-strain diagrams for the unidirectional and $(\pm 45)_{2s}$ laminates are shown in figures 4-2 to 4-5. Average properties are summarized in Table 4-2. Included on this table are the values of fiber content and specific gravity. Specific gravity was determined by accurately weighing and measuring a volume of the material. Fiber content was determined from several photomicrographs of the unidirectional material. A typical photomicrograph is shown in figure 4-6.

The cumulative distribution functions of both the tensile and compressive strength of the unidirectional material obtained by using the maximum likelihood method for estimating the parameters of a two-parameter Weibull distribution from the experimental data are shown in figures 4-7 and 4-8.

Specimens of all other laminates used in this study were instrumented and tested to determine the laminate tensile modulus (E_x), Poisson's ratio (ν_{xy}) and laminate ultimate tensile strength. Typical stress-strain diagrams for each laminate are shown in figures 4-9 to 4-13. Average laminate properties are summarized in Table 4-3.

These basic material data are required as input information for the subsequent fracture analysis.

C. Static Load-Damage Tests

During the course of the static tests, specimens of the $(\pm 25/90)_n$, $n = 1, 2, 3$, and the $(0_2/90_s)_s$ and $(0_2/90_3)_s$ laminates were periodically

removed from the testing machine, treated with DIB, and subjected to X-radiographic inspection. The intervals for this inspection procedure corresponded to step load increases of 10% of the UTS of each laminate until the detection of damage at which point the interval was reduced to step load increases of 5% of the UTS. Figures 4-14, 4-15, and 4-16 show the photographs of the results of this inspection process for a $(0_2/90_2)_s$ specimen, a $(0_2/90_3)_s$ specimen, and a $(\pm 25/90)_s$ specimen respectively. For the first two cases there is no sign of delamination; however, the number of transverse cracks increases with increasing load. For the third case, delamination is observed at a slightly higher load than that where transverse cracks were first detected.

These inspection records are used to construct the load-damage (S-a) relationships for each laminate. This is accomplished by counting the number of transverse cracks detected on the photographs in a four and one-half inch length of the specimen at each load level. Results are shown in figures 4-17 to 4-21 where the S-a relations are presented as graphs of the transverse crack density, i. e., number of cracks per inch vs. laminate stress for each laminate. Also indicated on these figures is the load at which delamination has occurred.

By examining these load-damage graphs, the onset loads for transverse cracking and delamination may be determined. Results are shown in Table 4-4. Other features of the damage progression may be determined from these figures. It is seen that there is no sign of delamination in either the $(0_2/90_2)_s$ laminate or the $(0_2/90_3)_s$ laminate. The transverse crack density is an increasing function of the load although for these two laminates, the crack density appears to level off near final failure, indicating a "saturation"

density of 45 cracks per inch for the $(0_2/90_2)_s$ laminate and of 37 cracks per inch for the $(0_2/90_3)_s$ laminate. For the other laminates, delamination always proceeds final failure. In the $(\pm 25/90)_s$ laminate, a few transverse cracks appear in some specimens before the initiation of delamination; however, the predominant mode of damage is delamination. In the $(\pm 25/90_2)_s$ and $(\pm 25/90_3)_s$ laminates, transverse cracking proceeds delamination. The onset load for transverse cracking is lower for the $(\pm 25/90_3)_s$ laminate than for the $(\pm 25/90_2)_s$ laminate, indicating the thickness effect of the 90° -layer. For this family of laminates, it is seen that an increase of the load by less than 20% over the onset load for delamination produces final failure (100% delamination).

Finally, several of the static tests were halted before final failure of the specimen in order to obtain photomicrographs of the internal damage. Two such specimens are shown in figures 4-22 and 4-23. Figure 4-22(a) shows the X-radiograph of a $(\pm 25/90_3)_s$ specimen after transverse cracking has begun. As can be seen, each transverse crack extends across the full width of the specimen. In figure 4-22(b), the photomicrograph of the indicated area, it is seen that the transverse crack also extends through the full thickness of the 90° -layers and is arrested of the 25/90 interfaces. Figure 4-23(a) shows the X-radiograph of a $(\pm 25/90_2)_s$ specimen after the initiation of delamination. In figure 4-23(b), the photomicrograph of the damage in the indicated region, it is seen that the delamination wanders between the mid-plane 90/90 interface and the 25/90 interface and that the transverse cracks apparently arrest the delamination at each interface.

D. Constant Amplitude Fatigue Tests

All constant amplitude tests have been performed under load control,

tension-tension conditions with $R = 0.1$. Three maximum fatigue load levels were selected for each laminate at values approximately 20% below, 10% below, and 10% above the damage initiation loads determined from static tests. These load levels are shown in Table 4-5. Note that the levels for the $(\pm 25/90_2)_s$ and $(\pm 25/90_3)_s$ laminates differ slightly from the levels indicated above. These changes were made because it was found that the lowest load level (20% below initiation) resulted in very little damage even at one million cycles. As the purpose of these tests is to determine a cycle-damage relationship, the above levels would provide little useful data and, thus, these levels were increased to those shown.

During the course of the fatigue tests, each specimen was periodically removed from the testing machine, treated with DIB, and subjected to X-radiographic inspection. The photographic plates resulting from this inspection procedure were then used to determine the nature and extent of the fatigue induced damages. For all laminates under study, it has been found that the mode of fatigue induced damage at all load levels is identical to the mode of damage under static loading. Specifically, the $(0_2/90_2)_s$ and $(0_2/90_3)_s$ exhibit damage only in the transverse cracking mode; the $(\pm 25/90)$ laminate exhibits delamination preceding transverse cracking; and the $(\pm 25/90_2)_s$ and $(\pm 25/90_3)_s$ laminates exhibit transverse cracking preceding delamination. The photographic plates were also used to obtain quantitative information on the damage state in each specimen. For transverse cracking, the total number of cracks in a four and one-half inch length of the specimen were counted; for edge delamination, the maximum extent of the delaminated region into the width of the specimen was measured. These data are shown graphically in figures 4.23 to 4.27.

From these figures it can be seen that, in all cases, damage (either transverse cracking or delamination) occurs at a lower number of cycles as the maximum fatigue load is increased. For the case of transverse cracking damage, the number of transverse cracks increases steadily with the continued cycling and, in general, at a given number of cycles a specimen fatigued at a low load level has fewer cracks than a specimen cycled at higher load. For the $(\pm 25/90)_s$ laminate which exhibits only delamination damage, it can be seen in figure 4.25 that after initiation, the percent delamination increases steadily until approximately the 30% damage level at which point catastrophic failure occurs. For the $(\pm 25/90_2)_s$ and $(\pm 25/90_3)_s$ laminates, delamination initiates when the transverse crack density (number of cracks per inch) attains a value of approximately 10 or 20 cracks/inch, which is in agreement with the static test results.

The objective of these fatigue tests was to determine a cycle-damage relationship for each laminate at fixed fatigue loads. The previously reported static tests were used to obtain load-damage relationships for each laminate. Using these results, a relation between load and cycles may be obtained at constant damage states for each laminate. This load-cycle relationship will then be used for the development of a cumulative damage model.

The concept of constant damage is illustrated in figure 4.28. The vertical coordinate of figure 4.28 represents the static loading. When the applied load reaches σ_c , onset of delamination occurs. This state of damage can be independently produced by a fatigue load, say at $\sigma_1 < \sigma_c$. Then, under σ_1 , it takes N_1 cycles to induce onset of delamination. Similarly, the same state of damage can also be reached by a different fatigue load,

say σ_2 , by N_2 cycles. Points defining the same damage state in the σ_f -log(N) plane define a "constant" damage curve. In figure 4.28, a curve representing 20% delamination and a curve representing 100% delamination are depicted. The 100%-curve corresponds to the final failure of this laminate; it is the same curve as the commonly generated fatigue S-N curve.

Experimental data has been used to construct these constant damage relations for all laminates used in this study and results are shown in figures 4.29 to 4.33 respectively.

E. Cumulative Damage Tests

Upon the construction of the constant damage curves in the load (σ_f) - life (N) plane, cumulative damage in the laminate under a given load spectrum may be evaluated in the following manner. Consider, as an example, the load history shown in figure 4.34. When it is applied to a given laminate, the state of damage at the end of the period of constant amplitude loading, σ_1 is represented by point A in the load-life plane. The constant damage curve passing point A is denoted as curve a_1 (say e. g., the onset of delamination). At the end of N_1 -cycle, the fatigue load σ_f is raised to σ_2 . Then the state of damage in the laminate at N_1 moves from point A to point B along curve a_1 . Under σ_2 and for a period of (N_2-N_1) cycles, the damage state in the laminate is represented by point C; through C passes the constant damage curve a_2 . Clearly, the damage state represented by curve a_2 is more extensive than the damage state represented by curve a_1 . At the end of the N_2 -cycle, the fatigue load is lowered to σ_1 again; and the corresponding damage state moves from point C to point D along the constant damage curve a_2 . Finally, at the completion of the loading history at N_3 , the damage state moves from D to E, where the damage is represented by curve a_3 .

A series of tests has been designed to study this concept of cumulative damage. The laminates selected for the study are the $(0_2/90_2)_s$, $(0_2/90_3)_s$ and $(\pm 25/90)_s$ laminates. These were selected because, as described above, each has a unique fatigue damage mode. Thus, any complication arising from the interaction of damage modes is eliminated in this first-round study. The test program is given in Table 4-6 where the load levels and number of cycles at each level were selected on the basis of cycling at high level followed by low level, low level followed by high, and cycling both above and below the damage initiation level. Data are given in Appendix C. Results will be discussed in the following section.

Table 4-1: DESIGN OF TEST PROGRAM

LAMINATE	TEST TYPE	MODE OF DAMAGE	PURPOSE OF TEST
1) (0_8)	Static Tension	Fiber Breakage	Material Characterization
2) (0_{12})	Static Compression	Compressive	Material Characterization
3) $(\pm 45)_2$	Static Tension	Transverse Cracking	G_{LT} Determination
	Static Compression	Compressive	G_{LT} Determination
4) $(\pm 25/90)_8$	Static Tension	Delamination Preceding Transverse Cracking	a_c, G_{IC} Determination, S-a Relation
	Fatigue Tension	Same as Static	Parameters of Model; S-N, N-a Relations
5) $(\pm 25/90_2)_8$	Static Tension	Transverse Cracking Preceding Delamination	a_c, G_{IC}, S -a Relation
	Fatigue Tension	Same as Static	Parameters of Model; S-N, N-a Relations
6) $(\pm 25/90_3)_8$	Static Tension	Transverse Cracking Preceding Delamination	a_c, G_{IC}, G_{IIC}, S -a Relation
	Fatigue Tension	Same as Static	Parameters of Model; S-N, N-a Relations
7) $(0_2/90_2)_8$	Static Tension	Transverse Cracking Preceding Delamination	a_c, G_{IC}, S -a Relation
	Fatigue Tension	Same as Static	Parameters of Model; S-N, N-a Relations
8) $(0_2/90_3)_8$	Static Tension	Transverse Cracking Preceding Delamination	a_c, G_{IC}, S -a Relation
	Fatigue Tension	Same as Static	Parameters of Model; S-N, N-a Relations

TABLE 4.2: MATERIAL PROPERTIES

A) Material Properties as Obtained From Unidirectional Laminates

E_L (comp) MPa (ksi)	132.3×10^3	(19.19×10^3)
E_L (Ten) MPa (ksi)	139×10^3	(20.17×10^3)
E_T MPa (ksi)	11.1×10^3	(1.6×10^3)
ν_{LT}	0.269	
$\sigma_{ult, L}$ MPa (ksi)	1826	(264.86)
$\sigma_{ult, T}$ MPa (ksi)	60	(8.7)
Fiber Volume, %	66.48	
Sp. Gravity	1.55	

B) Material Properties as Obtained From $(\pm 45)_2$ Laminates

G_{LT} (comp) MPa (ksi)	4861	(705)
G_{LT} (ten) MPa (ksi)	4792	(695)

TABLE 4-3: LAMINATE PROPERTIES

LAMINATE	E_x		ν_{xy}	σ_{ULT}		SPECIFIC GRAVITY
	MPa	(ksi)		MPa	(ksi)	
$(\pm 45)_2s$	19.1×10^3	(2780)	0.83	157.7	(22.87)	1.64
$(0_2/90_2)_s$	72.1×10^3	(10460)	0.0704	859	(124.6)	1.67
$(0_2/90_3)_s$	63.6×10^3	(9220)	0.045	782	(113.5)	1.59
$(\pm 25/90_3)_s$	42×10^3	(6100)	0.101	274.9	(39.87)	1.58
$(\pm 25/90_2)_s$	46.1×10^3	(6700)	0.162	315.4	(45.75)	1.57
$(\pm 25/90)_s$	63.8×10^3	(9250)	0.29	406.8	(59)	1.56

TABLE 4-4: ONSET LOADS FOR DAMAGE

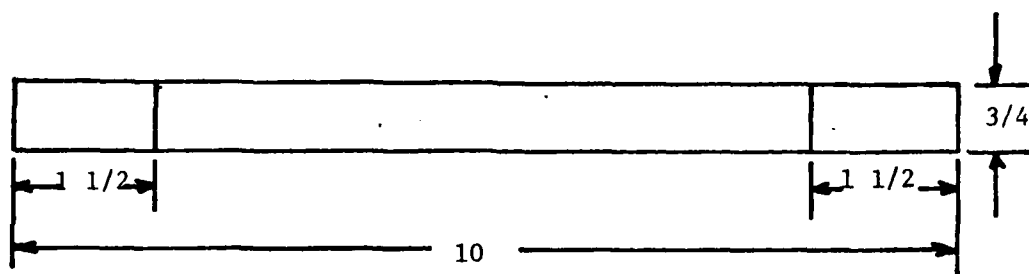
<u>LAMINATE</u>	TRANSVERSE CRACKING		DELAMINATION	
	<u>ONSET LOAD σ, MPa (ksi)</u>		<u>ONSET LOAD σ, MPa (ksi)</u>	
$(\pm 25/90)_s$	254.93	(37)	310.05	(45)
$(\pm 25/90_2)_s$	172.25	(25)	261.82	(38)
$(\pm 25/90_3)_s$	124.02	(18)	279.14	(36)
$(0_2/\pm 45_2)_s$	330.72	(48)	--	
$(0_2/\pm 45_3)_s$	234.26	(34)	--	

TABLE 4-5: MAXIMUM STRESS LEVELS FOR FATIGUE TESTS

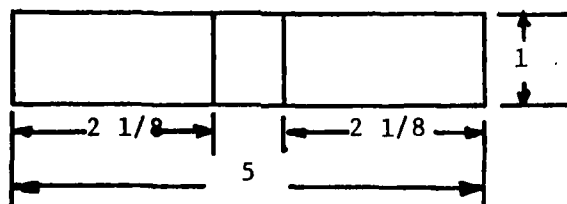
<u>Laminate</u>	Maximum Stress Level, σ_f , MPa (ksi)					
	I		II		III	
$(\pm 25/90)_s$	199.81	(29)	227.37	(33)	275.6	(40)
$(\pm 25/90_2)_s$	151.58	(22)	186.03	(27)	213.59	(31)
$(\pm 25/90_3)_s$	130.91	(19)	151.58	(22)	172.25	(25)
$(0_2/90_2)_s$	261.82	(38)	296.27	(43)	365.17	(53)
$(0_2/90_3)_s$	179.14	(26)	206.7	(30)	261.82	(38)

TABLE 4-6 CUMULATIVE DAMAGE TESTS

<u>Laminate</u>	<u>Maximum Fatigue Load, MPa (ksi)</u>	<u>Cycles @ Load</u>
(0 ₂ /90 ₂)	551.6 (80)	100
	413.7 (60)	100,000
	413.7 (60)	100,000
	551.6 (80)	100,000
	344.7 (50)	1,000
	482.6 (70)	1,000
	344.7 (50)	100,000
(0 ₂ /90 ₃) _s	103.4 (15)	100,000
	344.7 (50)	1,000,000
	551.6 (80)	10
	275.8 (40)	1,000,000
	179.2 (26)	10,000
	206.8 (30)	30,000
	179.2 (26)	100,000
(±25/90) _s	137.9 (20)	100,000
	206.8 (30)	300,000
	137.9 (20)	100,000
	344.7 (50)	1,000
	344.7 (50)	10
	206.8 (30)	300,000
	275.8 (40)	1,000
	344.7 (50)	1,000
	137.9 (20)	300,000
	275.8 (40)	1,000
	206.8 (30)	100,000



A. TYPICAL TENSION SPECIMEN



B. TYPICAL COMPRESSION SPECIMEN

ALL DIMENSIONS ± 0.001 "

Figure 4-1: Typical Specimen Dimensions

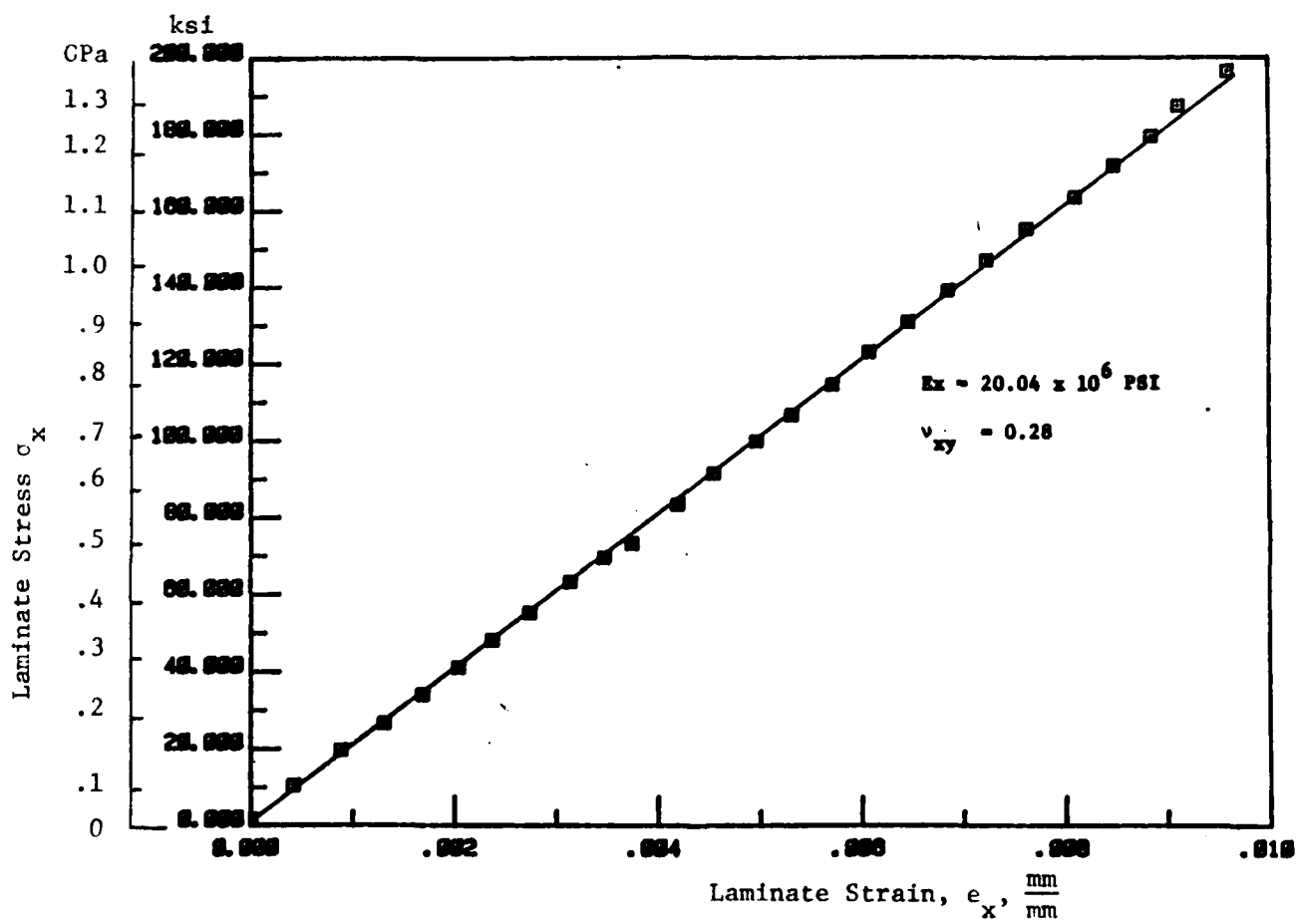


Figure 4.2: Tensile Stress-Strain Diagram: Unidirectional Material.

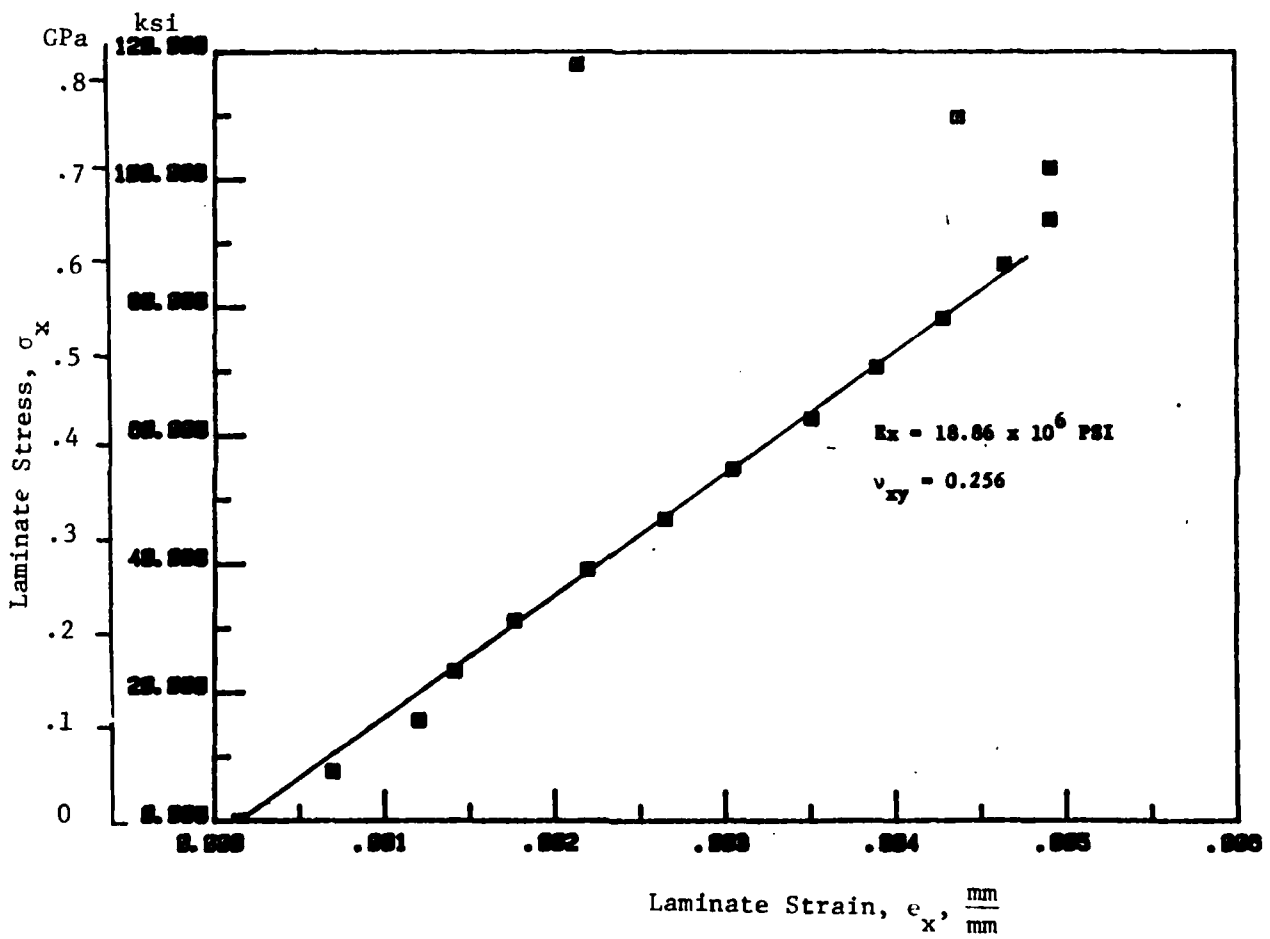


Figure 4.3: Compressive Stress-Strain Diagram: Unidirectional Material.

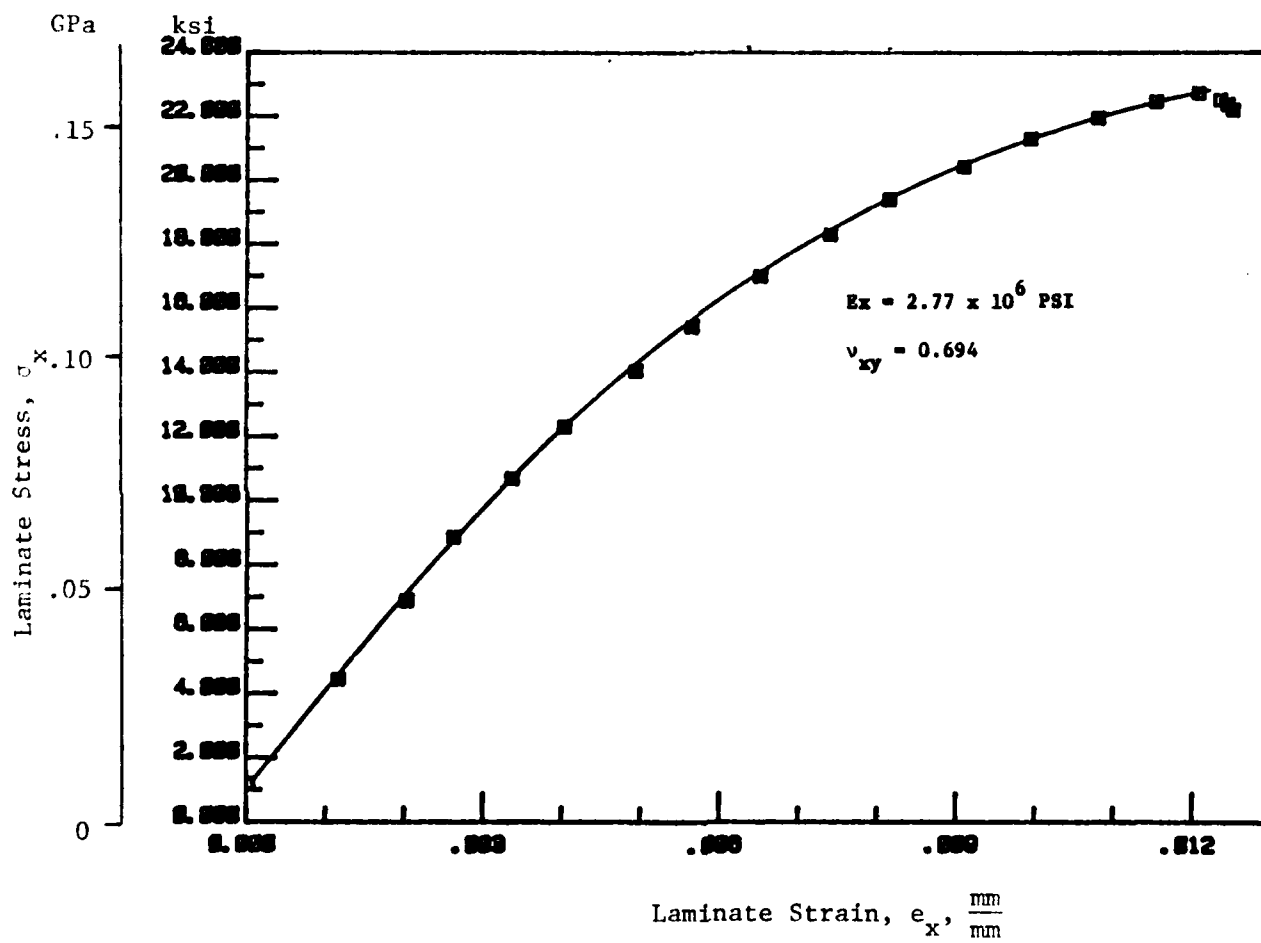
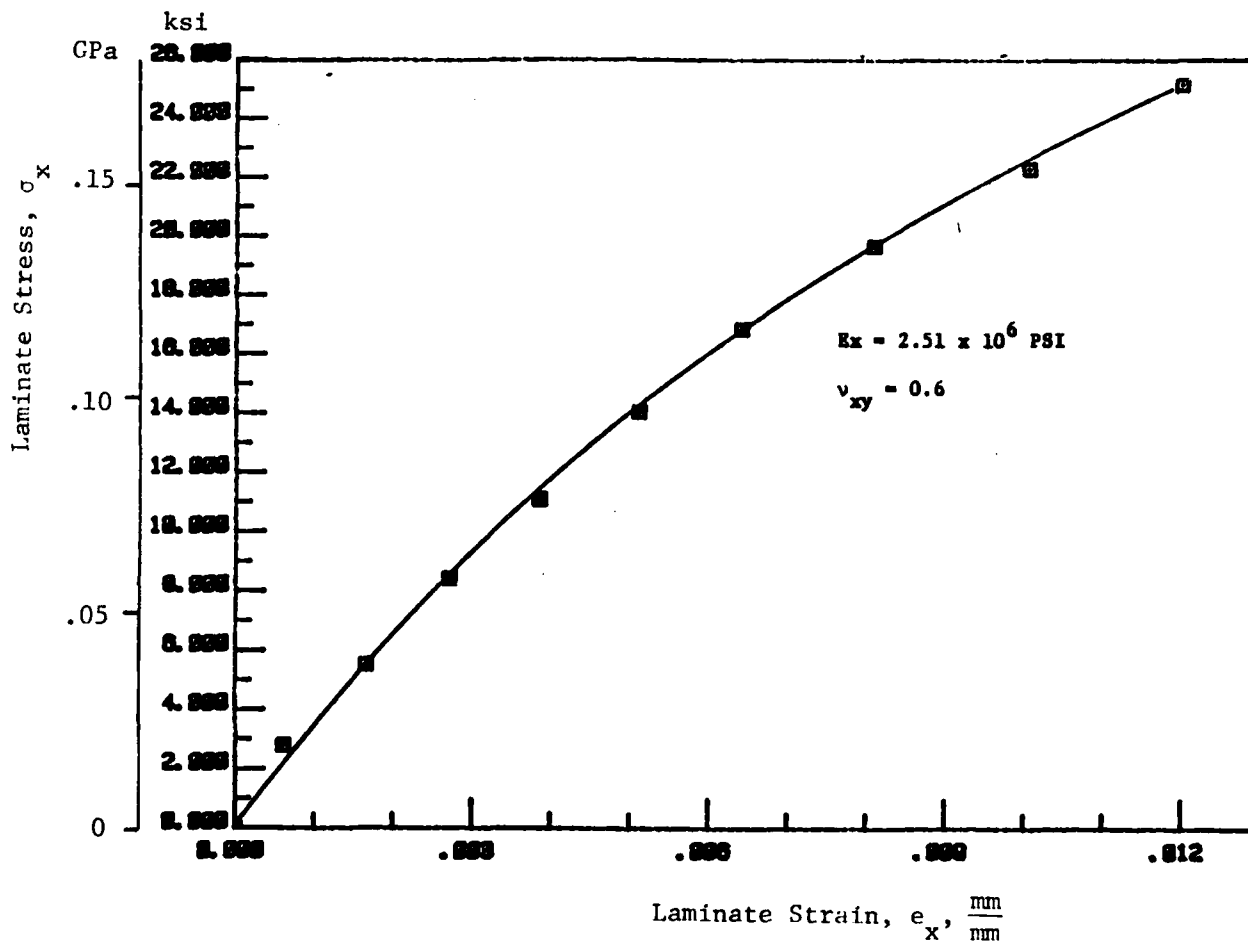


Figure 4.4: Tensile Stress-Strain Diagram: $(\pm 45)_{2s}$ Laminate.



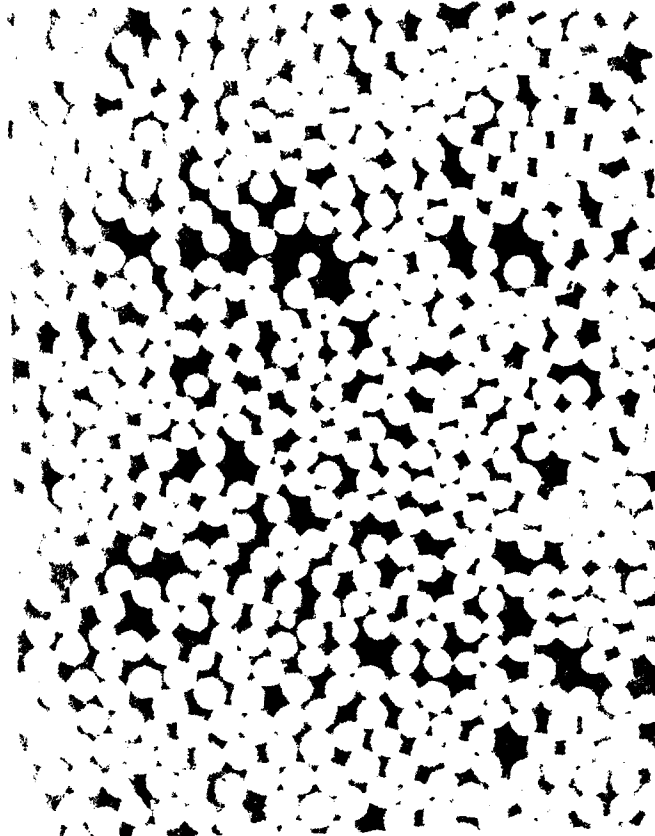


Figure 4.6: PHOTOMICROGRAPH OF CROSS SECTION
OF UNIDIRECTIONAL MATERIAL, 500x

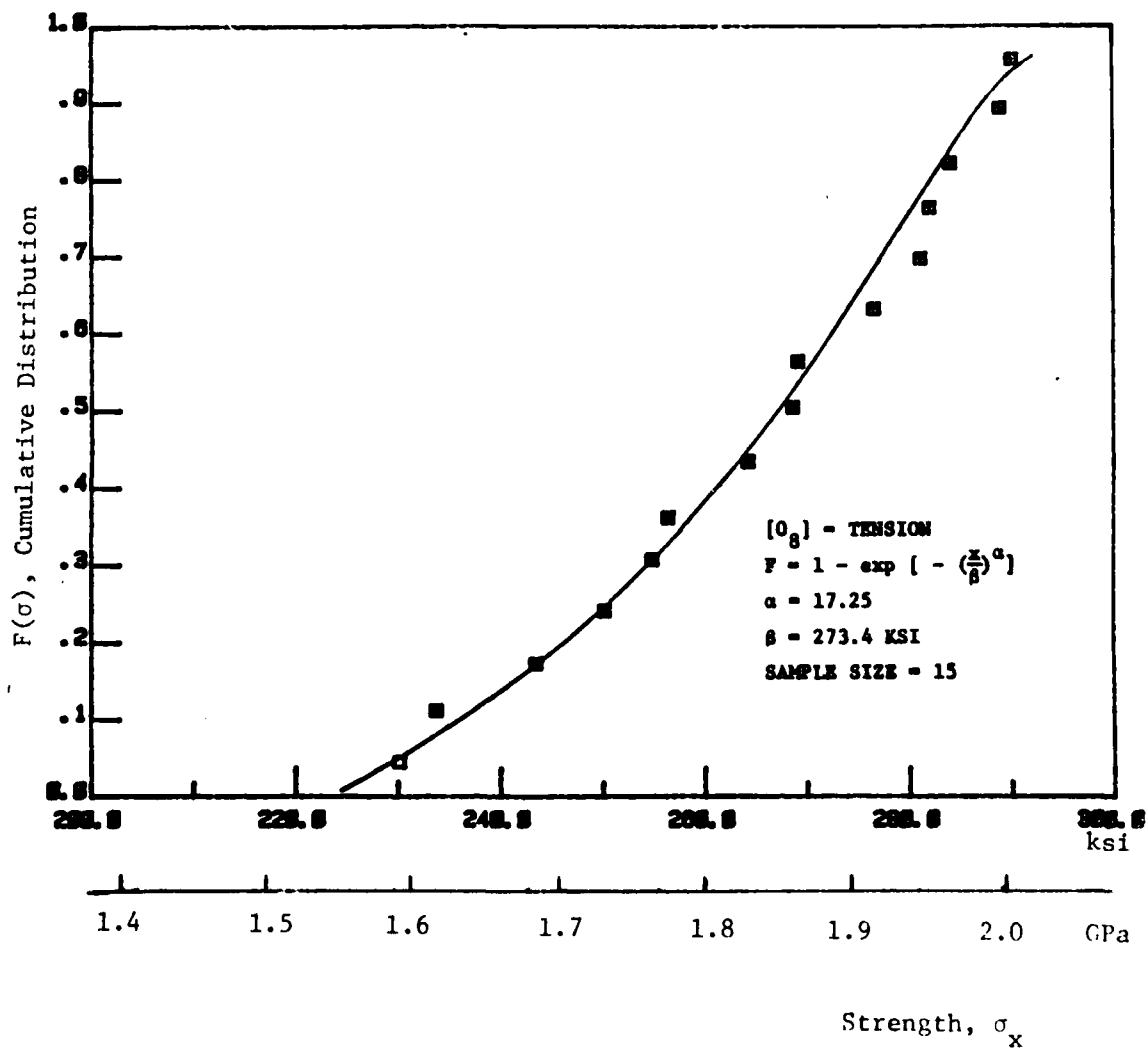


Figure 4.7: Two Parameter Weibull Cumulative Distribution for Ultimate Tensile Strength of Unidirectional Material.

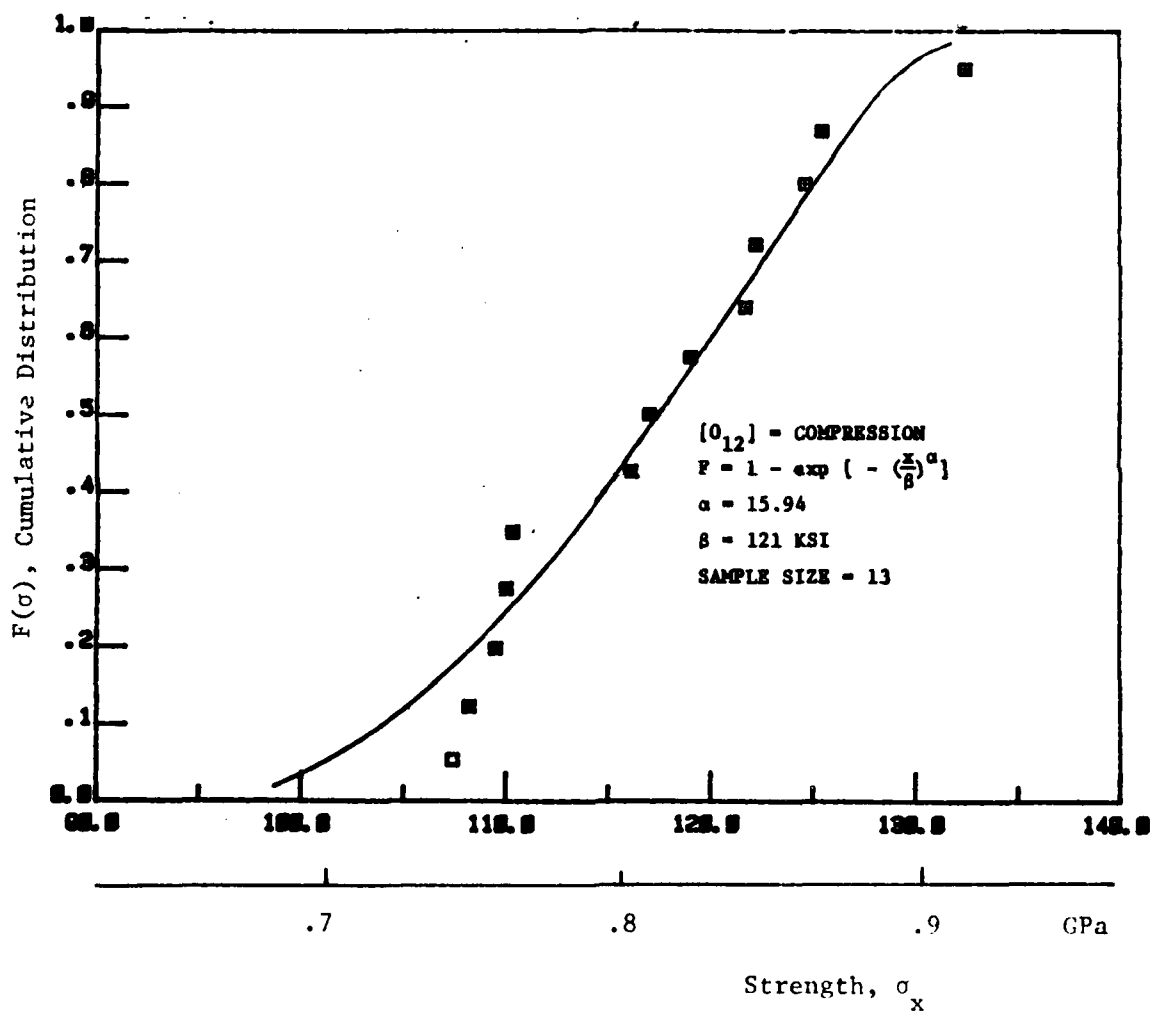


Figure 4.8: Two-Parameter Weibull Cumulative Distribution of Ultimate Compressive Strength of Unidirectional Material.

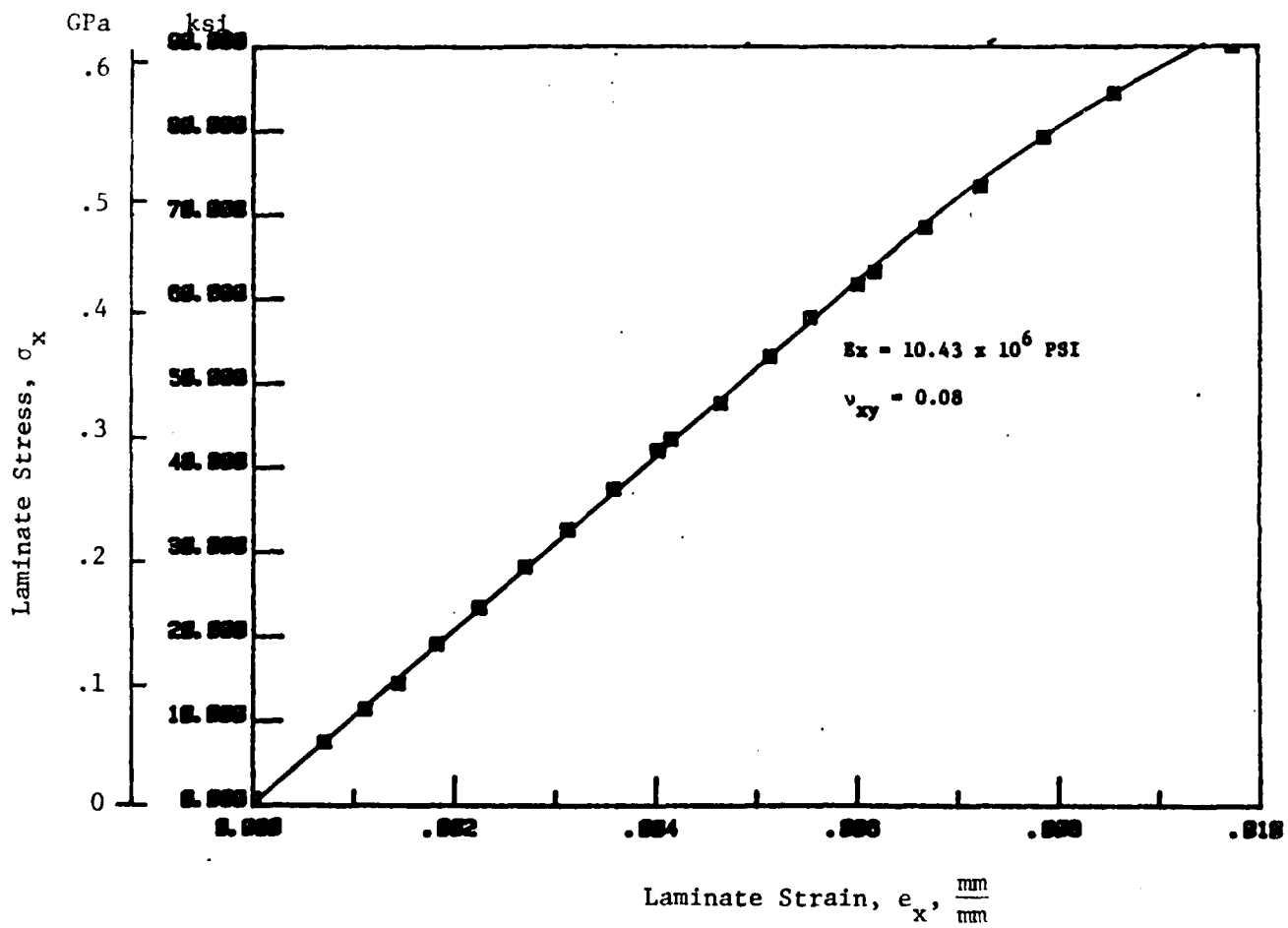


Figure 4.9: Typical Tensile Stress-Strain Diagram for $(0_2/90_2)_s$ Laminates.

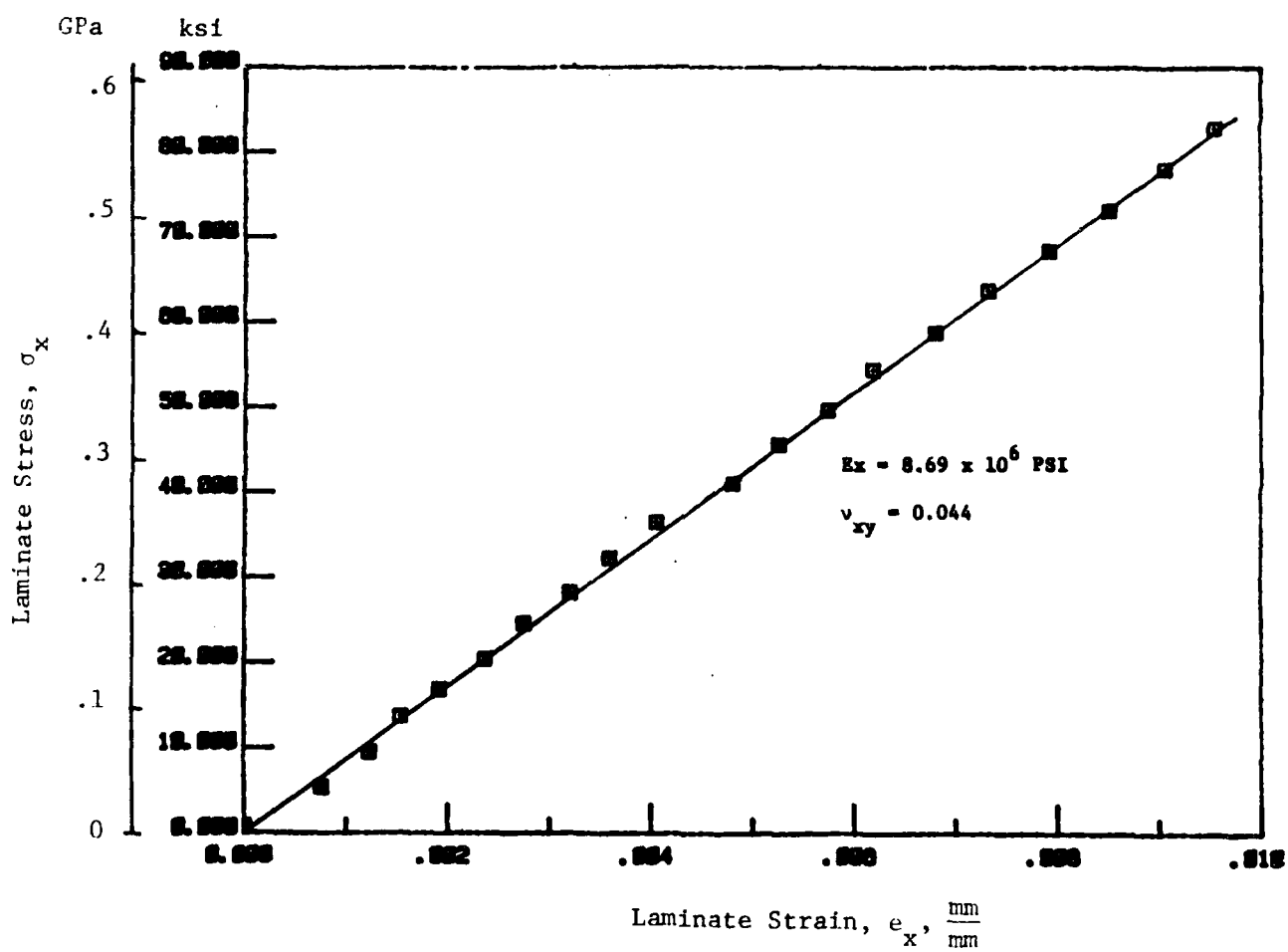


Figure 4.10: Typical Stress-Strain Diagram for $(0_2/90_3)_s$ Laminates.

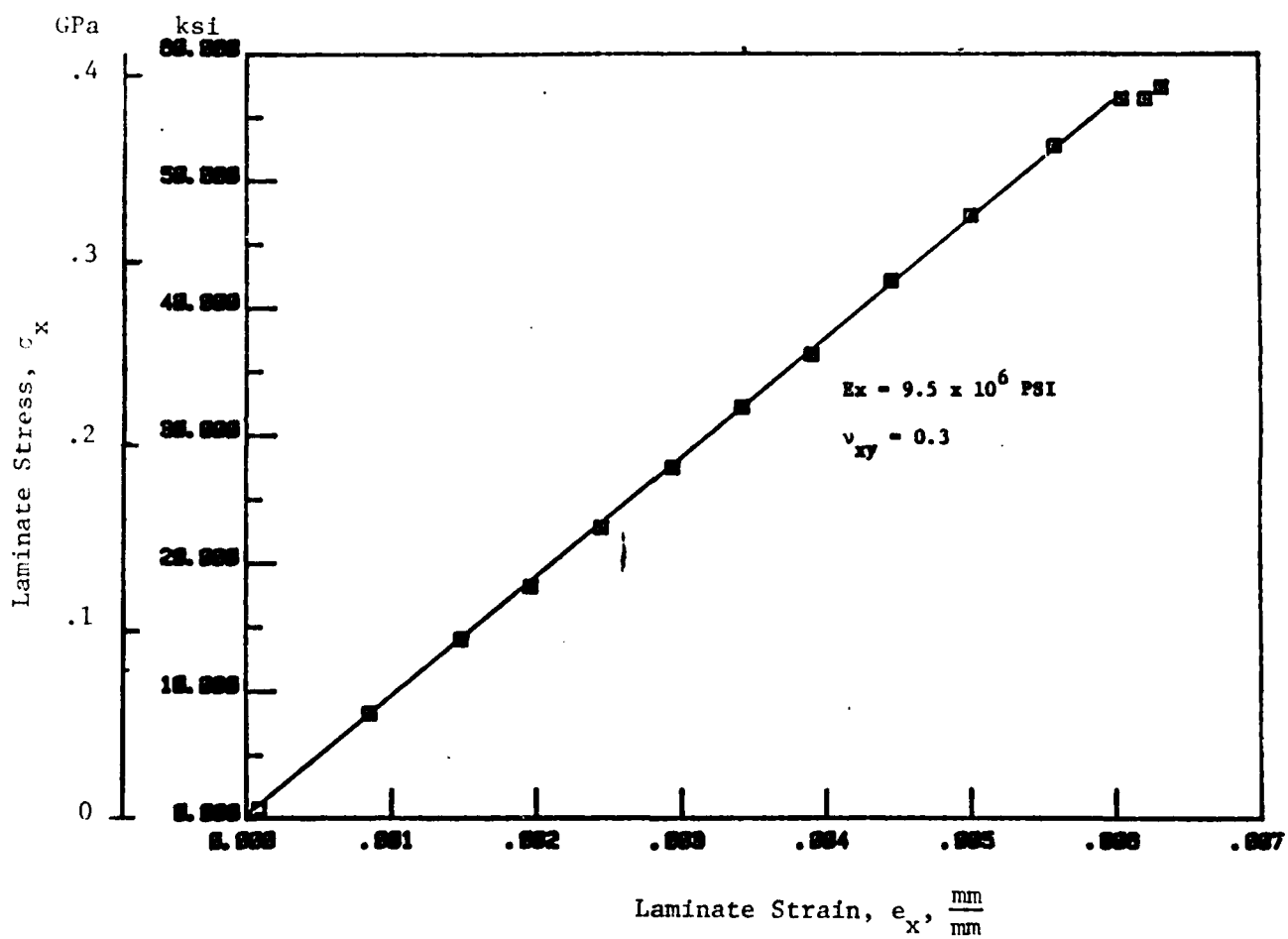


Figure 4.11: Typical Tensile Stress-Strain Diagram for $(\pm 25/90)_s$ Laminates.

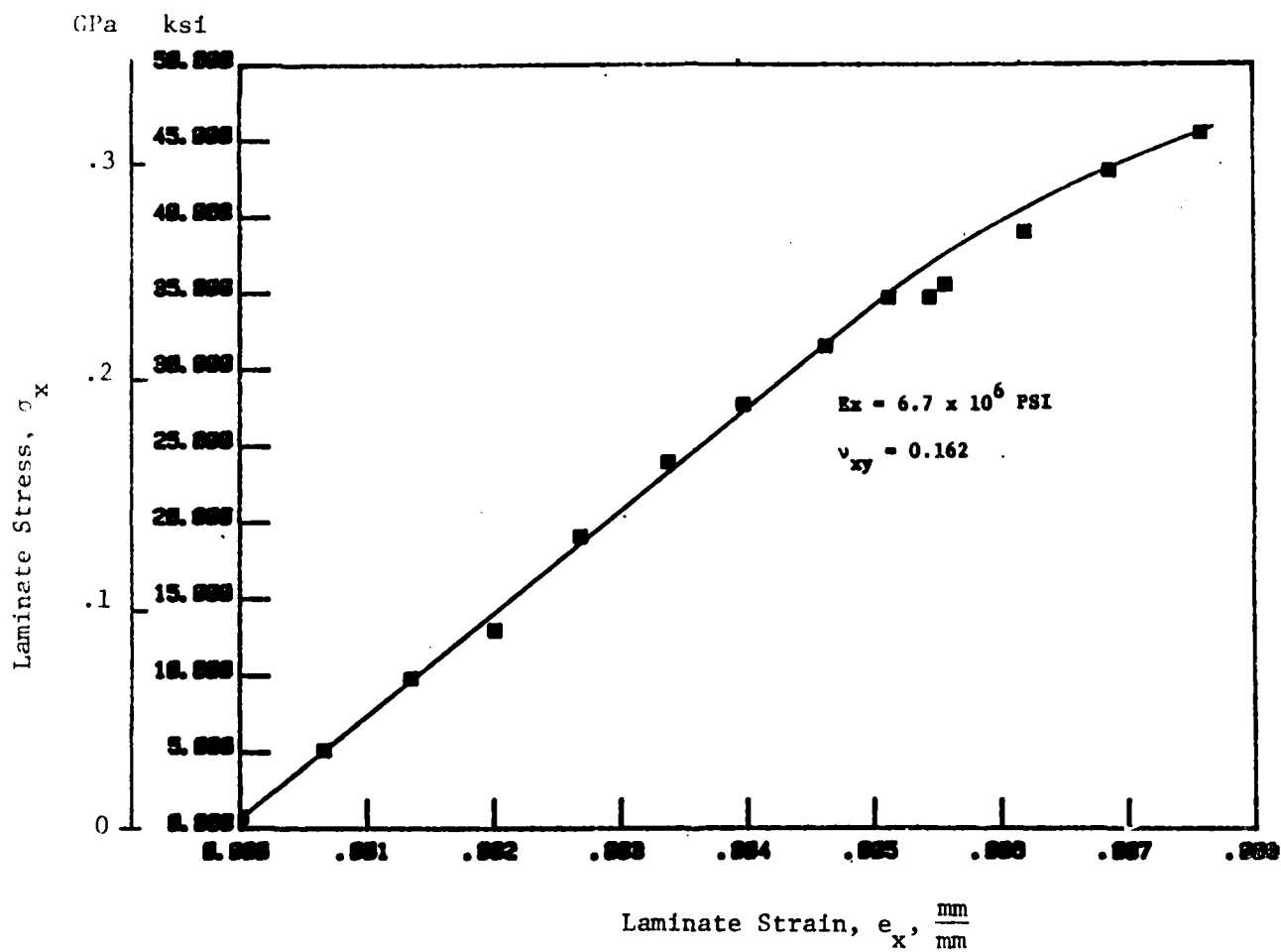


Figure 4.12: Typical Tensile Stress-Strain Diagram for $(\pm 25/90)_2$ Laminates.

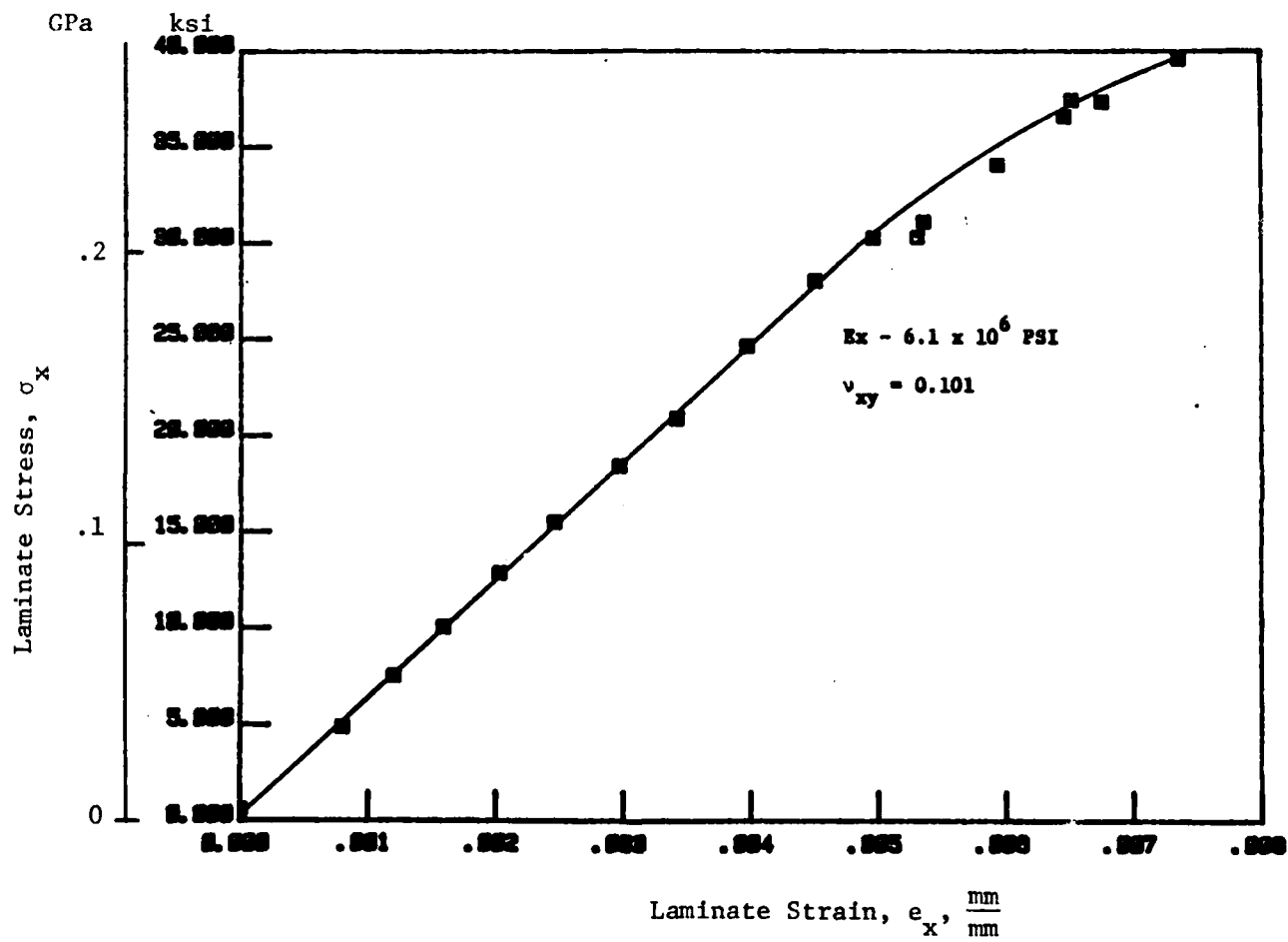


Figure 4.13: Typical Tensile Stress-Strain Diagram for $(\pm 25/90)_3/2s$ Laminates.



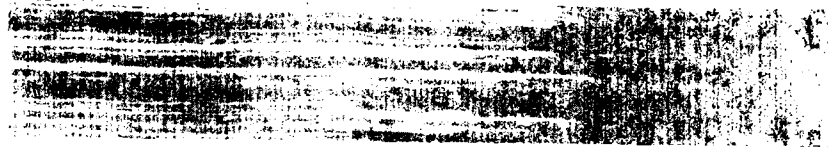
e) $\sigma = 63\% \sigma_{ult}$
 $n = 94$



f) $\sigma = 75\% \sigma_{ult}$
 $n = 126$

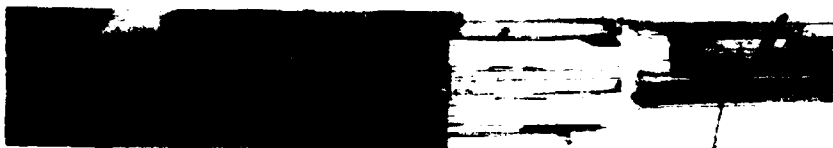


g) $\sigma = 83\%$
 $n = 143$

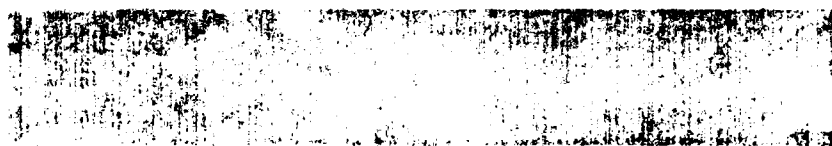


h) $\sigma = 90\% \sigma_{ult}$
 $n = 155$

Figure 4.14, continued.

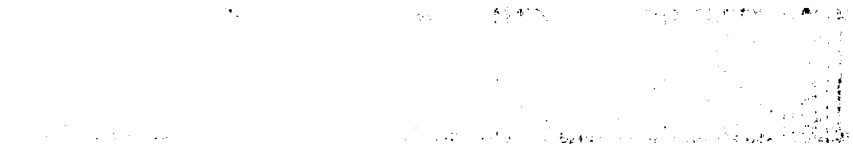


j) $\sigma = \sigma_{ult}$



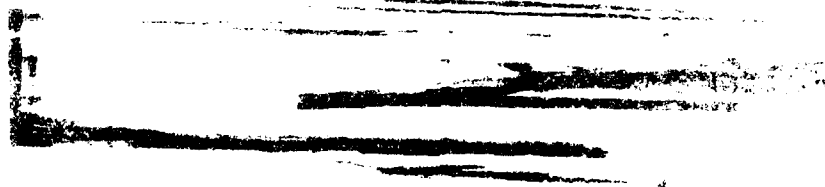
i) $\sigma = 96\% \sigma_{ult}$
 $n = 163$

Figure 4.14: continued.



- f) $\sigma = 57\% \sigma_{ult}$ $d = 16.2$
- g) $\sigma = 68\% \sigma_{ult}$ $d = 22.7$
- h) $\sigma = 80\% \sigma_{ult}$ $d = 28.2$
- i) $\sigma = 86\% \sigma_{ult}$ $d = 31.1$
- j) $\sigma = 91\% \sigma_{ult}$ $d = 34$

Figure 4.15: continued.



k) $\sigma = 96\% \sigma_{ult}$ 1) $\sigma = \sigma_{ult}$
 $d = 34.2$

Figure 4.15: continued.

- a) $\sigma = 0$
- b) $\sigma = 34\% \sigma_{ult}$
- c) $\sigma = 69\% \sigma_{ult}$
n = 3
- d) $\sigma = 81\% \sigma_{ult}$
n = 27

Figure 4.16: Series of X-radiographs showing damage progression in $(\pm 25/90)_s$ specimen: σ = applied load; n = number of transverse cracks.

AD-A122 859

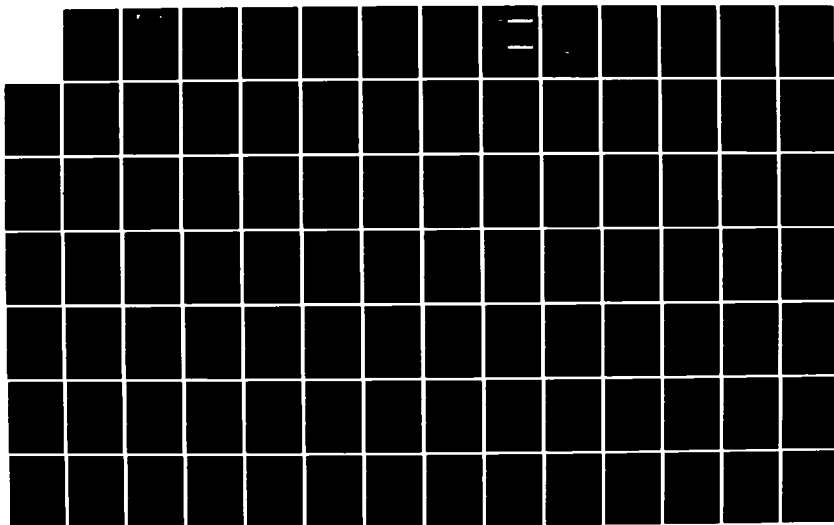
CUMULATIVE DAMAGE MODEL FOR ADVANCED COMPOSITE
MATERIALS(U) DYNA EAST CORP WYNNWOOD PA
P C CHOU ET AL. SEP 82 AFWAL-RR-82-4083
F33655-80-C-5039

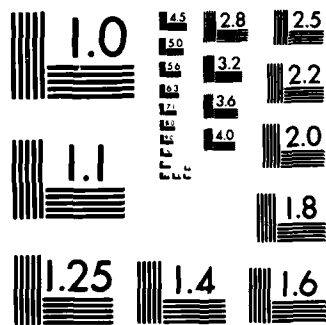
2/3

UNCLASSIFIED

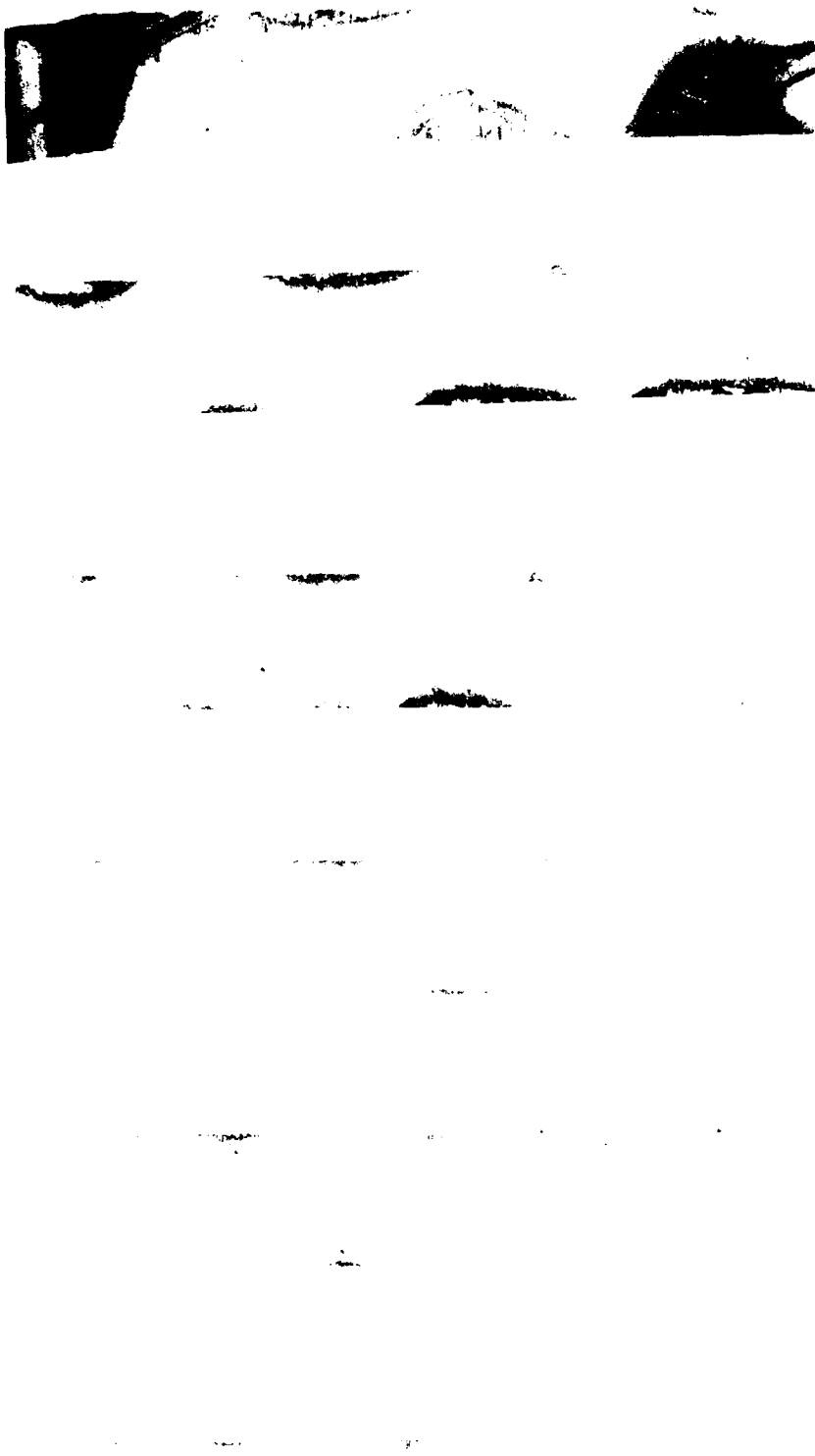
F/G 11/4

NL





MICROCOPY RESOLUTION TEST CHART
NATIONAL BUREAU OF STANDARDS-1963-A



- e) $\sigma = 85\% \sigma_{ult}$ $n = 37$ f) $\sigma = 88\% \sigma_{ult}$ $n = 60$ g) $\sigma = 91\% \sigma_{ult}$ $n = 72$ h) $\sigma = 95\% \sigma_{ult}$ $n = 98$ i) $\sigma = 99\% \sigma_{ult}$ $n = 127$ j) $\sigma = c_{ult}$

Figure 4.16, continued.

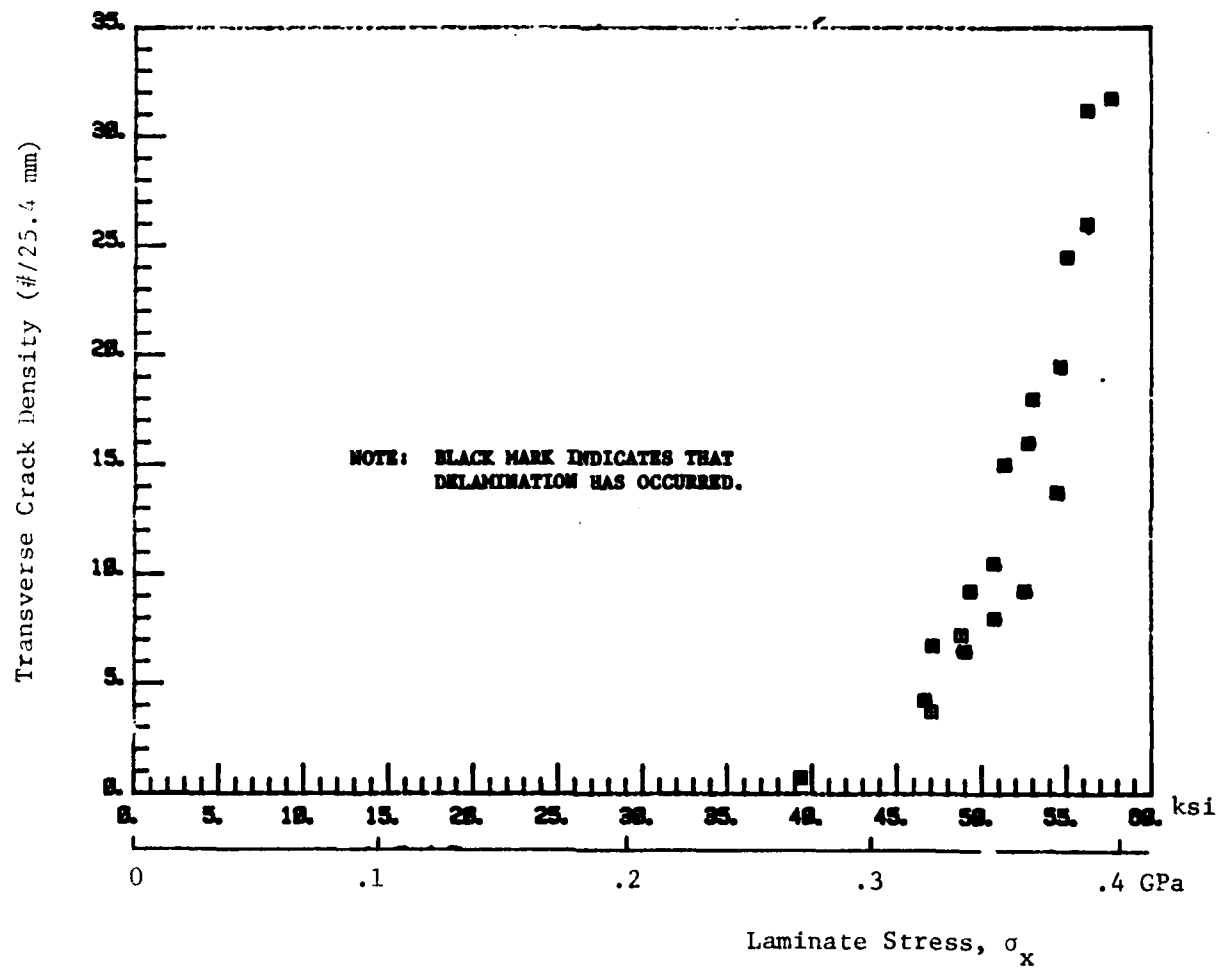


Figure 4.17: Load-Damage Relation for $(\pm 25/90)_s$ Laminate.

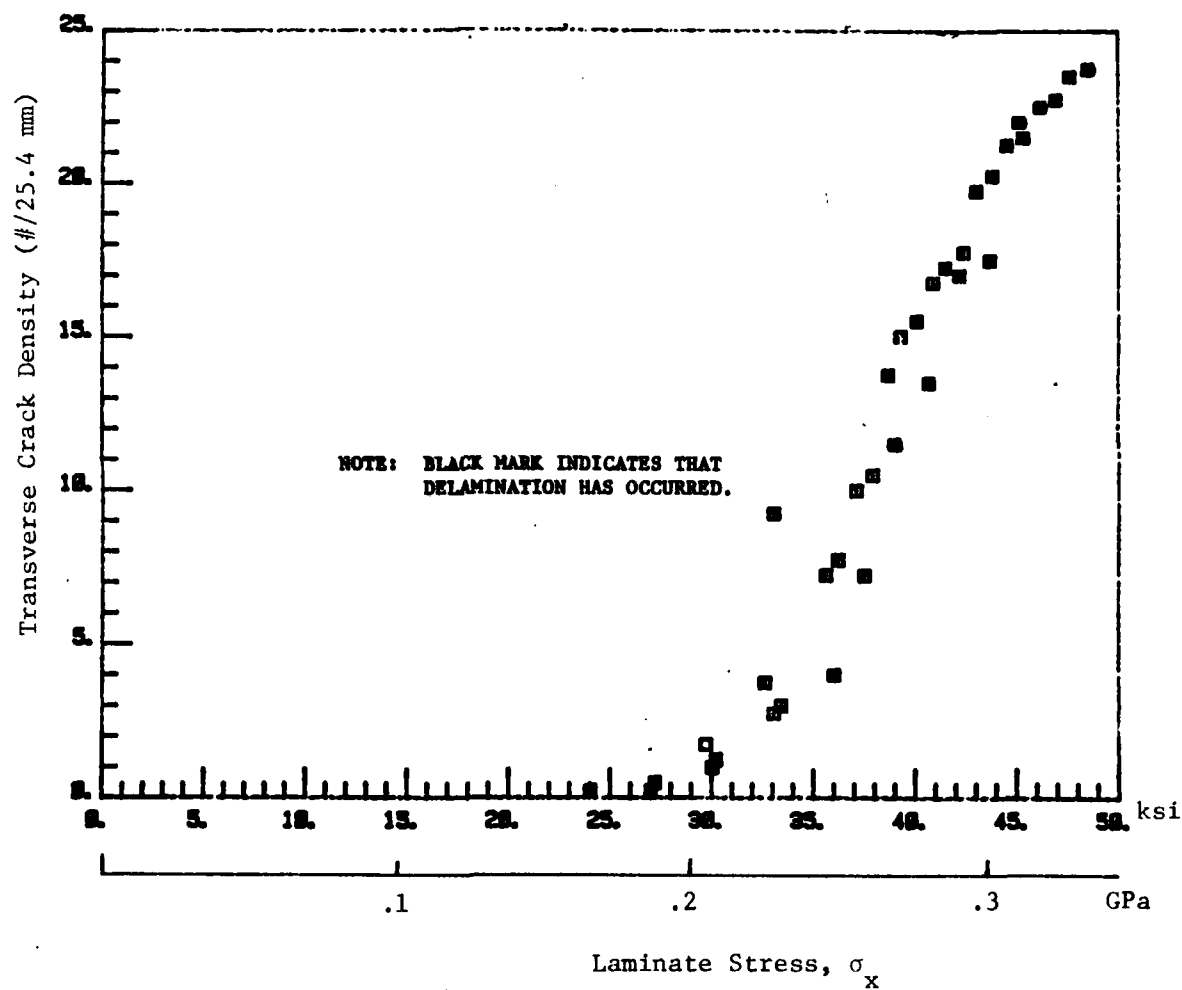


Figure 4.18: Load-Damage Relation for $(\pm 25/90_2)_s$ Laminate.

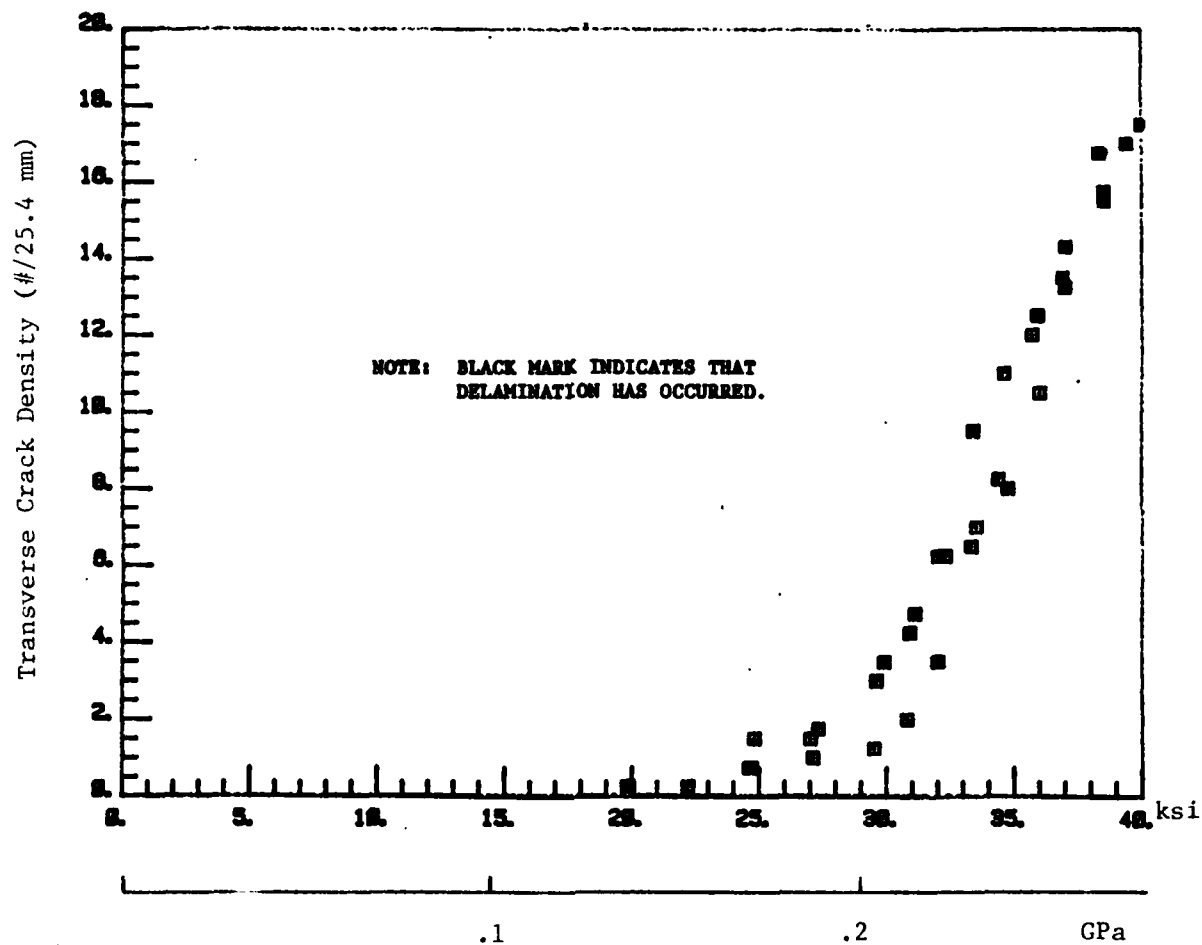


Figure 4.19: Load-Damage Relation for $(\pm 25/90)_3$ s Laminate.

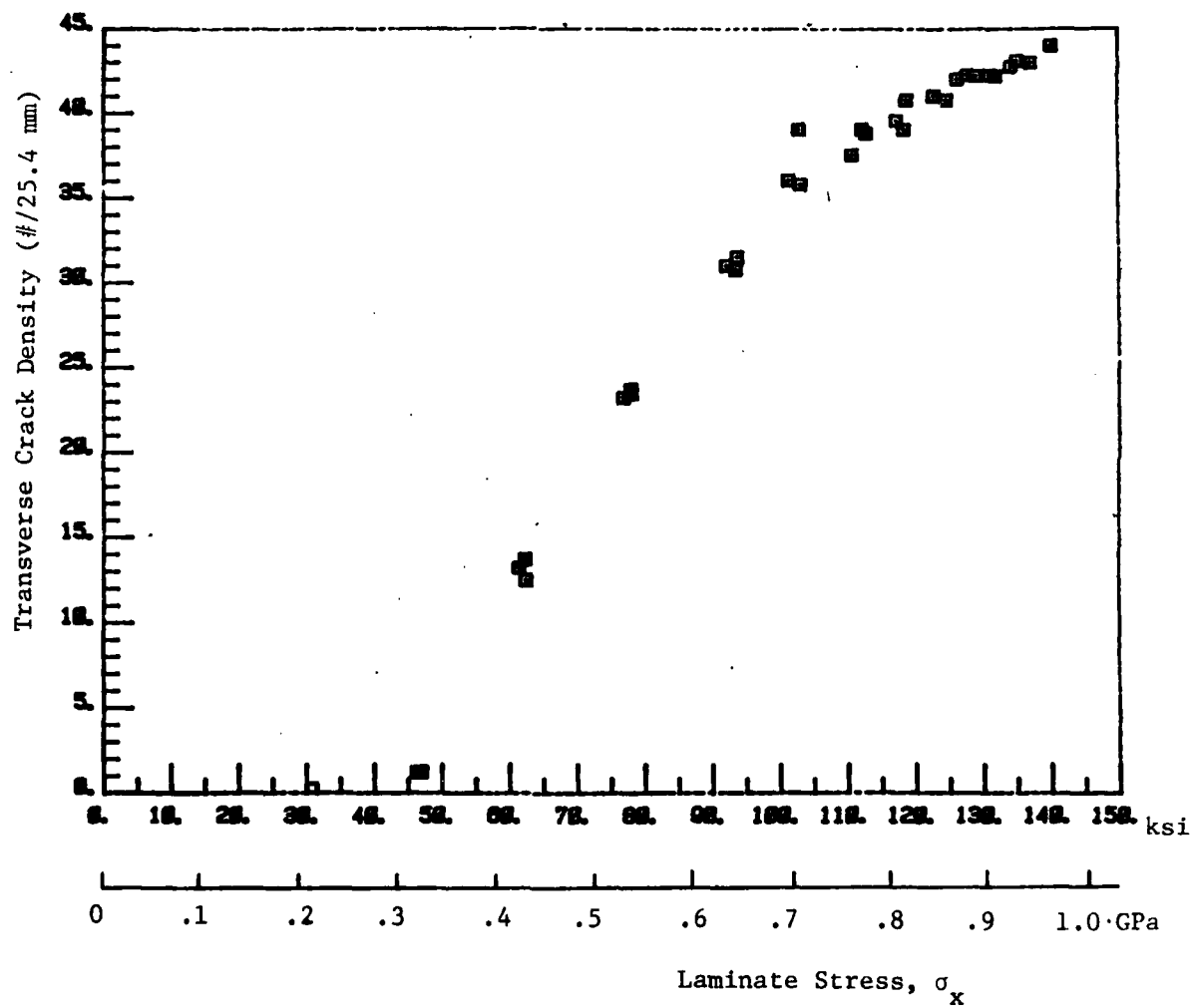


Figure 4.20: Load-Damage Relation for $(0_2/90_2)_s$ Laminate.

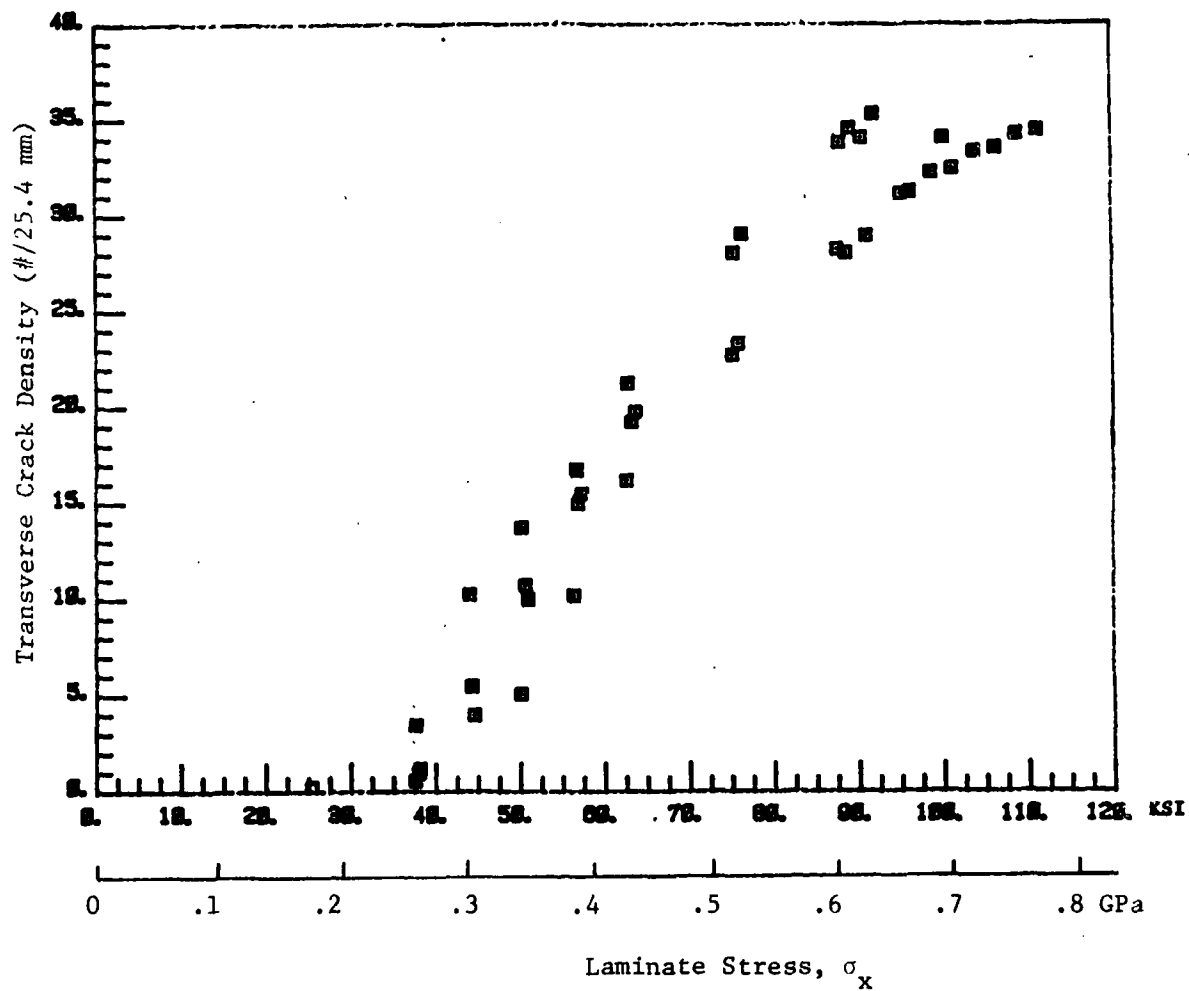
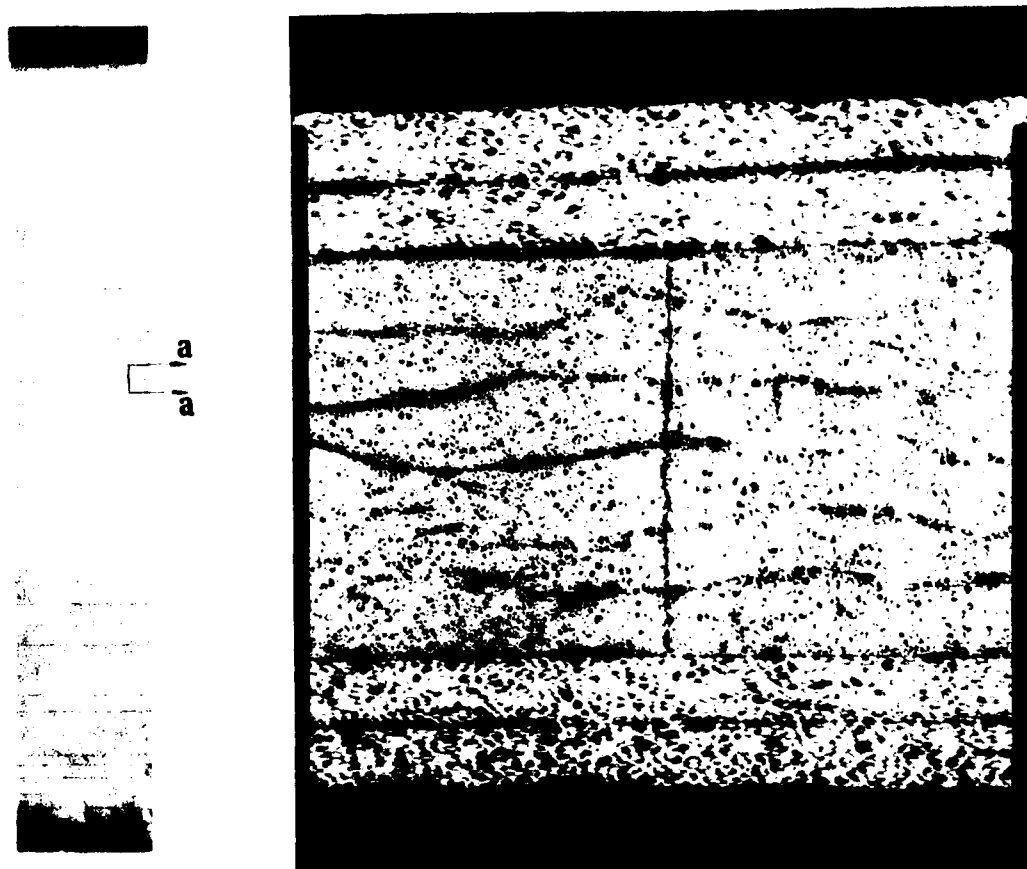


Figure 4.21: Load-Damage Relation for $(0_2/90_3)_s$ Laminate.



Section a-a ; 50x

a

b

Figure 4.22: a) X-radiograph of damage in a $[+25/90_3]_s$ specimen
 b) Photomicrograph of damage region showing typical transverse crack

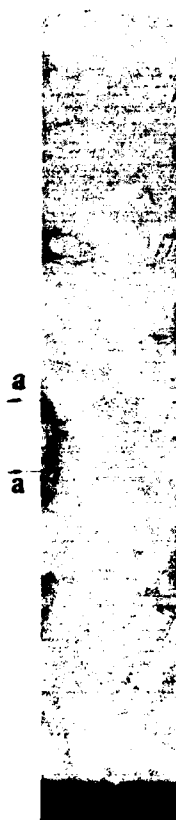
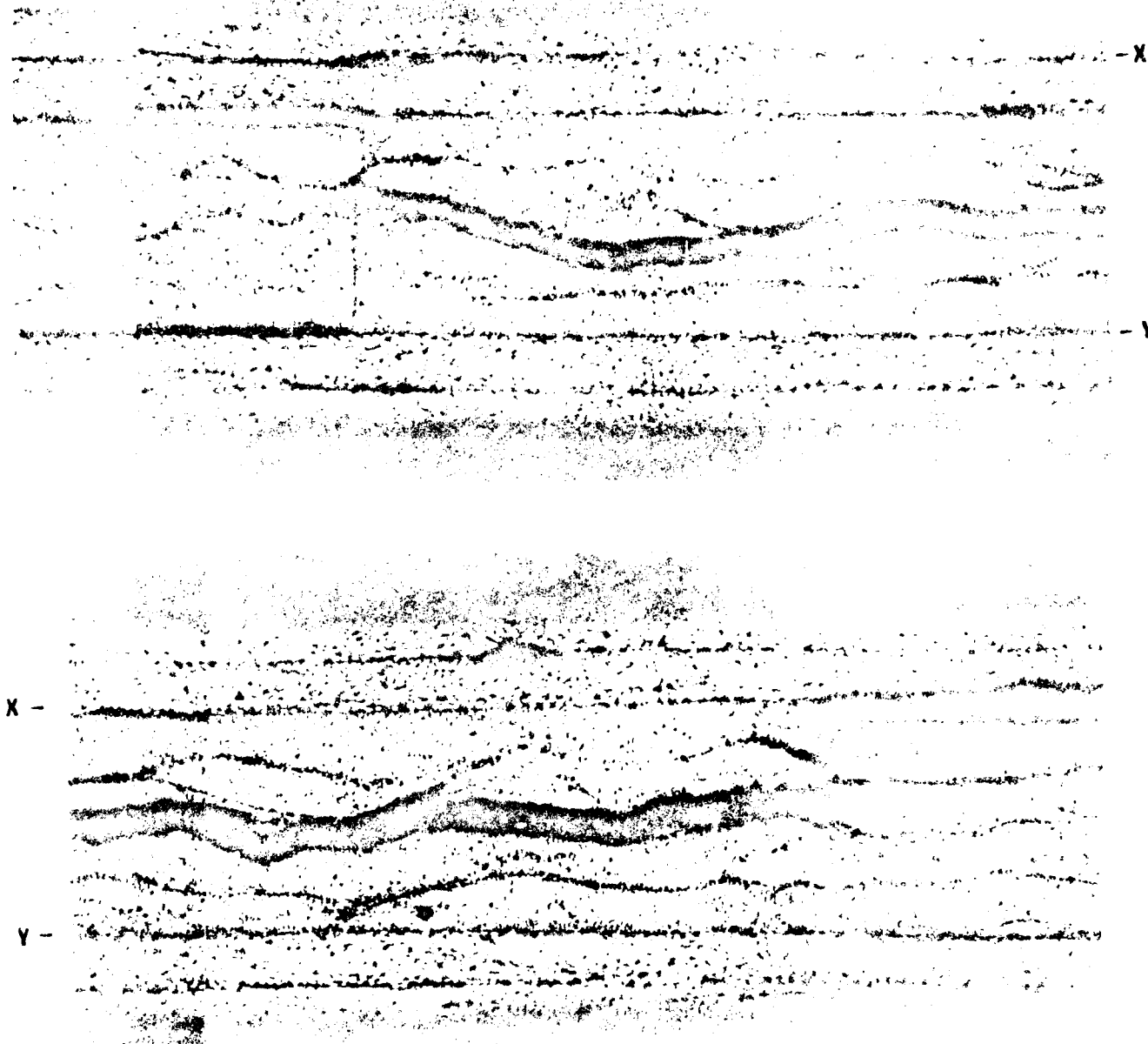


Figure 4.22(a): a) X-radiograph of damage in a $[+25/90_2]_s$ specimen



Section a a; 50x

Figure 4.22 (a): continued.

b) Photomicrograph of damage region

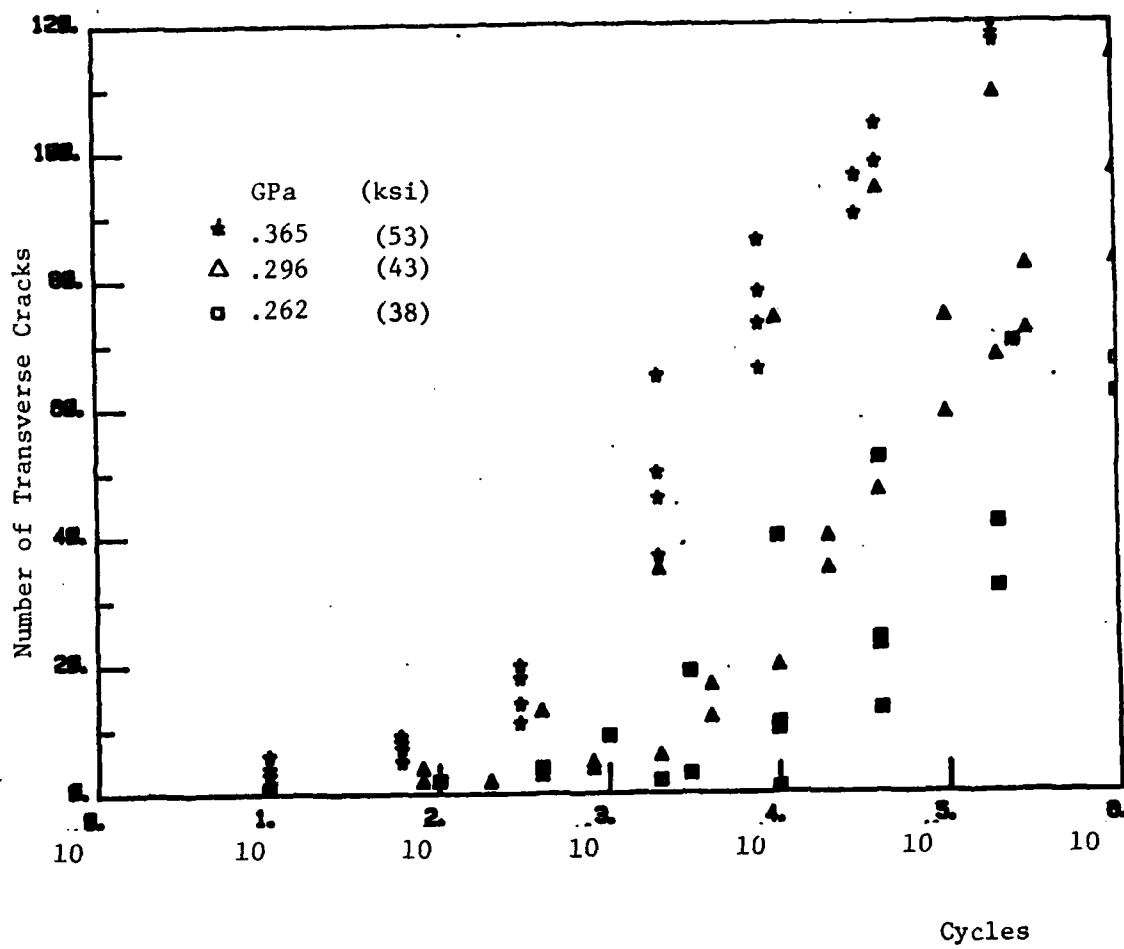


Figure 4.23: Cycles vs. Number of Transverse Cracks for $(0_2/90_2)_s$.

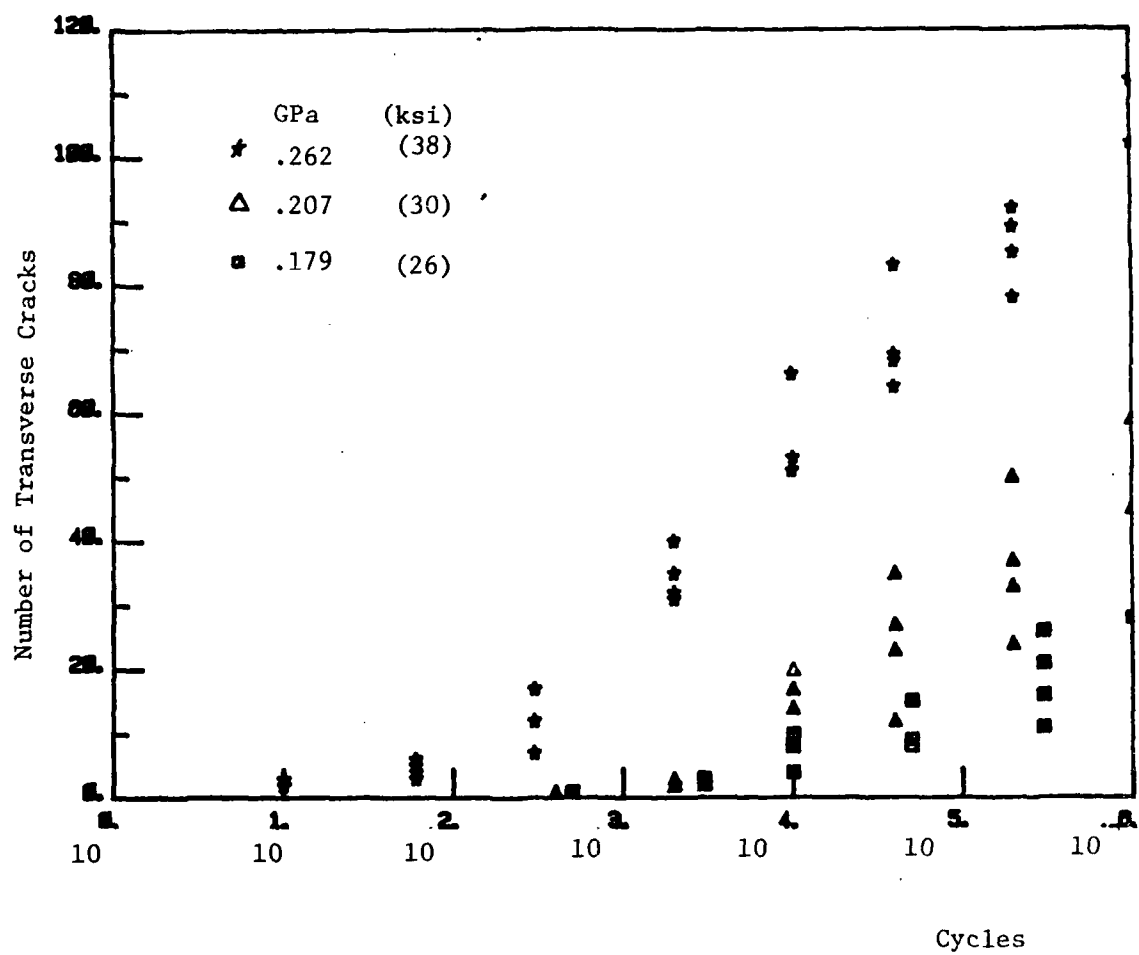


Figure 4.24: Cycles vs. Number of Transverse Cracks for $(0_2/90_3)_s$.

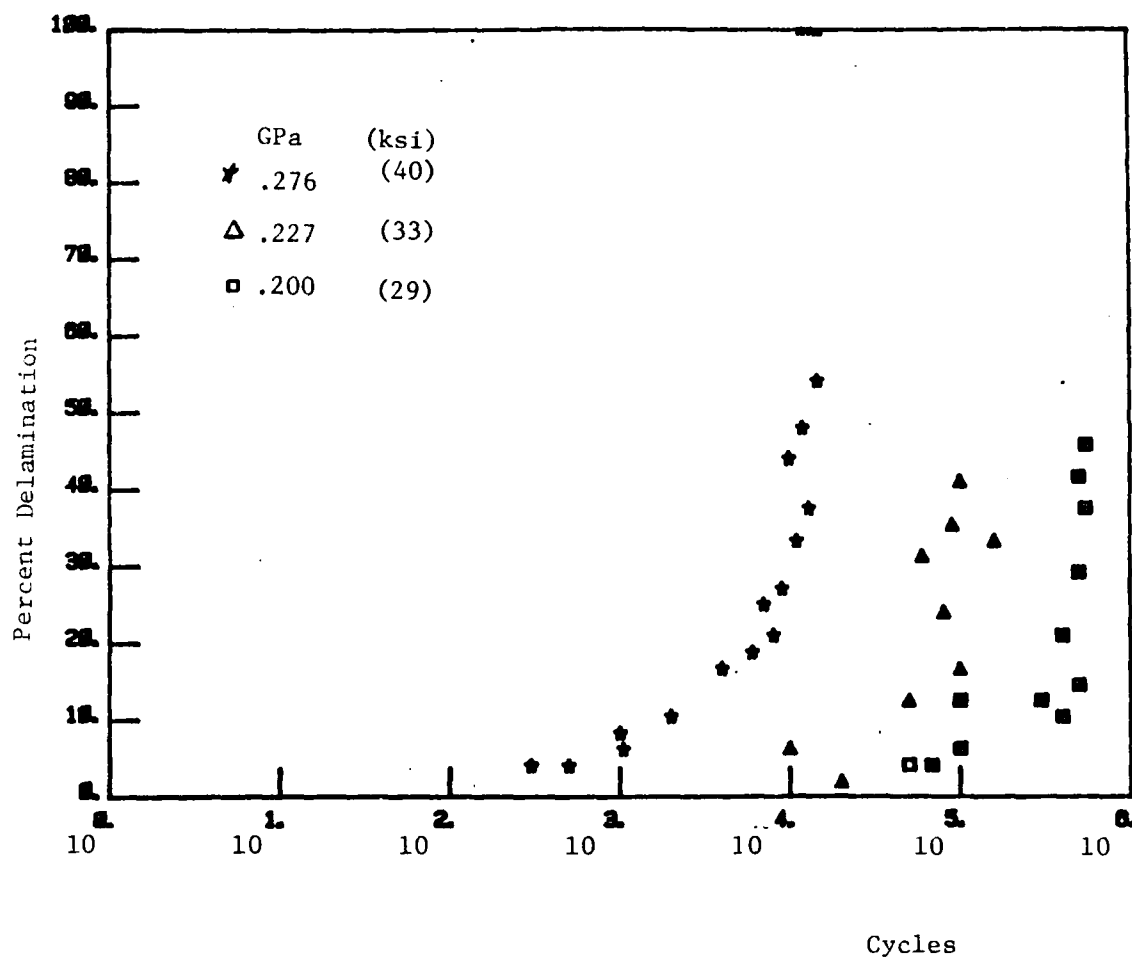


Figure 4.25: Cycles vs. Percent Delamination for ($\pm 25/90$).

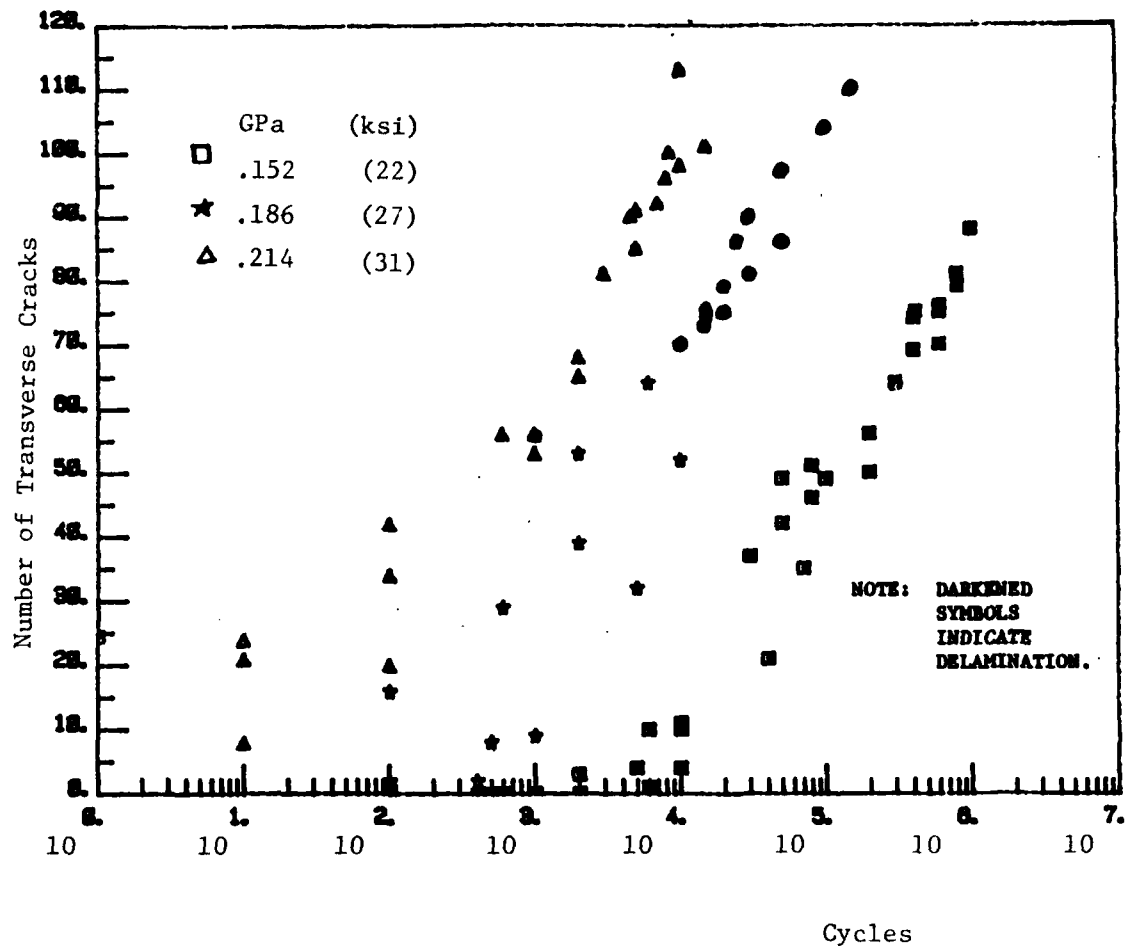


Figure 4.26(a): Cycles vs. Number of Transverse Cracks for $(\pm 25/90)_s$.

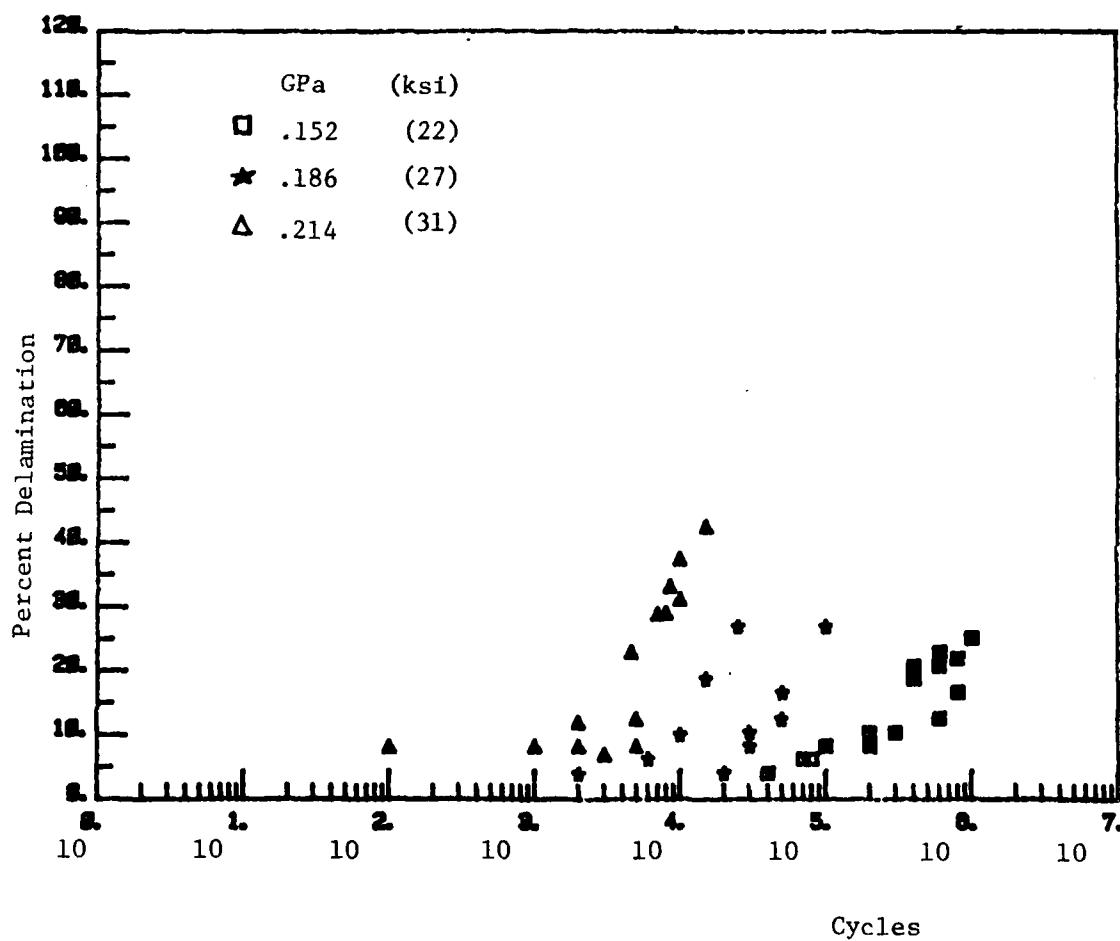


Figure 4.26(b): Cycles vs. Percent Delamination for $(\pm 25/90_2)_s$.

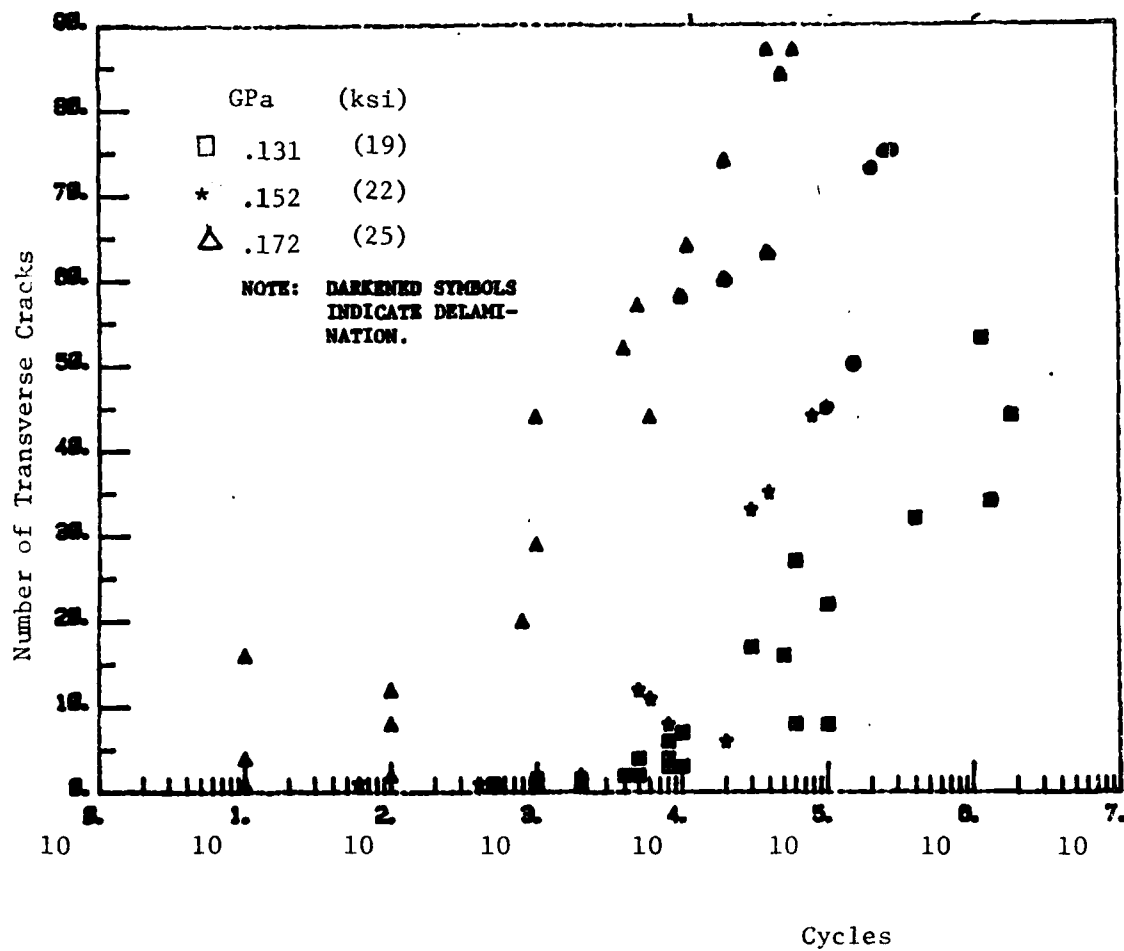


Figure 4.27(a): Cycles vs. Number of Transverse Cracks for $(\pm 25/90)_3$.

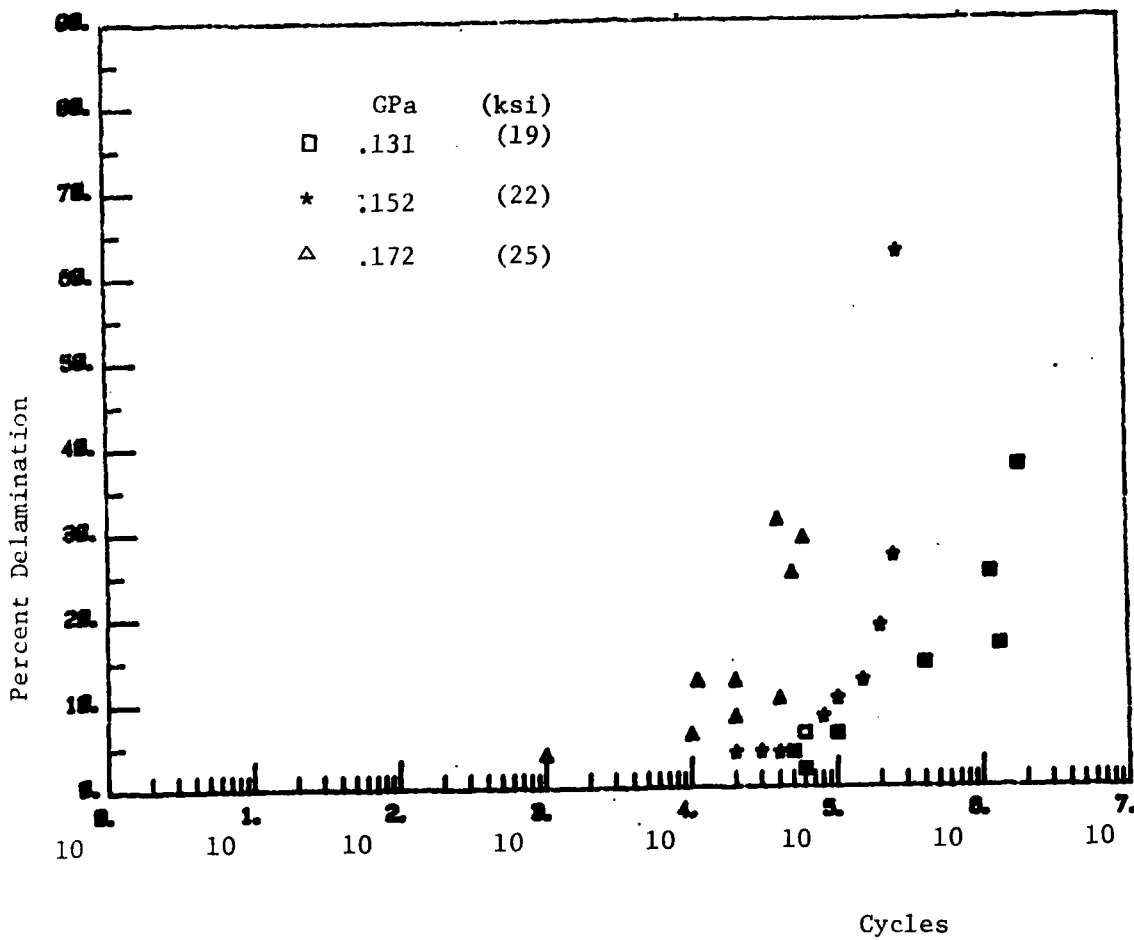


Figure 4.27(b): Cycles vs. Percent Delamination for $(\pm 25/90)_3$.

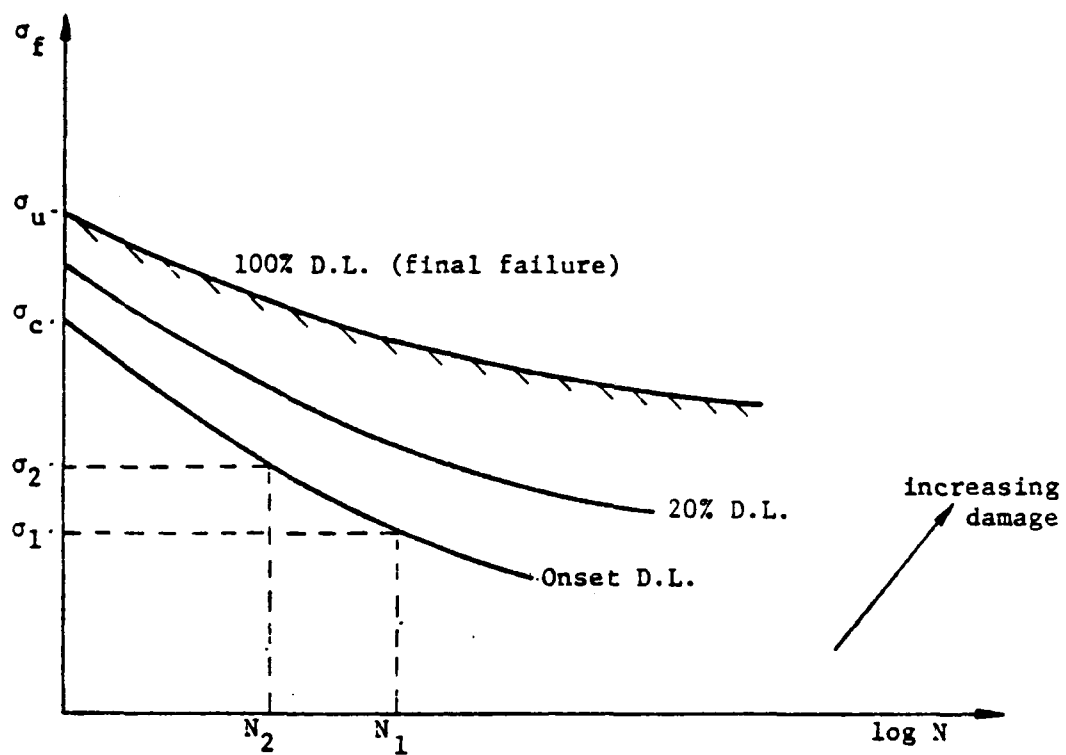


Figure 4-28 Schematics for the Concept of Constant Damage Curves

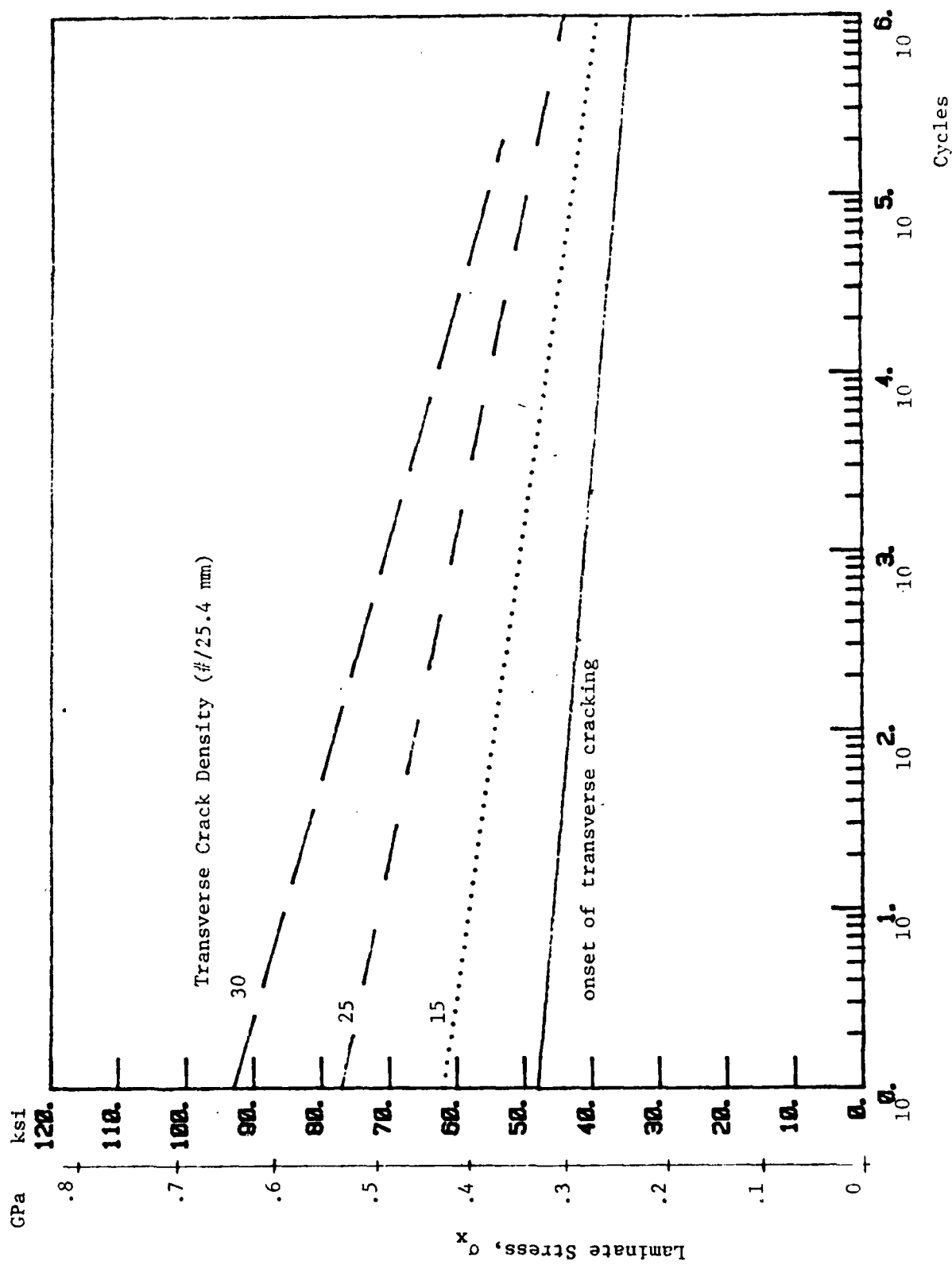


Figure 4.29: Constant Damage Curves for $(O_2/90)_2$ s.

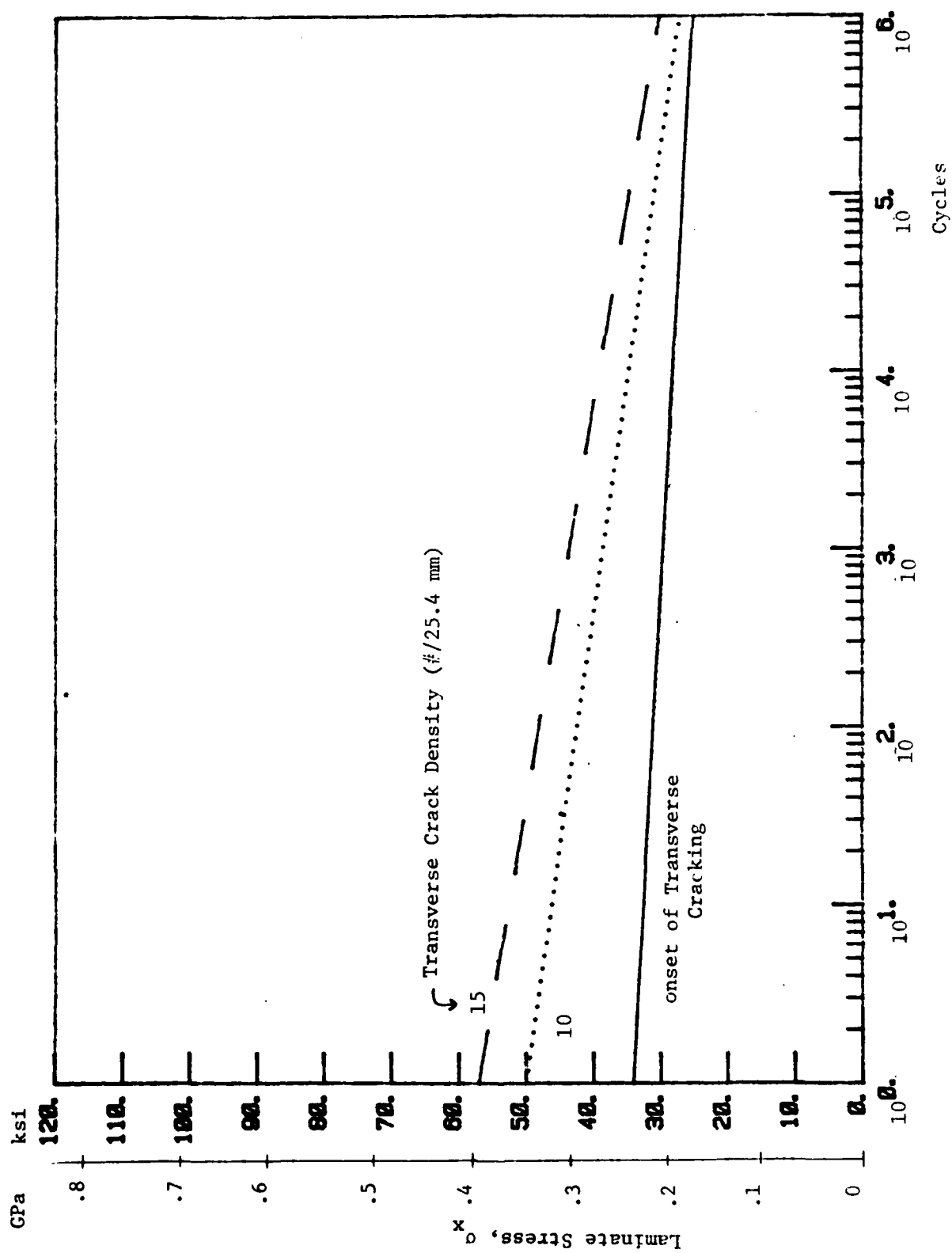


Figure 4.30: Constant Damage Curves for $(0/90)_3s$.

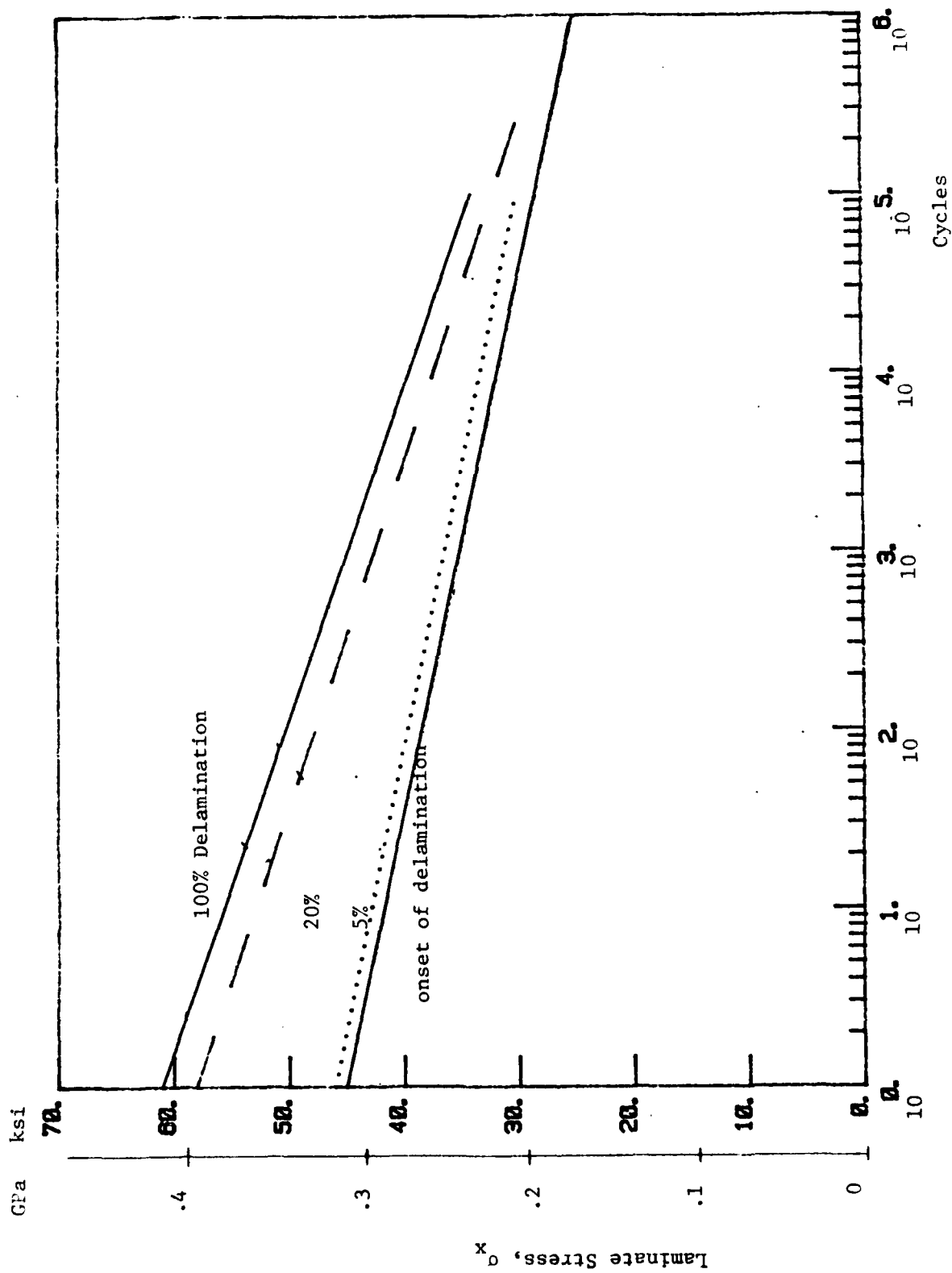


Figure 4.31: Constant Damage Curves for $(\pm 25/90)_s$.

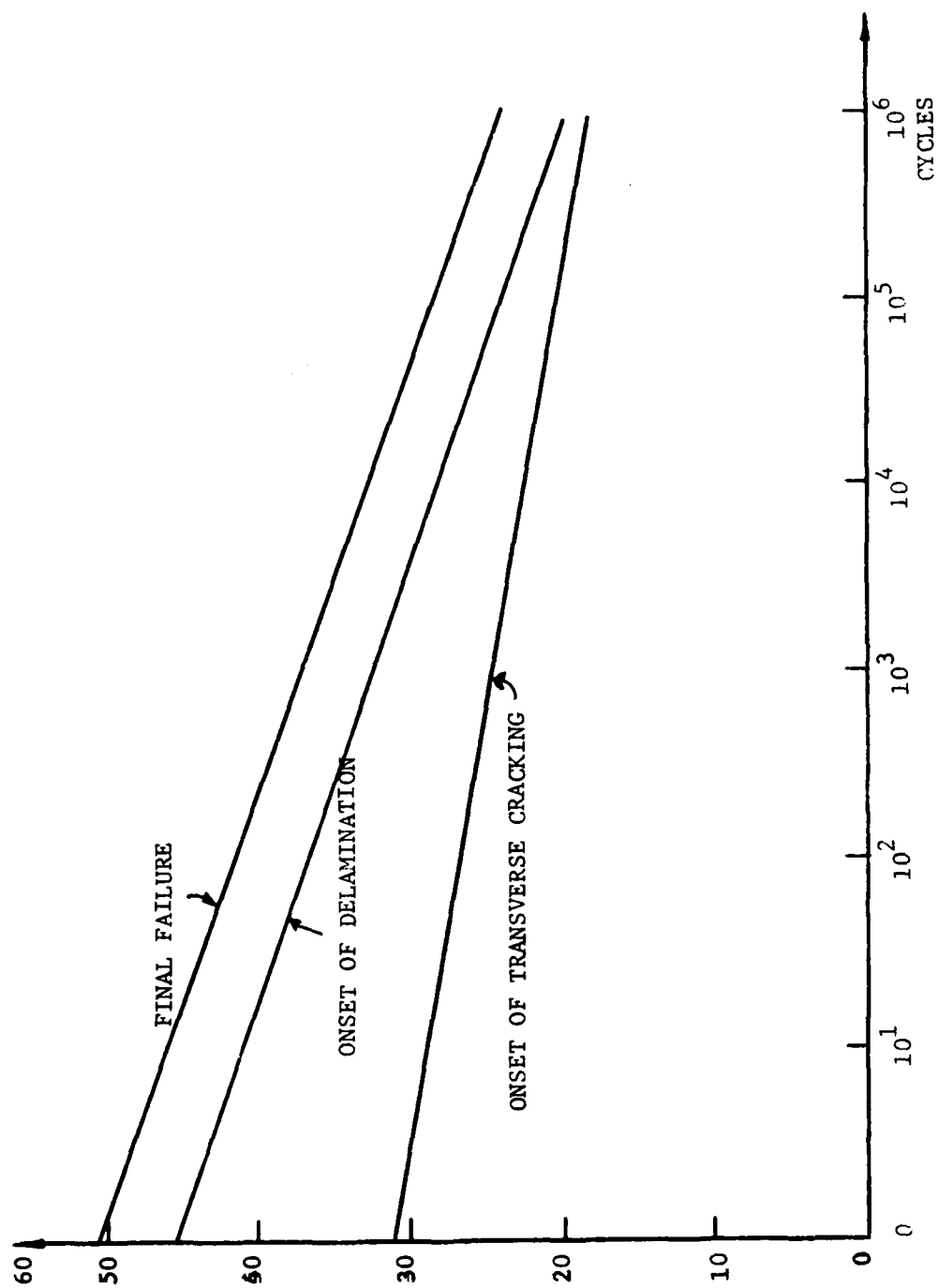


Figure 4.32: CONSTANT DAMAGE CURVES FOR (±25/90)₂s.

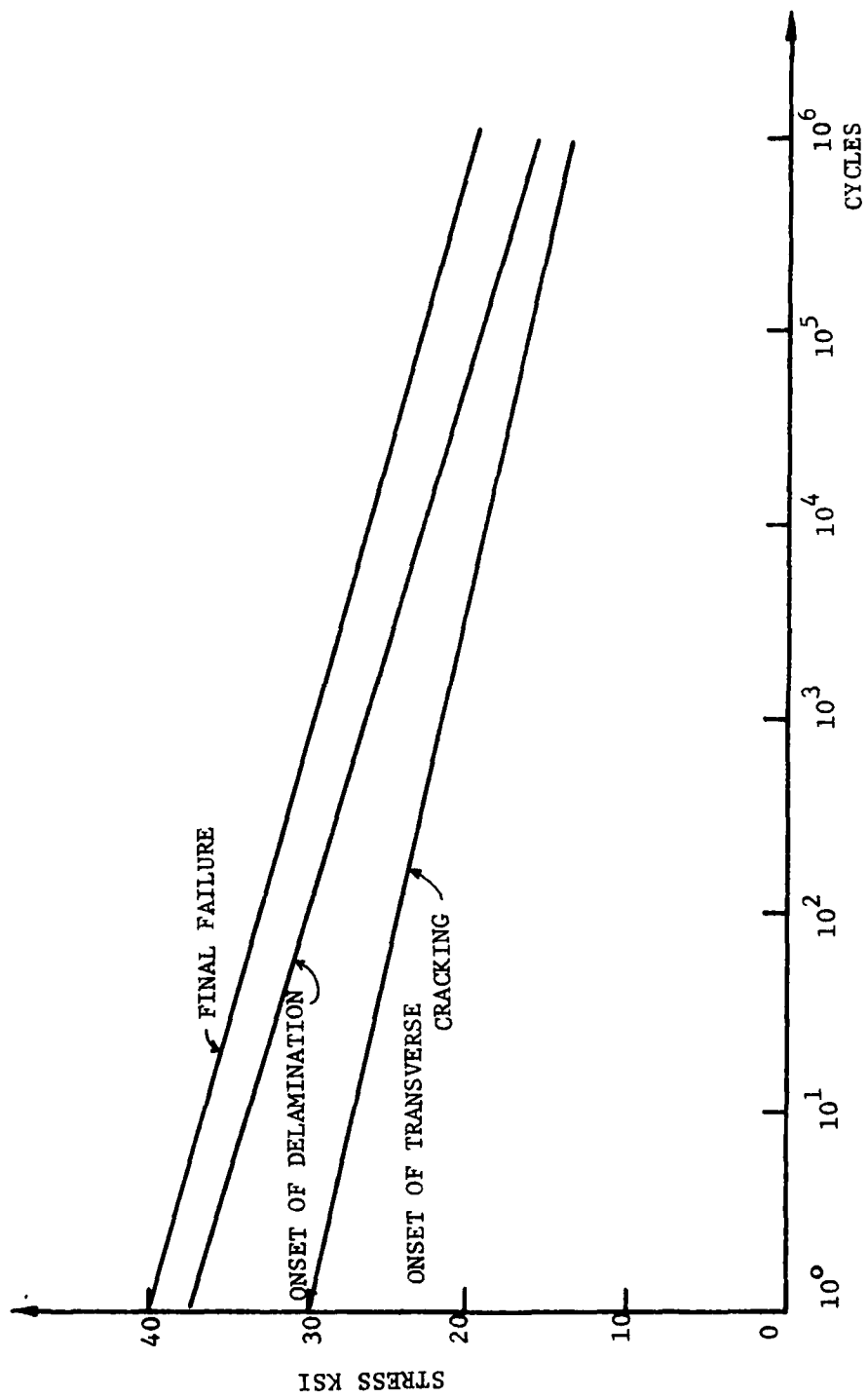
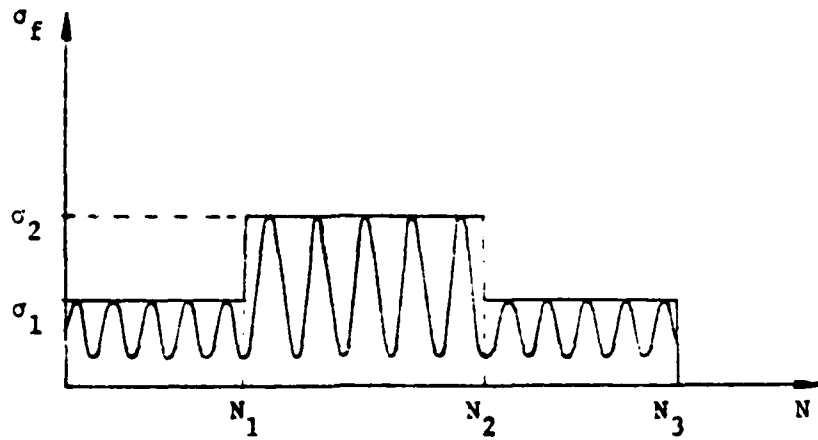
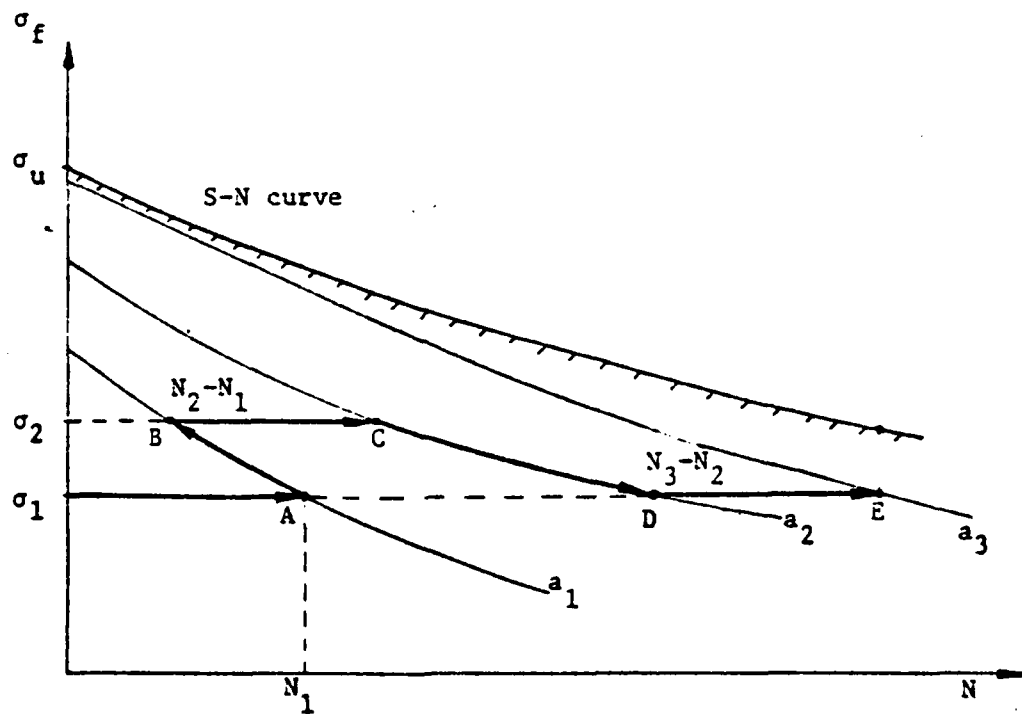


Figure 4-33: CONSTANT DAMAGE CURVES FOR $(\pm 25/90)_3$ s.



(a) Schematic of A Spectrum Loading History



(b) Damage Growth Path in the Load-Life Plane

Figure 4-34 Cumulative Damage Based on the Concept of Constant Damage State.

V. CORRELATION OF DATA WITH MODEL

A. Introduction

In Section III the approach to the development of a cumulative damage model for transverse cracking and free edge delamination was detailed. The model was seen to be an extension of existing models for the onset of damage under static loading and to have as its basis the concept of the energy release rate as a fracture criterion. In Section IV, details of the experimental program were given. It was seen that the laminates used in this study exhibited only the transverse cracking and delamination modes of damage before final failure, and that the damage sequence was the same under fatigue loading as under static loading. In this section, the experimental results will be correlated with the cumulative damage model concept.

B. Static Fracture Model

In this report, the only sub-laminate cracks investigated are the 90°-cracking and the free-edge delamination. In order to set up a crack initiation and growth criterion for each of the two types of cracking, it is assumed that micro-flaws exist along the fiber-matrix interface, and also along the ply-to-ply interface. As previously discussed, these initial flaws are described by an assumed distribution $f(a_c)$ which is then regarded as a known macroscopic material property. The Griffith criterion, when applied to predict the initiation of sub-laminate cracking, is:

$$G(a) \geq G_c \quad (5-1)$$

where a is the largest member of the distribution $f(a_c)$. For the specific modeling of transverse cracking and free edge delamination, $G(a)$ must be

appropriately calculated by the finite element crack-closure procedure as discussed in detail in Appendix B. The energy release rate is given by:

$$G(a) = t[C_e e^2 + C_{et} e \Delta T + C_t \Delta T^2] \quad (5-2)$$

or equivalently:

$$G(a) = t[\sqrt{C_e} e + \sqrt{C_t} \Delta T]^2 \quad (5-3)$$

where

e = far field strain,

t = ply thickness, taken as 0.0052",

ΔT = thermal load, taken as -225°F., and

C_e , C_t , and C_{et} are the mechanical, thermal, and mixed shape functions, respectively, determined from the finite element program.

These shape functions are shown in figure 5.1 for transverse cracking in the $(0_2/90_2)_s$ and $(0_2/90_3)_s$ laminates; in figure 5.2 for transverse cracking in the $(\pm 25/90_n)_s$ family of laminates; in figure 5.3 for mid-plane delamination of the $(\pm 25/90_n)_s$ family; and, in figure 5.4 for mixed-mode delamination in the $(\pm 25/90_n)_s$ family. Thus, the left hand side of equation 5.1 may be calculated for any value of a and for any value of the far field laminate strain.

As in any analytical model construction, idealization and simplification are made in order to reduce mathematical complexity. In the case of free-edge delamination, for instance, one may idealize the crack growth as a self-similar, or co-planar crack contained in an interface between two layers.

The growth is one-dimensional and the crack front is represented by a point. Similarly, transverse cracking may also be idealized as a self-similar crack along the matrix-fiber interface in the 90° -layer. In either case, the crack surface is assumed flat and smooth. In reality, of course, the crack surface is ragged and warped depending on the exact nature of the crack, even when viewed at the macroscopic level. But, the idealization may be tolerated in the overall modeling, if the material property (e. g., the critical energy release rate, G_c or K_c , is measured as a bulk quantity, and the size of the crack is large. This kind of idealization is, on one hand, a mathematical necessity; and on the other hand, it must be adjudicated by physical experiment.

The above consideration brings upon another conceptual question, which is how G_c or K_c should be physically determined. Although transverse cracks and edge delamination may all be regarded as matrix-dominant cracks, their individual resistance against crack growth when measured macroscopically could differ considerably. Consider, for example, the two different crack actions in a unidirectional laminate as shown in figure 5.5. Case (a) illustrates a mode-I delamination action between $0^\circ/0^\circ$ layers, and case (b) depicts a mode-I crack action between $90^\circ/90^\circ$ layers. The two crack actions may produce distinctive crack surfaces at the microscopic level, and thus give different values for G_c which is measured at the macroscopic level. This clearly raises the question of whether G_c can be regarded as a general material property for the class of the so-called matrix-dominated cracks. The difficulty comes, obviously, from the fact that G_c is measured without regard to the microscopic details of the cracking surfaces.

In a series of tests, conducted recently at Texas A & M University different values for the critical energy release rate, G_c were found for a unidirectional composite, depending on how the crack is propagated. In

particular, for the AS-3502 composite system, G_c measured under $0^\circ/0^\circ$ delamination action, case (a) figure 5.5 was about $140 \sim 160 \text{ J/m}^2$; while G_c , under $90^\circ/90^\circ$ cracking action, case (b), figure 5.5, was found to be $210 \sim 225 \text{ J/m}^2$. G_c for the neat resin (without reinforcement) has a value of only $60 \sim 70 \text{ J/m}^2$. The differences all stem from the individual characteristics of the crack surfaces. These results and results from other investigators are summarized in Table 5.1. Also shown are the values of G_c used in this study for each of the cracking modes. As can be seen, the values of G_c determined in this study are in general agreement with the results independently obtained by others for similar materials and crack geometries.

With the values of G_c known for each cracking mode, predictions of the laminate load for the onset of damage may be made using equation 5.1. Clearly a value of the initial flaw length must be selected for these calculations, and, for the onset of damage, this flaw length must correspond to the largest of the initial flaws in the material. Values for this largest flaw may be obtained by considering the fracture of the 90° material, for which $\sigma_u = 7 \text{ ksi}$, $E_x = 1.6 \text{ msi}$, and G_c (on a $0/0$ interface) $\approx 130 \text{ J/m}^2$ (0.9 lb/in). Calculations produce values of the initial flaw length a_c of $a_c = 1.75t$ for transverse cracking and $a_c = 2.0t$ for delamination, where t is the thickness of a ply. Calculating the energy release rate shape functions at these values, and using the appropriate values of G_c , allows the solution of equation 5.1 for the laminate strain (or stress) at the onset of damage under static load. Results are shown in Table 5-2 where both the calculated and the average experimental values of onset load are shown for each laminate used in this study. As can be seen, agreement is good in all cases with the possible exception of the $(\pm 25/90)_s$ laminate in which damage occurs experi-

mentally at a load 25% below that predicted.

In previous sections, the mechanics of the appearance of the first transverse cracks have been discussed in detail and the concept of the method of extending the damage initiation model to a model for multiple transverse cracking discussed. In the following, details of the multiple fracture model will be given. Emphasis will be placed on the application of the model to the $(0_2/90_2)_s$ and $(0_2/90_3)_s$ laminates which have transverse cracking as the only mode of damage preceding final failure.

Under static load, the first transverse crack per unit length forms at some critical load, σ_c , the second crack forms at a different cross-section under a higher load, and so forth. Assuming that each transverse crack forms as the result of an initial material defect (or crack), it may thus be postulated that a distribution of initial defects per unit length exists in the material. Thus, the first transverse crack will form at the cross-section with the largest initial crack, the second at the cross-section with the next largest initial crack, and so on. Under fatigue, the entire distribution may grow larger with increasing number of cycles.

Calculations have been performed with regards to this concept. Using the available energy release rate curves for the $(0_2/90_2)_s$ and $(0_2/90_3)_s$ laminates and using the value of $G_c = 1.3$, the values of a_c necessary for the initiation of transverse cracking at various laminate strain loads were calculated for each laminate. Results are shown in figure 5.6. In order to determine the initial flaw size distribution, the load-damage relations for these laminates were organized as histograms as shown in figures 5.7 and 5.8. For example, in figure 5.7 it is seen that, between stress levels of 67.5 and 72.5 ksi, 3 new cracks have formed per unit length. Using figure 5.6, it is thus determined that each unit length of this laminate contains 3 initial cracks of $a_c = 0.0032$ ".

This process is repeated for each stress level and each laminate. The values of a_c are then fit by a two-parameter Weibull distribution. Results are shown in figure 5.9. It was hoped that these distributions would be nearly identical, which would thus indicate that the distribution of flaws is common for the material. However, as can be seen, the distributions are different. It can be seen, however, that a nearly 3-2 relation is maintained. This 3-2 relation is not only the ratio of the 90°-plies in these laminates, it is also approximately the ratio of the transverse crack saturation density for these laminates.

For the convenience of the model development, we shall make the following assumptions. The length of the initial flaws (cracks), a_c , has a fixed distribution, independent of laminate thickness and volume. This distribution gives the percentage of flaw within each length interval, not the exact number. The cracks in any part of the specimen will have the same distribution, provided the volume considered is of sufficient size. This assumption ignores the extremely long cracks, which cannot exist in thin specimens. It also ignores the existence of the boundaries between the 90/90 plies. It is felt that these effects are minor.

For the present initial approach, we shall also assume that once a crack is propagated to full width, no crack will form within the shear-lag zone on both sides of it. This is just for mathematical simplicity at the present. This restriction will be relaxed later. In the actual case, cracks do not form within the shear-lag zone of previous cracks, although this occurs only when the load is near the maximum and the crack density is approaching the maximum.

For a given specimen, the initial flaws in the 90°-layer are distributed along its length. Assume a_c has a two-parameter Weibull distribution, with a

density function:

$$f(a_c) = \frac{\alpha}{\beta^\alpha} (a_c)^{\alpha-1} \exp \left[- \left(\frac{a_c}{\beta} \right)^\alpha \right] \quad (5-4)$$

and the corresponding distribution function:

$$F(a_c) = 1 - \exp \left[- \left(\frac{a_c}{\beta} \right)^\alpha \right] \quad (5-5)$$

Assume that 99% of all the initial flaws have a length greater than a_{co} , then:

$$F(a_{co}) = 0.01 \quad (5-6)$$

The deterministic relation between laminate strain and flaw length a_c as shown in figure 5.6 may be written as a relation $\sigma = \sigma(a_c)$, between the initial flaw length a_c and the laminate load stress σ which would cause a_c to propagate to full width of the 90° -layer. As a first order approximation, this relation can be represented by a linear equation:

$$\sigma = -C a_c + B \quad (5-7)$$

We shall use this linear equation for the subsequent development; a more exact equation may be used if necessary, although the final results may have to be obtained by numerical method, whereas for the linear case assumed here, closed form results can be obtained.

In equation 5.7, C and B are positive constants. In the σ vs. a_c coordinate, equation 5.7 is a straight line, whose intercept with the σ axis equal to B :

$$\sigma = B, \text{ when } a_c = 0$$

and its intercept with the a_c axis equal to $\frac{B}{C}$, or:

$$a_c = \frac{B}{C}, \text{ when } \sigma = 0$$

Since a_c is a random variable, σ must also be a random variable, whose distribution can be determined from equations 5.4 and 5.7. Inverting equation 5.7, we have:

$$a_c = -\frac{1}{C} (\sigma - B) \quad (5-8)$$

It can be shown that the density function of σ is related to that of a_c by:

$$f(\sigma) = f(a_c) \left| \frac{d a_c}{d \sigma} \right| \quad (5-9)$$

where a_c is treated as a function of σ through equation (5). Substituting equations 5.4 and 5.8 into 5.9, we obtain:

$$f(\sigma) = \frac{\alpha}{(\beta C)^\alpha} (B - \sigma)^{\alpha - 1} \exp \left[- \left(\frac{B - \sigma}{\beta C} \right)^\alpha \right] \quad (5-10)$$

Integrating, we have:

$$F(\sigma) = \exp \left[- \left(\frac{B - \sigma}{\beta C} \right)^\alpha \right] \quad (5-11)$$

Now let:

$$\sigma_o = -C a_{co} + B \quad (5-12)$$

that is, σ_0 is the load under which the initial crack with length a_{c0} propagates to full width. Since 99% of the initial flaws have lengths larger than a_{c0} , therefore under the load σ_0 , 99% of the initial flaws have propagated to full width, or:

$$F(\sigma_0) = 0.99 \quad (5-13)$$

Denoting the number of full width cracks per unit length formed at load σ by n_σ , and noting that at load σ_0 , n_σ , and n_m :

$$n_\sigma = n_m F(\sigma) \quad (5-14)$$

If n_m is known, then equation 5.14 provides a relationship between the load σ and the number of full width cracks per unit length at that σ .

Let us elaborate on the meaning of $F(\sigma)$. It may be considered as the percent of saturation of the fully developed cracks under the load σ . The load σ will cause cracks of a particular length a_c or larger to propagate to full width; there are $[1 - F(a_c)]$ percent of cracks that have a length of a_c or larger. After combining $f(a_c)$ and $a_c = a_c(\sigma)$, therefore, $F(\sigma)$ is the percent of fully developed cracks under σ .

Note that the saturation crack density, n_m , must be determined by experiment or by shear-lag analysis. In the present derivation, we only know that:

$$F(\sigma) = \frac{n}{n_m}$$

If the σ vs. a_c curve is represented by two straight line segments, as shown in figure 5.10 we can still obtain closed form solutions. The equations

for these two straight lines are of the form of equation 5.4, with the lower segment of constants B and C , and the upper segment of constants B' and C' . These two segments intersect at the point:

$$a_c = p, \quad \sigma = q$$

Now, the density function of σ is the same form as the single segment case, equation (7), with the modification that B and C are without prime in the lower segment, and with prime in the upper segment.

Upon integration, we obtain:

$$\begin{aligned} F(\sigma) &= \int_0^{\sigma} f(\sigma) d\sigma \\ &= \exp \left[- \left(\frac{B - \sigma}{\beta C} \right)^{\alpha} \right], \quad \text{for } \sigma < q \end{aligned} \quad (5-15)$$

This is identical to the single segment case. For $\sigma > q$, we have:

$$\begin{aligned} F(\sigma) &= \int_0^q f(\sigma) d\sigma + \int_q^{\sigma} f(\sigma) d\sigma \\ &= \exp \left[- \left(\frac{B - q}{\beta C} \right)^{\alpha} \right] - \exp \left[- \left(\frac{B' - q}{\beta C'} \right)^{\alpha} \right] \quad (5-16) \\ &\quad + \exp \left[- \left(\frac{B' - \sigma}{\beta C'} \right)^{\alpha} \right], \quad \text{for } \sigma > q \end{aligned}$$

A two-parameter Weibull distribution with parameters $\alpha = 3.0$ and $\beta = 0.004$ inches is taken as the distribution of inherent flaws (a_c) in both the $(0_2/90_2)_s$ and $(0_2/90_3)_s$ laminates. A two-segment approximation

to the $\sigma - a_c$ relation calculated from the finite element code is also used. The distribution of σ (equations 5.15 and 5.16) have been calculated using the values:

$$\begin{array}{ll} B = 93 & B' = 200 \\ C = 7.5 \times 10^3 & C' = 45 \times 10^3 \\ q = 70 & n_m = 45 \end{array}$$

for the $(0_2/90_2)_s$ laminate and:

$$\begin{array}{ll} B = 68 & B' = 120 \\ C = 5.87 \times 10^3 & C' = 19.45 \times 10^3 \\ q = 46 & n_m = 37 \end{array}$$

for the $(0_2/90_3)_s$ laminate. Results are shown in figures 5.11 and 5.12 for each laminate. Note that the values of n_m here are those that have been determined experimentally. As discussed elsewhere, a shear-lag approach may also be employed for the determination of n_m . Referring to figure 5.13, a shear-lag zone corresponding to an approximate 90% reduction in peak shear stress (i. e., a value of normal stress in the 90° -layer of 90% of the far field stress) produces a shear lag zone of $x/b = 2.5$. This corresponds to a saturation crack density of 38 cracks per inch in the $(0_2/90_2)_s$ laminate. From figure 5.14, it is seen that a spacing of 2.5 produces a ratio of energy release rates of 65%; that is, the energy release rate for the second crack has values of 65% of that for the first crack. Since energy release rate is proportional to σ^2 , it is seen that only a 20% increase in the far field stress is required to form cracks with this spacing. The resulting

load-damage relation using the distribution of σ and $n_m = 38$ is shown in figure 5.15. Agreement between the predicted and experimental load-damage relations is good, regardless of the method of selection of n_m . However, we shall use the experimentally determined value in subsequent correlations.

C. Constant Amplitude Fatigue Model

In Section III, the basis for the constant amplitude fatigue model was shown to be the existence of damage growth functions F_{TC} and F_{DL} which map the damage-load curve onto the damage-cycle plane. A general form of a growth rate equation:

$$\frac{da}{dN} = \alpha \left(\frac{G}{G_c} \right)^p \quad (5-17)$$

and an alternate form for the case of transverse cracking:

$$\frac{dn}{dN} = \alpha \left(\frac{G}{G_c} \right)^p \quad (5-18)$$

were introduced. In this subsection, the experimental data will be incorporated into the model. Emphasis will be placed on the $(0_2/90_2)_s$, $(0_2/90_3)_s$ and $(\pm 25/90)_s$ laminates which exhibit unique damage modes until final failure.

(i) Transverse Cracking Model

As discussed in the section on experimental results, the transverse crack formation under constant load fatigue cycling is similar to that in the static case. Under a load smaller than the crack onset load, there is no crack formed after one cycle. After repeated fatigue cycling under this load, cracks start to appear and increase in number as the cycle increases.

Our experiments have not carried high enough cycles to reach crack saturation, but it is believed that the saturation density under fatigue is the same as under static load, both in number and in appearance.

In this section, we shall formulate a model to represent the crack formation under fatigue loading. Again, we assume there are initial flaws (cracks) of length a_c in the specimen. The distribution of a_c is determined from the static case. It has a two-parameter Weibull distribution given by equations 5.4 and 5.5.

A deterministic rule of crack growth per cycle of fatigue loading will be assumed. In general, this rule may contain many parameters:

$$\frac{da}{dN} = g(N, a, \bar{G}, \dots) \quad (5-19)$$

where,

$$\bar{G} = \frac{G}{G_c} \quad (5-20)$$

is the ratio of the energy release rate based on the current crack length, and the critical energy release rate. The reason for including the variable N , a , and \bar{G} in equation 5.19 has been discussed elsewhere.

For the present study, we shall assume a specific form for the crack propagation rule as follows,

$$\frac{da}{dN} = k \frac{a}{N} \quad (5-21)$$

where $k = k(\bar{G})$. This rule is based on some physical reasoning. The energy

release rate, or the stress intensity factor, increases as the crack length increases. Therefore, da/dN is proportional to a or G . Here we have included "a" explicitly, and included G implicitly in \bar{G} . Similarly, da/dN should be proportional inversely with N . In rules proposed by others, N may not appear explicitly, but it is implicitly included in ΔG , or ΔK terms.

In a given specimen, there are inherent initial cracks. These cracks will increase in length due to every cycle of fatigue loading according to equation 5.22. Consider a crack of original length a_c , after N cycles of fatigue, the crack length increased from a_c to a , which can be obtained by integrating equation 5.21 or:

$$\int_{a_c}^a \frac{da}{a} = \int_1^N k \frac{dN}{N} \quad (5-22)$$

which yields, after integration:

$$\ln a - \ln a_c = k \ln N \quad (5-23)$$

where $k(\bar{G})$ has been assumed to be constant. Now we shall define a value a^* , which is the crack length that under the load σ will propagate to the full width of the 90°-layer. When the load is very small, "a" could be almost equal to the full width and still cannot produce enough energy release rate to cause the crack to propagate to full width due to static fracture mechanics. In that case, the crack will grow according to the fatigue rule of equations 5.19 and 5.23 to the full width and the static fracture mechanics criterion is not needed.

Also, we define the fatigue cycle that causes a crack to grow to length a^* as N^* , or from equation 5.23:

$$\ln a_c = \ln a^* - k \ln N^* \quad (5-24)$$

or:

$$a_c = \frac{a^*}{(N^*)^k} \quad (5-25)$$

Now we shall treat a^* as a constant, a_c as a random variable. It follows that N^* is a random variable. The distribution of N^* can be related to that of a_c by:

$$f(N^*) = f(a_c) \left| \frac{d a_c}{d N^*} \right| \quad (5-26)$$

From equation 5.25, we have:

$$\frac{d a_c}{d N^*} = - \frac{a^* k}{(N^*)^k + 1} \quad (5-27)$$

Substituting 5.27 into 5.26, we obtain:

$$f(N^*) = \frac{k \alpha a^{*\alpha}}{\beta^\alpha} (N^*)^{-1 - k\alpha} \exp\left[-\left(\frac{a^*}{\beta}\right)^\alpha (N^*)^{-k\alpha}\right] \quad (5-28)$$

After integration, this yields:

$$F(N^*) = \exp\left[-\left(\frac{a^*}{\beta}\right)^\alpha (N^*)^{-k\alpha}\right] \quad (5-29)$$

The meaning of $F(N^*)$ is similar to that of $F(\sigma)$ in the static case. It is the percentage of saturation cracks at cycle N^* . If the saturation crack

density n_m is known, the crack density under cycle N^* is then:

$$n = n_m F(N^*) \quad (5-30)$$

The constant amplitude fatigue data for the $(0_2/90_2)_s$ and $(0_2/90_3)_s$ laminates has been used. The parameters α and β are again taken as 3 and 0.004, respectively. The value of a^* is determined for each loading from the static fracture criteria. In the case of the $(0_2/90_2)_s$ laminate, $a^* = .0104$ in. ($= 2t$) for $\sigma_f = 38$ ksi and $\sigma_f = 43$ ksi, and $a^* = 0.008$ in. for $\sigma_f = 53$ ksi. For the $(0_2/90_3)_s$ laminate, $a^* = 0.0156$ in. ($= 3t$) for the two lowest stress levels and $a^* = 0.010$ for $\sigma = 38$ ksi. The values of n_m were taken as the static experimental values. The value of k was determined by a best fit procedure with the data for each case. As can be seen in figures 5.16 and 5.17, agreement between the data and predicted values is quite good, indicating that the growth law has captured the trend of the experiments. Also, note that the value of the parameter k seems to be nearly constant. At this time, however, the exact nature of this parameter and its relation to \bar{G} has not been determined.

As previously indicated, an alternate approach to forming a transverse cracking model is possible through the use of equation 5.18. This approach uses the transverse crack density (or the total number of cracks in a specified length) directly. The quantity $\frac{\Delta n}{\Delta N}$, the change in number of cracks per change in number of fatigue cycles, is found from the experimental data. This quantity is then used as an approximation of the damage growth rate, $\frac{dn}{dN}$, which in turn may be integrated to obtain the cycle-damage relation.

Data for the $(0_2/90_2)_s$ and $(0_2/90_3)_s$ laminates have been reduced and

are shown in figures 5.18 and 5.19 respectively. As can be seen the quantity $\ln \frac{\Delta n}{\Delta N}$ for each laminate at each stress level varies linearly with the log of fatigue cycles, suggesting that the general form of the growth rate equation is:

$$\frac{dn}{dN} = \alpha(\bar{G})^{\beta \ln N} \quad (5-31)$$

where α and β are empirical constants and \bar{G} is the ratio G_f/G_c .

From equation 5.31, the damage growth relation is:

$$n = \int_{N_0=1}^N \alpha \bar{G}^{\beta \ln N} dN \quad (5-32)$$

strictly speaking, \bar{G} is a complicated function; $\bar{G} = \bar{G}(G_c, a, \sigma_f)$. Thus, equation 5.32 is a complicated integral. For approximation, we shall take $\bar{G} = \text{constant}$. Then, equation 5.32 becomes:

$$n = \alpha \left(\frac{1}{1 + \beta \ln \bar{G}} \right) \bar{G}^{\beta \ln N} N \quad (5-33)$$

or, by taking logs,

$$\ln n = \ln \alpha - \ln(1 + \beta \ln \bar{G}) + (1 + \beta \ln \bar{G}) \ln N \quad (5-34)$$

which is a straight line in $\ln n - \ln N$ coordinates. Data are shown in these coordinates in figures 5.20 and 5.21. Also shown are linear regression fits to the data. As can be seen, the data at all load levels seem to follow this linear relation, although the experimental values at large fatigue

cycles tend to flatten out.

The constants obtained from a linear regression fit of the $\frac{\Delta n}{\Delta N}$ data may be used for the determination of the parameters α and β in equation 5.31. These constants are shown in Table 5.3. A value of $\beta = -0.4325$ was determined for all load levels for the $(0_2/90_2)_s$ laminate and a value $\beta = 1.46$ was determined for all load levels for the $(0_2/90_3)_s$ laminate. Using these values for β and values of α obtained directly from Table 5.3, equation 5.33 is plotted against the experimental data in figures 5.22 and 5.23. Again, agreement is good.

(2) Free Edge Delamination Model

The damage growth equation for free edge delamination after the initiation of macroscopic damage has been given as:

$$\int_{a^*}^a da = \int_{N_{DL}}^N \alpha \bar{G}^p dN \quad (5-35)$$

where $\bar{G} = \frac{G}{G_c}$, and where a^* represents a macroscopically definable delamination size corresponding to the damage initiation cycle N_{DL} . The problem of the growth of an edge flaw from size a_c to a^* will not be addressed here.

Equation 5.35 corresponds to a growth rate equation:

$$\frac{da}{dN} = \alpha \bar{G}^p. \quad (5-36)$$

Unlike the case of transverse cracking, the quantity $\frac{da}{dN}$ may be determined directly from the experimental data; i. e., the crack size "a" is directly observable. Data for the delamination of the $(\pm 25/90)_s$ laminate has been

reduced to $\frac{da}{dN}$ information. Results are shown in figure 5.24 in $\ln \frac{da}{dN}$ vs. $\ln N$ coordinates. Also shown are linear regression fits to the data at each fatigue load level. As can be seen, the damage rate per cycle appears weakly dependent on the number of cycles, although data for the two lower load levels may be said to be independent of N . Data for this laminate are shown in $\ln a$ vs. $\ln N$ coordinates in figure 5.25. Again, the data at each load level appears to follow a linear trend indicating that the damage growth rate rule can again be taken as:

$$\frac{da}{dN} = \alpha \bar{G}^{\beta} \ln N \quad (5-37)$$

Values of α and β can be determined using the linear regression constants given in Table 5.3. Values for N_{DL} are estimated from figure 5.25 as 60 cycles for $\sigma_f = \text{ksi}$, 4000 cycles for $\sigma = 33 \text{ ksi}$, and 10000 cycles for $\sigma = 29 \text{ ksi}$. The resultant damage-cycle relations obtained by performing the integration of equation 5.35 are also shown in figure 5.25. It is seen that the model provides a good description of the data.

(3) Mixed Damage Modes

The damage sequence in the $(\pm 25/90_2)_s$ and $(\pm 25/90_3)_s$ laminates has been seen to be transverse cracking followed by delamination, which in turn leads to the final failure. Analysis of these laminates is more complicated than that for the $(0_2/90_n)_s$ family and the $(\pm 23/90)_s$ laminate because of this interaction of damage modes. In particular, it is seen that the transverse crack density may no longer be bounded by a value n_m as the number of transverse cracks increases rapidly in a delaminated region. Alternatively, the onset and growth of delamination is certainly influenced by the

pre-existence of transverse cracks. Because of these complications, detailed study of data from these laminates will be performed in the subsequent phase of the project.

Following the insight into the damage growth gained from the $(0_2/90_n)_s$ and $(\pm 25/90)_s$ laminates, similar data reduction techniques have been applied on a preliminary basis to the data from these two laminates. Data in the form $\frac{dn}{dN}$ vs. N are shown in log-log coordinates in figure 5.26 for the $(\pm 25/90_2)_s$ laminate and in figure 5.27 for the $(\pm 25/90_3)_s$ laminate. Delamination growth rates are shown in similar coordinates in figures 5.28 and 5.29. It is seen these relations are similar to those from the single damage mode laminates. Transverse cracks versus cycle data for these two laminates are shown in log-log coordinates in figures 5.30 and 5.31, and delamination vs. cycle data are shown in figures 5.32 and 5.33. The linear nature of all these relations indicates that growth laws of the form used in the analysis of the single damage mode laminates are again applicable to these laminates, although details of the actual modeling will have to be modified.

D. Cumulative Damage

As shown in the previous subsection, the damage-cycle relation can be determined for any constant amplitude fatigue load using any appropriately determined damage growth rate per cycle law and some empirical constants. The ability to construct these relations was demonstrated in details using:

$$\frac{da}{dN} = k(\bar{G}) \frac{a}{N} \quad (5-38)$$

for transverse cracking, and:

$$\frac{da}{dN} = \alpha G^{-\beta} \ln N \quad (5-39)$$

for delamination. The extension of constant amplitude fatigue damage to cumulative damage through the concept of constant damage states was described in Section 3-C. Consider, for example, a laminate subjected to a fatigue load σ , for N_1 cycles followed by N_2 cycles at load σ_2 , and which experiences only transverse cracking under each load. Then, the cycle-damage relation, as given above, is:

$$n = n_m F(N^*) \quad (5-40)$$

Damage accumulates under each load in the same manner as under constant amplitude fatigue. Thus, after N_1 cycles at σ_1 , the damage is given by:

$$\begin{aligned} n_1 &= n_m F_1(N_1) \\ &= n_m \left[\exp - \left(\frac{a_1^*}{\beta} \right)^\alpha N_1 - k_1 \alpha \right] \end{aligned} \quad (5-41)$$

Thus, when the load is changed from σ_1 to σ_2 , the laminate has the damage state of n_1 . An equivalent number of cycles, N'_1 , to produce this damage state at σ_2 may be determined as:

$$N'_1 = \left[\exp - \frac{1}{k_2 \alpha} \ln \ln \left(\frac{n_m}{n_1} \right) \left(\frac{a_2^*}{\beta} \right)^{-\alpha} \right] \quad (5-42)$$

The total damage after N_2 cycles at σ_2 is thus:

$$\begin{aligned}
n_T &= n_m F_2 (N_2 + N'_1) \\
&= n_m \exp \left[- \left(\frac{a^*_2}{\beta} \right)^\alpha (N_2 + N'_1)^{-k_2 \alpha} \right] \quad (5-43)
\end{aligned}$$

This concept may easily be extended on a cycle by cycle basis to spectrum loadings. Thus, the constant damage curves which were constructed from the experimental data in figures 4.29 to 4.33 may not be constructed from the analytical model.

The results of a series of cumulative damage tests are compared to the predicted results. At this time, the experimentally constructed constant damage curves are used to form the predicted damage, as the exact forms of damage growth laws have not been determined. The cumulative damage tests which were performed on the $(0_2/90_2)_s$, $(0_2/90_3)_s$, and $(\pm 25/90)_s$ laminates are shown superimposed on the constant damage curves in figures 5.34 through 5.40. Averages of experimental data are shown in parentheses at critical points on graph. These results are summarized in figure 5.41 for transverse cracking and in figure 5.42 for delamination. As can be seen, the agreement between the predictions and the data is good in all cases. Thus, we conclude that the use of constant amplitude fatigue damage and the constant damage state concept is an appropriate method of modeling cumulative damage for these damage modes.

Table 5-1: SUMMARY OF TEST RESULTS FOR G_{Ic} AND $G_{(I,II)c}$

	<u>G_{Ic} (0/0)</u>	<u>$G_{(I,II)c}$ (0/0)</u>	<u>G_{Ic} (90/90)</u>
G. D. AS-3501-06	130 J/m ²	365 - 475*	-
Texas A & M AS-3501-02		230 - 475	210 - 245
Wang & Kishore T300/934	155	160 - 490	-
Wang & Crossman	140	-	225 - 230

* $G_{II}/G_{TOT} = 0.765$

VALUES USED IN THIS STUDY (AS-3501-06)

For transverse cracks;

$$G_{Ic}(90/90) = 230 \text{ J/m}^2 \text{ (1.3 lb/in)}$$

For mid-plane delamination;

$$G_{Ic}(90/90) = 230 \text{ J/m}^2 \text{ (1.3 lb/in)}$$

For mixed mode delamination (off mid-plane);

$$G_{(I,II)c} = 265 \text{ J/m}^2 \text{ (1.5 in/lb)}$$

Table 5-2: SOME RESULTS BASED ON THE FRACTURE MODELS

<u>Laminates</u>	<u>Onset Transverse Crack</u>	<u>Onset Delamination</u>
$[0_2/90_2]_s$	47 (48), ksi	--
$[0_2/90_3]_s$	34 (34)	--
$[\pm 25/90]_s$	61 (48)	60 (48)
$[\pm 25/90_2]_s$	26 (28)	45 (42)
$[\pm 25/90_3]_s$	22 (23)	40 (38)

*values in parentheses are averaged experimental results.

**predictions are based on: $G_c = 1.3 \text{ lb/in (230 J/m}^2\text{)}$

$\Delta T = -225^\circ\text{F.}$

$a_c = 1.75t$ for transverse cracking

$= 2.0t$ for delamination

Table 5-3: DAMAGE RATE EQUATION CONSTANTS
DETERMINED BY LINEAR REGRESSION

$$Y = A + BX$$

where: $Y = \ln \frac{da}{dN}$

$A = \ln \alpha$

$X = \ln N$

$B = \beta \ln \bar{G}$

LAMINATE	MAXIMUM FATIGUE LOAD σ_f , ksi	A	B
$(0_2/90_2)_s$	38	-.885	-.675
	43	-.044	-.73
	53	.842	-.755
$(0_2/90_3)_s$	26	.255	-.852
	30	-1.216	-.661
	38	.437	-.767
$(\pm 25/90)_s$	29	-8.161	-.125
	33	-6.971	-.114
	40	-2.62	-.356

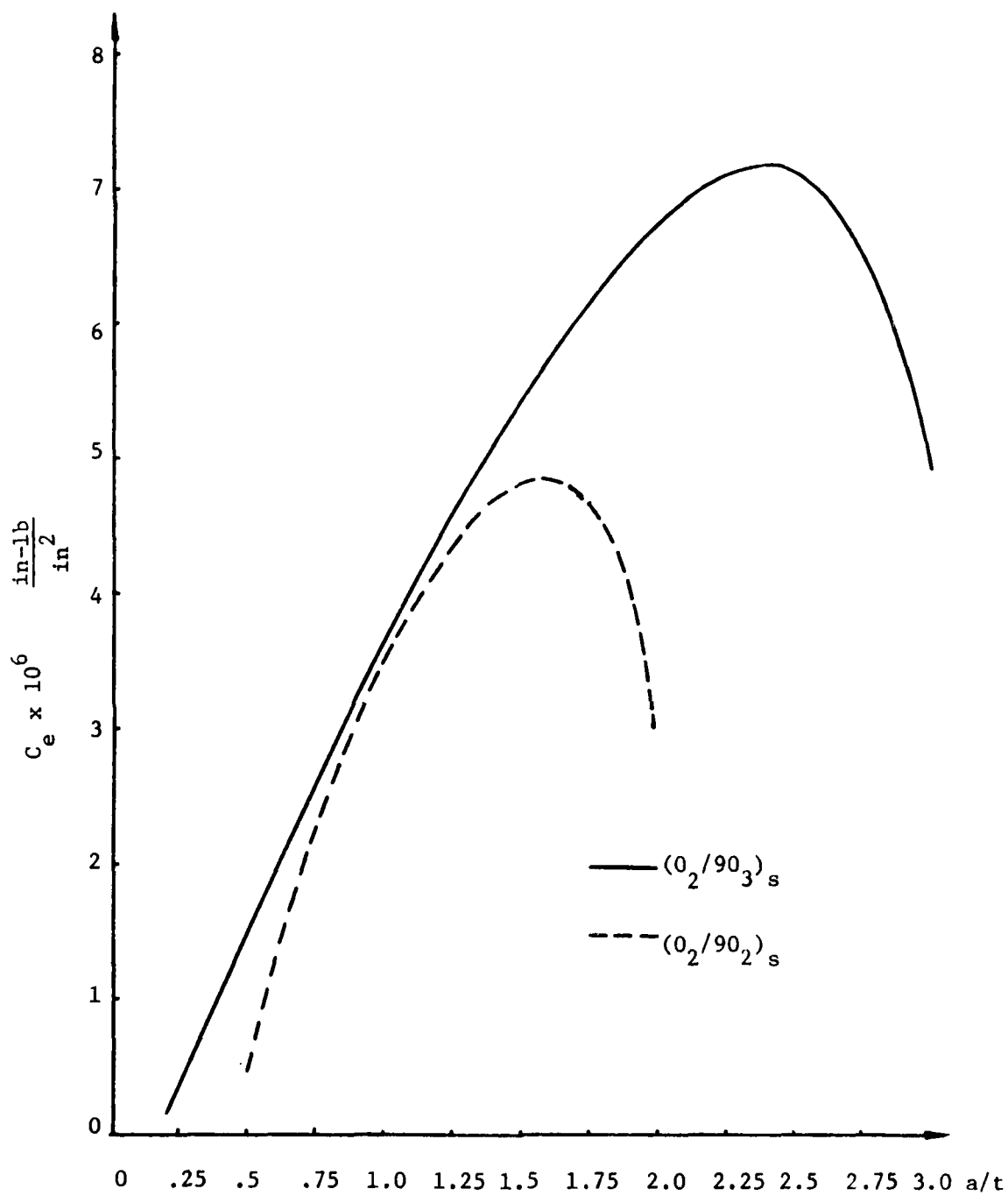


Figure 5-1a: MECHANICAL LOAD SHAPE FUNCTIONS VS. RELATIVE CRACK LENGTH FOR $(0_2/90_2)_s$ AND $(0_2/90_3)_s$ LAMINATES.

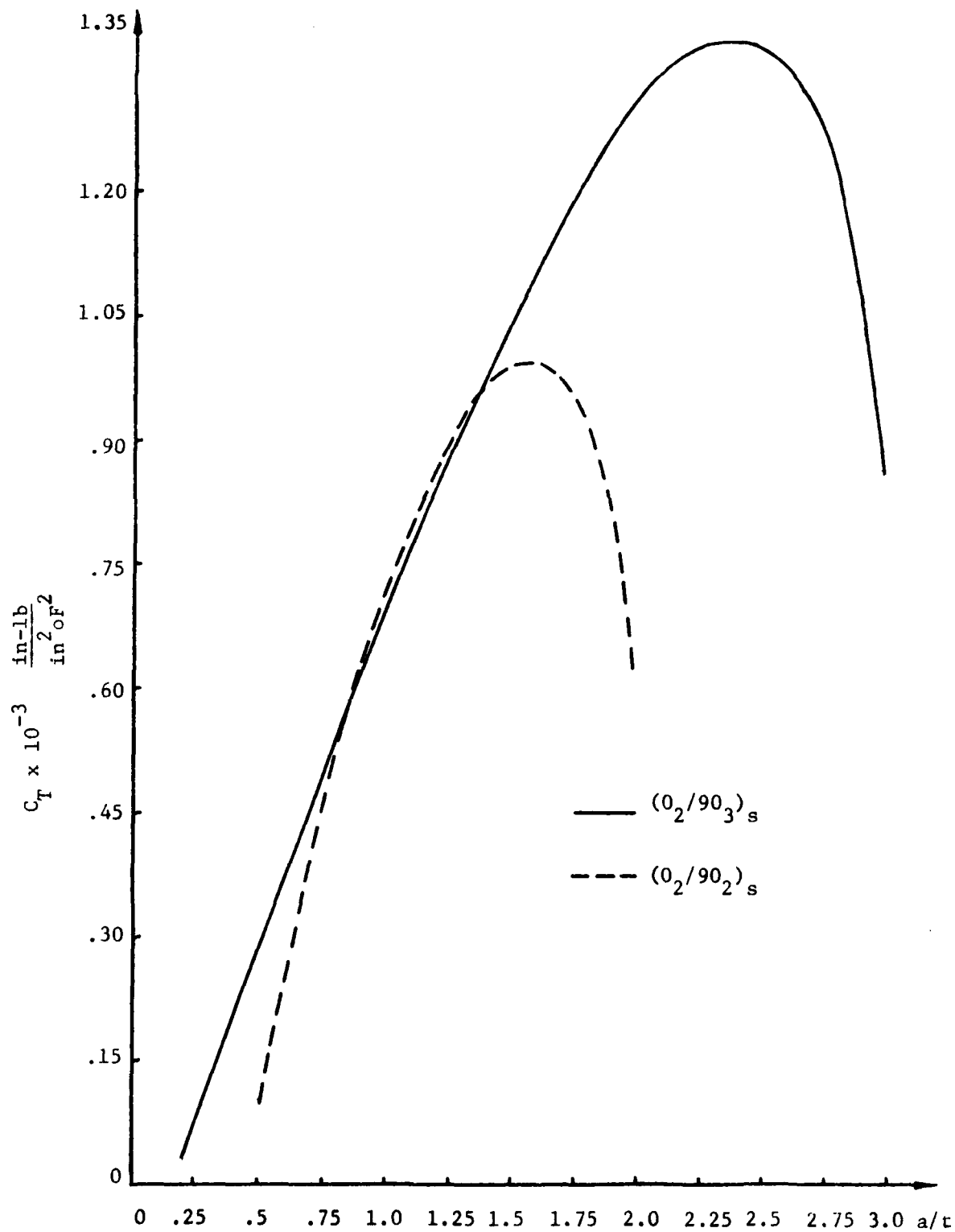


Figure 5-1b: THERMAL LOAD SHAPE FUNCTIONS VS. RELATIVE CRACK LENGTH FOR $(0_2/90_2)_s$ AND $(0_2/90_3)_s$ LAMINATES.

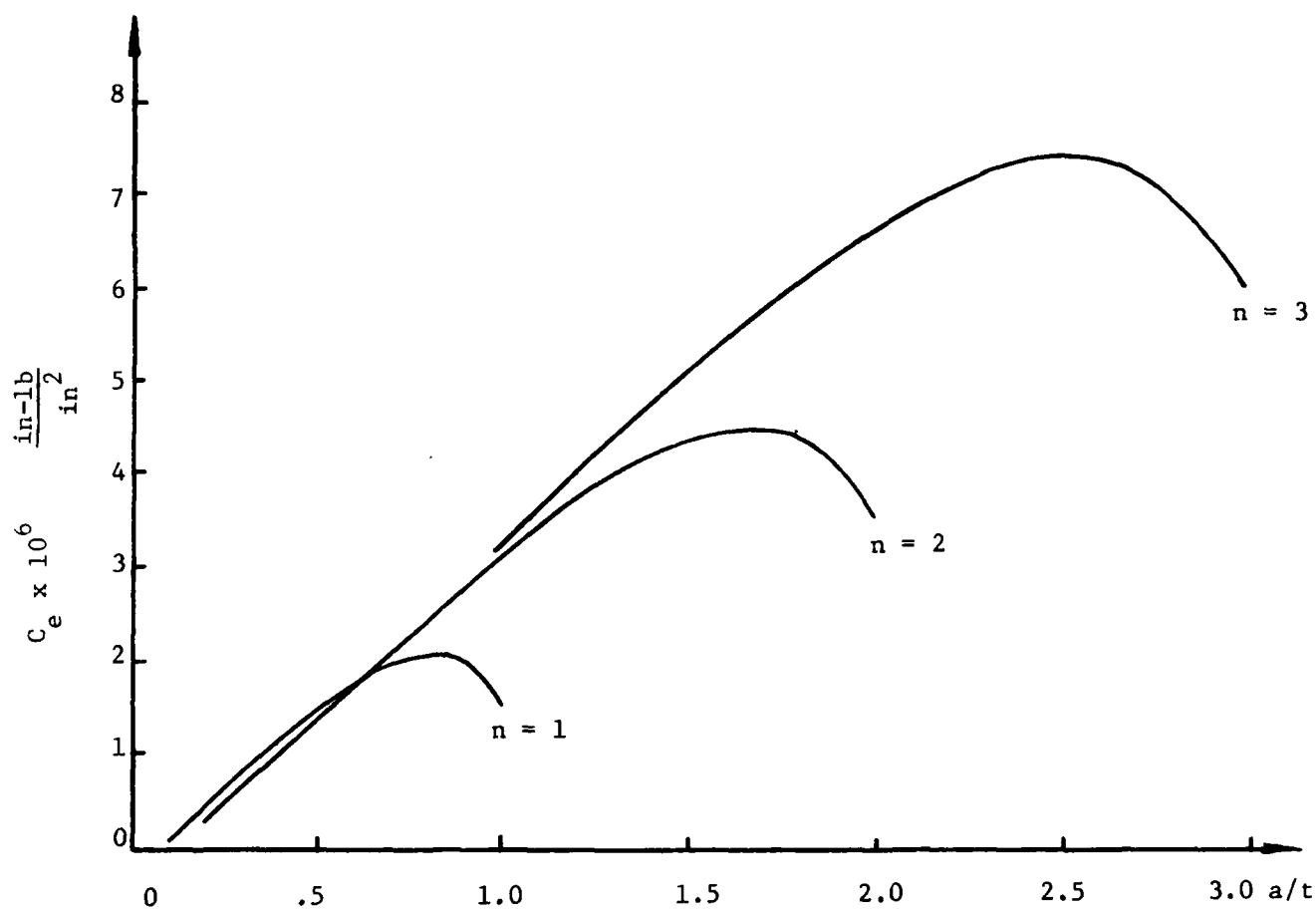


Figure 5-2a: MECHANICAL LOAD SHAPE FUNCTIONS FOR TRANSVERSE CRACKING IN $(\pm 25/90)_n$ LAMINATES.

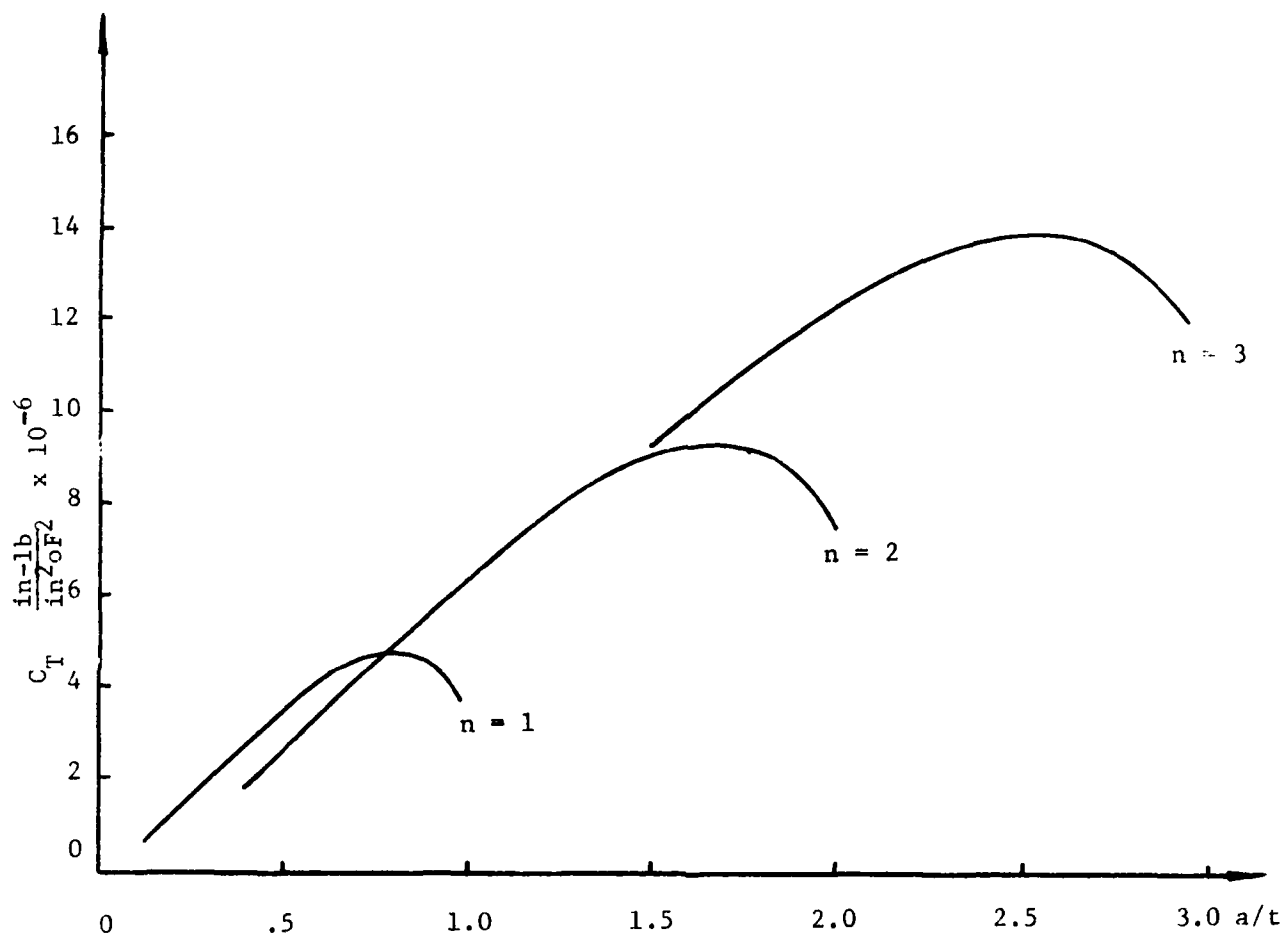


Figure 5-2b: THERMAL LOAD SHAPE FUNCTIONS FOR TRANSVERSE CRACKING IN $(\pm 25/90)_n$ LAMINATES.

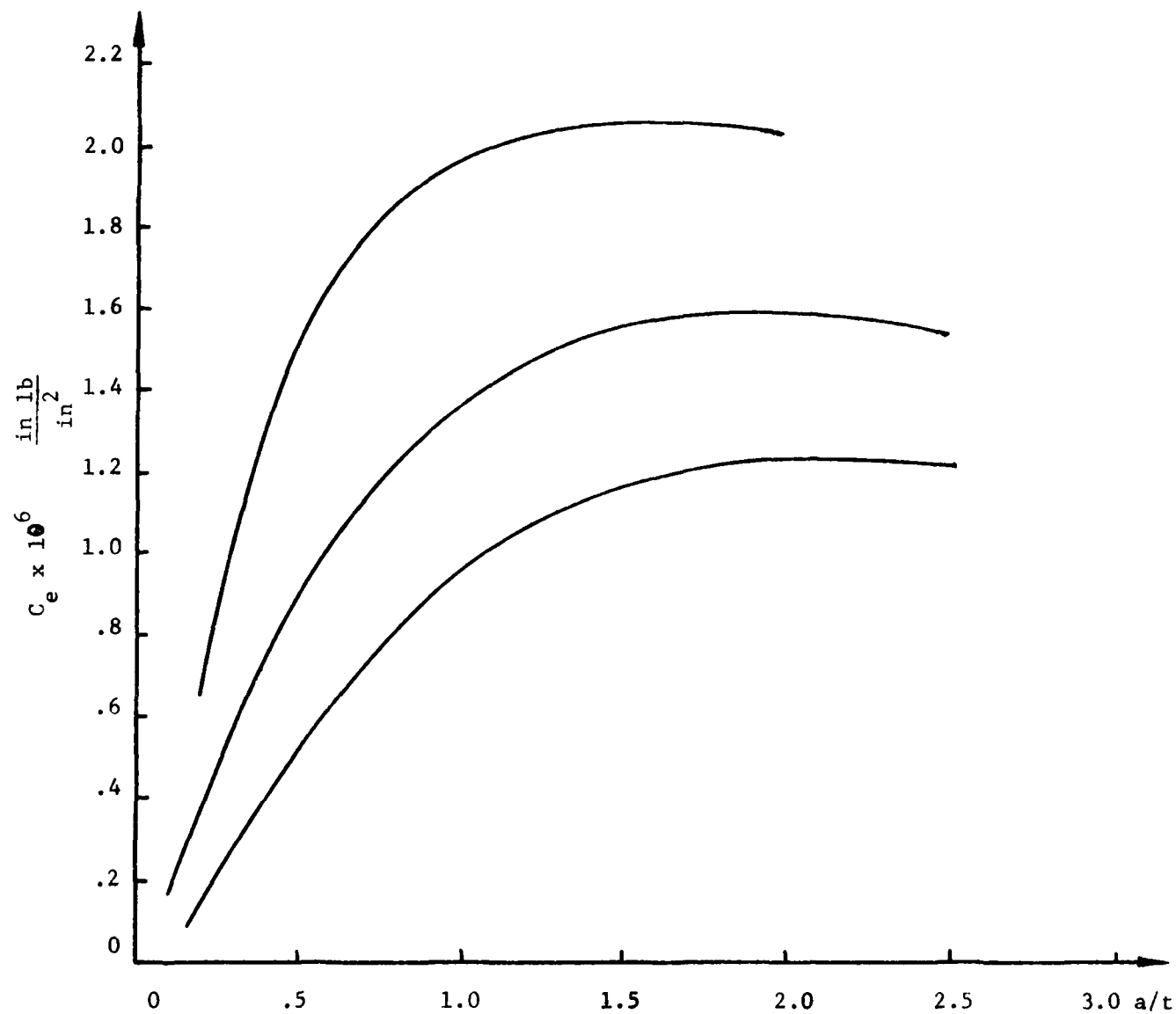


Figure 5-3a: MECHANICAL LOAD SHAPE FUNCTIONS FOR MID-PLANE DELAMINATION OF $(\pm 25/90)_{n_s}$ LAMINATES.

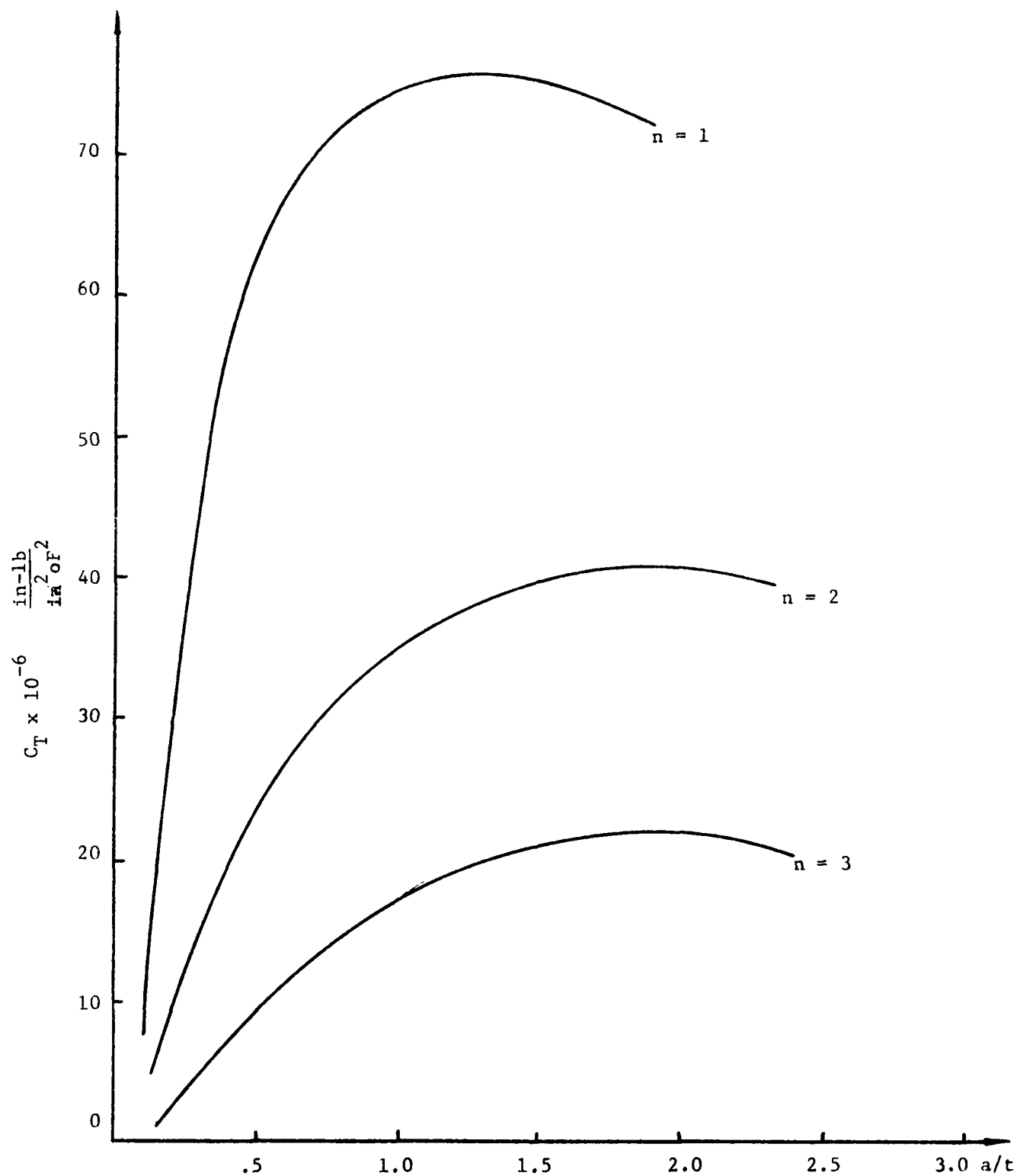


Figure 5-3b: THERMAL LOAD SHAPE FUNCTIONS FOR MID-PLANE DELAMINATION OF $(\pm 25/90)_n$ LAMINATES.

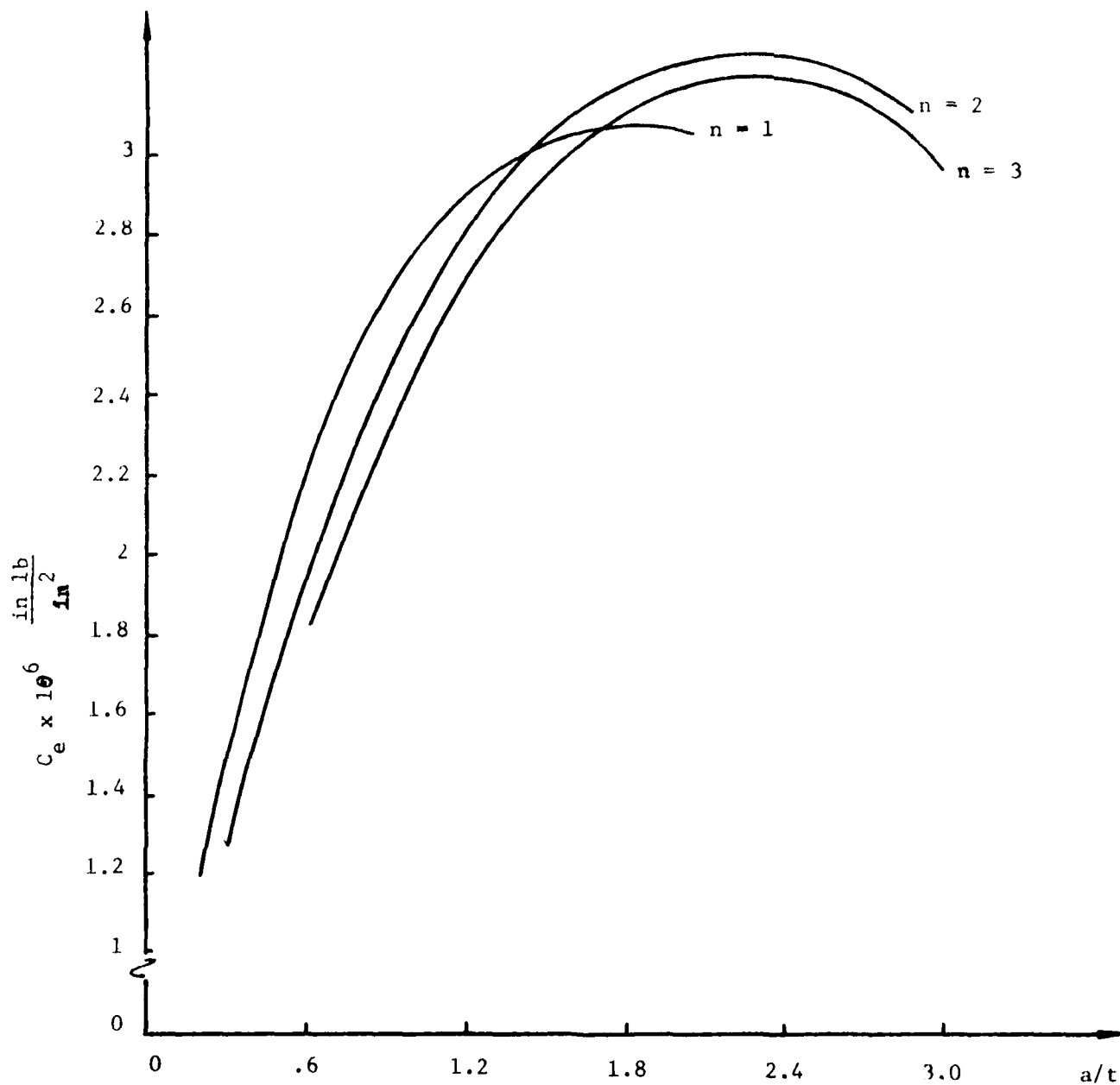


Figure 5-4a: MECHANICAL LOAD SHAPE FUNCTIONS FOR MIXED MODE DELAMINATION OF $(\pm 25/90)_n$ LAMINATES.

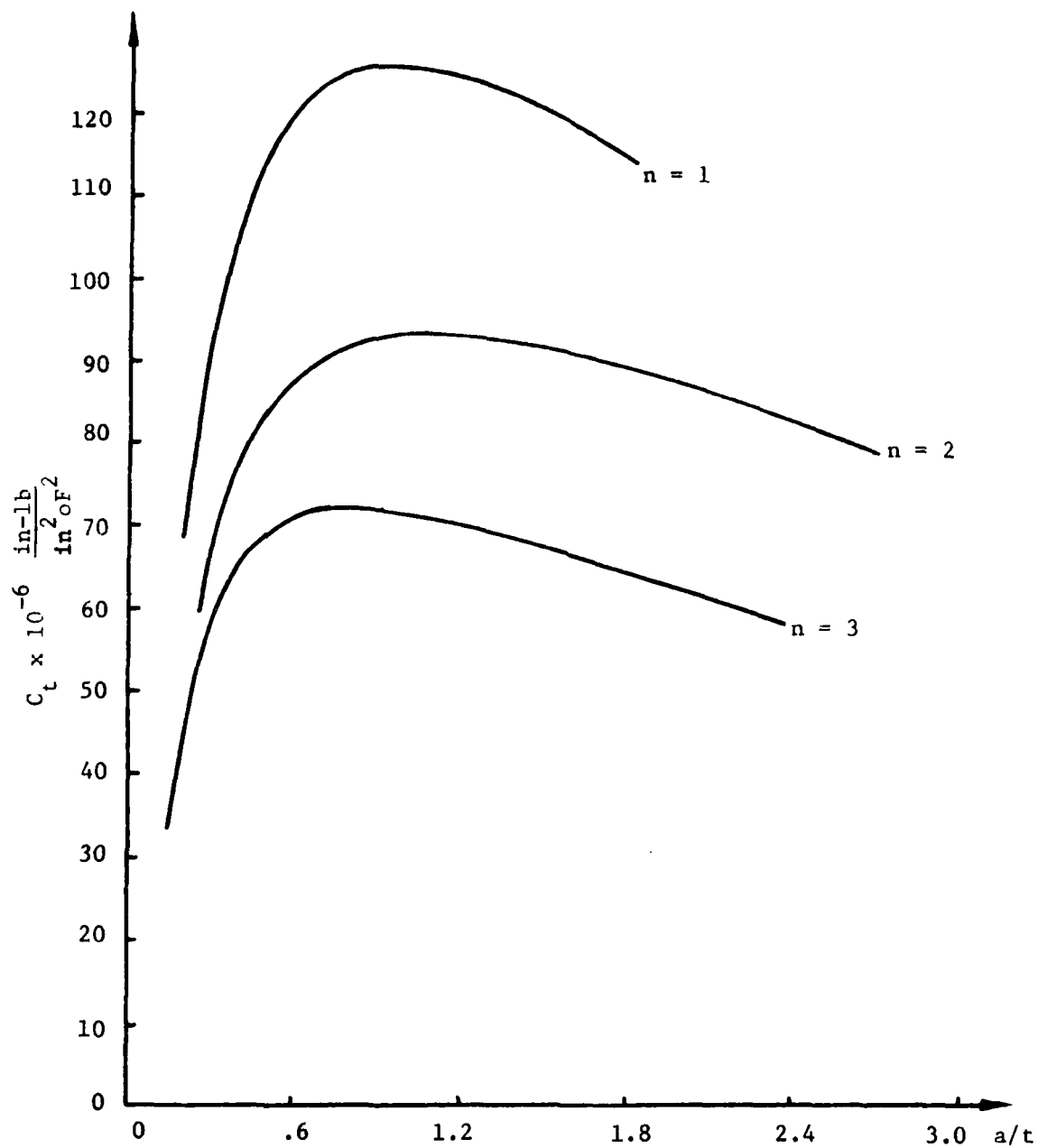
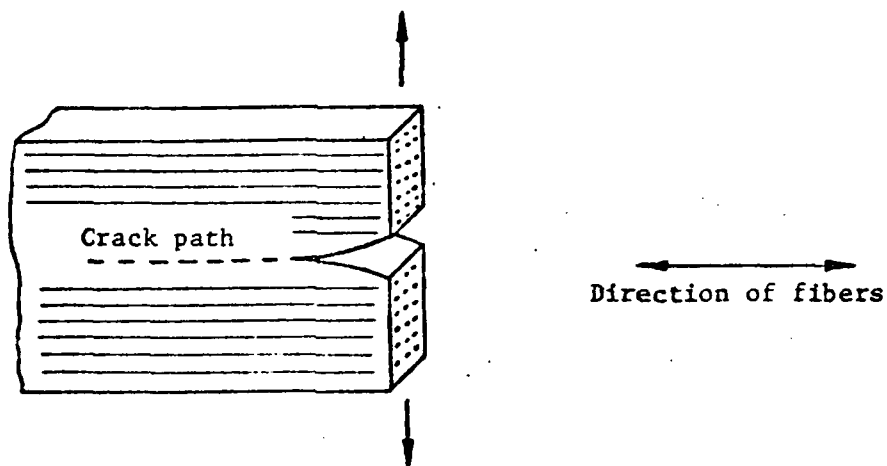
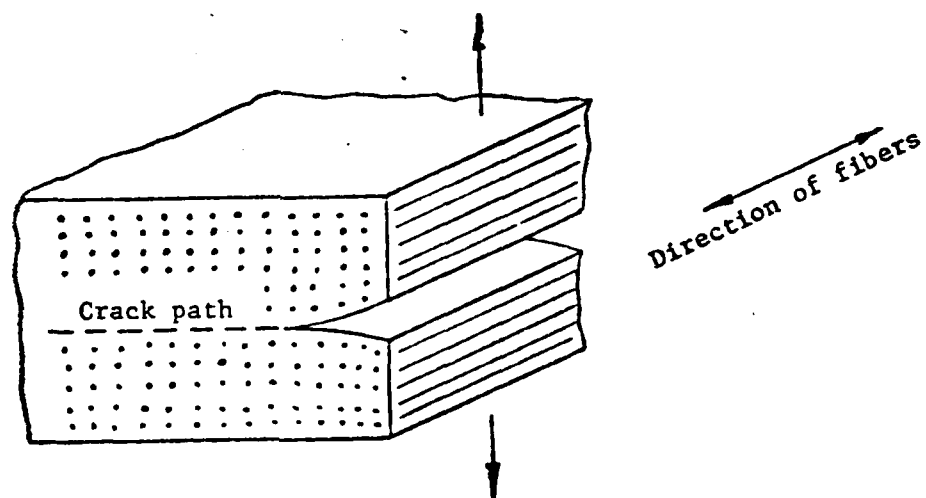


Figure 5-4b: THERMAL LOAD SHAPE FUNCTIONS FOR MIXED MODE DELAMINATION OF $(\pm 25/90)_n$ LAMINATES.



(a) $0^\circ/0^\circ$ Delamination Action



(b) Transverse Cracking Action

Figure 5-5 Schematics of Two Different Cracking Actions in Unidirectional Laminate

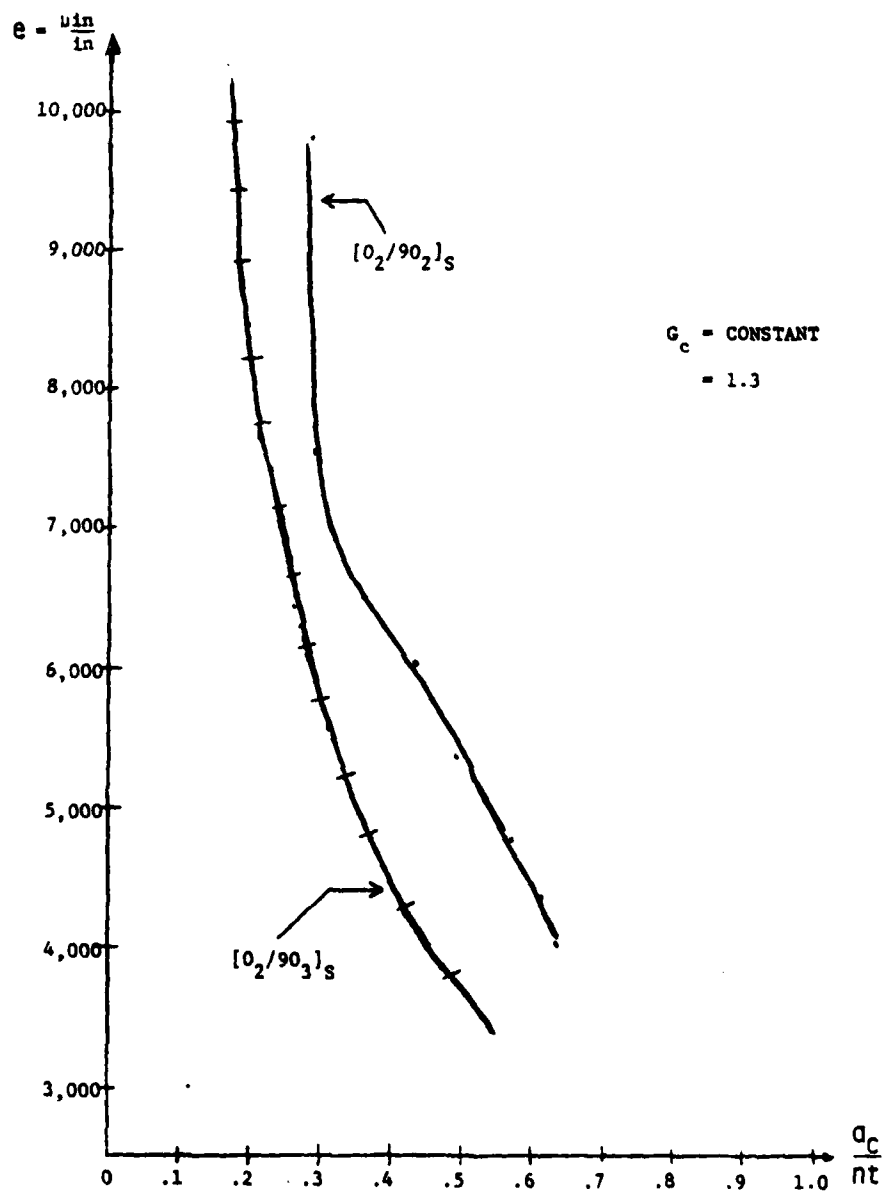


Figure 5.6: Transverse Crack Initiation Strain vs. Relative Critical Crack Length; $(0_2/90_2)_S$ and $(0_2/90_3)_S$.

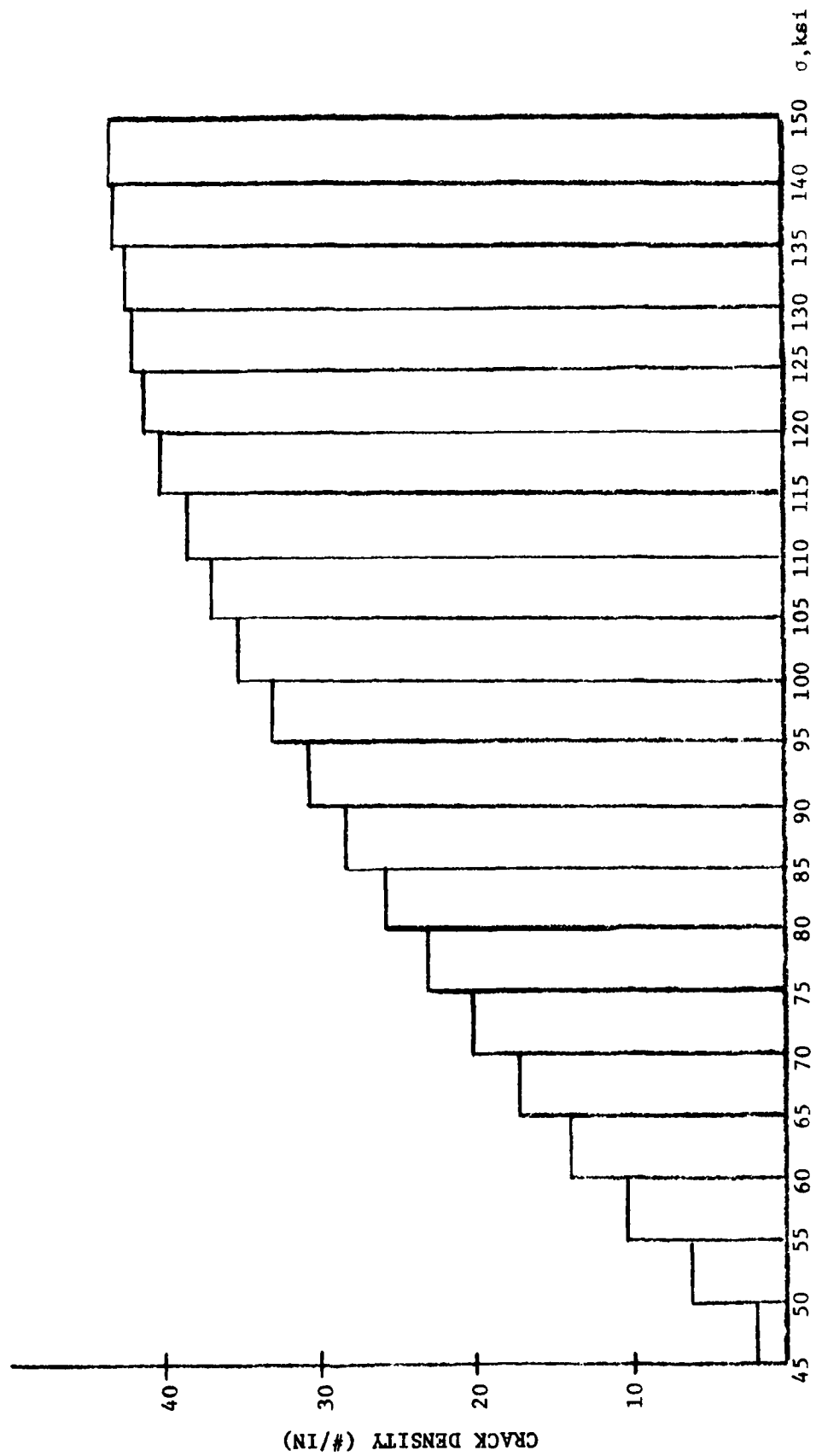


Figure 5-7: Histogram Representation of Load-Damage results for $[0_2/90_2]_S$ Laminate.

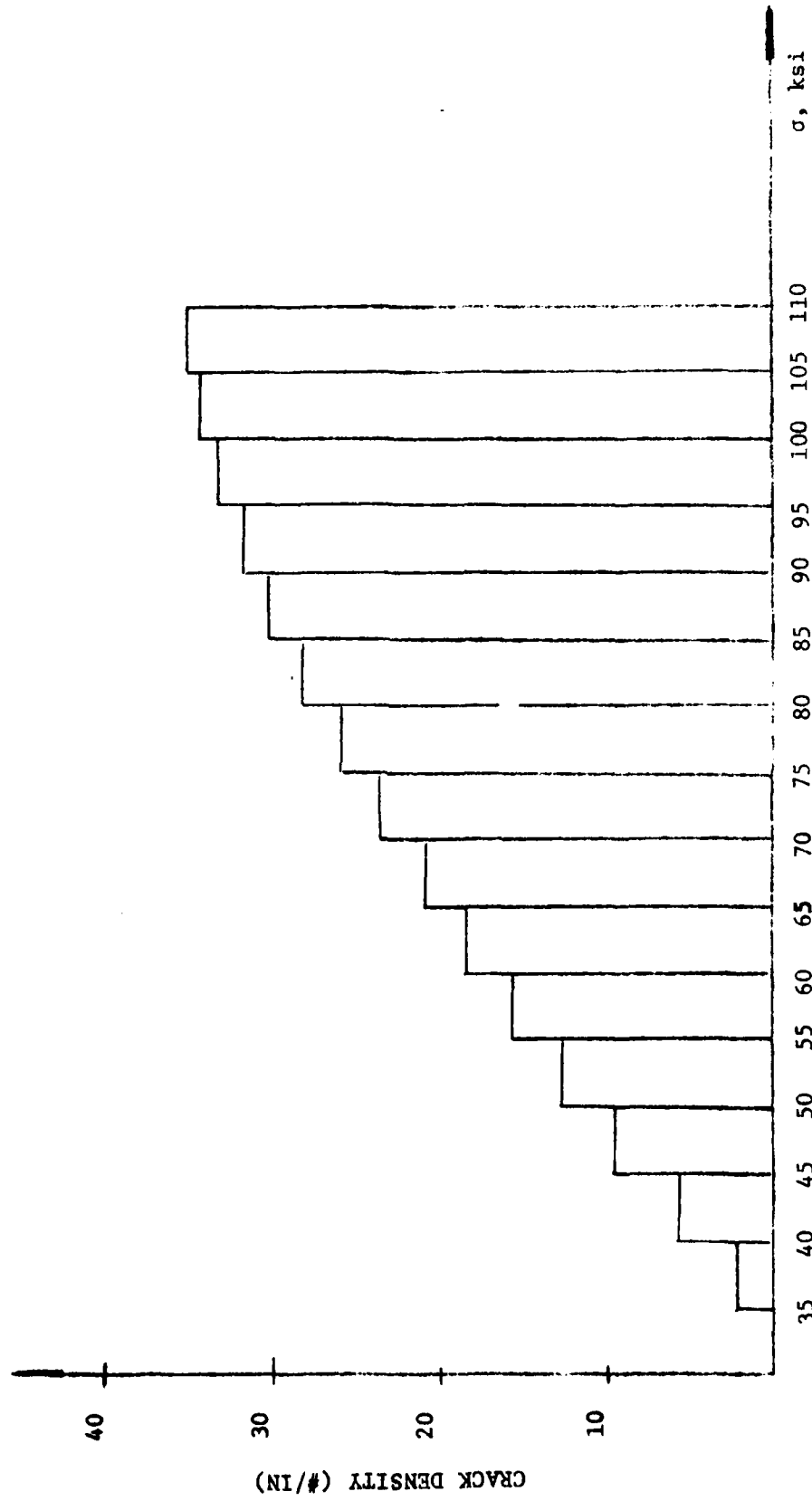


Figure 5-8: HISTOGRAM REPRESENTATION OF LOAD-DAMAGE RESULTS FOR $[0_2/90_3]_s$ LAMINATE.

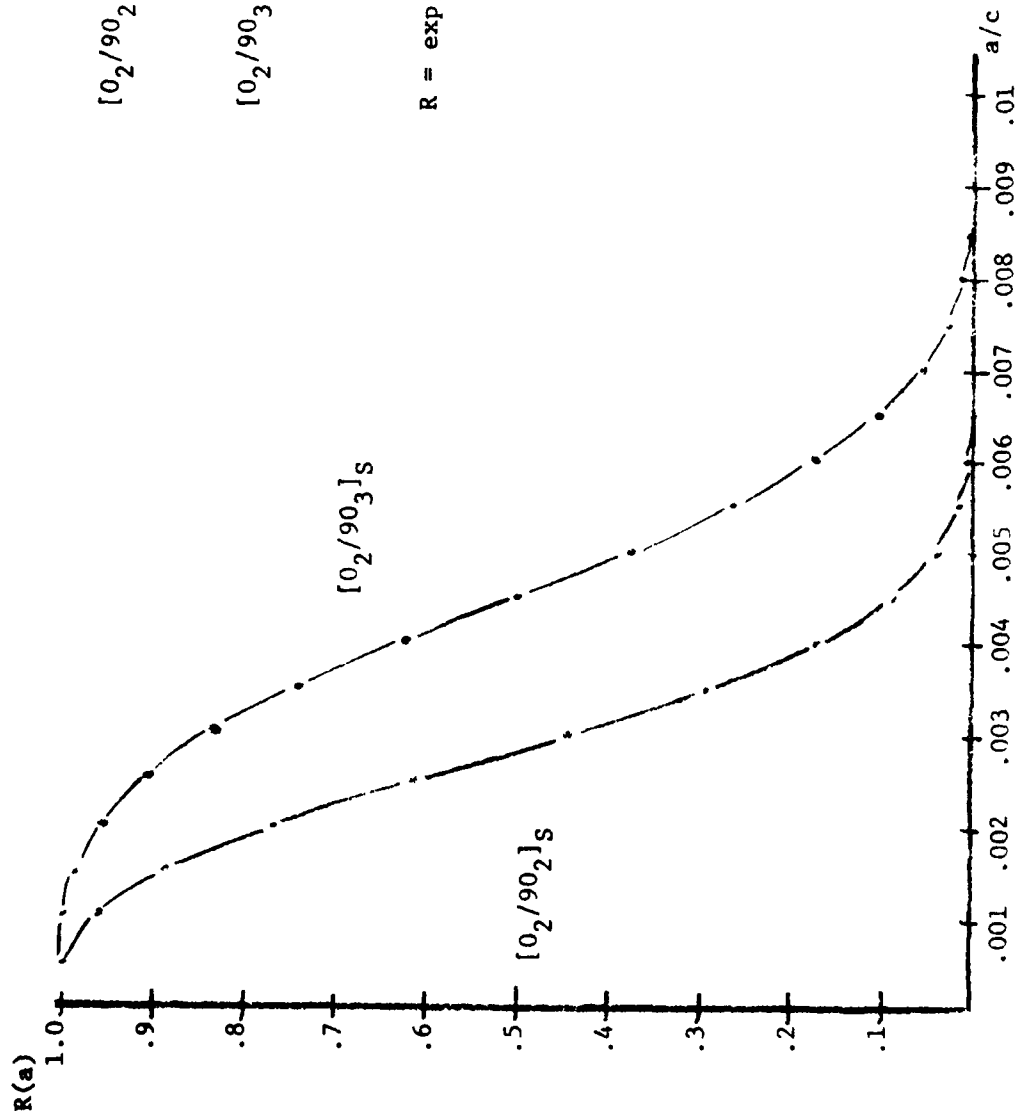


Figure 5-9
Distributions of Initial Flaws Per Unit Length for $[0_2/90_2]_S$ and $[0_2/90_3]_S$ Laminates.

$$[0_2/90_2]_S: \alpha = 2.727$$

$$\beta = 0.00325''$$

$$[0_2/90_3]_S: \alpha = 3.232$$

$$\beta = 0.00503''$$

$$R = \exp\left[-\left(\frac{x}{\beta}\right)^\alpha\right]$$

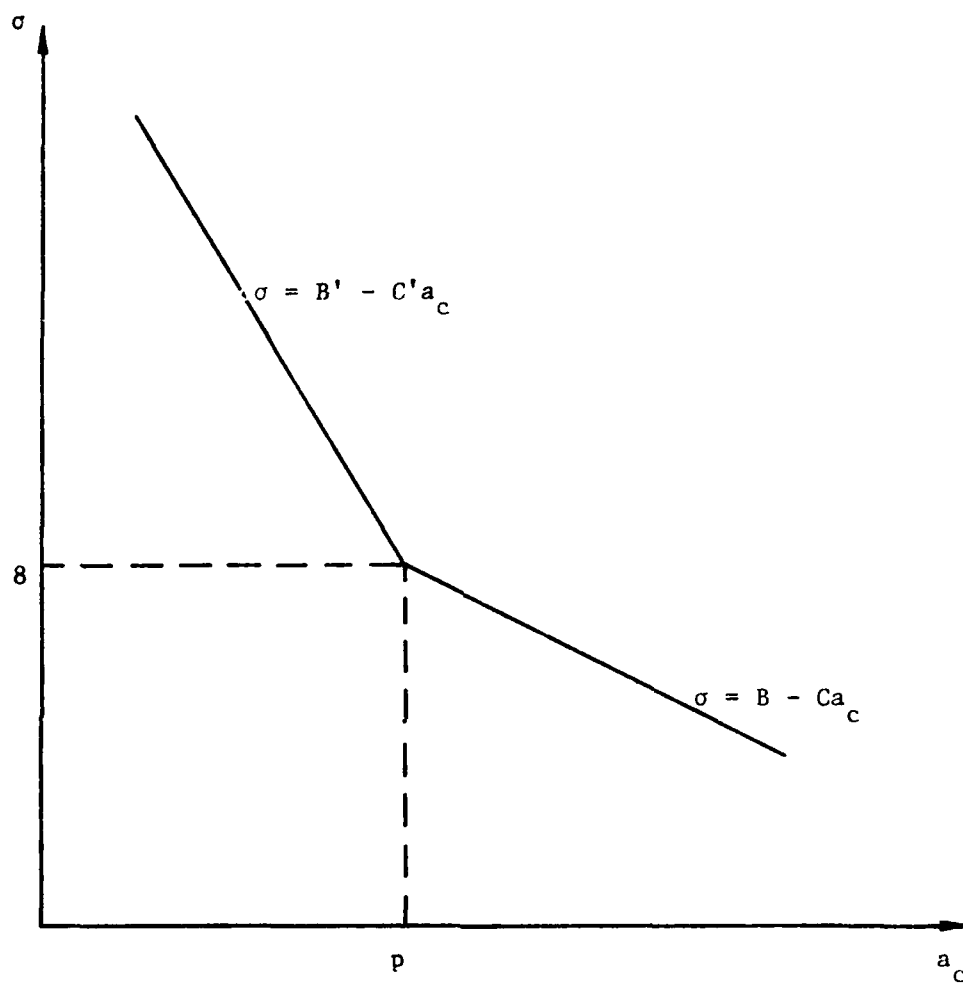


Figure 5-10: TWO SEGMENT APPROXIMATION TO THE $\sigma - a_c$ RELATION.

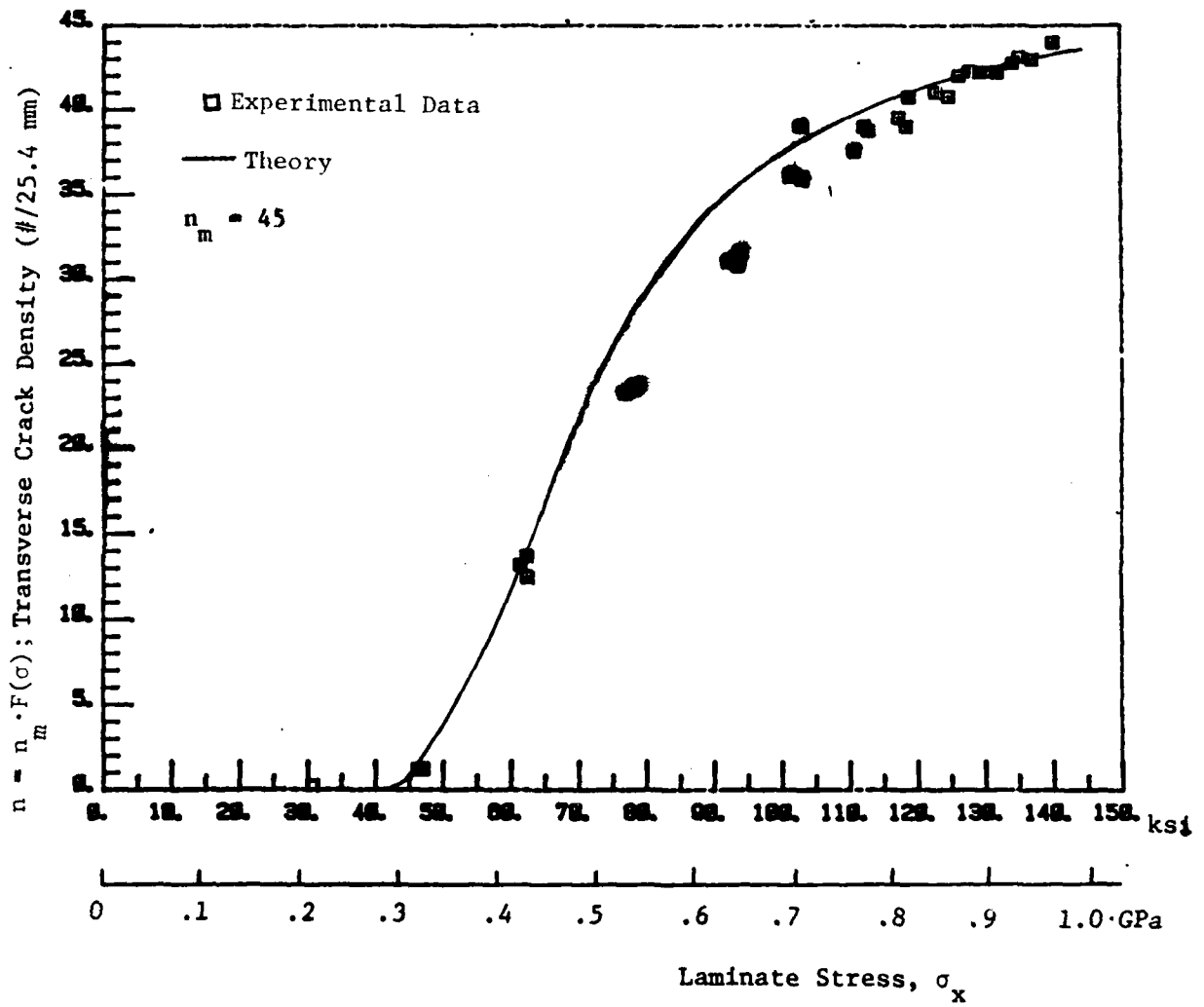


Figure 5.11: Load-Damage Relation for $(0_2/90_2)_s$ Laminate.

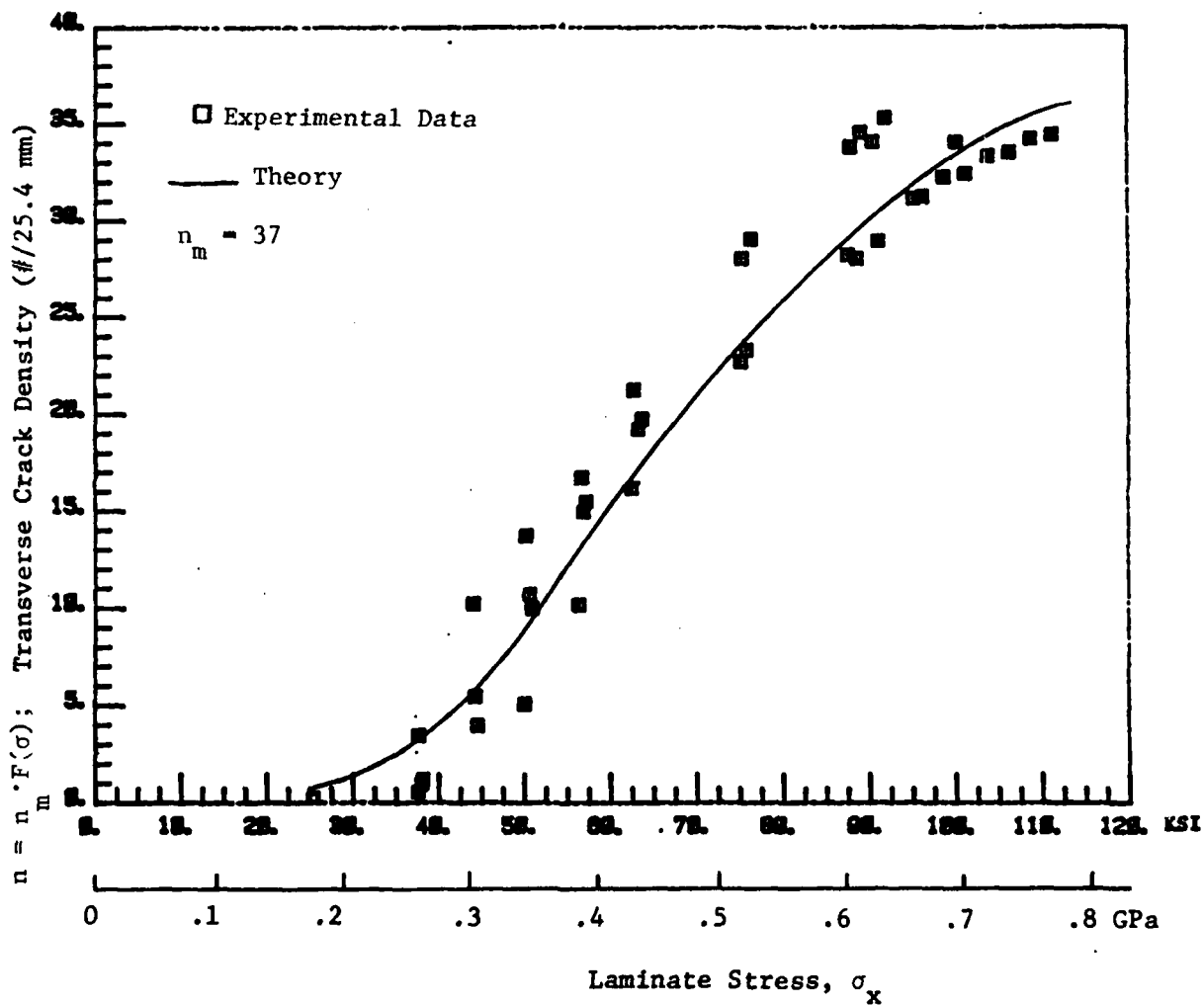


Figure 5.12: Crack Density vs. Static Load for $(0_2/90_3)_s$.

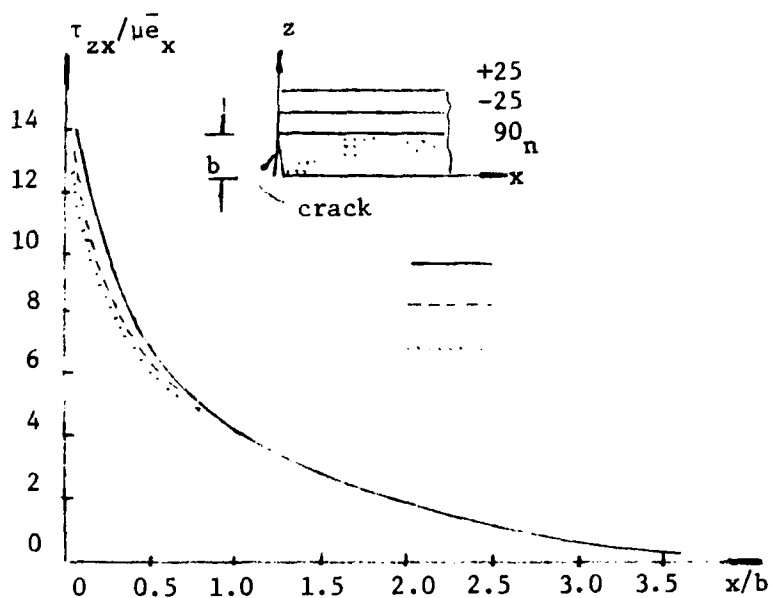


Figure 5-13: Interlaminar Shear Stress on -25/90 Interface.
 x is measured from the root of the crack.

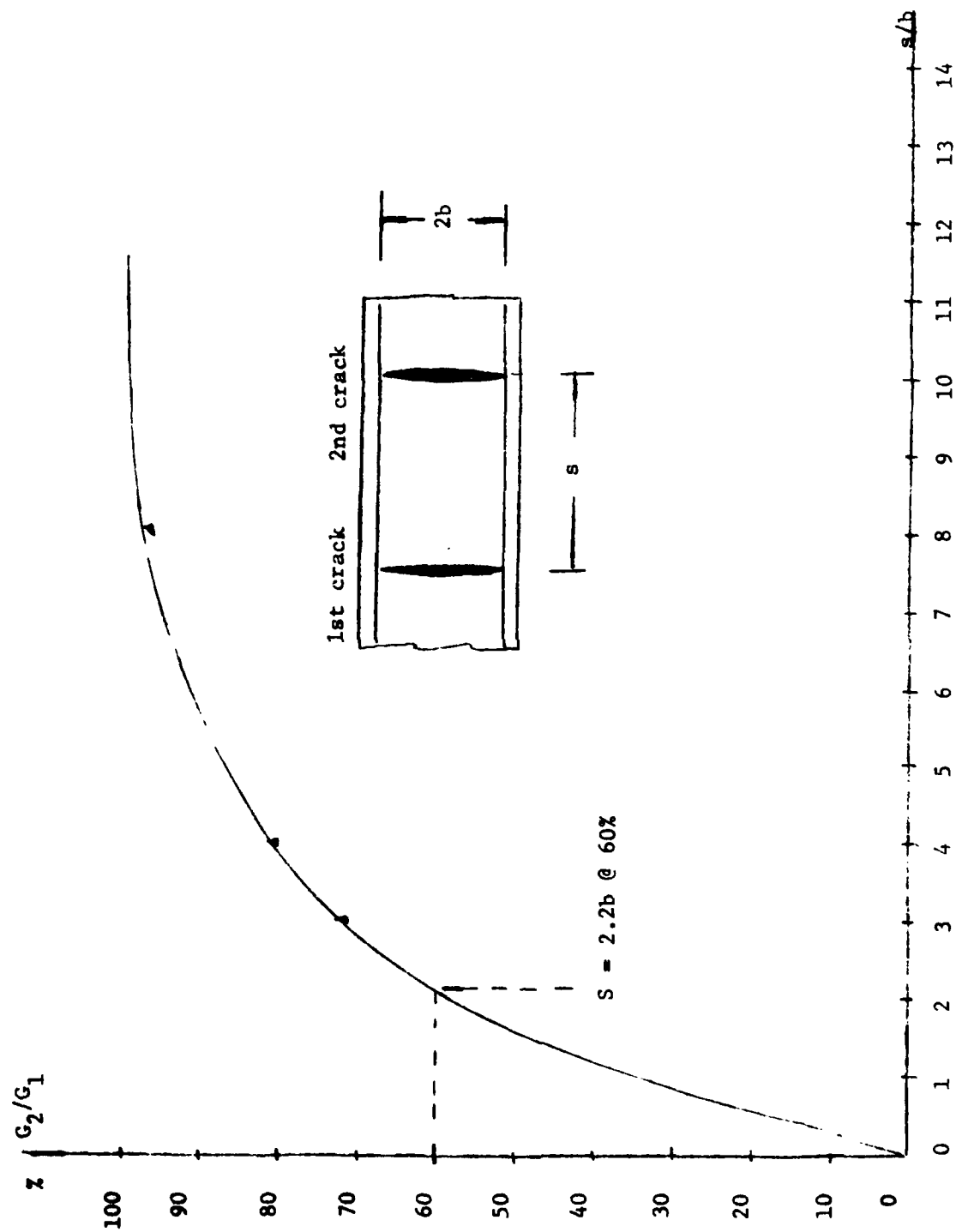


Figure 5-14: Ratio of Energy Release Rates for a Crack Placed a Distance, s , From a Previously Formed Crack.

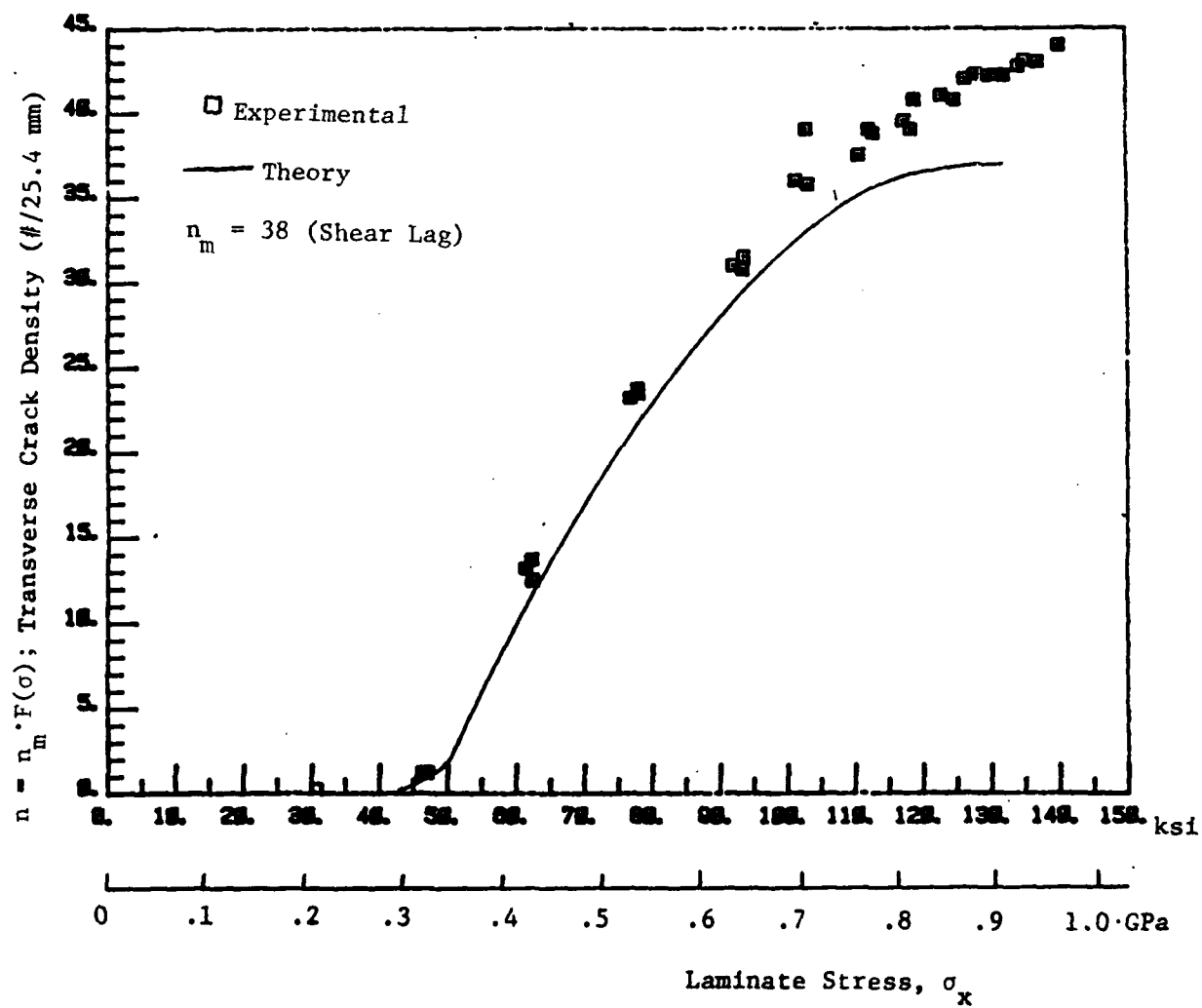


Figure 5.15: Load-Damage Relation for $(0_2/90_2)_s$ Laminate.

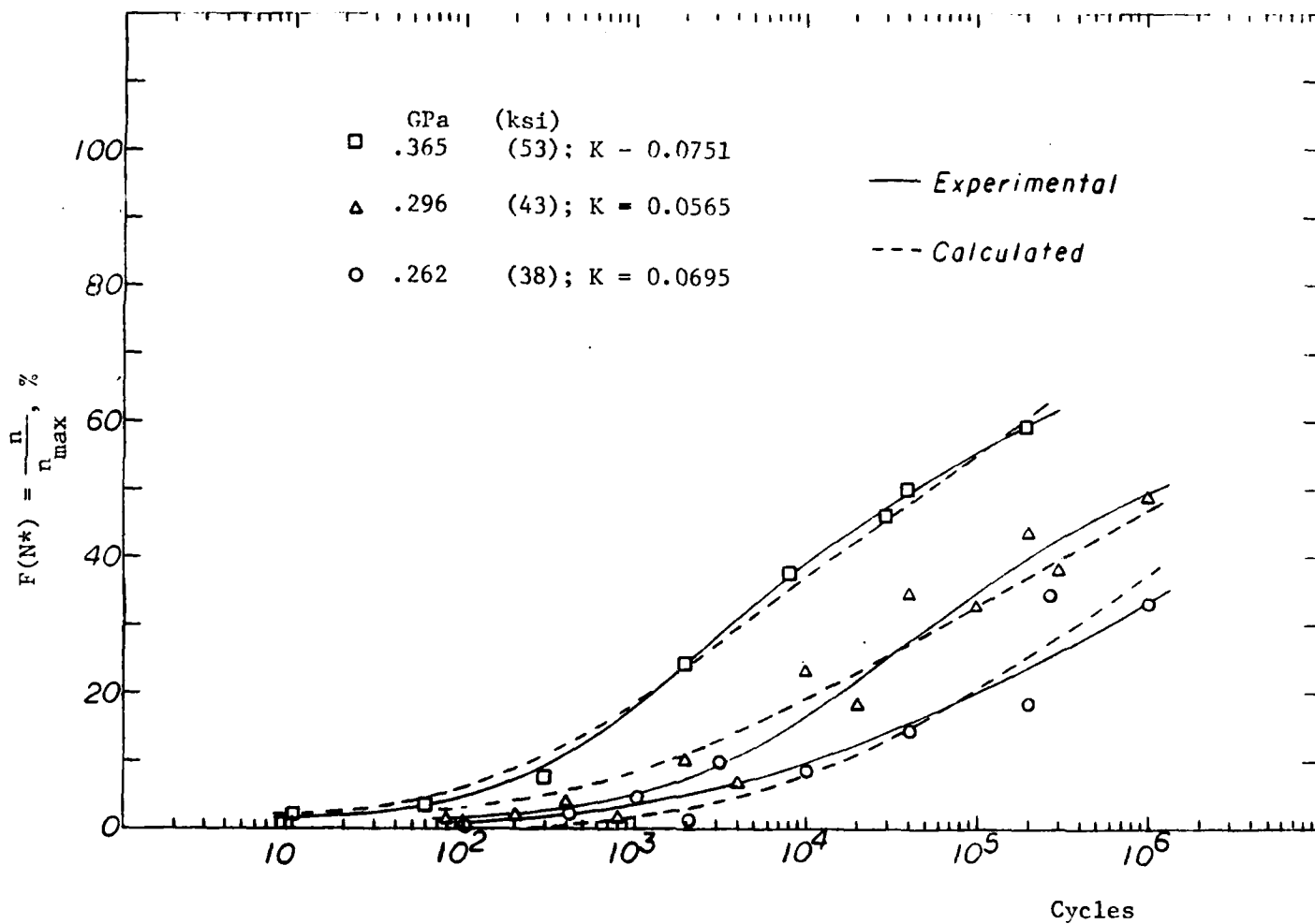


Figure 5.16: Distribution of N^* for $(0_2/90_2)_s$ Lmainate for Three Maximum Loads Under Constant Amplitude Fatigue.

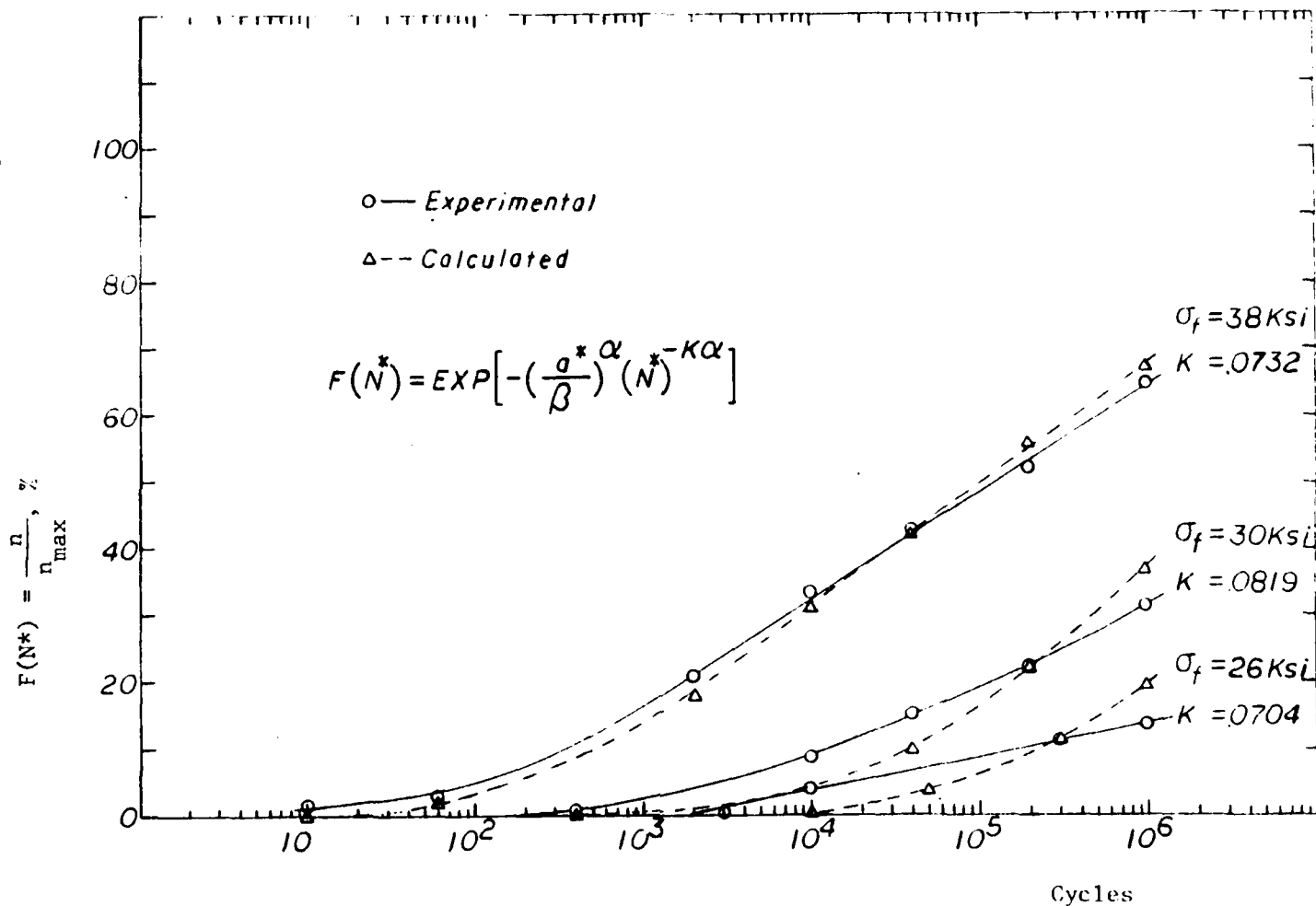


Figure 5.17: Distributions of N^* for $(0_2/90_3)_s$ Laminate for Three Maximum Fatigue Loads Under Constant Amplitude Fatigue.

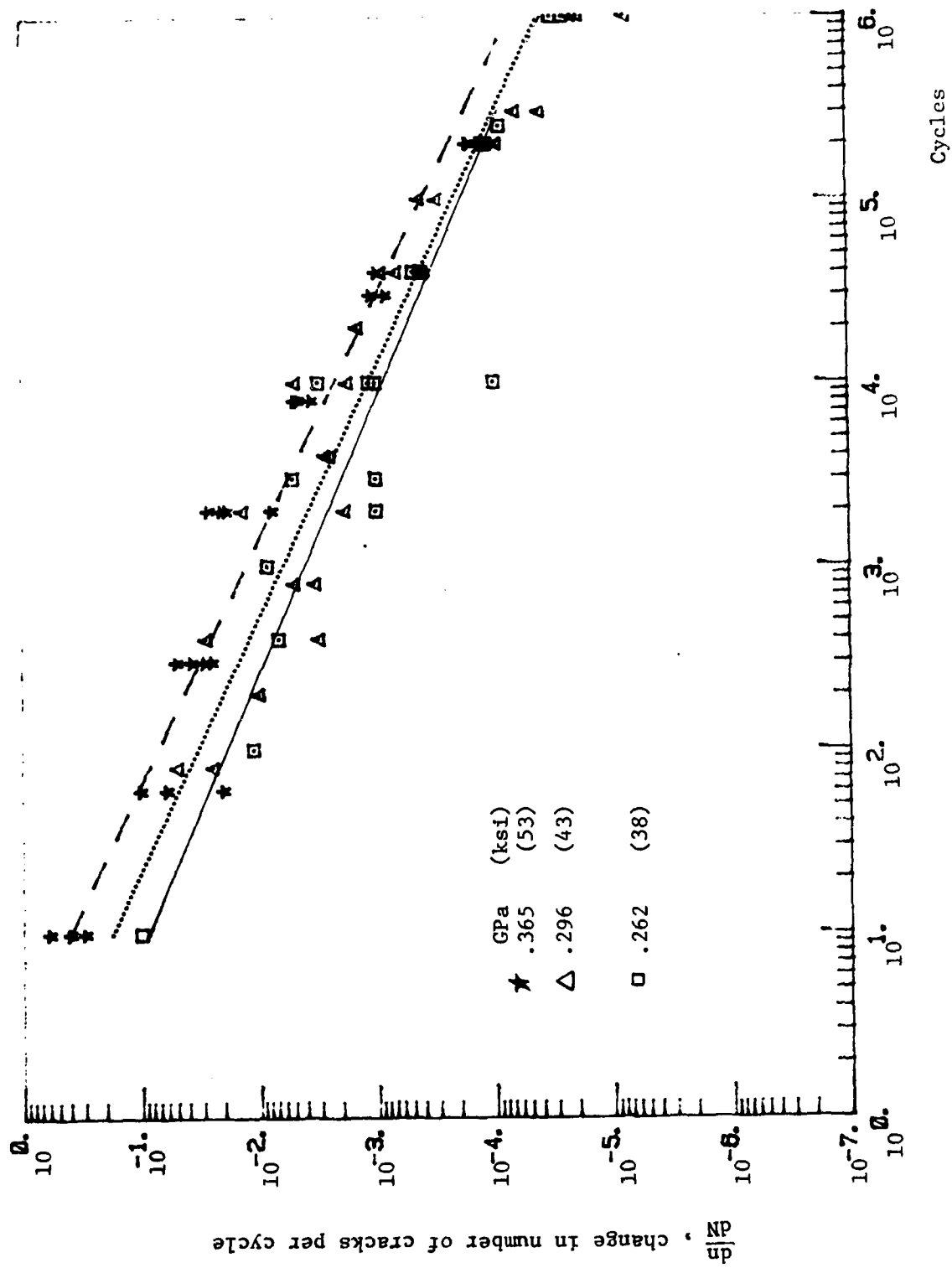


Figure 5-18: Cycles vs. Damage Growth Rate for $(O_2/90_2) s$.

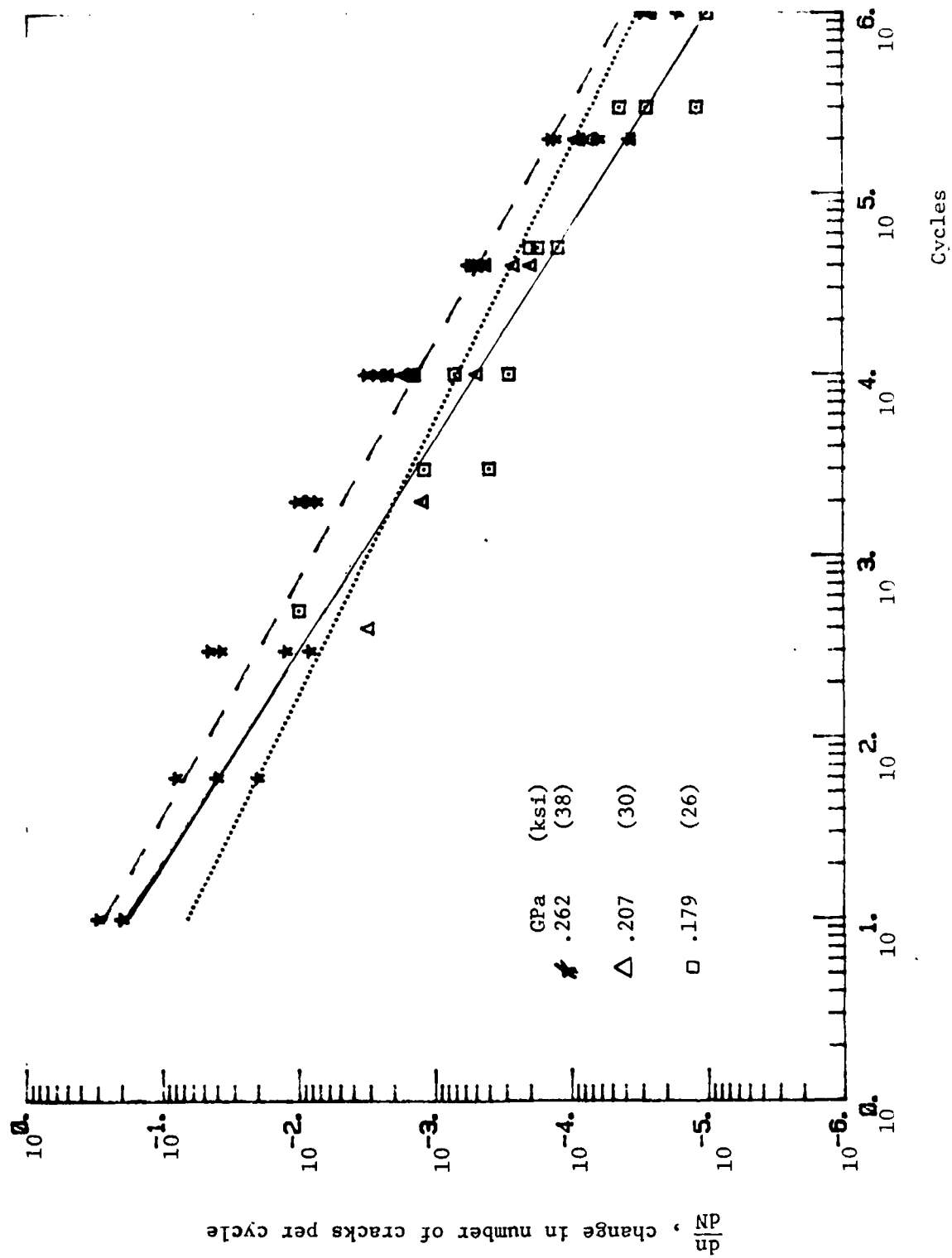


Figure 5-19: Cycles vs. Damage Growth Rate for $(O_2/90)_3 s$.

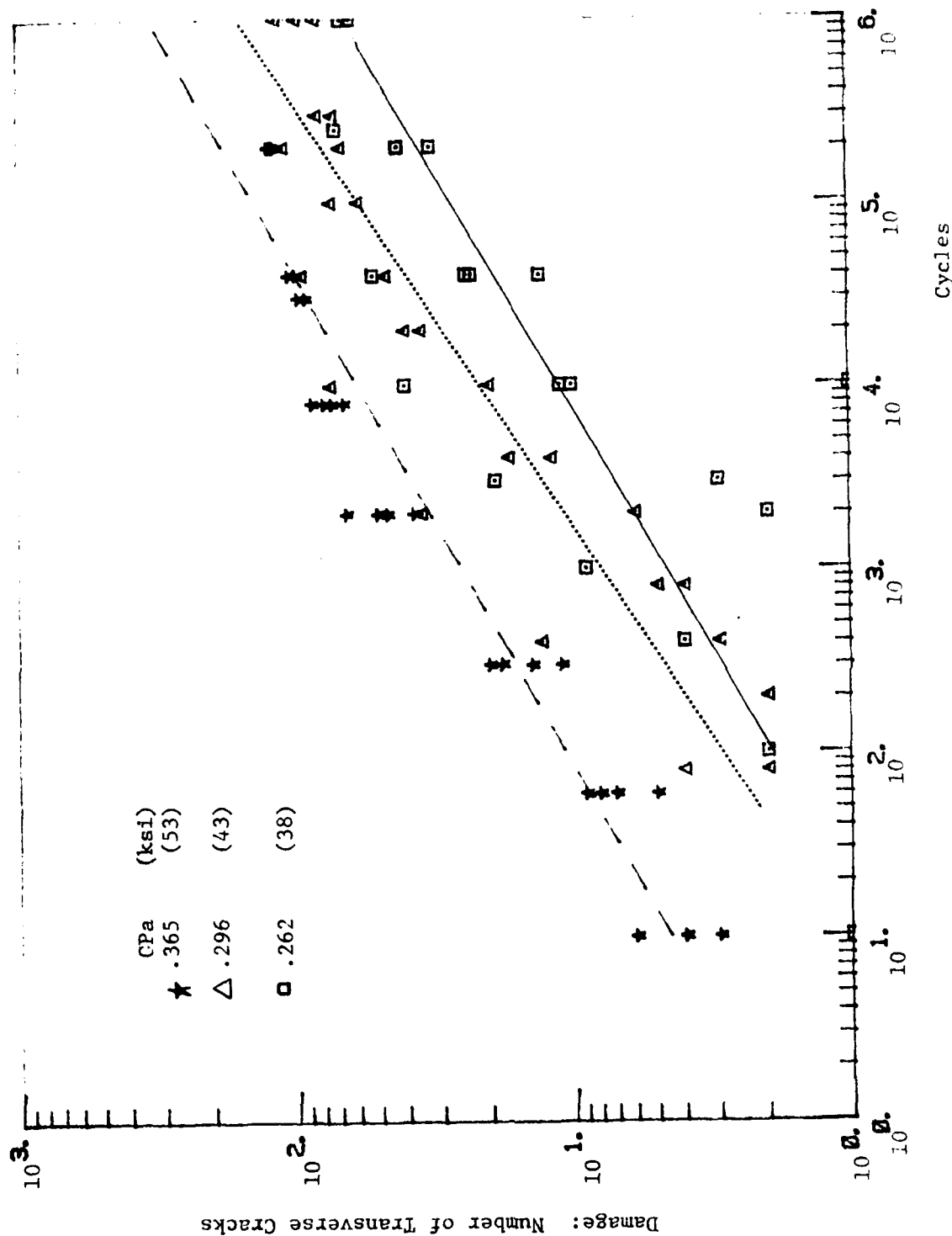


Figure 5-20: Cycles vs Number of Transverse Cracks for $(O_2/90_2)_s$.

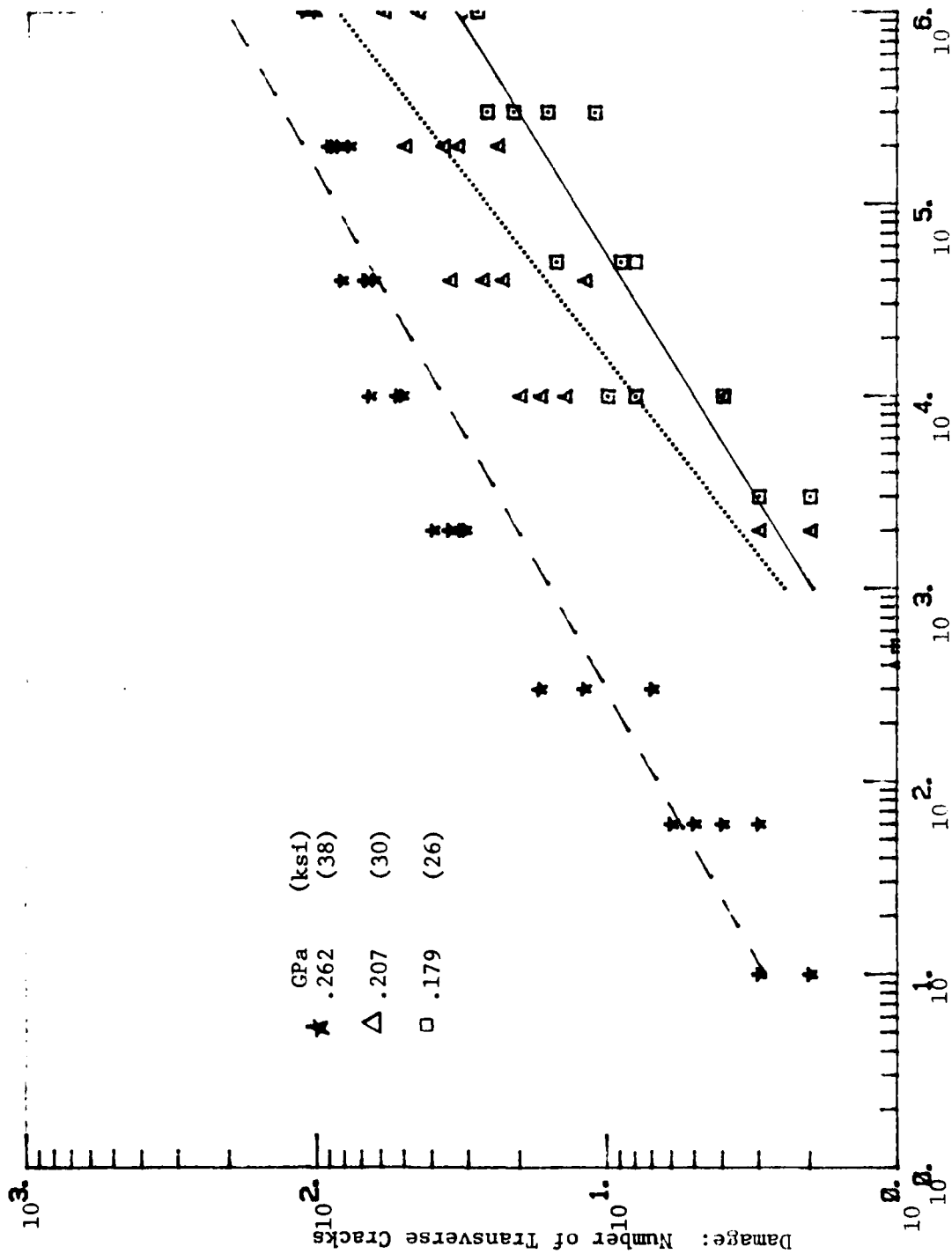


Figure 5-21: Cycles vs Number of Transverse Cracks for $(O_2/90_3)s$.

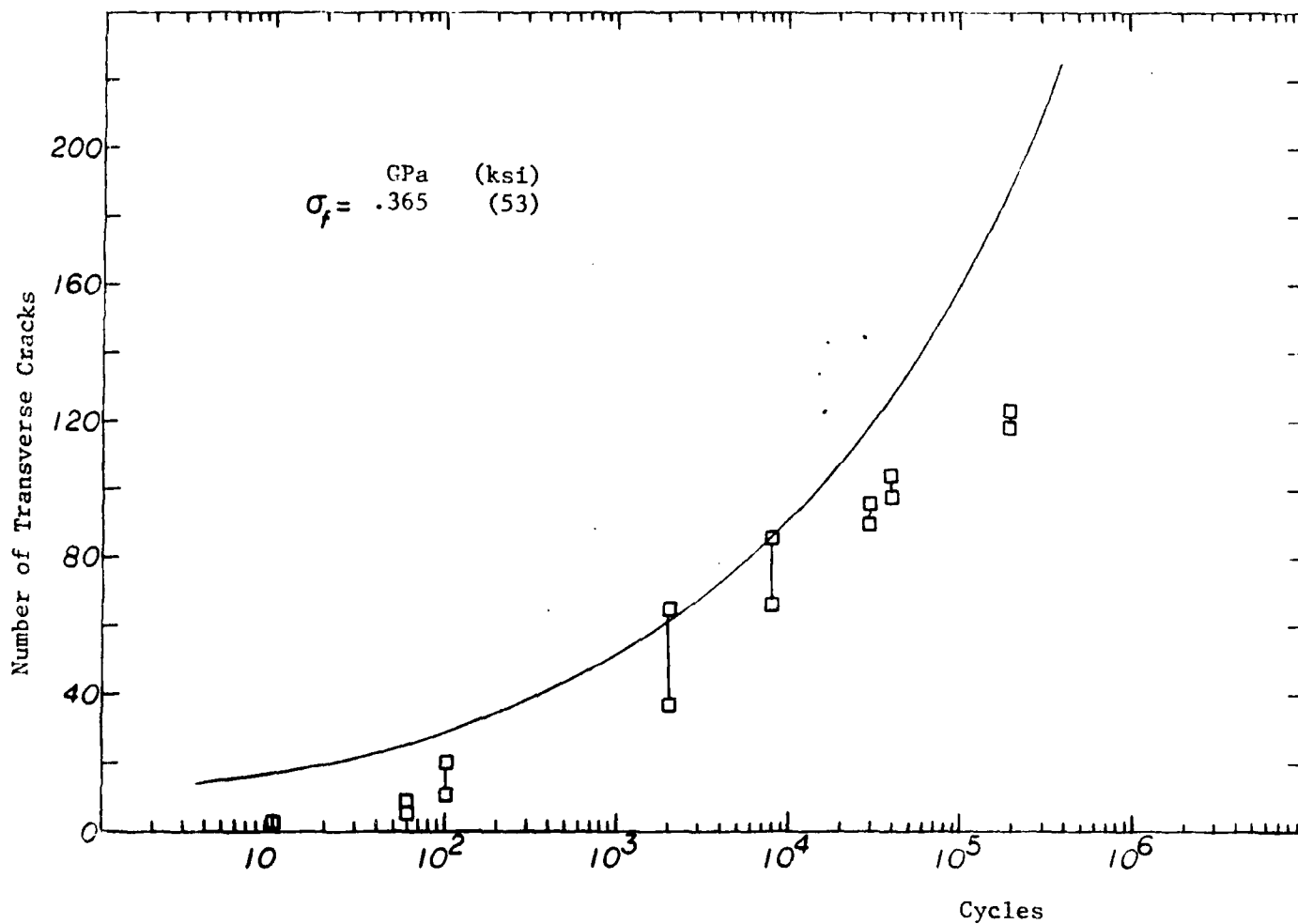


Figure 5.22(a): Number of Cracks vs. Cycles for $(0_2/90_2)_s$.

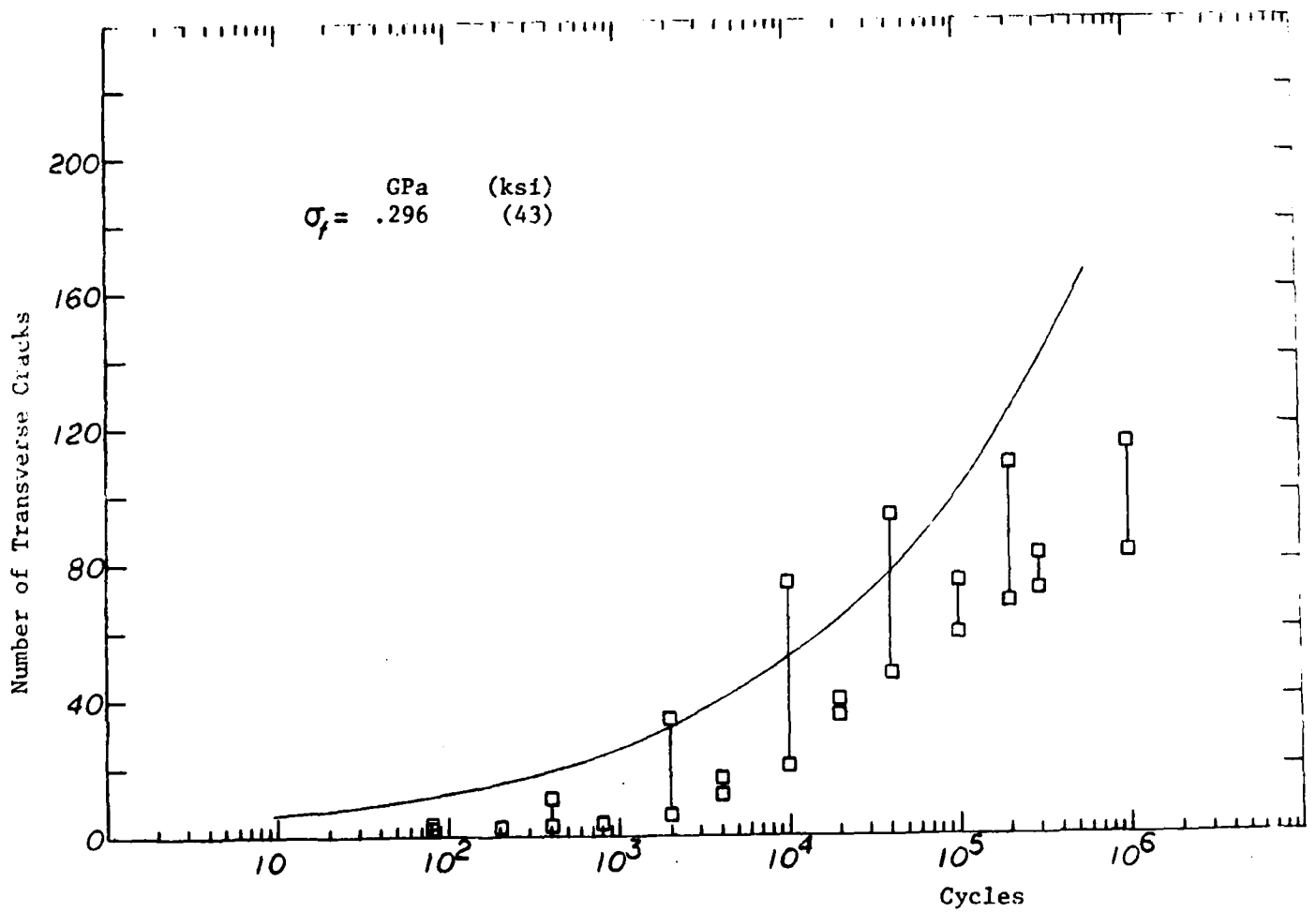


Figure 5.22(b): Number of Cracks vs. Cycles for $(0_2/90_2)_s$.

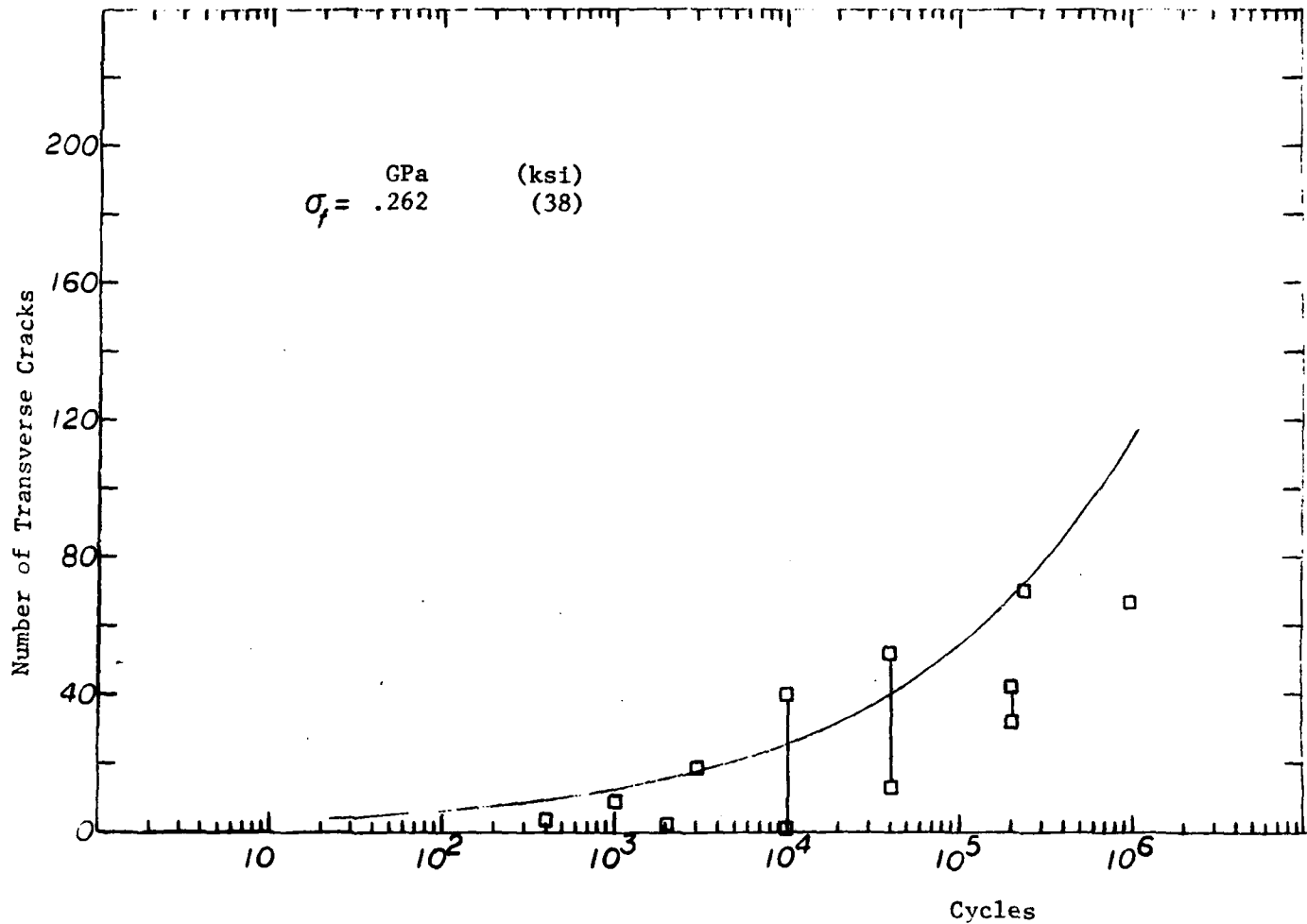


Figure 5.22(c): Number of Cracks vs. Cycles for $(0_2/90_2)_s$.

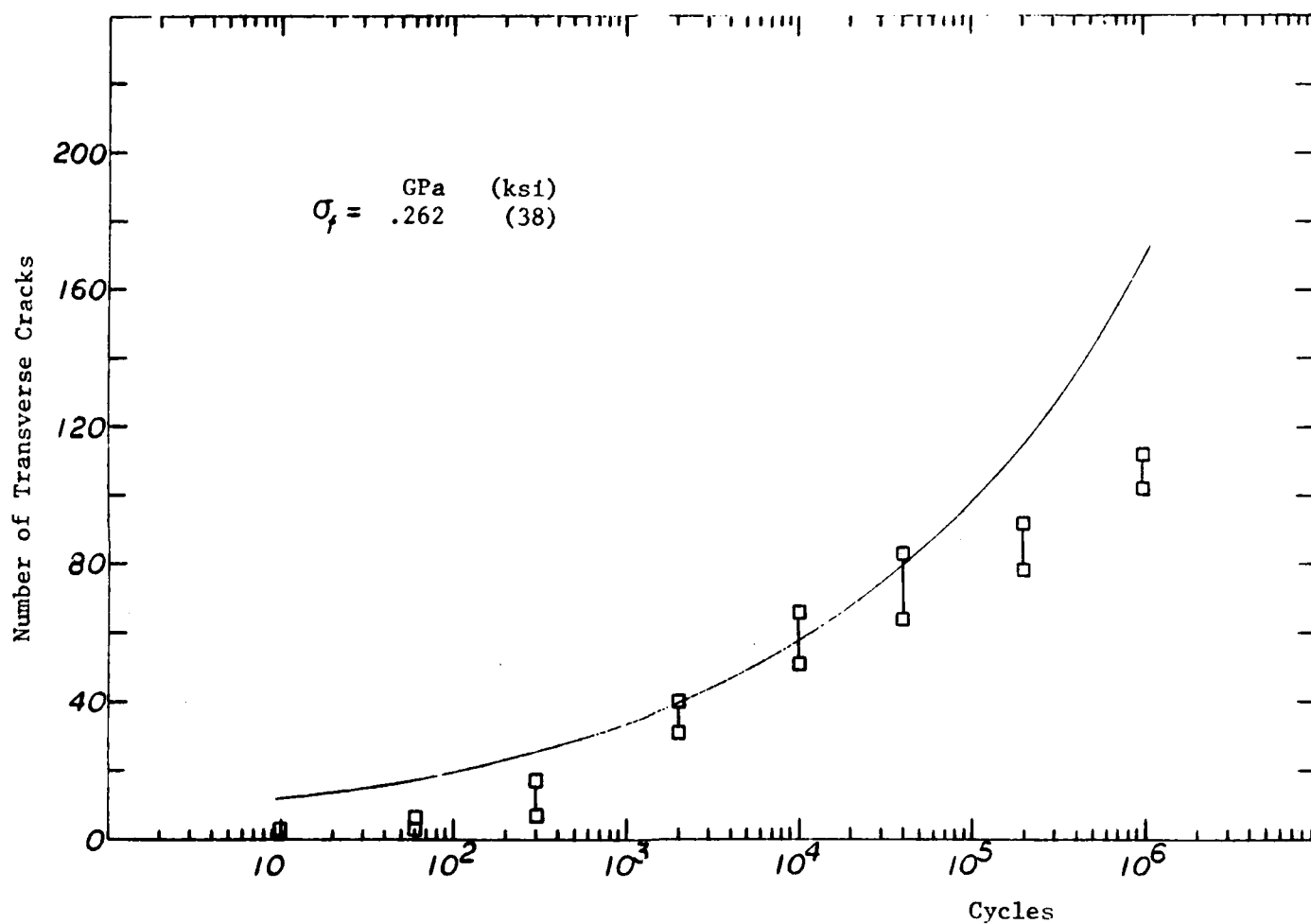


Figure 5.23(a): Number of Cracks vs. Cycles for $(0_2/90_3)_s$.

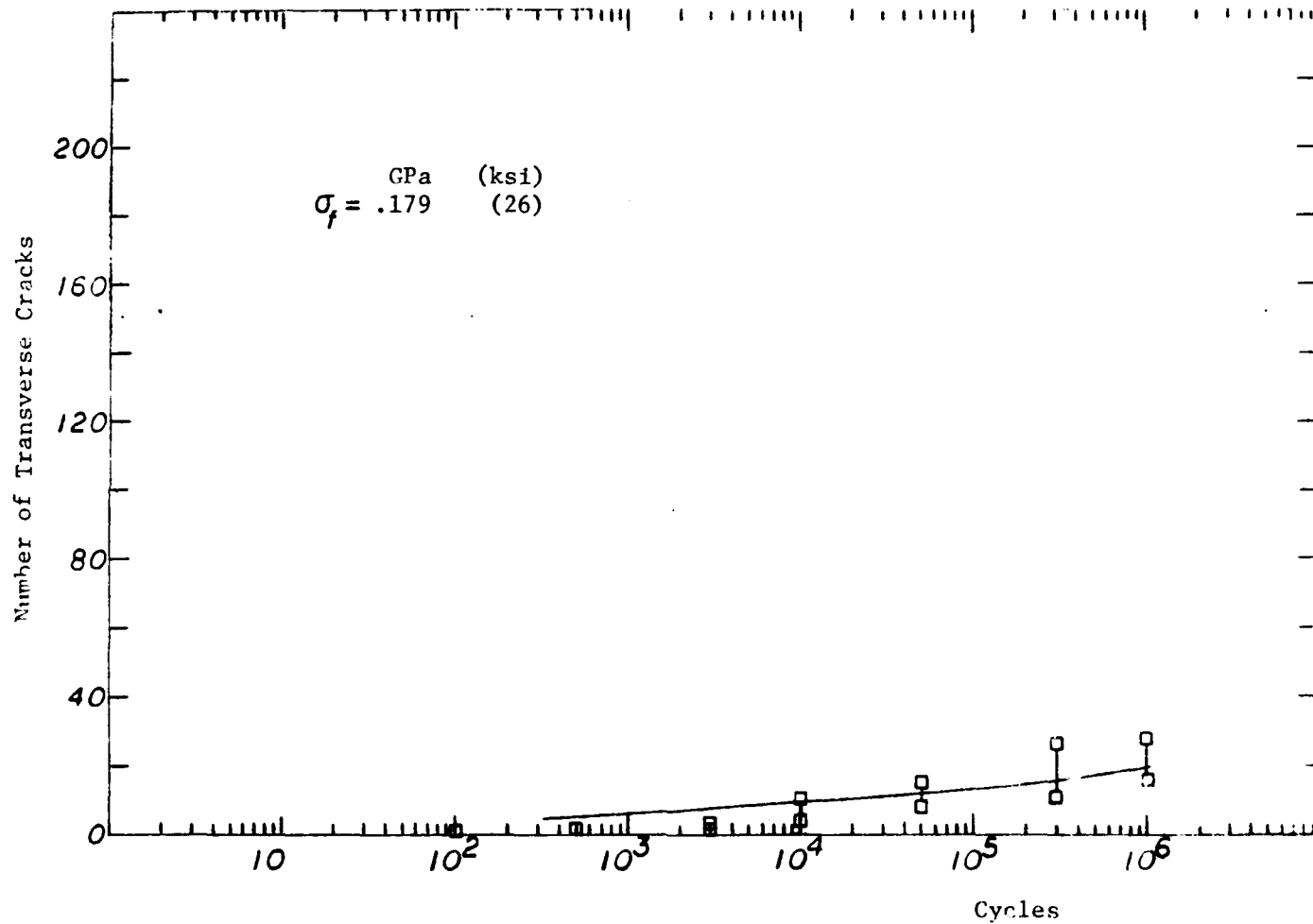


Figure 5.23(c): Number of Cracks vs. Cycles for $(0_2/90_3)_s$.

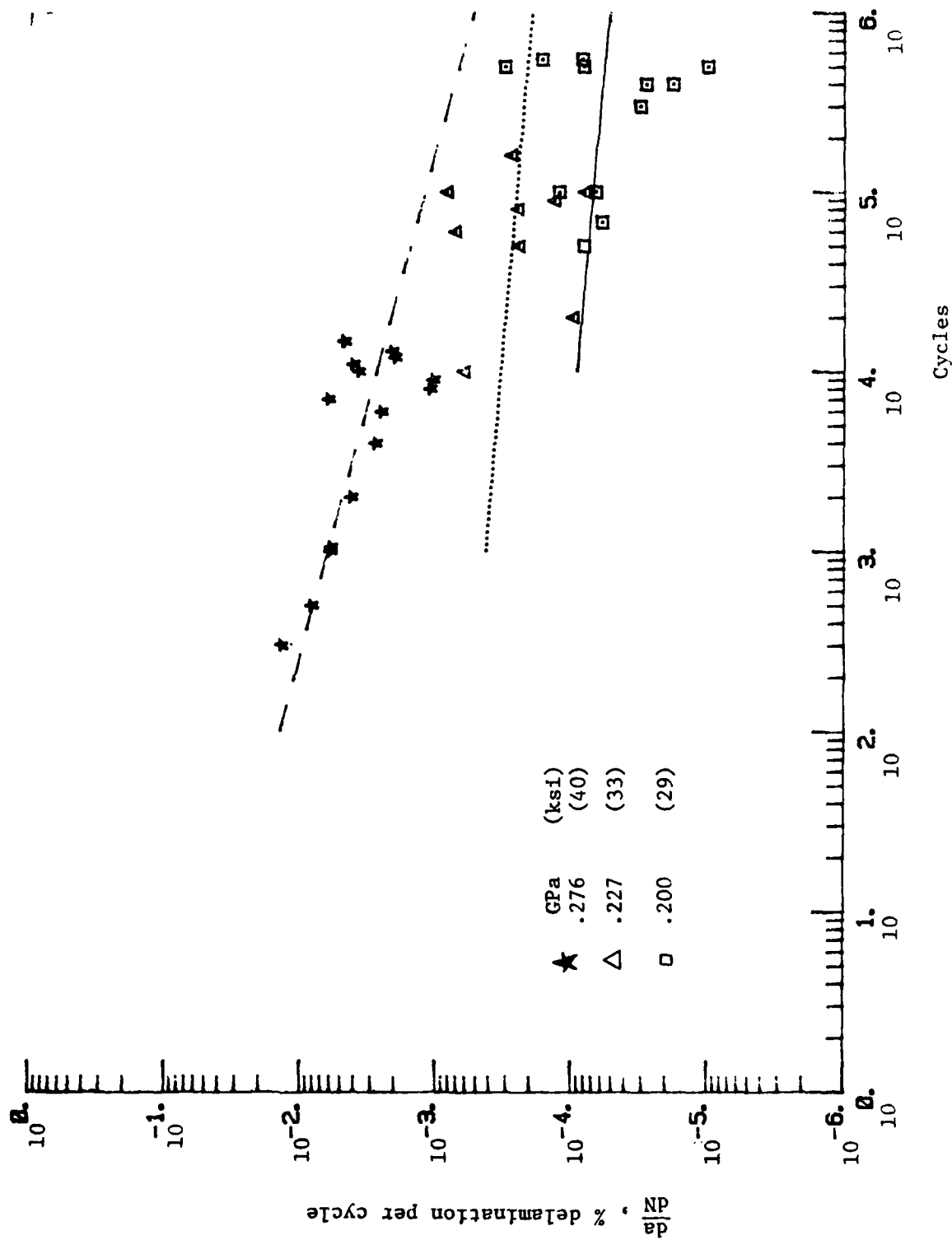


Figure 5-24: Cycles vs Damage Growth Rate for (+25/90)_s.

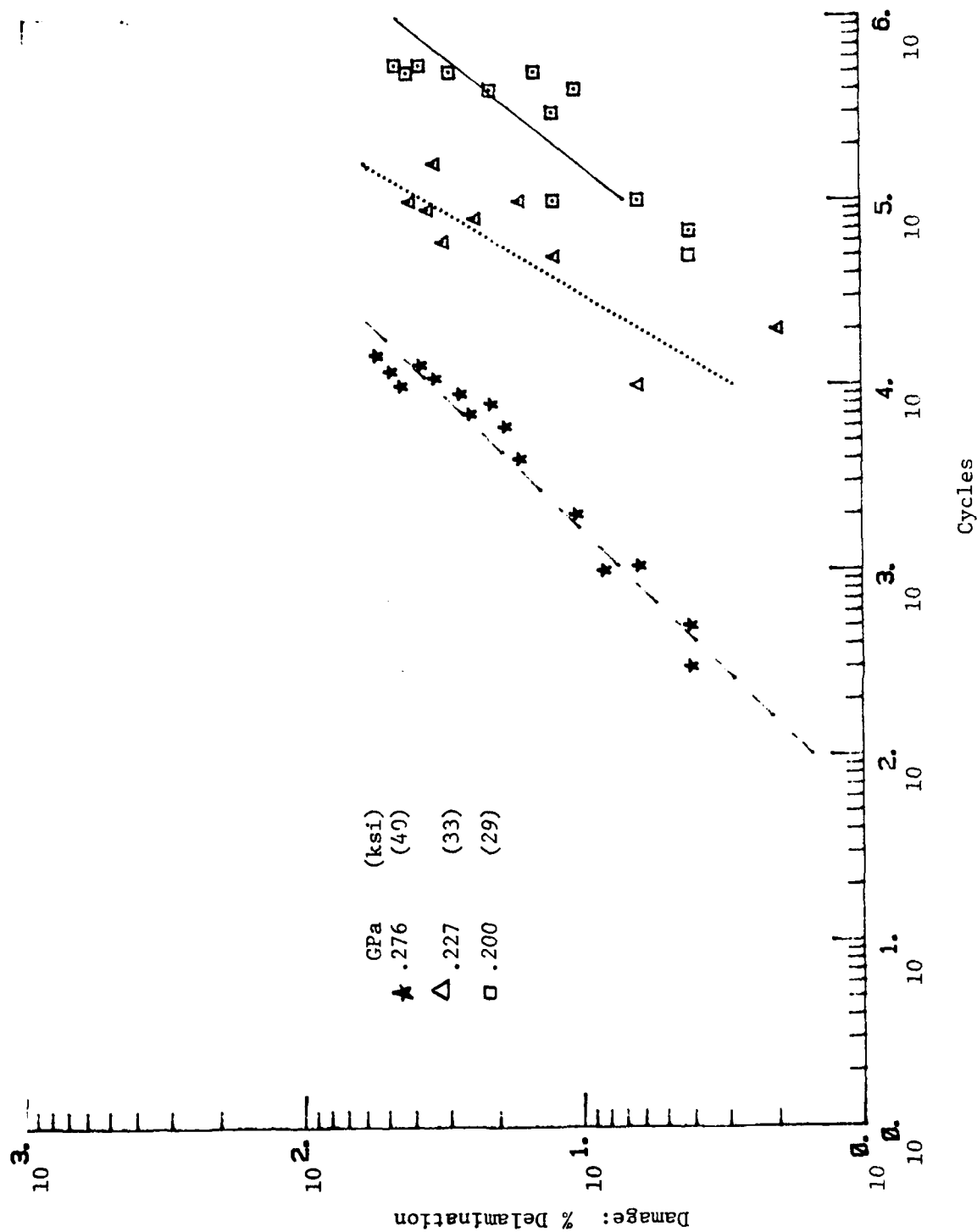


Figure 5-25: Cycles vs Percent Delamination for (+25/90)_s.

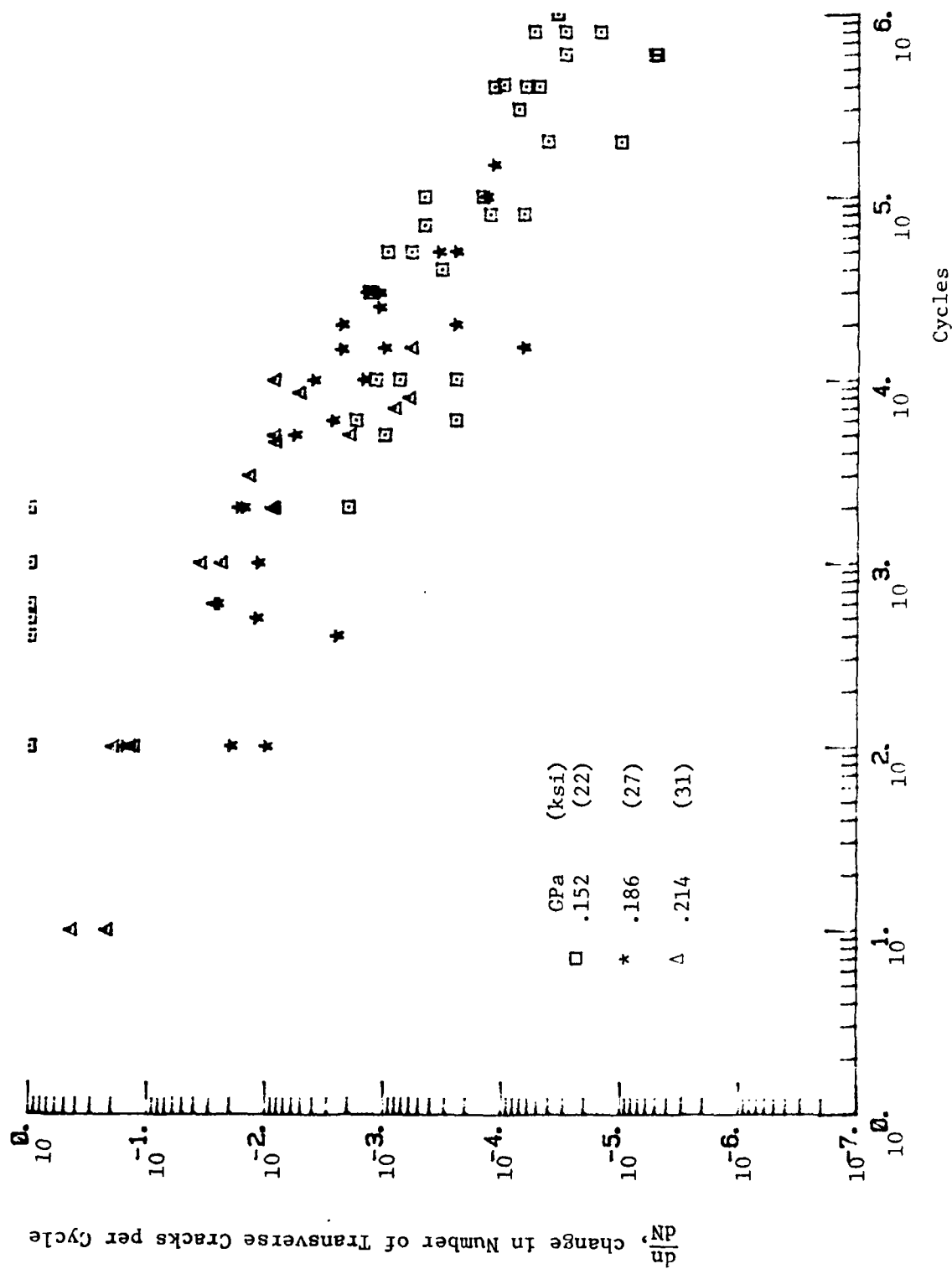


Figure 5-26: Damage Rate vs. Cycles for Transverse Cracking in ($\pm 25/90_2$) Laminate

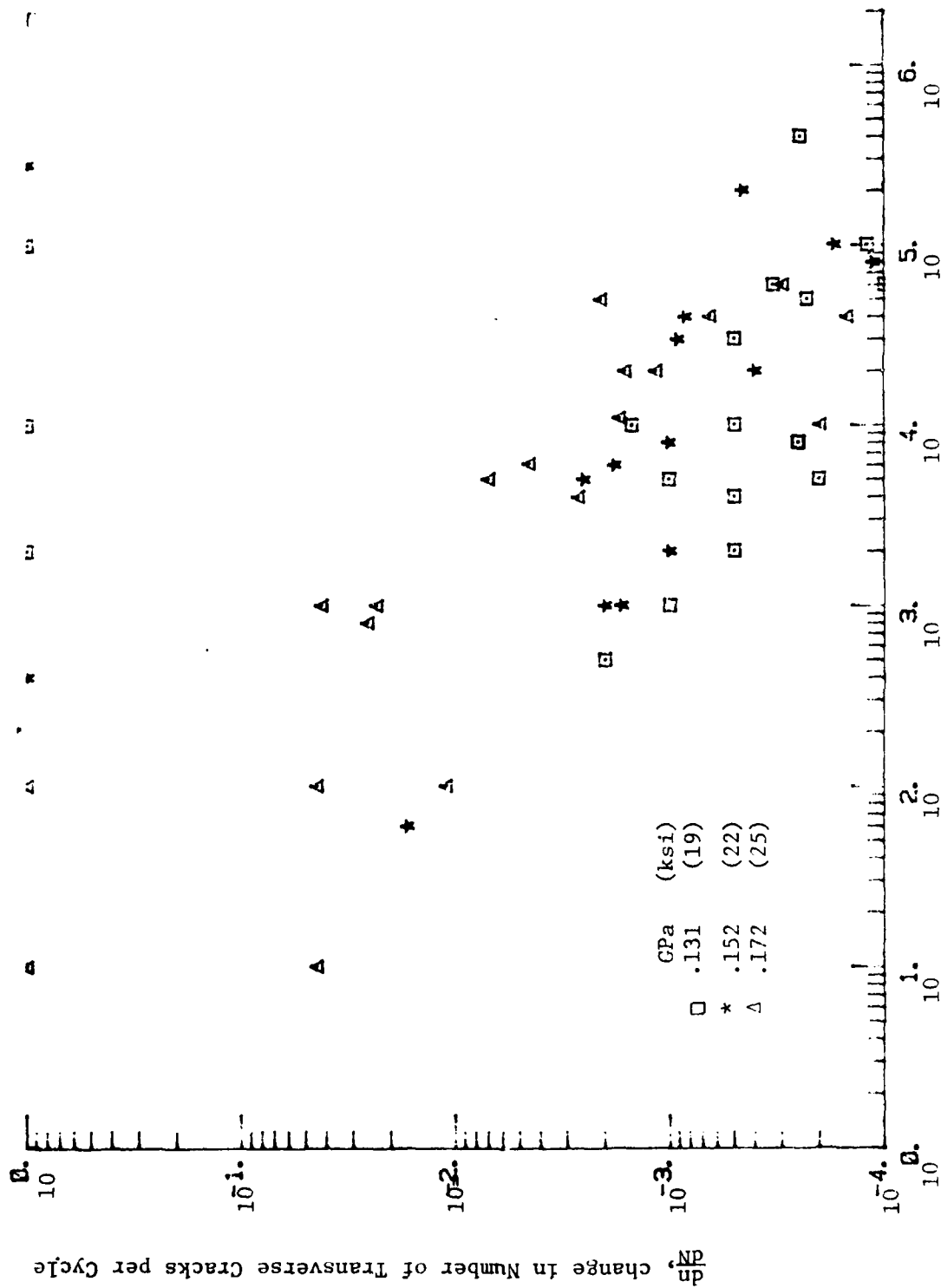


Figure 5-27: Damage Rate vs. Cycles for Transverse Cracks in $(\pm 25/90)_3$ Laminate

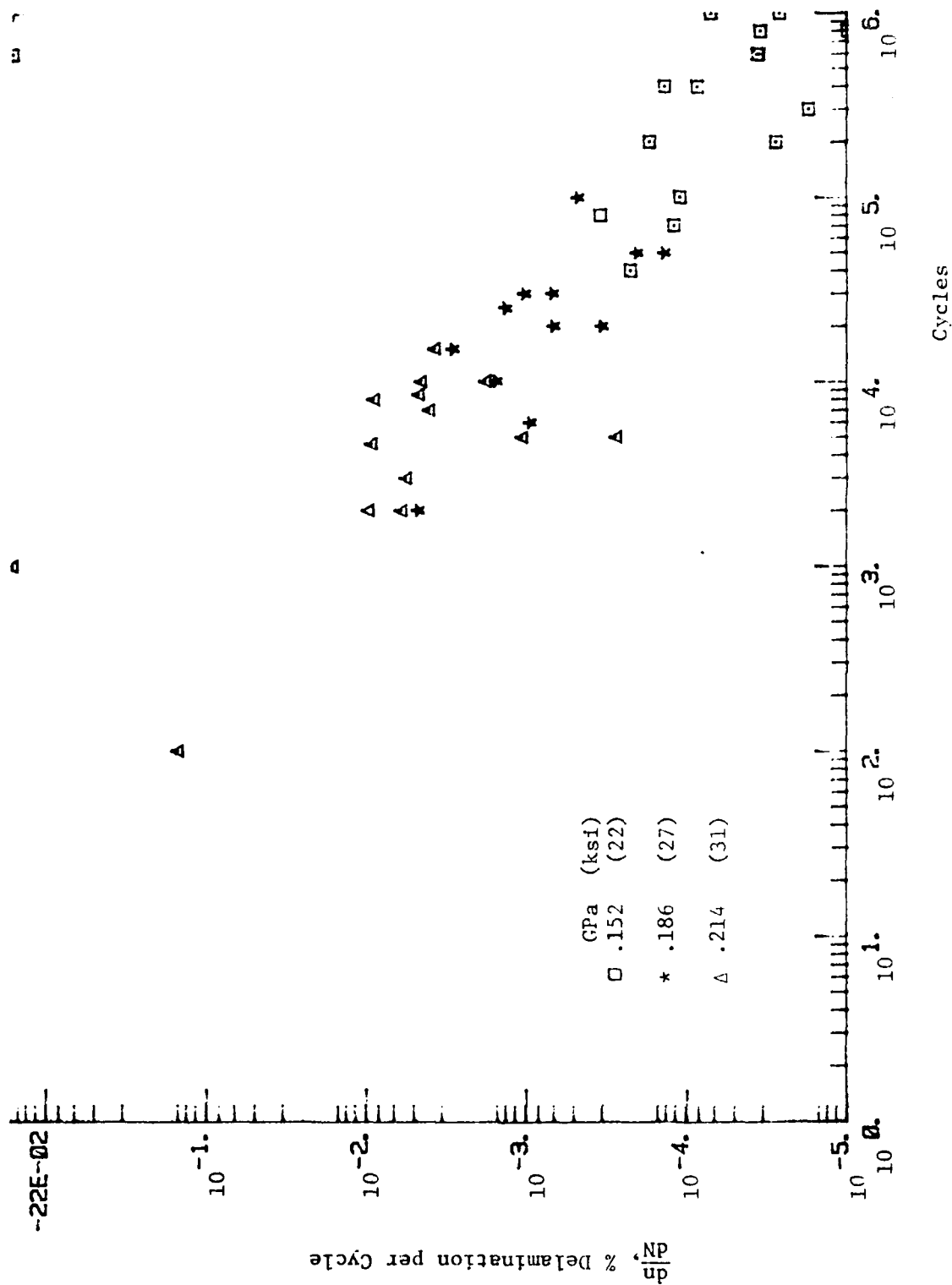


Figure 5-28: Damage Rate vs. Cycles for Delamination in $(\pm 25/90_2)_s$ Laminate

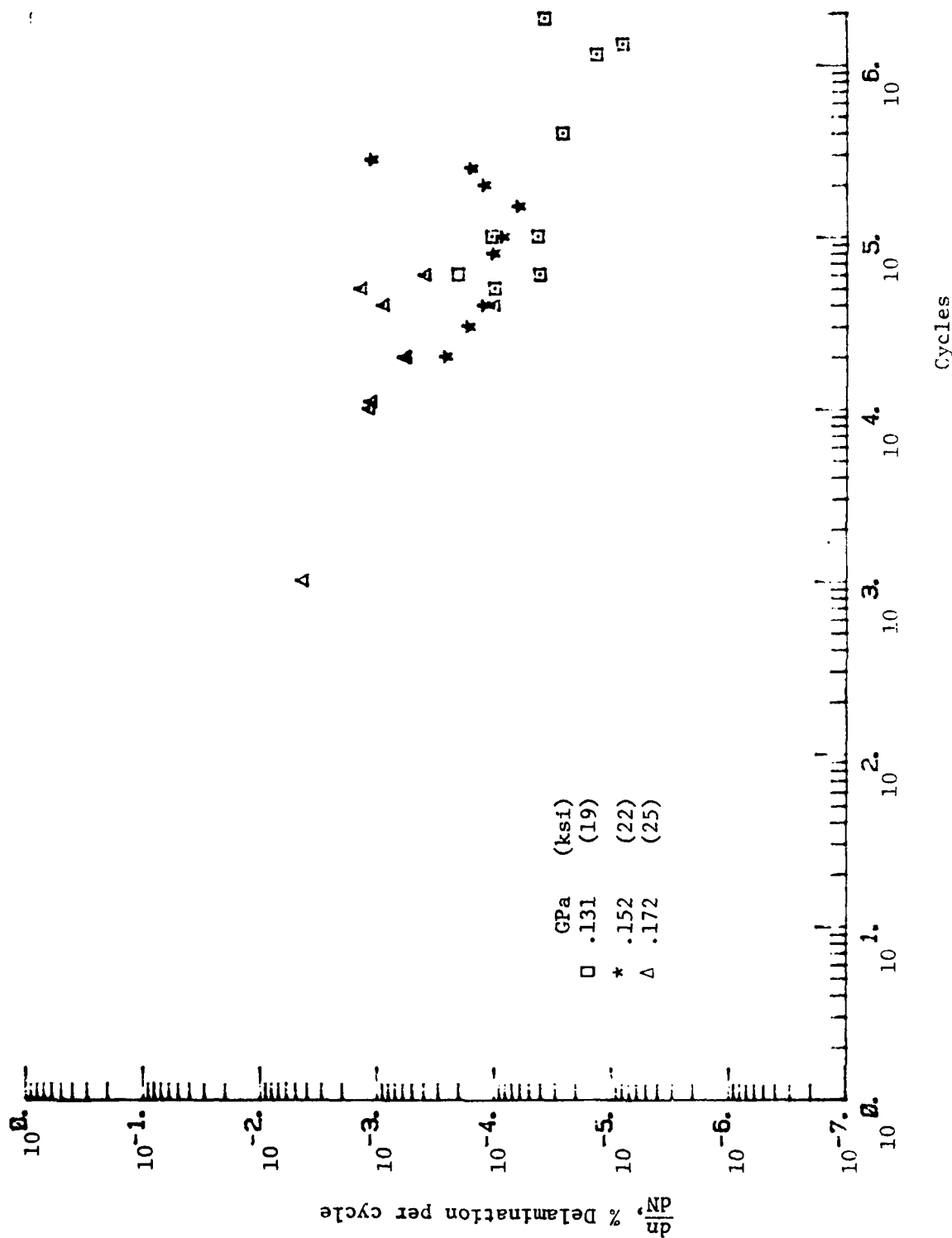


Figure 5-29: Damage Rate vs. Cycles for Delamination in $(\pm 25/90)_3$ Laminate

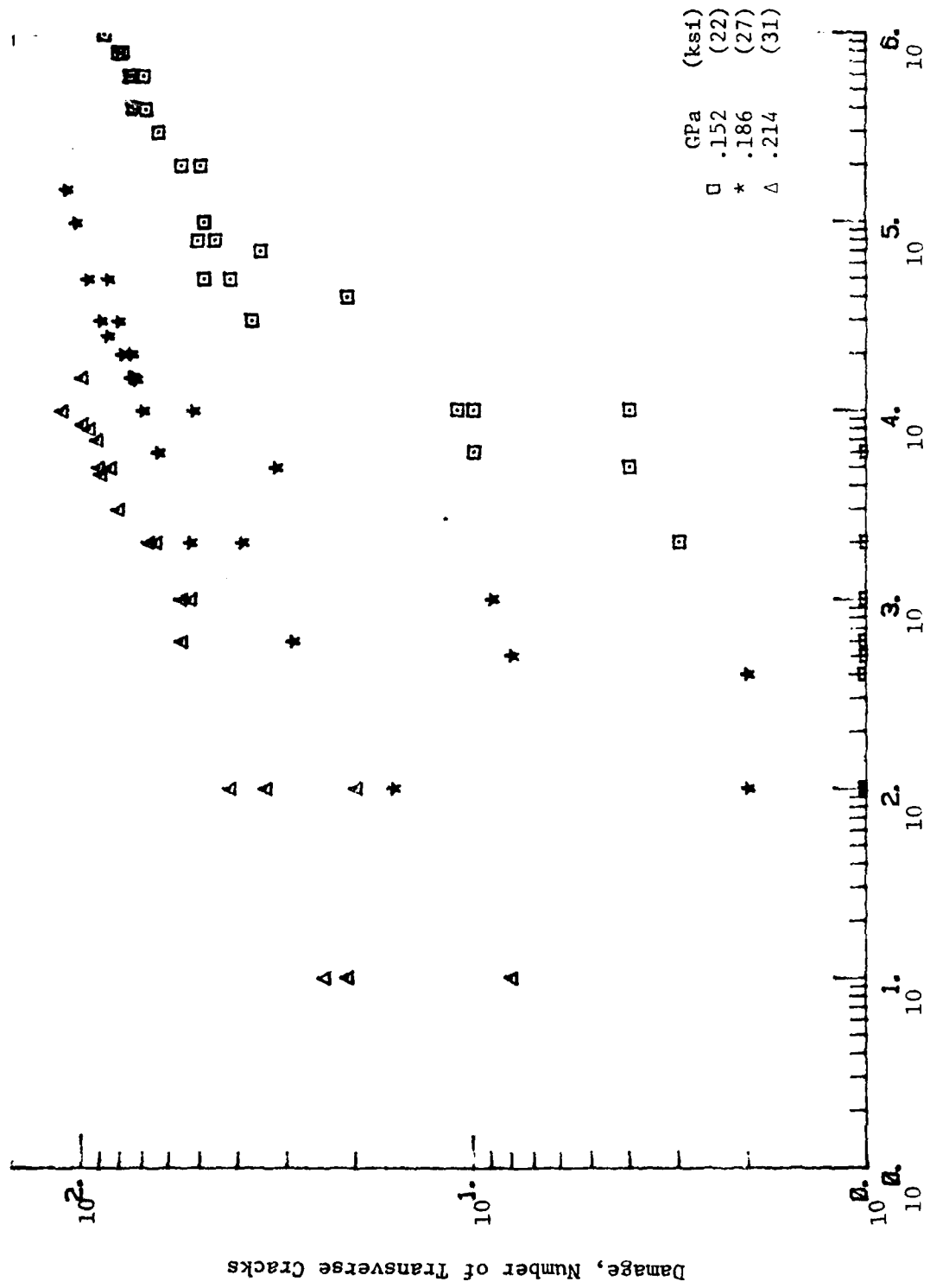


Figure 5-30: Number of Transverse Cracks vs. Cycles for $(+25/90)_2$ Laminate

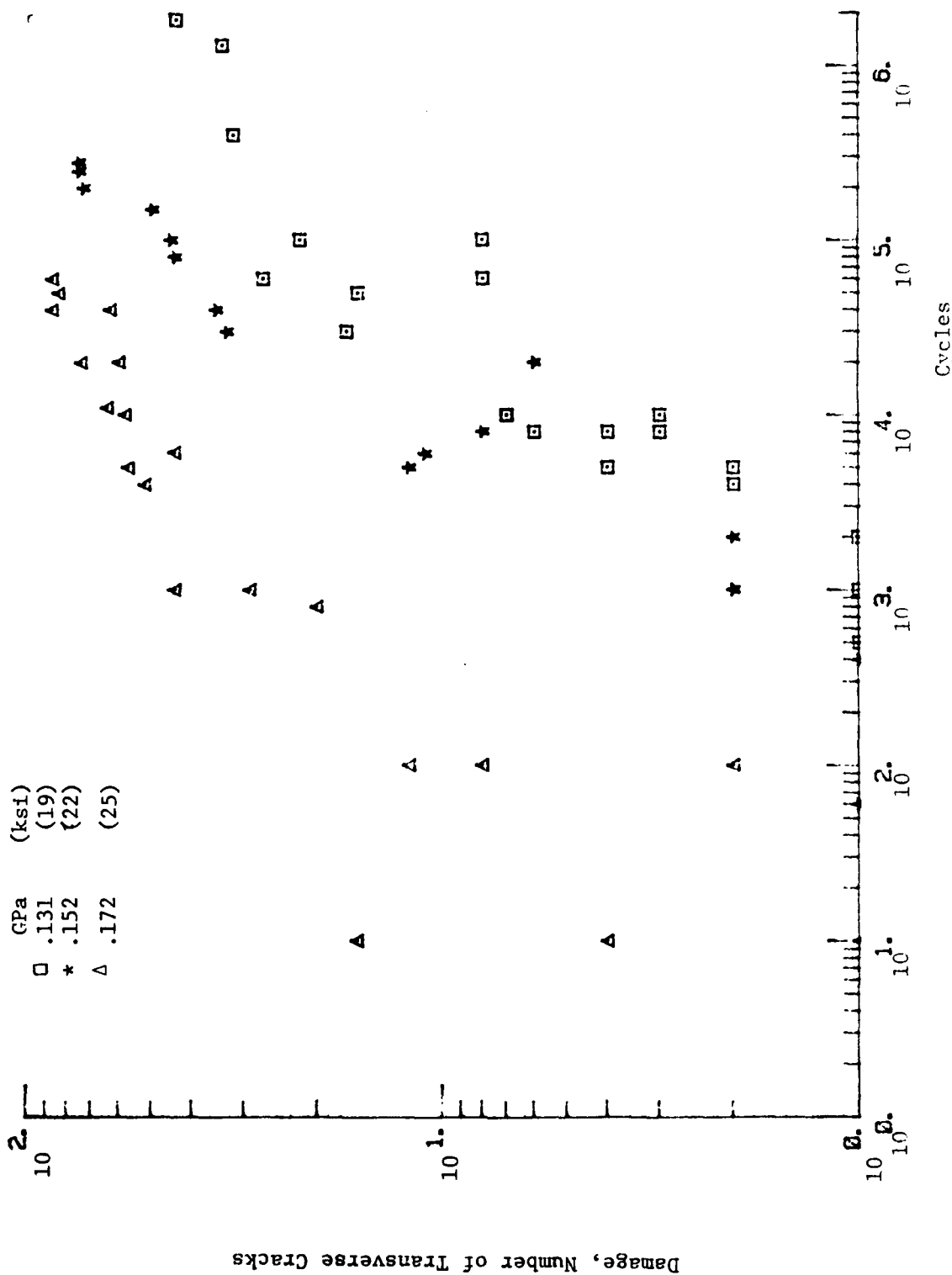


Figure 5-31: Number of Transverse Cracks vs. Cycles for $(+25/90)_3$ Laminate

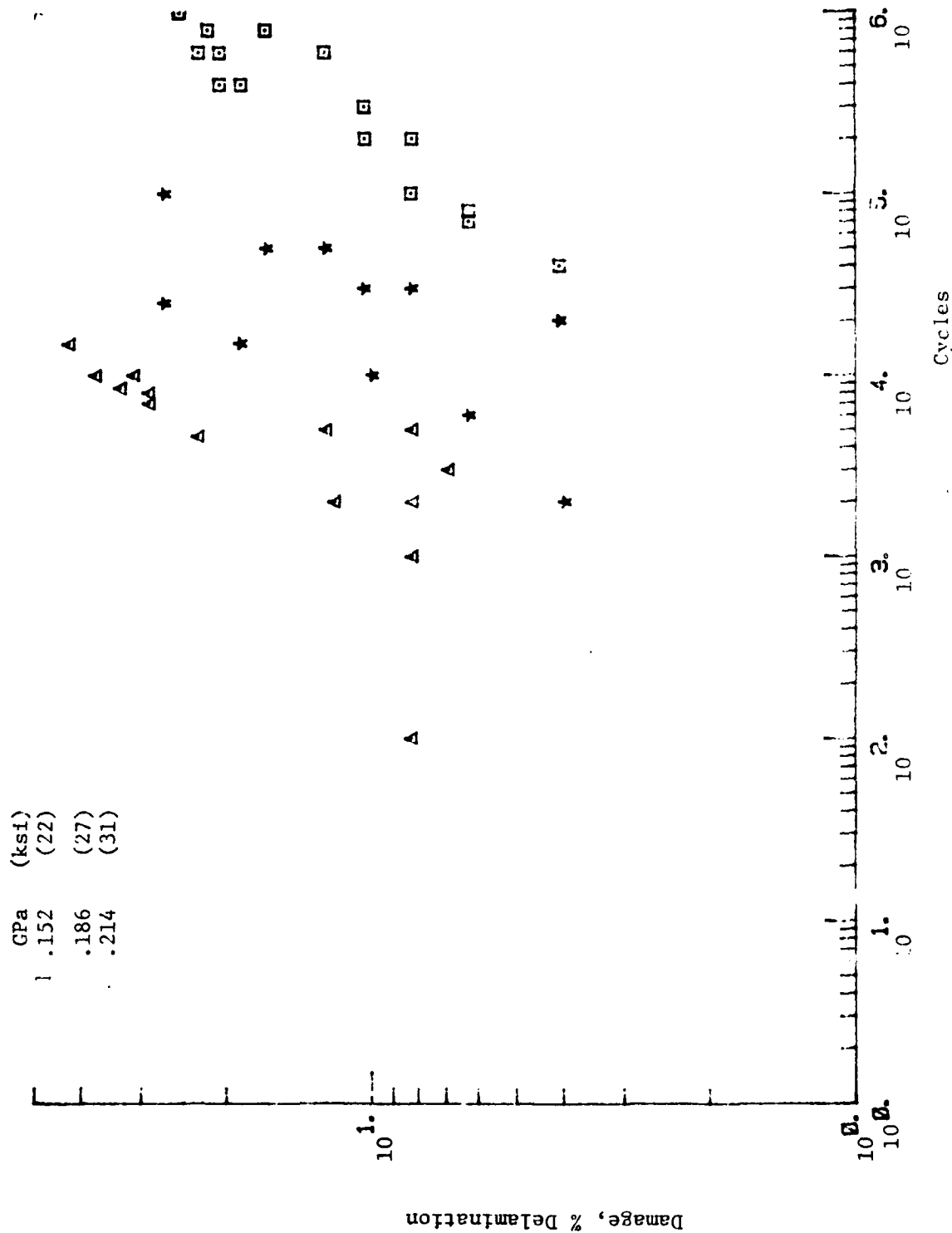


Figure 5-32: % Delamination vs. Cycles for $(\pm 25/90)_2$ Laminate

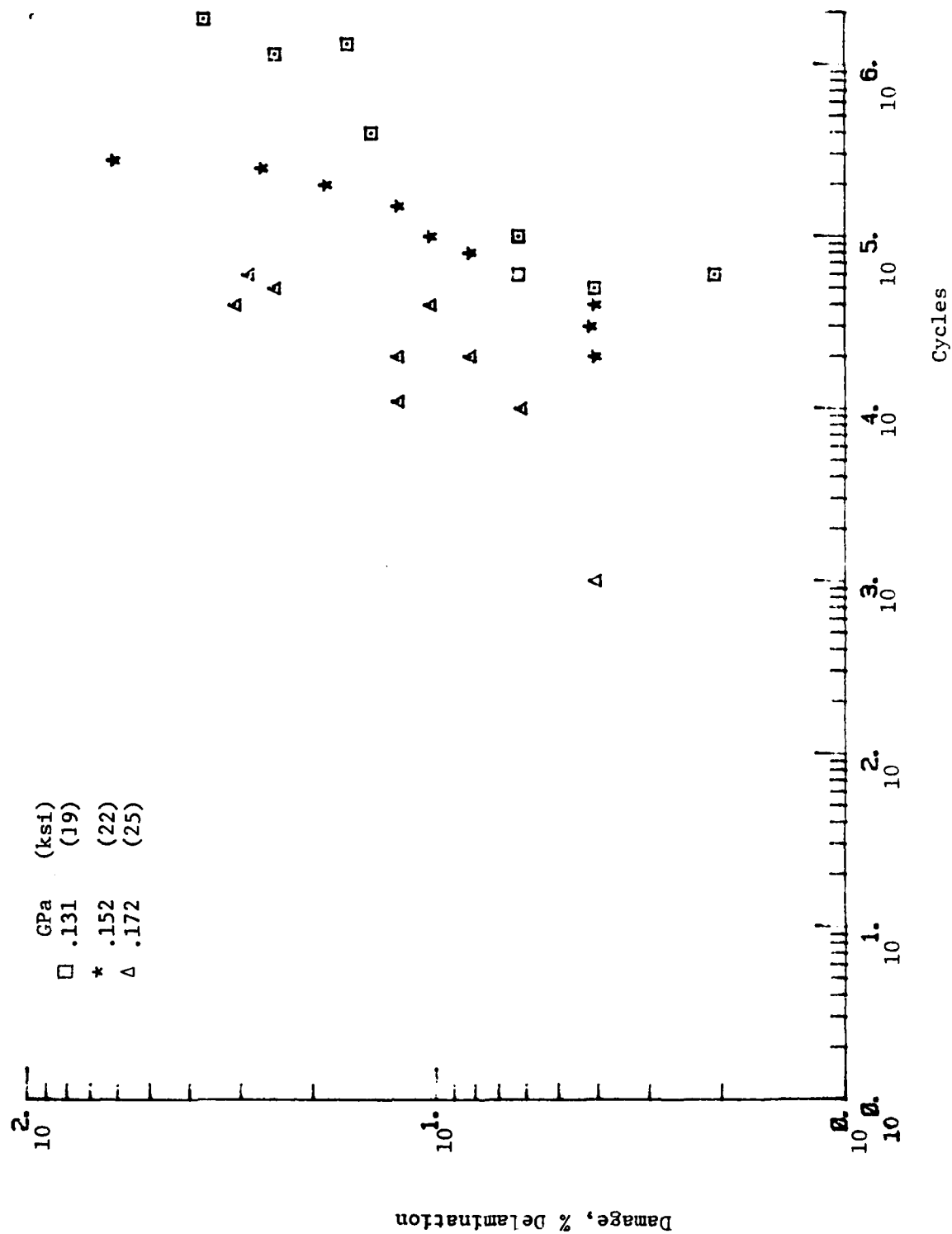


Figure 5-33: % Delamination vs. Cycles for ($\pm 25/90$)₃ Laminate

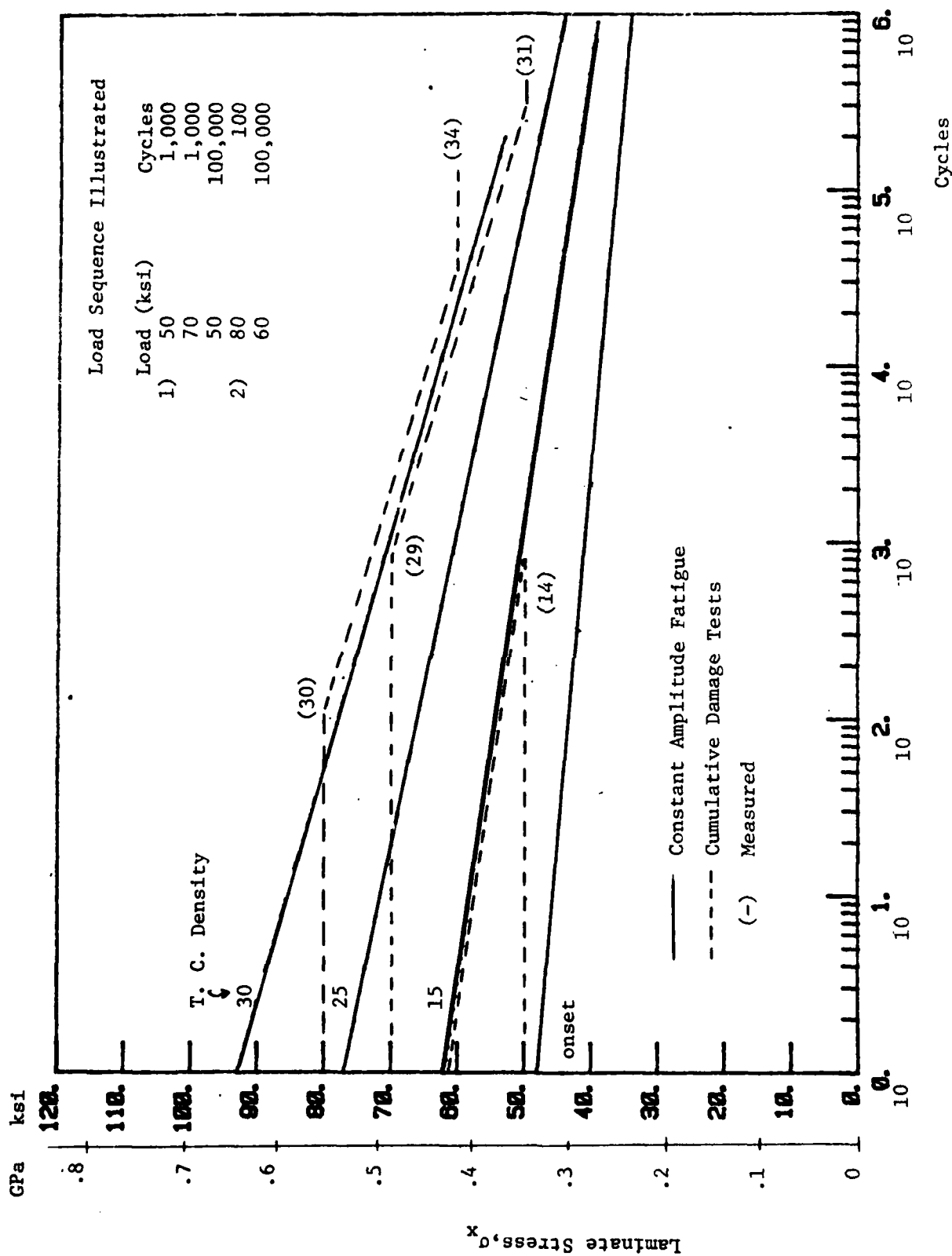


Figure 5.34: Cumulative Damage Tests: $(0/90)_2$ s.

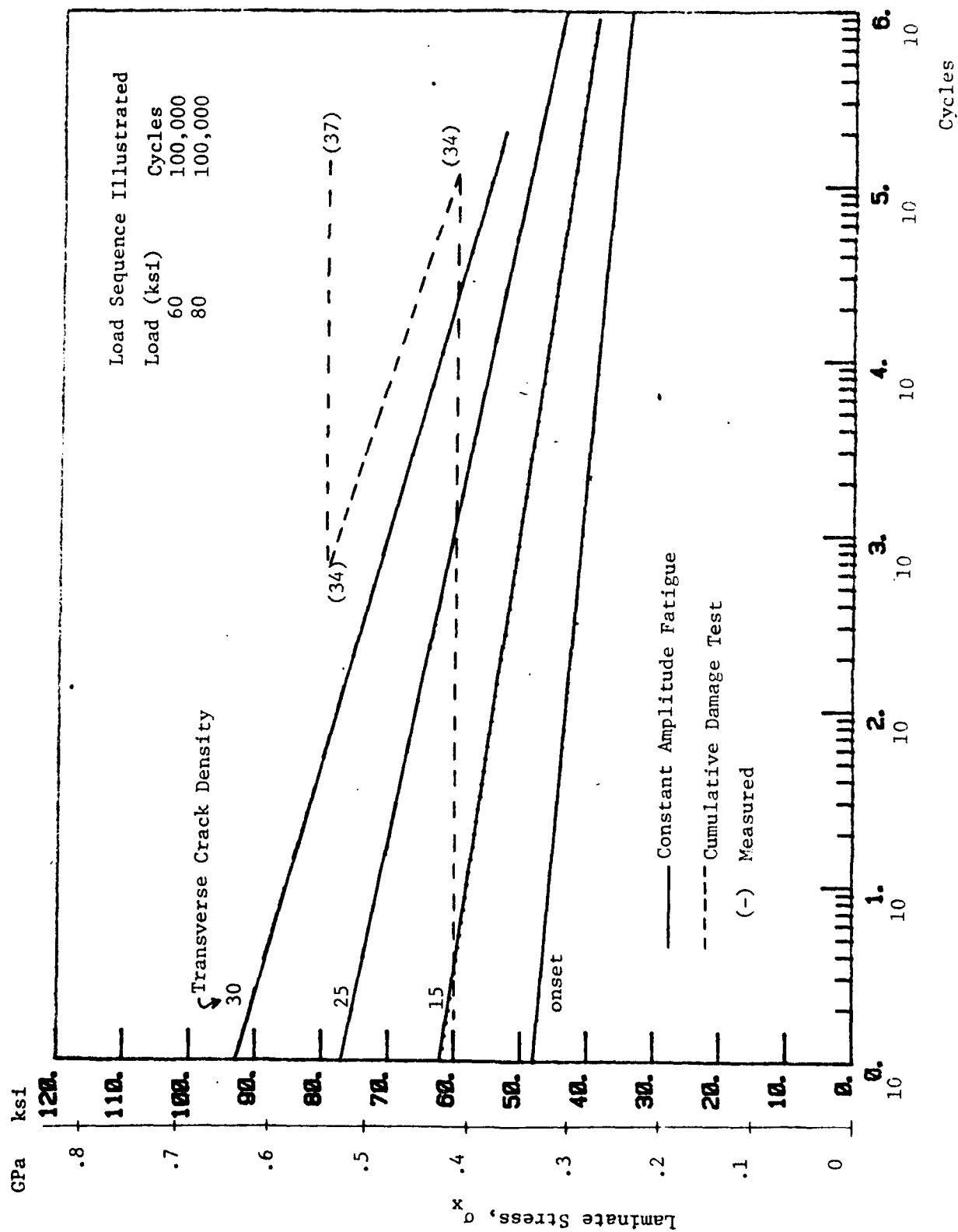


Figure 5.35: Cumulative Damage Tests: $(C_2/50)_2$ s.

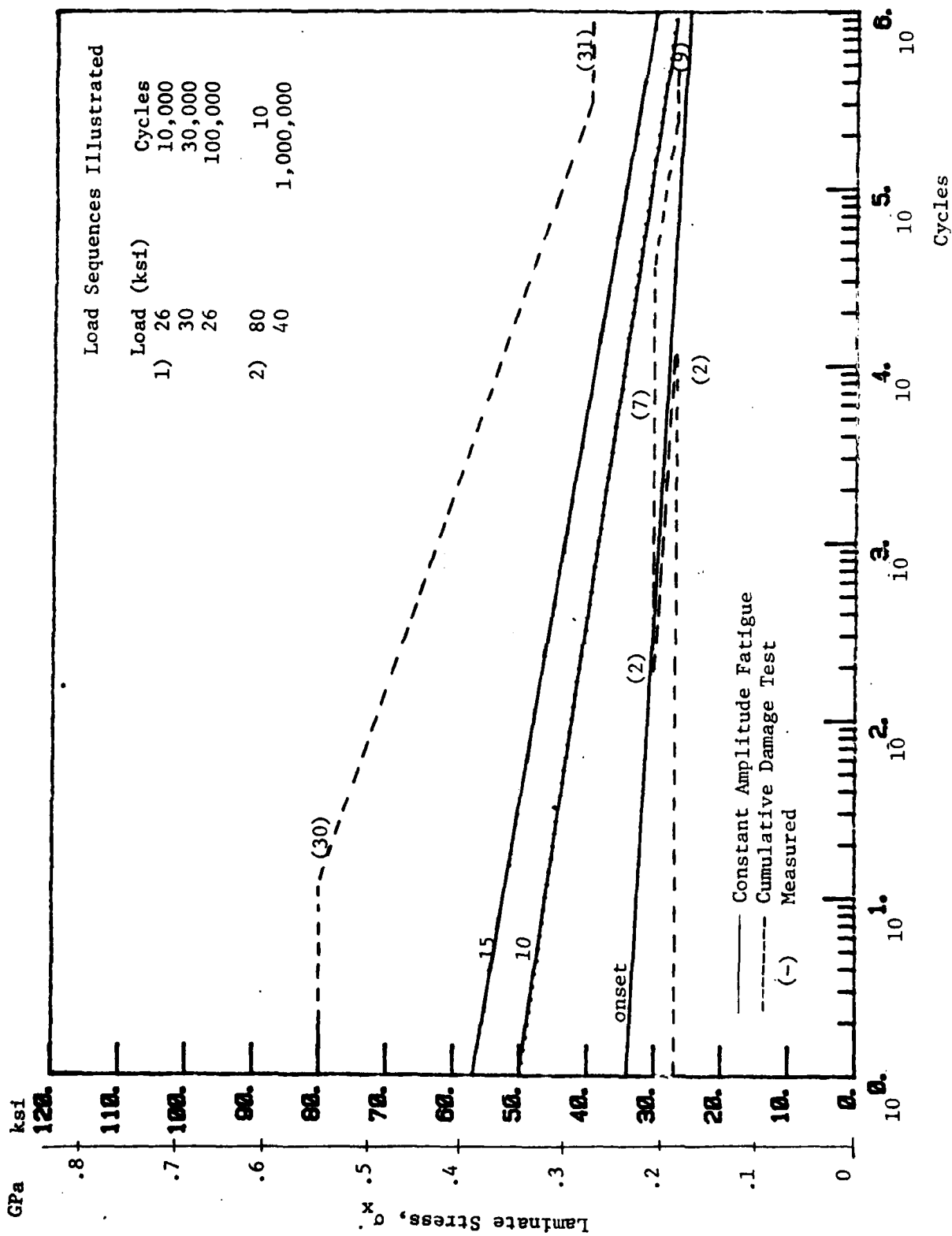


Figure 5.36: Cumulative Damage Tests: $(0_2/90_3)_s$

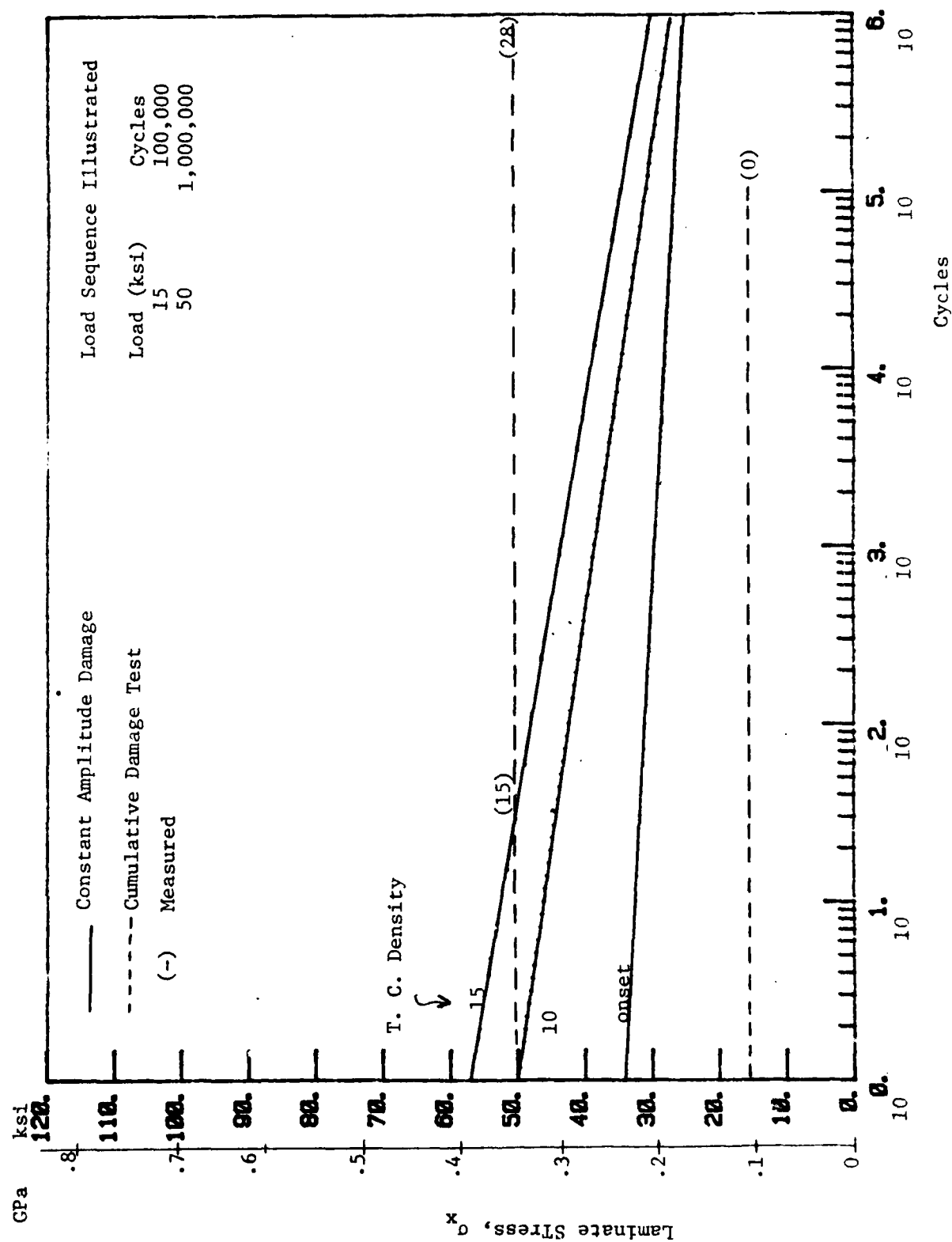


Figure 5.37: Cumulative Damage Tests: ($O_2/90_3$)_s.

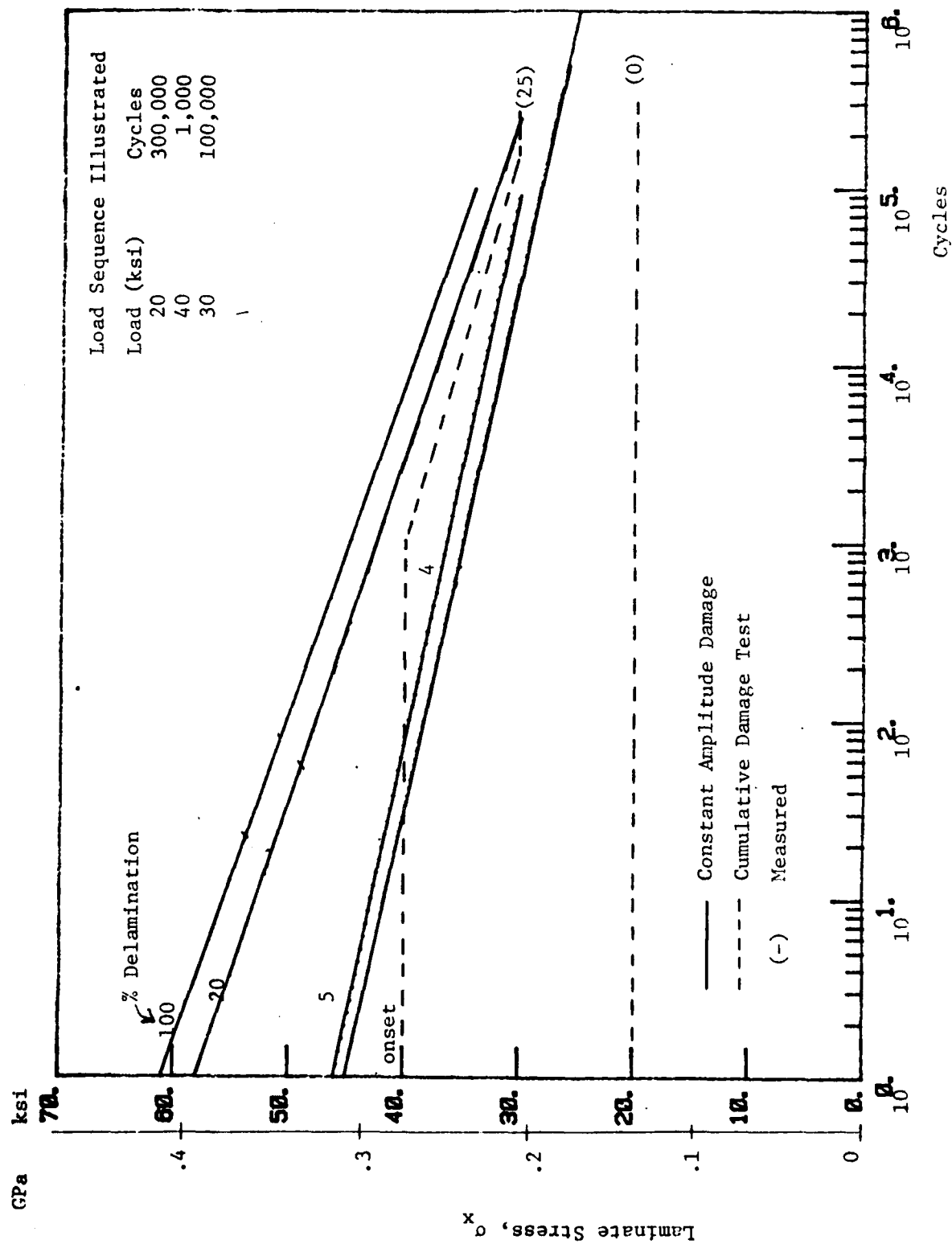


Figure 5.38: Cumulative Damage Tests: $(\pm 25/90)_s$.

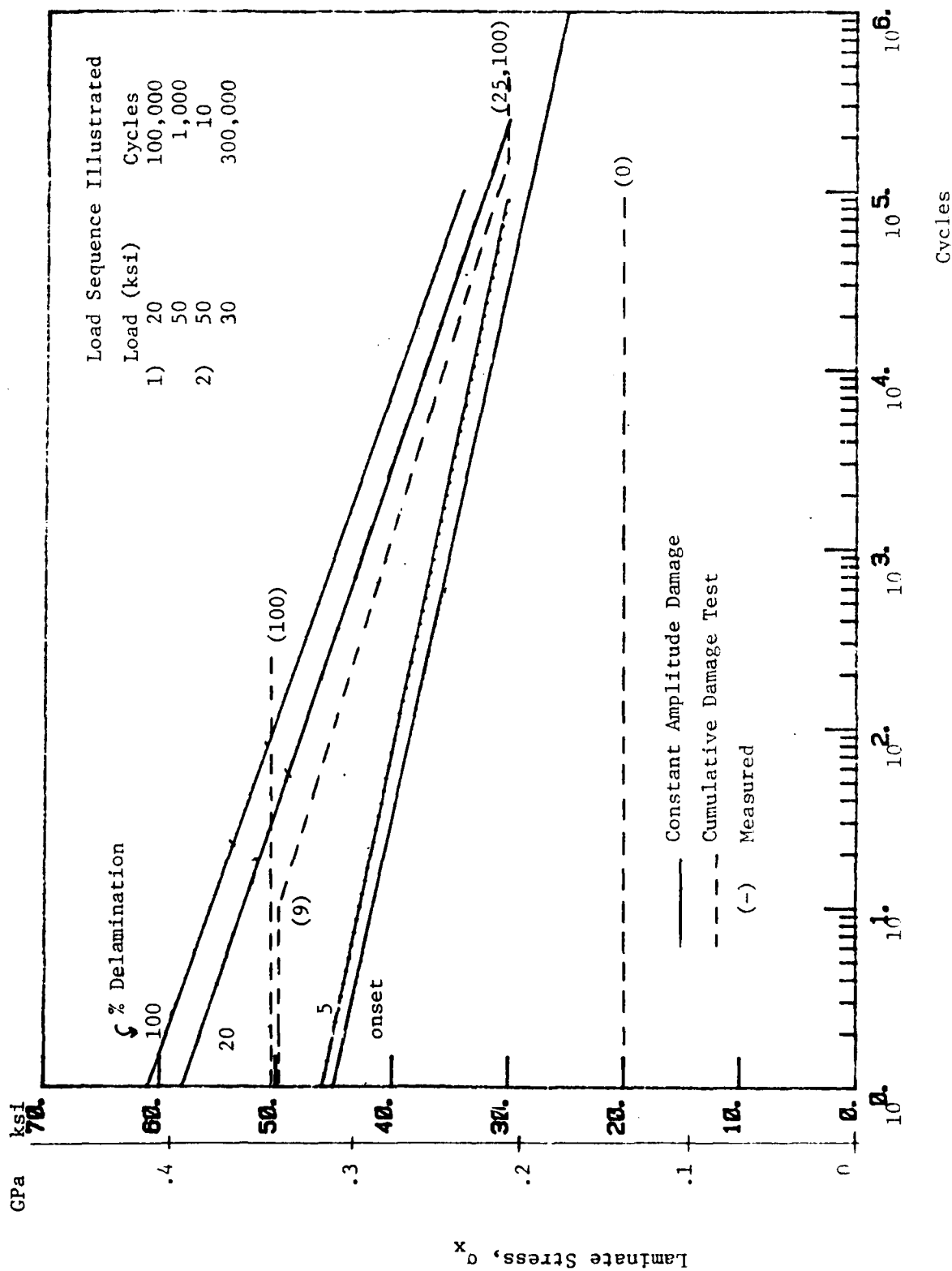


Figure 5.39: Cumulative Damage Tests: $(\pm 25/90)_s$.

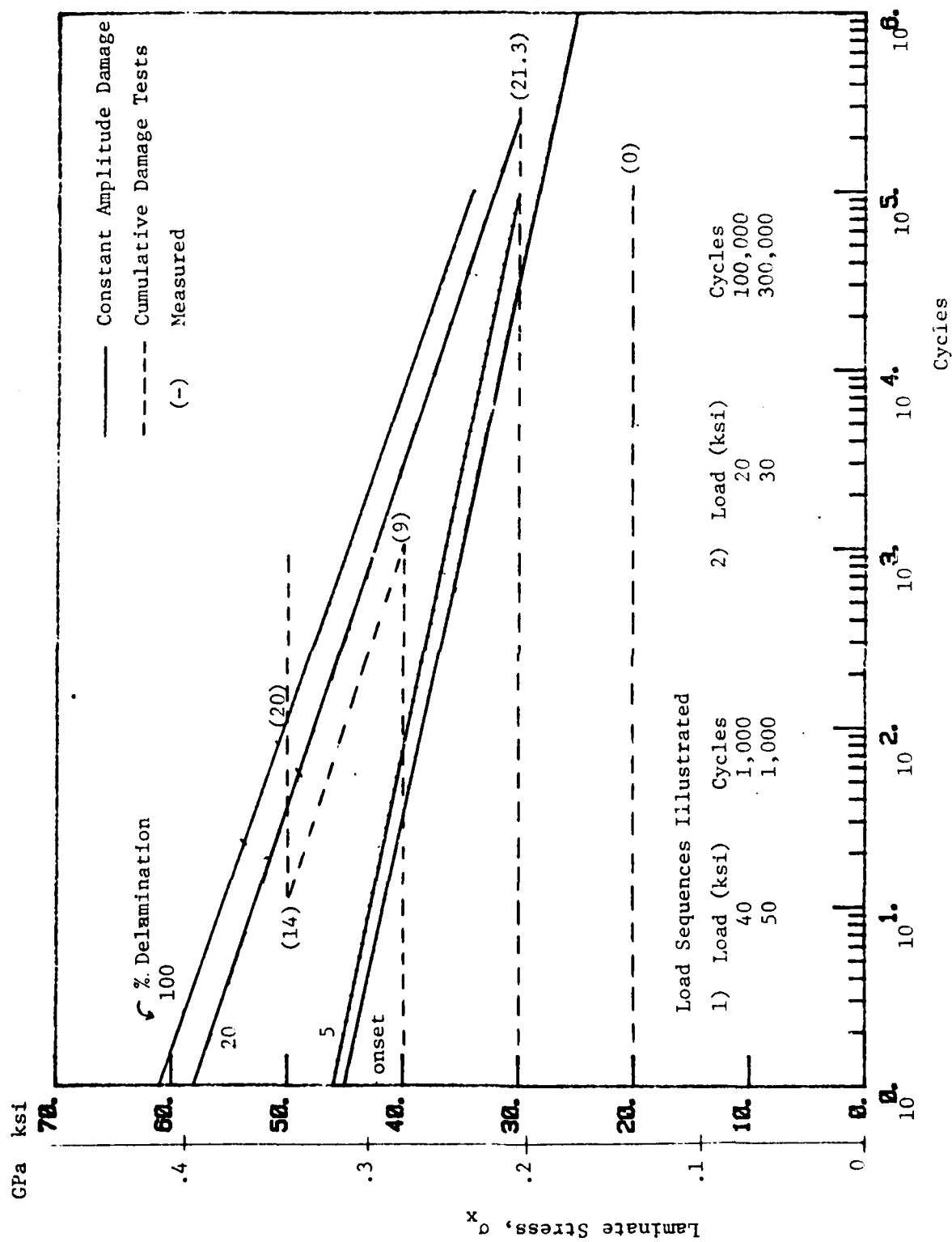


Figure 5.40: Cumulative Damage Tests: $(\pm 25/90)_s$.

AD-A122 859

CUMULATIVE DAMAGE MODEL FOR ADVANCED COMPOSITE
MATERIALS(U) DYNA EAST CORP WYNNWOOD PA
P C CHOU ET AL SEP 82 AFWAL-RR-82-4083

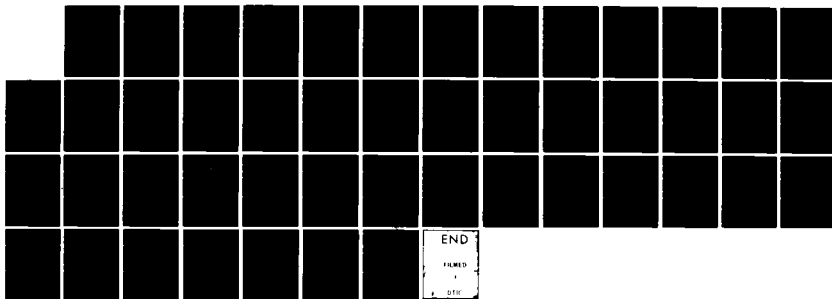
3/3

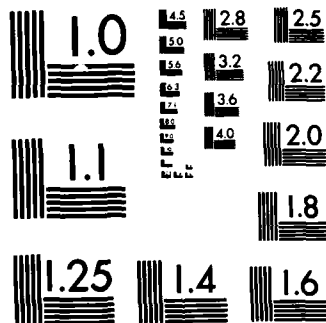
UNCLASSIFIED

F33655-80-C-5039

F/G 11/4

NL





MICROCOPY RESOLUTION TEST CHART
NATIONAL BUREAU OF STANDARDS-1963-A

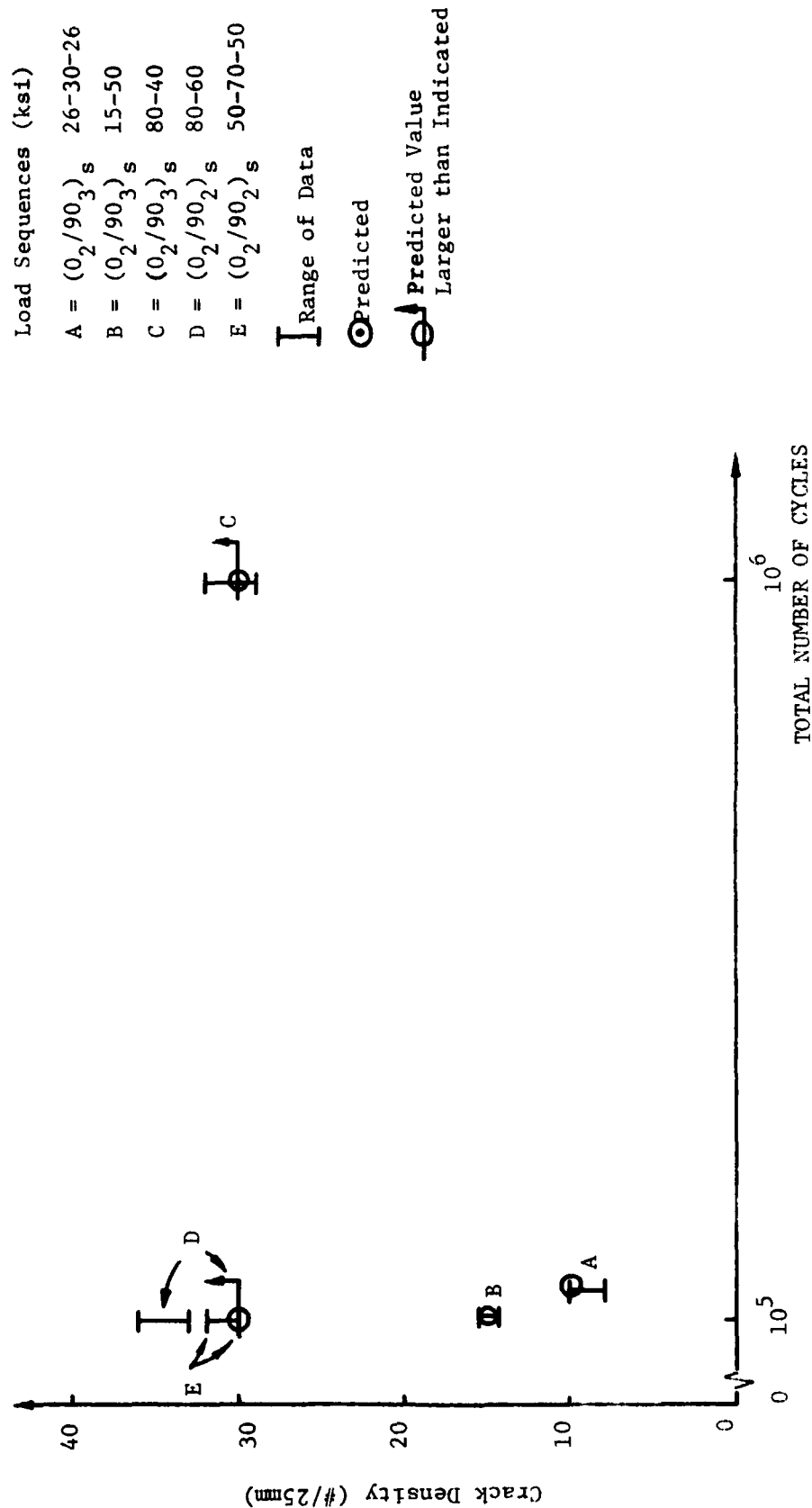


Figure 5-41: COMPARISON OF PREDICTED AND OBSERVED TRANSVERSE CRACK DENSITY AT COMPLETION OF CUMULATIVE DAMAGE TESTS.

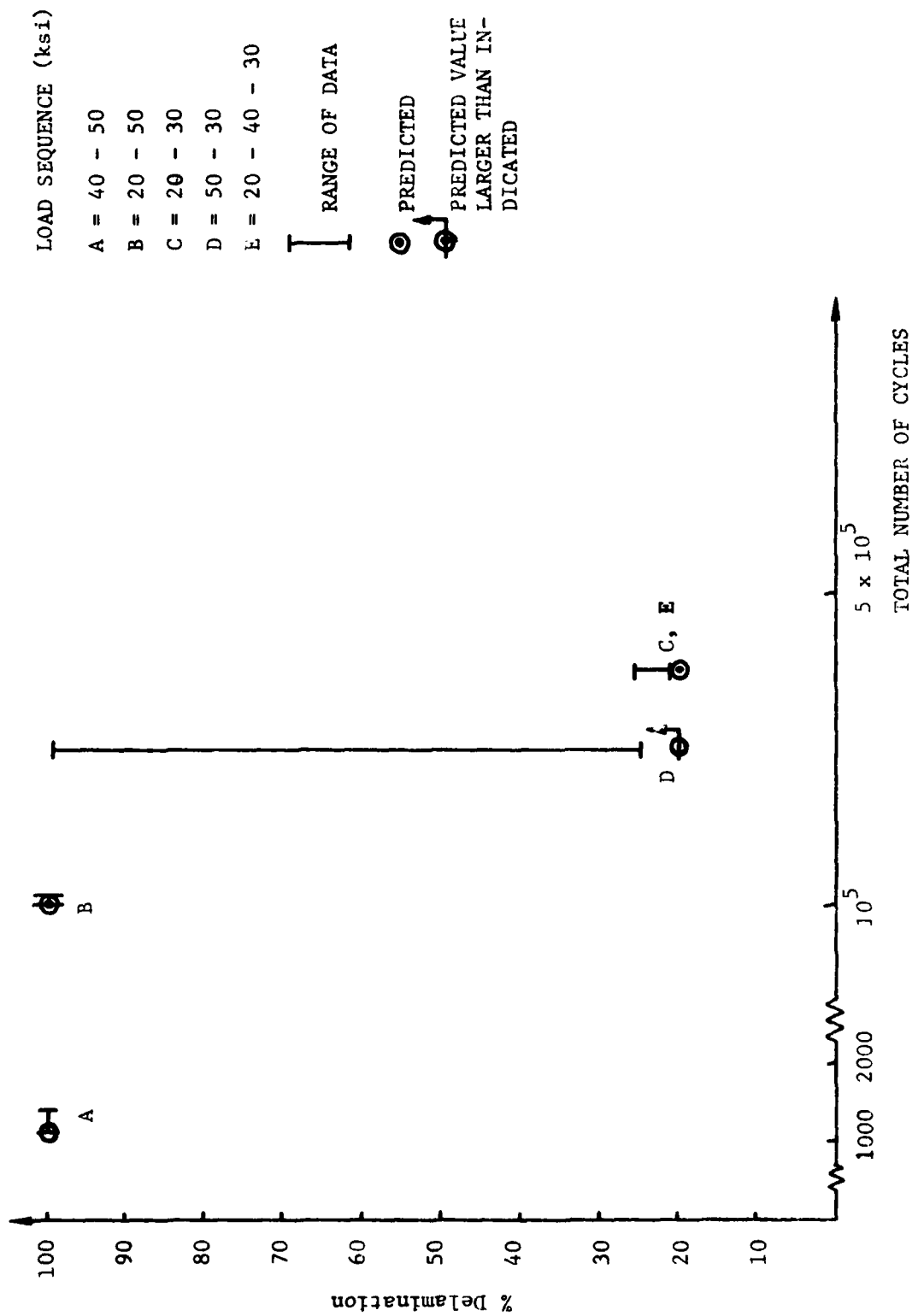


Figure 5.42: COMPARISON OF PREDICTED AND OBSERVED % DELAMINATION AT COMPLETION OF CUMULATIVE DAMAGE TESTS OF ($\pm 25/90$)_s LAMINATE.

VI. SUMMARY AND RECOMMENDATIONS

In this report, we have presented the research results obtained during Phase I of the AFML sponsored program, A Cumulative Damage Model for Advanced Composites, under contract F33615-80-C-5039. In this section, these results will be summarized and recommendations for future work will be presented.

There are five major steps to the approach to the development of a cumulative damage model. These are:

- 1) Development of the basic fracture mechanics approach for the static onset of transverse cracking and edge delamination.
- 2) Development of a static model for multiple transverse cracks.
- 3) Development of the fatigue model for the two damage modes.
- 4) Extension of the fatigue model to cumulative damage, and
- 5) Extension to final laminate failure.

The development of the static onset model of step 1 was previously performed by Wang and Crossman [19-26]. The finite element code they developed for the calculation of strain energy release rate was implemented on an HP-1000 computer system under this project.

A literature review on failure modes and mechanisms in composites and on methods of life prediction was conducted as part of steps 2 through 5. A summary of this review, with particular emphasis placed on transverse cracking and delamination, has been included as Section 2 of this report.

A static model for multiple transverse cracks has been developed by assuming the existence of a distribution of initial defects in the material. This distribution is taken as a material property which, when combined with the deterministic load-crack length relation and with prior knowledge of the maximum number of cracks that can form in a specimen, produces a relation

between the load and the transverse crack density. Comparison of this theory and experimental results from the $(0_2/90_2)_s$ and $(0_2/90_3)_s$ laminates has shown good agreement.

The static models for transverse cracking and delamination have been extended to describe damage under constant amplitude fatigue by the introduction of a damage growth rate per cycle equation. An underlying assumption is that damage under fatigue loading of a given laminate is of the same mode as damage under static load. The general form of the growth rate equation is:

$$\frac{da}{dN} = \alpha \bar{G}^p \quad (6-1)$$

where $\bar{G} = \bar{G}(G_f, G_c)$ and α and p are determined empirically. Here, it is believed that \bar{G} embodies information such as the load, material properties, and lamination; thus, in the exact form of equation 6.1, α and p should have been calculated for both transverse cracking and delamination using assumed forms of equation 6.1. Comparison with experimental results is good. However, further experimental data are required in order to determine the exact nature of equation 6.1.

A cumulative damage model based on the concept of constant damage states has been proposed. In this model, the static load-damage relation and the constant amplitude fatigue damage-cycle relation are combined to form a relation between load and cycles. This relation is then used to form an equivalence between the number of cycles at one load that produces a given damage state and the number of cycles at another load which produces the same damage state. The results of a brief series of cumulative damage

experiments show good agreement between the observed and predicted values.

As described above, further experimental data is required in order to fix the exact form of the equations of the models and to determine the range and significance of the parameters. A sequence of tests involving the $(0_2/90_2)_s$, the $(0_2/90_3)_s$ and the $(\pm 25/90)_s$ laminates is planned for the following phase of this project. These tests will involve different fatigue load levels and different environmental conditions than the tests performed during Phase I. In addition, a study of a more realistic laminate, such as a quasi-isotropic, is planned.

Several questions remain to be resolved analytically. First is the description of the delamination under fatigue load. Here, it is felt that further study of the random distribution of pre-existing edge flaws will be useful. Second is the analysis of laminates that experience several modes of damage before final failure. This falls, however, under the more general topic of extending the fatigue damage models developed here to the determination of final failure of the laminate.

We can classify the damage progression to final failure in laminates under tensile load into three types. A type I sequence is the formation of transverse cracks in the off-axis plies followed by fiber breakage in the load-carrying plies which then produces final failure. Type II shows transverse cracking followed by a delamination that initiates at the transverse crack tip and that grows in the load direction. Type III shows delamination which grows in the direction normal to the applied load along with transverse cracks which form under the delaminated region. These types of damage progression are shown schematically in figure 6.1.

The model for the type III laminate has been established during Phase I.

This model, though developed for free-edge delamination, may be applied to internal delaminations as long as the two-dimensional field equations and the one-dimensional growth assumptions are valid.

It is felt that the current energy release rate approach may be used to describe both the type I and II failures. For the type I sequence, the transverse cracking portion has been modeled in Phase I. This model may be extended to include fiber breakage by assuming that the 0° -layer is a homogeneous anisotropic layer. When a transverse crack is arrested at the 0° interface, it is assumed that the process of arresting the crack produces damage in the 0° -layer. This damage may be idealized as an equivalent crack in the homogeneous layer. The existing finite element code can then be used to calculate the energy release rate as this crack extends through the 0° -layer. Thus, a model similar to the existing transverse cracking model would be developed. Of course, the value of G_c and the extent of damage done by an arrested crack needs to be determined experimentally.

For the type II sequence, the finite element code may be used to calculate the energy release rate for the delamination (which is a combined mode I and mode II). The properties of the 90° -layers may be reduced to reflect the presence of the transverse cracks in this layer. For this case, final failure may occur when the delaminated region has propagated throughout the specimen or when the 0° -layer fails. Here, one approach to failure of the 0° -layer is through a probabilistic chain of bundles concept. As the delaminated region grows larger, the length of the unsupported 0° region becomes larger and thus the probability of failure of the 0° -layer increases. Limited work on this type of model was done by Law [25] for the static load case. Under this program, this model would be extended to fatigue.

TYPES OF LAMINATES

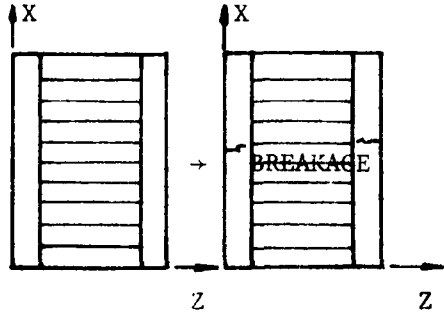
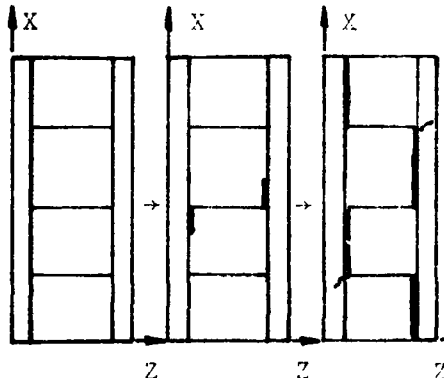
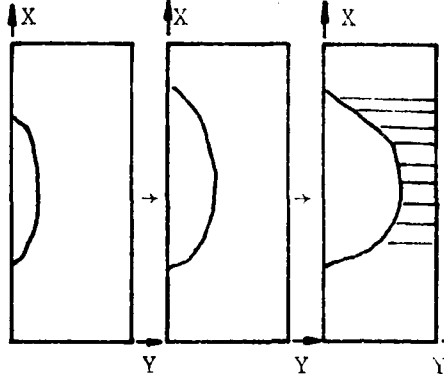
FAILURE TYPES	TYPICAL LAMINATES	FAILURE SEQUENCE
<p>I.</p> <p>T. C. → FIBER</p> <p>BREAKAGE → FAIL</p>	<p>$(0_2/90_2)_s$</p> <p>$(0_2/90_3)_s$</p>	
<p>II.</p> <p>T. C. → DEL._{y→x}</p> <p>→ FAIL</p>	<p>$(0_2/90_n)_s$</p> <p>$n \geq 4$</p> <p>$(\pm 25/90_n)_s$</p> <p>$n \geq 4$</p>	
<p>III.</p> <p>DEL_{x→y} → T. C.</p> <p>→ FAIL</p>	<p>$(\pm 25/90_n)_s$</p> <p>$n \leq 3$</p>	

Figure 6-1: Schematic of Damage Progression Leading to Final Failure.

REFERENCE

- [1] Tsai, S. W. and Hahn, H. T., Introduction to Composite Materials, Technomics Publishing Co., Inc. Westport, Conn. (1980).
- [2] Pipes, R. B. and Pagano, N. J., "Interlaminar Stresses in Composite Laminates Under Uniform Axial Tension," J. Composite Materials, Vol. 4 (1970), P. 538.
- [3] Tang, S., "Interlaminar Stresses of Uniformed Loaded Rectangular Composite Plates," J. Composite Materials, Vol. 10, (1976), p. 69.
- [4] Hsu, P. W. and Herakovich, C. T., "A Perturbation Solution for Interlaminar Stresses in Composite Laminates," ASTM STP 617, (1977), p. 296.
- [5] Wang, A. S. D. and Crossman, F. W., "Some New Results on Edge Effects in Symmetric Composite Laminates," J. Composite Materials, Vol. II, (1977), p. 92.
- [6] Wang, S. S. and Choi, I., "Boundary-Layer Effects in Composite Laminates," Paper #F9-0803, AIAA/ASME/AHS 20th Structures, Structural Dynamics and Materials Conference, St. Louis, (1979).
- [7] Baker, R. M., Dena, J. R. and Pryor, C. W., "Stress Concentrations Near Holes in Laminates," J. Engineering Mechanics, ASCE, (1974), p. 477.
- [8] Rybicki, E. F. and Schmueser, D. W., "Effect of Stacking Sequence and Lay-up Angle on Free-Edge Stresses Around a Hole in a Laminated Plate under Tension," J. Composite Materials, Vol. 12, (1978), p. 314.
- [9] Pagano, N. J. and Pipes, R. B., "The Influence of Stacking Sequence on Laminate Strength," J. Composite Materials, Vol. 5, (1971), p. 229.
- [10] Whitney, J. M. and Kin, R. Y., "Effect of Stacking Sequence on the Notched Strength of Laminated Composites," ASTM STP 617, (1977), p. 229.
- [11] Bjeletich, J. G., Crossman, F. W. and Warren, W. J., "The Influence of Stacking Sequence on Failure Modes in Quasi-Isotropic Graphite-Epoxy Laminates," Failure Modes in Composites-IV, AIME, (1978).
- [12] Reifsnider, K. L., Henneke, E. G. and Stinchcomb, W. W., "Delamination in Quasi-Isotropic Graphite-Epoxy Laminates," ASTM STP 617, (1977), pp. 93-105.
- [13] Rodini, B. T. and Eisenmann, J. R., "An Analytical and Experimental Investigation of Edge Delamination in Composite Laminates," Proc. 4th Conf. Fibrous Composites, San Diego, (1978).
- [14] Aveston, J. and Killy, A., "Theory of Multiple Fracture of Fibrous Composites," J. Matl. Sciences, Vol. 8, (1973), p. 352.
- [15] Reifsnider, K. L. and Masters, J. L., "Investigation of Characteristic Damage States in Composite Laminates," ASME paper no. 78-WA/AERO-4, (1978).
- [16] Bader, M. G., Bailey, J. E., Curtis, P. T. and Parvizi, A., "The Mechanisms of Initiation and Development of Damage in Multi-Axial Fiber-Reinforced Plastics Laminates," Proc. 3rd Int. Symp. Mechanical Behavior of Materials, Cambridge, U. K., Vol. 3, (1979), p. 227.

- [17] Norita, T., "Transverse Cracking in [0/90]s Laminates of Two Resin Systems," Tech. Rep. Toray Industries, Japan, (1982).
- [18] Irwin, G. R., "Fracture," Hanbuch der Physik, Vol. V, Springer-Verlag, (1958), p. 551.
- [19] Wang, A. S. D. and Law, G. E., "Interlaminar Failure in Epoxy-Based Composite Laminates," Proc. 29th Symp. Failure Modes in Composites, NBS, (1979).
- [20] Wang, A. S. D. and Law, G. E., and Warren, W. J., "An Energy Method for Multiple Transverse Cracks in Graphite-Epoxy Laminates," in Modern Development in Composite Materials and Structures, Ed. J. R. Vinson, (1979), p. 17.
- [21] Wang, A. S. D. and Crossman, F. W., "Initiation and Growth of Transverse Cracks and Edge Delamination in Composite Laminates. Part I. An Energy Method," J. Composite Materials, Vol. 14, (1980), p. 71.
- [22] Crossman, F. W. Warren, W. J. Wang, A. S. D. and Law, G. E., "Initiation and Growth of Transverse Cracks and Edge Delamination in Composite Laminates, Experimental Correlation," J. Composite Materials, Vol. 14, (1980), p. 87.
- [23] Wang, A. S. D., "Growth Mechanisms of Transverse Cracks and Ply Delamination in Composite Laminates," in Advances in Composite Materials, Proc. ICCM-III, (1980), p. 170.
- [24] Crossman, F. W. and Wang, A. S. D., "The Dependence of Transverse Cracks and Delamination on Ply Thickness in Graphite Epoxy Laminates," in Damage in Composite Materials, ASTM STP.
- [25] Law, G. E. "Fracture Analysis of [+25/90n]s Graphite-Epoxy Composite Laminates," Thesis, Drexel University, (1981).
- [26] Wang, A. S. D. and Crossman, F. W., "Fracture Mechanics of Transverse Cracks and Edge Delamination in Graphite-Epoxy Composite Laminates," Technical Report, F 49620-79-C-0206 AFOSR, (1982).
- [27] Rybicki, E. F. and Kennenen, M. F., "A Finite Element Calculation of Stress Intensity Factors by A Modified Crack Closure Integral," Eng. Fracture Mechanics, Vol. 9, (1977), pp. 931-938.
- [29] Cullen, J. S., "Mode-I Delamination of Unidirectional Graphite-Epoxy Composite Under Complex Load Histories," Thesis Texas A & M University, (1981).
- [28] Rybicki, E. F. Schmueser, D. W. and Fox, J., "An Energy Release Rate Approach for Stable Crack Growth in the Free Edge Delamination Problem," J. Composite Materials, Vol. II, (1977), p. 470.
- [30] Williams, D., "Mode-I Transverse Cracking in an Epoxy and a Graphite Fiber Reinforced Epoxy," Theses, Texan A & M University, (1981).
- [31] Vanderkley, P. S., "Mode-I and Mode-II Delamination Fracture Toughness of an Unidirectional Graphite-Epoxy Composite," Thesis, Texas A & M University, (1981).
- [32] Wilkins, D. J., "A Comparison of the Delamination and Environmental Resistance of a Graphite-Epoxy and a Graphite-Bismaleimide," NAV-GD-0037; Naval Air System Command, (1981).

- [33] Jurf, R. A. and Pipes, R. B., "Interlaminar Fracture of Composite Material," Tech. Report, University of Delaware, (1982).
- [34] Wang, A. S. D., Kishore, N. N. and Feng, W. F., "On Mixed-Mode Fracture in Off-axis Unidirectional Graphite-Epoxy Composites," Proc. ICCM-IV, (1982).
- [35] Rosen, B. W., "Mechanics of Composite Strengthening," in Fiber Composite Materials, Amer. Soc. Metals, (1965).
- [36] Davis, J. G., "Compressive Strength of Fiber Reinforced Composite Materials," ASTM STP 580, (1975), p. 364.
- [37] Wang, A. S. D., "Certification of Composite Aircraft Structures Under Impact, Fatigue and Environmental Conditions, Part III. Environmental Effects on Compressive Strength," NADC-TR. 78259-60, (1978).
- [38] Wang, A. S. D. and Slomiana, M., "Fracture Mechanics of Delamination-Initiation and Growth," NADC-TR-79056-60, (1982).
- [39] Tirosh, J., "The Mixed-Mode Fracture of Unidirectional Fibrous Composites," Eng. Fracture Mechanics, Vol. 13, (1980), pp. 118-127.
- [40] Mandell, J. F. and Meir, V., "Fatigue CRack Propagation in 0°/90° E-Glass/Epoxy Composites," ASTM STP 569, (1975), p. 28.
- [41] Kanninen, M. F., Rybicki, E. F. and Griffith, W. I., "Preliminary Development of a Fundamental Analysis Model For Crack Growth in a Fiber-Reinforced Composite Materials," ASTM STP 617, (1977), pp. 53-69.
- [42] Sik, G. C. and Cheu, E. P., "Fracture Analysis of Unidirectional Composites," J. Composite Materials, Vol. 7, (1973), p. 230.
- [43] Zweben, C., "Fracture Mechanics and Composite Materials," in ASTM STP 521, (1973), pp. 65-97.
- [44] Harlow, D. G., "Properties of the Strength Distribution for Composite Materials," in ASTM STP 674, (1979), 484-501.
- [45] Phoenix, S. L., "Statistical Aspects of Failure of Fibrous Materials," in ASTM STP 674, (1979), pp. 455-483.
- [46] Sendekyj, G. P. and Stalnaker, H. D., "Effect of Time at Load on Fatigue Response of [0/I45/90]25 T300/5208 Graphite-Epoxy Laminate," ASTM STP 617, (1977), p. 79.
- [47] Stinchcomb, W. W. and Reifsnider, K. L., "Fatigue Damage Mechanisms in Composite Materials, A Review," ASTM STP 675, (1979), pp. 762-787.
- [48] Reifsnider, K. L. Stinchcomb, W. W. and Henneke, E. G., "Defect-Property Relationship in Composite Materials," AFML-TR-76-81, Part I, (1976), Part II (1977), and Part III (1979).
- [49] Owen, J. J. and Bishops, P. T., "Crack Growth Relationships for Glass Reinforced Plastics and Their Application to Design," J. Physics D. Applied Physics, Vol. 7, (1974), p. 1214.

- [50] Wilkins, D. J., Eisenmann, J. R., Carmin, R. A., Margolis, W. S. and Benson, R. A., "Characterizing Delamination Growth in Graphite-Epoxy," ASTM STP, (1981).
- [51] Ratwani, M. M. and Kan, H. P., "Compression Fatigue Analysis of Fiber Composites," NADC TR N62269-78-C-0241, (1979).
- [52] Howe, R. J. and Owen, M. J., Proc. 8th International Reinforced Plastics Congress, London, (1972).
- [53] Carswell, W. S., "Fatigue Damage in Notched Composites," Composites, Vol. 8, (1977), p. 251.
- [54] Rice, J. R., "Mathematical Analysis in the Mechanics of Fracture," in Fracture, An Advanced Treatise, Vol. II, H. Liebowitz, ed., Academic Press, (1968).
- [55] Hertzberg, R. W., Deformation and Fracture Mechanics of Engineering Materials, Wiley, (1976).
- [56] Griffith, A. A., "The Phenomenon of Rupture and Flow in Solids" Phil. Trans. Roy. Soc. London, Ser. A 221, (1920), pp. 163-198.
- [57] Westergaard, H. M., "Bearing Pressure and Cracks," Trans. ASME J. Appl. Mech., Vol. 6, (1939).
- [58] Sneddon, I. N., "Integral Transform Methods," Methods of Analysis and Solutions of Crack Problems, Noordhoff International Publishing, Leyden, The Netherlands, (1973), p. 315.
- [59] Zienkiewicz, O. C., The Finite Element Method in Engineering Science, McGraw-Hill, London, (1971).

Appendix A: REVIEW OF FRACTURE MECHANICS

In our study of texts on fracture mechanics, there seems to be some confusion regarding the definition of the energy release rate, particularly in discussions on fixed load and fixed displacement boundary tractions. One reason for this apparent confusion is that some authors define the energy release rate as the change of potential energy of the body while others define it as the change of strain energy of the body. Rice [54] has given a concise derivation of the energy release rate from general principles, although he did not formulate the energy release rate in terms of compliance.

Another reason for the apparent confusion is the lack of clear distinction between the potential energy and the strain energy. Some authors use the loose term "elastic energy." For instance, in [55] (Hertzberg), the energy release rate for the fixed grip case is shown to be the negative of that for the fixed load case (equations 8 - 16a & b). In a more precise sense, the release rate of potential energy for these two cases should be the same, not negative to each other.

Consider a linear elastic body containing a crack of length "a" which is loaded as shown in figure A.1. The potential energy of this body may be expressed as:

$$U = V - W \quad (A-1)$$

where:

V = stored strain energy

and:

W = work done by external forces.

For the crack to extend by an amount da the necessary additional surface energy is obtained from a change in the potential energy of the body which, in view of equation A.1, may be related to changes in strain energy and work done by external forces. Defining G , the energy release rate, as:

$$G = - \frac{dU}{da} \quad (A-2)$$

we may thus write:

$$G = - \frac{dU}{da} = \frac{dW}{da} = \frac{dV}{da} \quad (A-3)$$

Note that G is the decrease of potential energy per unit crack extension; it is the rate of energy released from the strain energy and work done of outside force.

A. Fixed Displacement Case

A typical load-displacement diagram for the linear elastic body is shown in figure A.2. In this figure, line OP_1 corresponds to the response of the body containing a crack of length " a " while line OP_2 corresponds to a crack length $(a + da)$. M_1 and M_2 are the respective stiffnesses of the body. Clearly, for this fixed displacement case, $d\delta = 0$ and therefore:

$$\frac{dW}{da} = 0 \quad (A-4)$$

Thus,

$$G = - \frac{dU}{da} = - \frac{dV}{da} \quad (A-5)$$

We may also relate the energy release rate to a change in the compliance of the body. Referring to figure A.2, the change in the strain energy as the crack extends from length "a" to (a + da) is:

$$\frac{dV}{da} = \frac{d}{da} \left(\frac{1}{2} P \delta \right) \quad (A-6)$$

where:

$$\delta = \text{constant} = \frac{P_1}{M_1} = \frac{P_2}{M_2} \quad (A-7)$$

or, in general:

$$\frac{P}{M} = \text{constant}. \quad (A-8)$$

Differentiation of equation A.8 results in:

$$\frac{1}{M} \frac{dP}{da} + P \frac{d}{da} (1/M) = 0$$

or

$$\frac{1}{M} \frac{dP}{da} = - P \frac{d}{da} (1/M).$$

Writing equation A.6 as:

$$\frac{dV}{da} = \frac{1}{2} \frac{d}{da} \left(\frac{P^2}{M} \right)$$

and performing the differentiation results in:

$$\frac{dV}{da} = \frac{1}{2} \left[\frac{2P}{M} \frac{dP}{da} + P^2 \frac{d}{da} (1/M) \right] \quad (A-10)$$

Substituting equation A.9 into equation A.10 produces:

$$\frac{dV}{da} = \frac{1}{2} \left[- 2P^2 \frac{d}{da} (1/M) + P^2 \frac{d}{da} (1/M) \right]$$

and simplifying:

$$\frac{dV}{da} = - \frac{1}{2} P^2 \frac{d}{da} (1/M). \quad (A-11)$$

Therefore, from equation A.5 we have:

$$G = + \frac{1}{2} P^2 \frac{d}{da} (1/M). \quad (A-12)$$

B. Fixed Load Case

Figure A.2 shows also the load displacement diagram for the fixed load case. Line OP_1 corresponds to the response of the body containing the crack of length "a". Line OP'_1 corresponds to the response of the body containing a crack of length $(a + da)$. As the crack increases, the displacement at the point of application of the load increases from δ_1 to δ_2 where:

$$\delta_2 = \delta_1 + d\delta \quad (A-13)$$

The change in strain energy may be expressed, as before,

$$\frac{dV}{da} = \frac{1}{2} \frac{d}{da} (P\delta)$$

or

$$\frac{dV}{da} = \frac{1}{2} P \frac{d}{da} (\delta) \quad (A-14)$$

since P is a constant.

The work done by outside force as the crack extends from "a" to (a + da) is:

$$\frac{dW}{da} = P \frac{d\delta}{da}. \quad (A-15)$$

Substitution of equation A.14 and equation A.15 into equation A.3 produces:

$$G = - \frac{dU}{da} = P \frac{d\delta}{da} - \frac{1}{2} P \frac{d\delta}{da} = \frac{1}{2} P \frac{d\delta}{da} \quad (A-16)$$

To obtain G in terms of compliance, we have in this case:

$$\delta M = P = \text{constant}. \quad (A-17)$$

Rearranging,

$$\delta = \frac{P}{M} \quad (A-18)$$

and differentiating:

$$\frac{d\delta}{da} = P \frac{d}{da} (1/M).$$

Substituting equation A.18 into equation A.16 produces:

$$G = \frac{1}{2} P^2 \frac{d}{da} (1/M). \quad (A-19)$$

The expression of G in equation A.19 (fixed load) is identical to that of equation A.12 (fixed displacement). We conclude, therefore, the potential energy release rate due to a crack extension is the same for both the fixed load case and fixed displacement case.

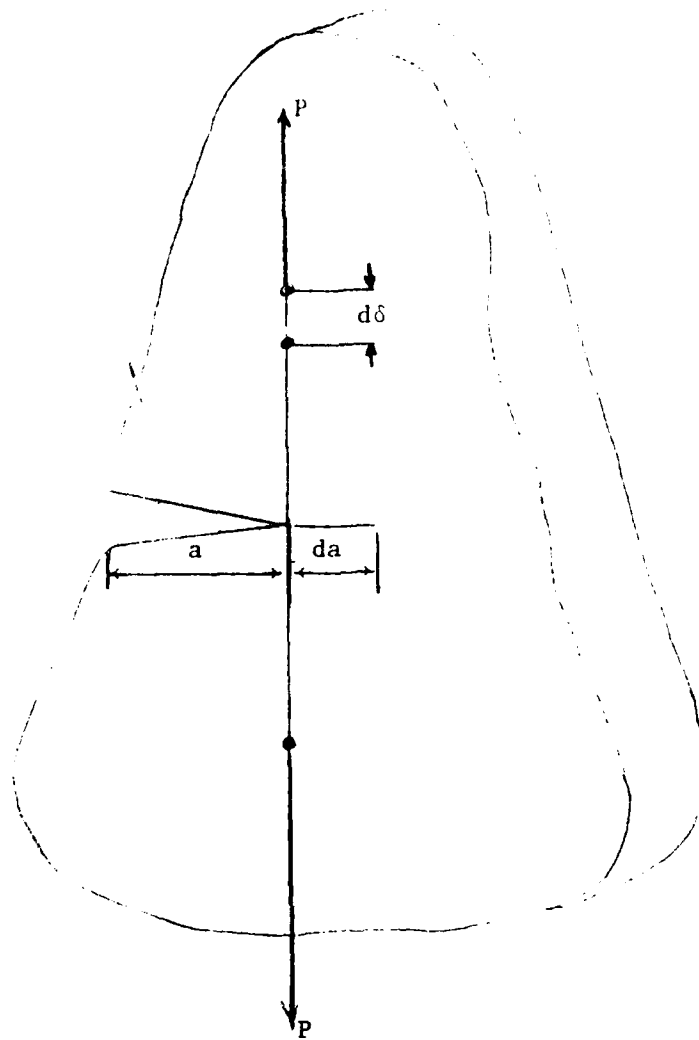


Figure A-1 Schematic Diagram of a Cracked Body under Uniaxial Load

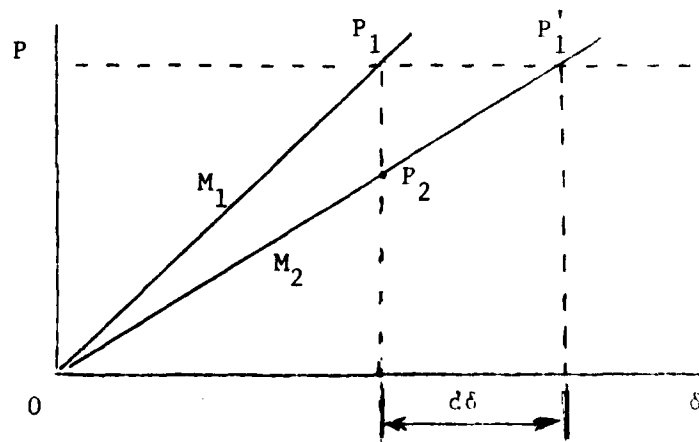


Figure A-2 Typical Load-Displacement Diagram for Cracked Body.

Appendix B: The Finite Element Scheme

The concept of the strain energy release rate as a fracture growth criterion for brittle cracks in elastic solids is one of long standing. In 1920, Griffith [56] attributed the ultimate tensile strength of glass to the fact that crack-like surface flaws exist in glass. He reasoned that the worst flaw propagates unstably when the rate of decrease of the strain energy becomes equal to or greater than the rate of increase of the surface energy during crack extension. Let U be the strain energy and S be the surface energy in the crack tip region. Then the Griffith postulation states that an initial flaw of size a will grow unstably if

$$\frac{\partial U}{\partial a} \geq \frac{\partial S}{\partial a} \quad (\text{B-1})$$

Note that $\frac{\partial U}{\partial a}$ is a quantity that depends on the stress field near the flaw as well as the geometry of the flaw. On the other hand, the quantity $\frac{\partial S}{\partial a}$ depends only on the material under consideration, and thus is a material property. The former, commonly referred to as the available energy release rate, is denoted by G . The latter, referred to as the critical energy release rate, is denoted by G_c . Thus, equation (B-1) may be rewritten as

$$G \geq G_c \quad (\text{B-2})$$

From an elastic energy balance consideration, Irwin [18] showed that the elastic strain energy released during a small incremental crack extension is equal to the work done in closing the crack to its original length. Let Δa represent an infinitesimal crack extension from the initial size of a as shown in Figure (B-1). Let $\Delta \bar{u}$ be the relative displacements between the mating crack surfaces along Δa when the crack is open as in Figure (B-1)b. Let $\bar{\sigma}$ be the normal and shearing surface stress distribution along Δa when the crack is closed as in Figure (B-1)c. Then the work done per unit thickness to close the crack extension may be expressed by

$$\Delta W = 1/2 \int_0^{\Delta a} \bar{\sigma} \cdot \Delta \bar{u} \, da \quad (\text{B-3})$$

Thus, by means of Irwin's crack closure equivalence, the available energy release rate G , for a crack of size a , is expressed by

$$G = \lim_{\Delta a \rightarrow 0} \frac{1}{2\Delta a} \int_0^{\Delta a} \bar{\sigma} \cdot \Delta \bar{u} \, da \quad (B-4)$$

Substituting the components of the surface stresses $\bar{\sigma}$ and the relative displacements $\Delta \bar{u}$ into the equation (B-4) yields G in component form as

$$\begin{aligned} G_I &= \lim_{\Delta a \rightarrow 0} \frac{1}{2\Delta a} \int_0^{\Delta a} \sigma_y \Delta v \, da \\ G_{II} &= \lim_{\Delta a \rightarrow 0} \frac{1}{2\Delta a} \int_0^{\Delta a} \tau_{xy} \Delta u \, da \\ G_{III} &= \lim_{\Delta a \rightarrow 0} \frac{1}{2\Delta a} \int_0^{\Delta a} \tau_{yz} \Delta w \, da \end{aligned} \quad (B-5)$$

where G_I , G_{II} , and G_{III} denote the mode I, mode II, and mode III crack extension modes respectively, and

$$G = G_I + G_{II} + G_{III} \quad (B-6)$$

As illustrated in Figure (B-2), mode I crack extension refers to an opening action, while a mode II crack refers to a sliding action, and mode III is an anti-plane shearing action.

In order to evaluate the integrals of (B-4) or (B-5), the exact stress field near the crack tip must be determined. But, it is well known that the distribution of stresses in the neighborhood of a sharp crack is singular in nature [57, 58]. One approach to determine the singular stress field is to introduce the well-known "stress intensity factor." For example, Sneddon [58] solved a plane problem that gives the stress field in the region of a "penny shaped" crack

undergoing mode I action as

$$\begin{aligned}\sigma_y &= \frac{K_I}{\sqrt{2\pi r}} \cos \frac{\theta}{2} \left[1 + \sin \frac{\theta}{2} \sin \frac{3\theta}{2} \right] \\ \sigma_x &= \frac{K_I}{\sqrt{2\pi r}} \cos \frac{\theta}{2} \left[1 - \sin \frac{\theta}{2} \sin \frac{3\theta}{2} \right] \\ \tau_{xy} &= \frac{K_I}{\sqrt{2\pi r}} \left[\sin \frac{\theta}{2} \cos \frac{\theta}{2} \cos \frac{3\theta}{2} \right] \\ \sigma_z &= \nu(\sigma_x + \sigma_y) = \frac{2\nu K_I}{\sqrt{2\pi r}} \cos \frac{\theta}{2} \\ \tau_{yz} &= \tau_{xz} = 0.\end{aligned}\tag{B-7}$$

Here, K_I is the mode I stress intensity factor that is a measure of the strength of the singularity. Similar stress intensity factors may be obtained for mode II and mode III crack extension actions.

Since the energy release rate G is computed from the crack tip stress field by equation (B-5), the relationship between the strain energy release rate and the stress intensity factor for a linear elastic isotropic material can be established. For example, under a plane strain condition, G is given by [18].

$$G = \frac{1-\nu^2}{E} \left[K_I^2 + K_{II}^2 \right]\tag{B-8}$$

where K_{II} is the mode II stress intensity factor.

For initially cracked, layered anisotropic materials, such as composite laminates, an explicit relationship between K and G is generally not available. Moreover, in a generally anisotropic solid, the mode I and mode II cracking actions are mutually coupled.

The methodology of the crack closure and stress intensity factor approaches requires a detailed knowledge of the stress distribution in the vicinity of the crack tip. In the case of composite laminates, analytical solutions of the stress distribution in the region of a crack tip are generally not available. Hence, numerical solution techniques, such as the finite element method, are often utilized.

A numerical technique to calculate the strain energy release rate has been presented by Rybicki and Kanninen [27]. Their approach involves a finite element solution of Irwin's crack closure integral given in (B-5). In the finite element representation, the continuous stress and displacement fields of the solid are approximated by the nodal forces and displacements respectively. Figure (B-3) illustrates the finite element representation of a crack tip region. Here, a crack of length a is shown with the crack tip at node c . The finite element solution determines the displacement components $(u, v, w)_c$ of the crack tip node c , under a prescribed loading. An incremental crack extension Δa is introduced by replacing the crack tip node c with two separate nodes f and g as shown in Figure (B-3)b. With this new crack geometry taken into account, the finite element solution for the nodal displacements $(u, v, w)_f$ and $(u, v, w)_g$ are found for nodes f and g respectively. The crack extension is closed by applying equal and opposite forces at nodes f and g such that their common displacements match the displacements found earlier for node c .

The work required to close the crack extension is approximated by

$$\Delta W \sim [F_x(u_f - u_g) + F_y(v_f - v_g) + F_z(w_f - w_g)]/2 \quad (B-9)$$

where F_x , F_y , and F_z are the components of the nodal forces required to close nodes f and g together. Thus, the energy release rates for the three crack extension modes are approximated by

$$G_I \sim F_y (v_f - v_g) / 2\Delta a$$

$$G_{II} \sim F_x (u_f - u_g) / 2\Delta a \quad (B-10)$$

$$G_{III} \sim F_z (w_f - w_g) / 2\Delta a$$

The method presented here does not require that the stresses be calculated because the stress and strain fields are approximated by the nodal forces and displacements in the finite element solution. Rybicki and Kanninen applied conventional constant strain finite elements to the solution of three fracture problems: the double cantilever beam specimens; a finite strip containing a central crack; and a bolt fastened double lap joint containing radial cracks. They reported that a coarse grid in the crack tip region was sufficient for a good comparison between their example problems and reference solutions.

In this analysis, both mechanical and thermal loadings may be considered. The mechanical load is uniaxial tension, and the thermal loading is due to the curing process. The thermal load is taken in the form of a uniform temperature change ΔT from the curing temperature to the ambient temperature [59]. Within the context of linear elasticity, the mechanical and thermal loading cases may be solved independently under unit load conditions and then superimposed to obtain the solution for a combined load condition. It is convenient to choose the mechanical load as the far field laminate strain ϵ equal to one micorstrain (1×10^{-6}). This represents a "fixed-grip" load condition. The thermal load ΔT is chosen as minus one degree Fahrenheit for convenience. Let \tilde{f}_m and \tilde{d}_m be the nodal forces and displacements respectively, due to the unit mechanical strain load as determined by the finite element solution.

Similarly, let \tilde{f}_T and \tilde{d}_T be the nodal forces and displacements respectively, due to the unit thermal load of $\Delta T = 1^\circ\text{F}$. Then, under a combined loading of ϵ and ΔT , the nodal forces and displacements can be expressed as

$$\tilde{f} = f_m e + f_T \Delta T$$

(B-11)

$$\tilde{d} = d_m e + d_T \Delta T$$

To calculate the strain energy release rate it is necessary to introduce a crack in the finite element network as described above. Referring to Figure (B-3), let \tilde{D} be the relative displacements of nodes f and g when the crack is extended to $a + \Delta a$ defined as

$$\tilde{D} = \tilde{u}_f = \tilde{u}_g \quad (B-12)$$

\tilde{D} may be represented in terms of a combined mechanical and thermal load of e and ΔT as

$$\tilde{D} = \tilde{D}_m e + \tilde{D}_T \Delta T \quad (B-13)$$

where \tilde{D}_m and \tilde{D}_T are the relative displacements associated with the unit mechanical and unit thermal loadings respectively. Let \tilde{F} be the nodal forces required to close nodes f and s together. \tilde{F} may be expressed in terms of a combined load of e and ΔT as

$$\tilde{F} = \tilde{F}_m e + \tilde{F}_T \Delta T \quad (B-14)$$

where \tilde{F}_m and \tilde{F}_T are the nodal closing forces associated with the unit mechanical and unit thermal loadings respectively. The energy release rate per unit thickness may then be expressed as

$$G = \frac{1}{2\Delta a} (\tilde{F}_m e + \tilde{F}_T \Delta T) \cdot (\tilde{D}_m e + \tilde{D}_T \Delta T) \quad (B-15)$$

where Δa is the incremental crack extension as shown in Figure (B-3). Equation (B-15) may be rewritten in the form

$$G = t[C_e(e)^2 + C_T(\Delta T)^2 + C_{eT}(e)(\Delta T)] \quad (B-16)$$

where

$$\begin{aligned} C_e &= (\tilde{F}_m \cdot \tilde{D}_m)/2\Delta at \\ C_T &= (\tilde{F}_T \cdot \tilde{D}_T)/2\Delta at \\ C_{eT} &= (\tilde{F}_m \cdot \tilde{D}_T + \tilde{F}_T \cdot \tilde{D}_m)/2\Delta at \end{aligned} \quad (B-17)$$

The parameter t , the thickness of a single ply, is introduced so that C_e , C_T , and C_{eT} are independent of the ply thickness. Note that, for a given geometry and material properties, equations (B-17) are a function of the non-dimensional crack length a/t and are independent of the applied loading. Thus, the functions C_e , C_T , and C_{eT} are characteristic for a particular crack growth problem and are hereafter denoted "shape functions." C_e , C_T , and C_{eT} are associated with the mechanical, thermal, and mixed load conditions respectively. C_e has units of energy per unit area, C_T has units of energy per unit area per $(\Delta T)^2$, and C_{eT} has units of energy per unit area per ΔT .

The mechanical load shape function C_e may be expressed in terms of the x , y , z components of \tilde{F}_m and \tilde{D}_m as

$$\begin{aligned} C_{eI} &= (F_{my} \cdot D_{my})/2\Delta at \\ C_{eII} &= (F_{mx} \cdot D_{mx})/2\Delta at \\ C_{eIII} &= (F_{mz} \cdot D_{mz})/2\Delta at \end{aligned} \quad (B-18)$$

The subscripts I, II, and III are identified with the mode I, mode II and mode III crack extension modes respectively. Similar expressions may be obtained for the thermal and mixed load shape functions. Thus, the mode I, mode II, and mode III components of the energy release rate may be expressed in terms of the shape function as

$$G_I = t[C_{eI}(e)^2 + C_{TI}(\Delta T)^2 + C_{eTI}(e)(\Delta T)]$$

$$G_{II} = t[C_{eII}(e)^2 + C_{TII}(\Delta T)^2 + C_{eTII}(e)(\Delta T)] \quad (B-20)$$

$$G_{III} = t[C_{eIII}(e)^2 + C_{TIII}(\Delta T)^2 + C_{eTIII}(e)(\Delta T)]$$

Thus, a methodology has been presented to superimpose the energy release rate for two load conditions. This is accomplished using shape functions that are characteristic for a given crack geometry and material. These shape functions are calculated from unit load finite element solutions for each loading condition. The mode I, II and III components of the energy release rate are explicitly calculated.

The finite element code has been installed for use on the HP-1000 computer system. Proper operation of the code has been confirmed by running several benchmark programs and comparing them with existing solutions [25]. In order to provide further confidence in both the energy release rate approach and the finite element computation, a comparison has been made for the case of transverse cracking in the $(0_2/90_2)_s$ laminate at the onset load between the G calculated by the finite element code and G as calculated from a reference solution using the stress intensity factor K_I . The reference problem and functional form of the shape function F are shown in Figure (B-4). For this comparison, only the mechanical load will be considered, i.e., the finite element computation produces

$$G = t C_e e^2$$

The value of G using the stress intensity factor approach is obtained from the relation

$$G = \frac{K^2}{E}$$

where E is taken as the modulus of the 90° -layer (E_T) and where K is calculated using

$$\beta = \frac{E_L}{E_T} \approx 13$$

and $\sigma = 6.44$ ksi,

which is the stress in the 90° -layer corresponding to the laminate transverse crack initiation strain of 4027 $\mu\text{in/in}$. Results of these calculations are shown in Figure (B-5). As can be seen, the agreement in both the magnitude and the shape of the two functions is quite good.

In the preceding example, the comparison was not exact largely because the properties of the laminate did not match those required by the exact solution. As a final comparison, a transversely isotropic laminate was analyzed. Properties were chosen to match exactly those required by the exact solution. The value of β was taken as 5. Results are shown in Figure B.6, where it is seen that the results are nearly identical.

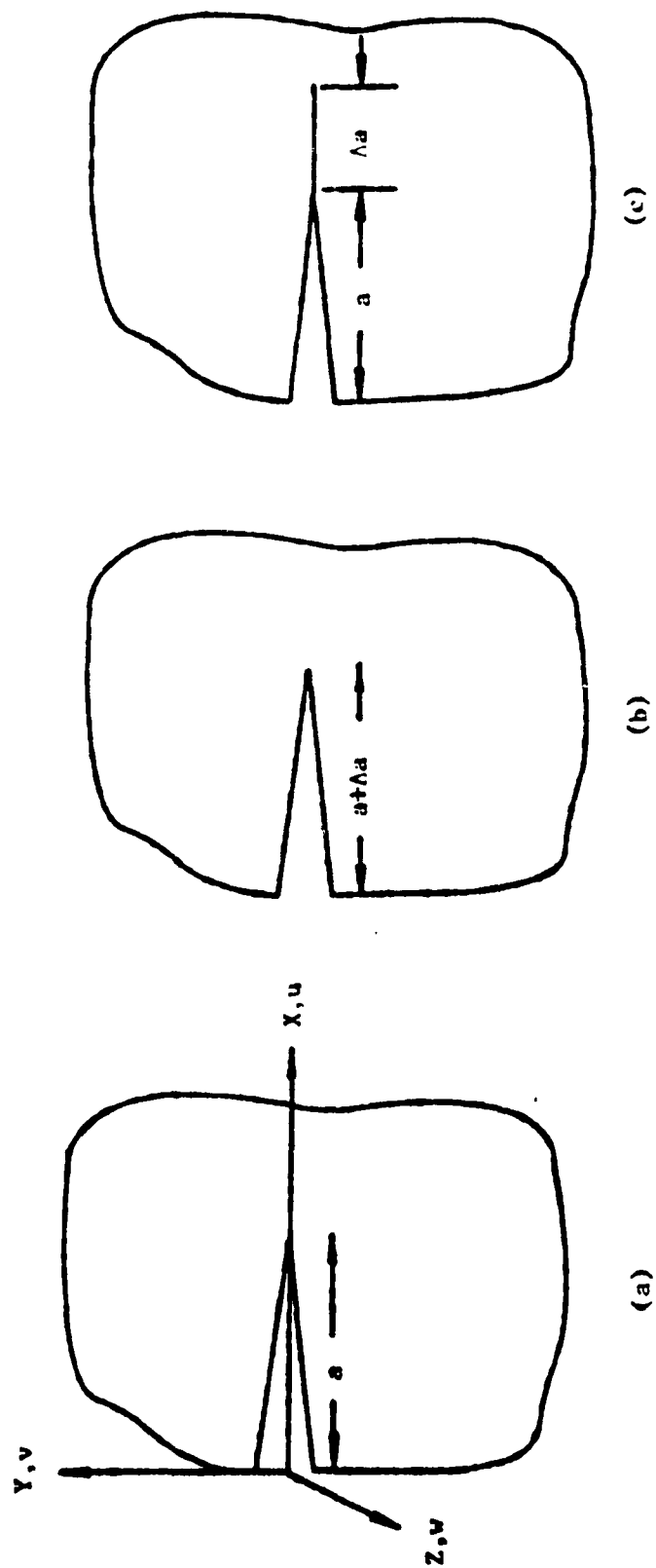
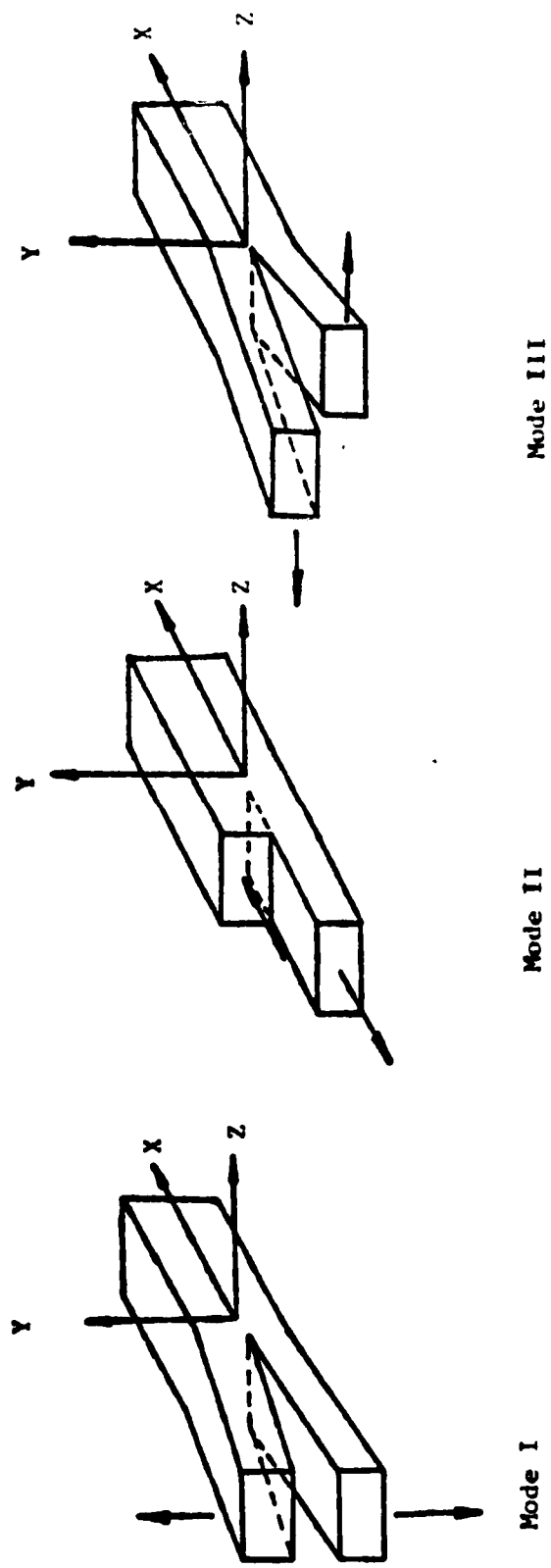


Figure B-1 Schematic of Crack Closure Technique



B-11

Figure B-2 The Three Crack Extension Modes.

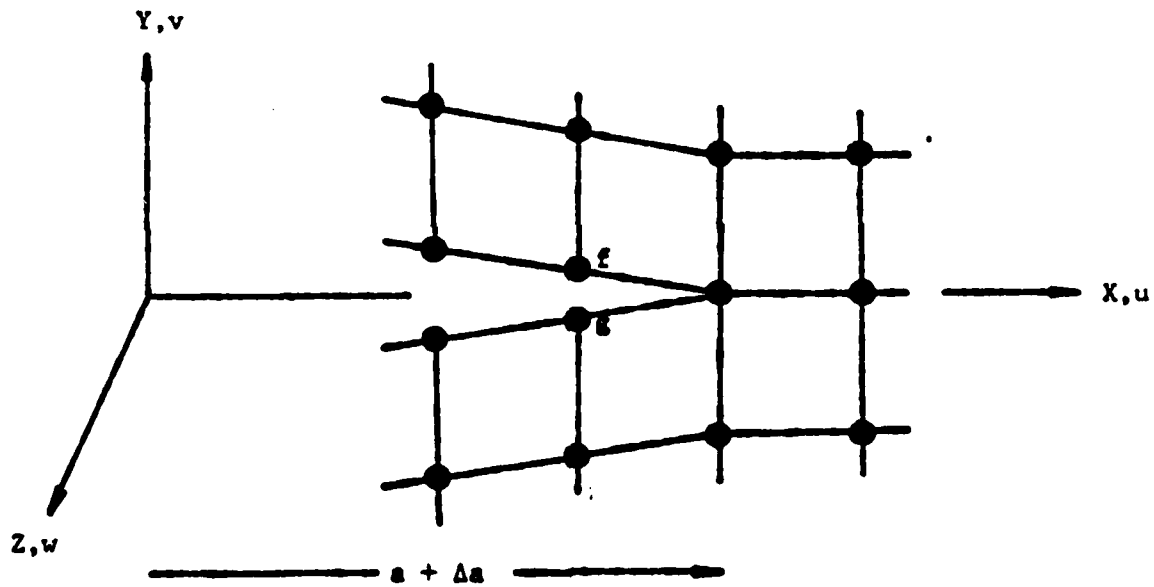
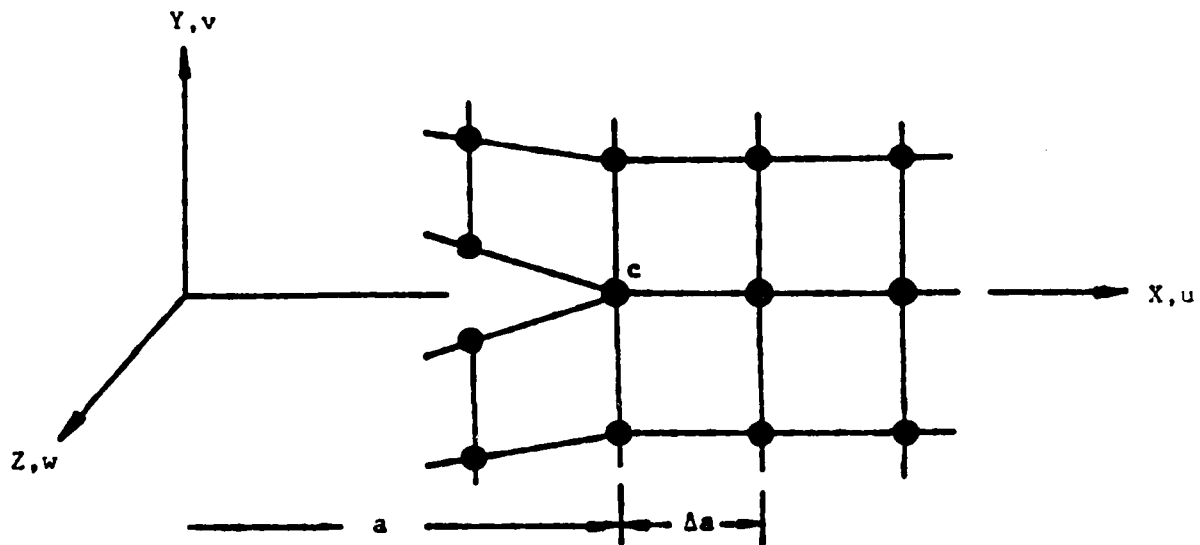
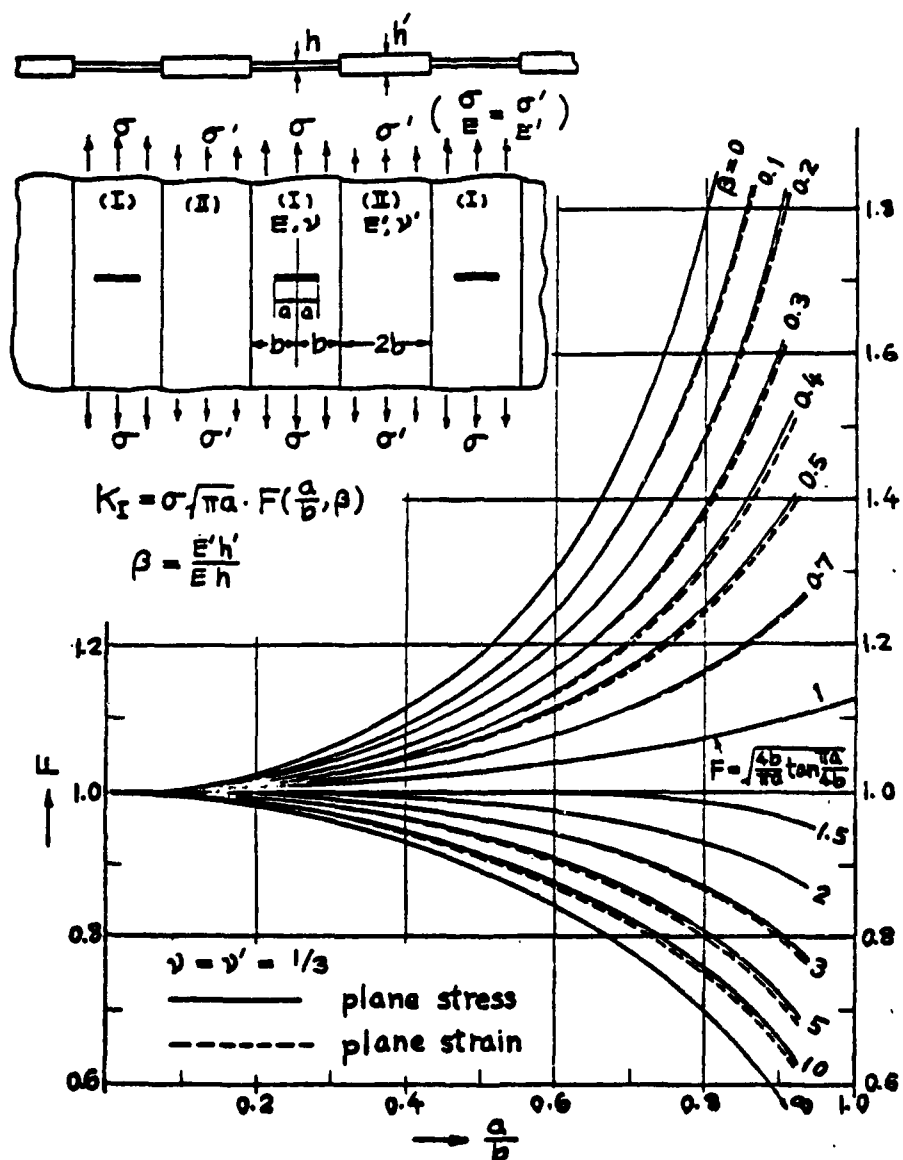


Figure B-3 Finite Element Mesh at a Crack Tip Illustrating the Crack Closure Technique.



Method: Expansions of Complex Stress Potentials
 Accuracy: Curves were drawn based on the results with 0.1% accuracy;
 Reference: Isida 1970a

Figure B-4: Stress Intensity Factor Approach Reference Solution

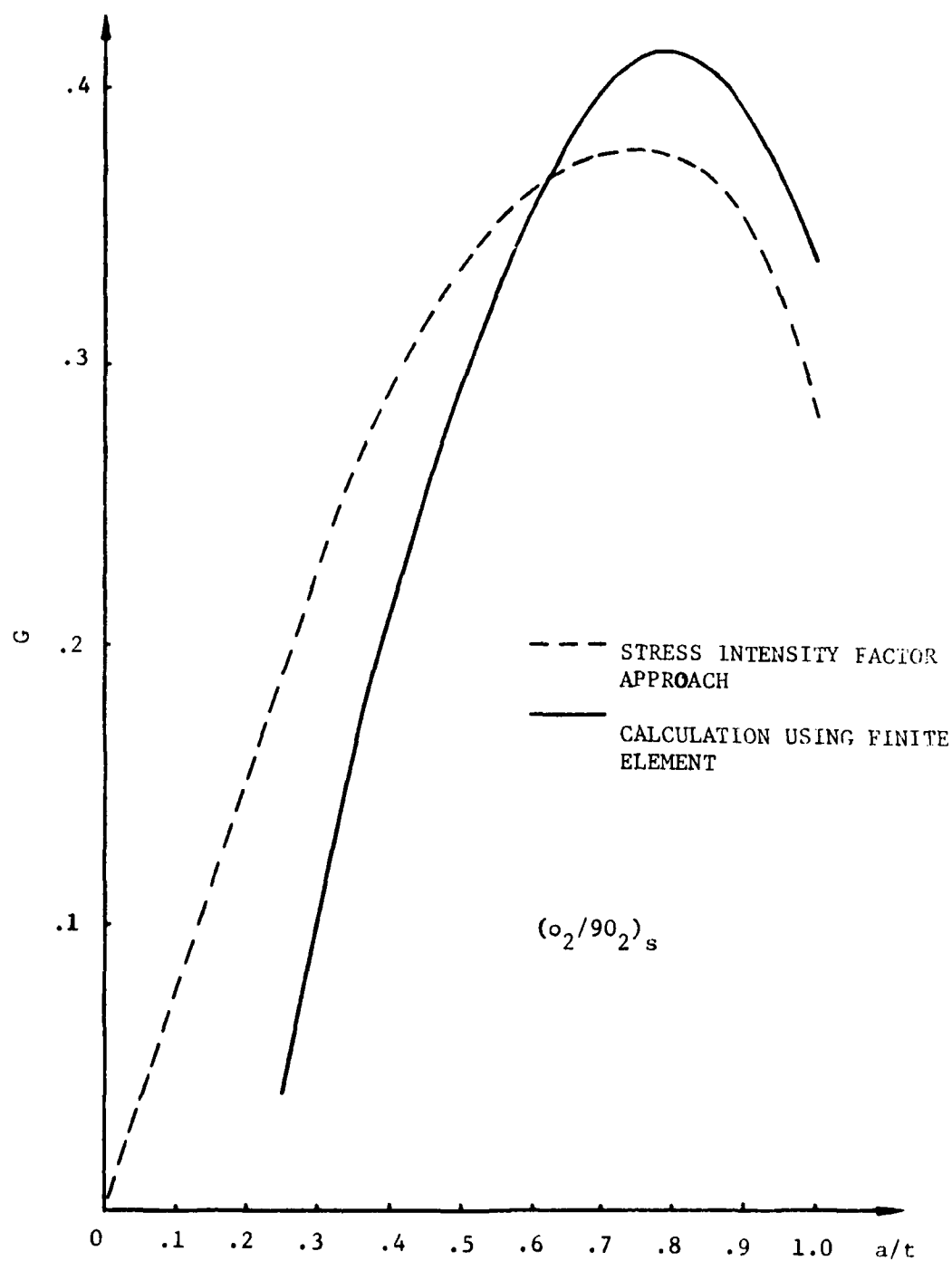


Figure B-5: COMPARISON OF ENERGY RELEASE RATE CALCULATED FROM STRESS INTENSITY FACTOR AND FROM FINITE ELEMENT CODE.

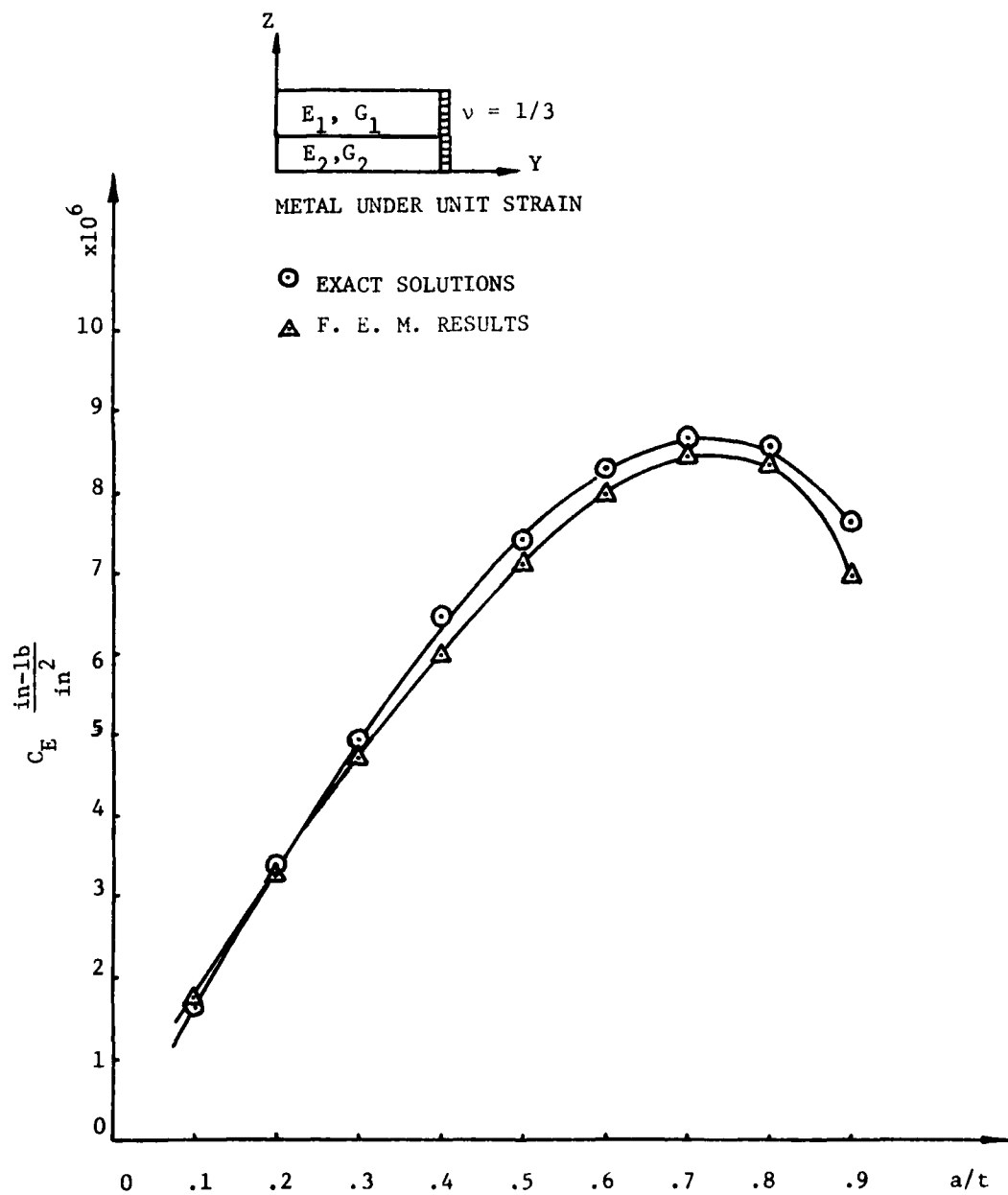


Figure B-6: COMPARISON OF G CALCULATED BY FEM TO EXACT VALUE OF G FOR TRANSVERSELY ISOTROPIC LAMINATE.

Appendix C
Tables of Experimental Data

TABLE C-1 CYCLE-DAMAGE DATA FOR $(0_2/90_2)_s$

Max. Stress $\sigma_f = 38$ ksi		Max. Stress $\sigma_f = 43$ ksi		Max. Stress $\sigma_f = 53$ ksi	
Cycles	Number of Transverse Cracks	Cycles	Number of Transverse Cracks	Cycles	Number of Transverse Cracks
10	1	200	2	10	3
100	2	800	4	60	8
400	4	4,000	12	300	20
1,000	9	20,000	35	2,000	65
3,000	19	100,000	59	8,000	86
10,000	40	300,000	72	40,000	98
40,000	52			200,000	117
250,000	70				
		200	2		
		800	5	10	4
2,000	2	4,000	17	60	5
10,000	11	20,000	40	300	11
40,000	23	100,000	74	2,000	46
200,000	42	300,000	82	8,000	73
1,000,000	67	1,000,000	97	40,000	104
				200,000	120
10,000	1	80	4		
40,000	13	400	13	10	4
200,000	32	2,000	35	60	7
		10,000	74	300	14
		40,000	94	2,000	37
		200,000	109	8,000	66
		1,000,000	115	30,000	90
				200,000	118
		80	2		
		400	3	10	6
		2,000	6	60	9
3,000	3	10,000	20	300	18
10,000	10	40,000	47	2,000	50
40,000	24	200,000	68	8,000	78
200,000	42	1,000,000	83	30,000	96
1,000,000	62			200,000	123

TABLE C-2 CYCLE-DAMAGE DATA FOR $(O_2/90_3)_s$

Max. Stress $\sigma_f = 26$ ksi		Max. Stress $\sigma_f = 30$ ksi		Max. Stress $\sigma_f = 38$ ksi	
Cycles	Number of Transverse Cracks	Cycles	Number of Transverse Cracks	Cycles	Number of Transverse Cracks
100	1	400	1	10	3
500	1	2,000	3	60	5
3,000	2	10,000	17	300	7
10,000	4	40,000	23	2,000	31
50,000	9	200,000	37	10,000	53
300,000	16	1,000,000	57	40,000	68
1,000,000	16			200,000	78
				1,000,000	102
3,000	2	10,000	4		
10,000	10	40,000	12		
50,000	14	200,000	24	10	2
300,000	21	1,000,000	45	60	6
1,000,000	28			300	17
				2,000	40
		2,000	2	10,000	66
3,000	3	10,000	14	40,000	83
10,000	8	40,000	27	200,000	89
50,000	15	200,000	33	1,000,000	112
300,000	26				
		2,000	2	10	2
50,000	8	10,000	20	60	4
300,000	11	40,000	35	300	7
		200,000	50	2,000	35
				10,000	53
				40,000	69
				200,000	92
				10	2
				60	3
				300	12
				2,000	32
				10,000	51
				40,000	64
				200,000	85

TABLE C-3 CYCLE-DAMAGE DATA FOR (+25/90)_s

Max. Stress $\sigma_f = 29$ ksi		Max. Stress $\sigma_f = 33$ ksi		Max. Stress $\sigma_f = 40$ ksi	
Cycles	% Delamination	Cycles	% Delamination	Cycles	% Delamination
6,000	0	3,000	0	500	4.1
50,000	4.1	10,000	7	2,000	10.4
400,000	10.4			10,000	44
500,000	41.6			12,000	48.9
550,000	45.8	3,000	0	12,020	100
		10,000	6.3		
		80,000	24		
6,000	0	100,000	41	300	4.1
100,000	12.5			1,000	8.3
400,000	21			4,000	16.6
500,000	29.2	5,000	0	8,000	21.0
550,000	30.0	20,000	2	11,000	33.3
600,000	33.0	60,000	31.3	13,000	44.0
		90,000	35.4	13,920	100
68,000	4.1	105,000	100		
100,000	6.25			50	0
300,000	12.5			1,050	6.25
500,000	13.3	10,000	0	6,000	18.75
600,000	16	50,000	12.5	7,000	25
800,000	33	100,000	16.6	9,000	27.1
900,000	42.7	160,000	33.3	14,700	54.1
		167,000	100	15,110	100
				50	0
				2,000	2

TABLE C-4 CYCLE-DAMAGE DATA FOR $(+25/90_2)_s$

Maximum Stress $\sigma_f = 22$ ksi			Maximum Stress $\sigma_f = 27$ ksi		
Cycles	Number of Transverse Cracks	% Delamination	Cycles	Number of Transverse Cracks	% Delamination
5,000	4	0	100	1	0
10,000	10	0	400	2	0
30,000	37	0	1,000	9	0
50,000	49	0	5,000	32	0
80,000	51	6.3	10,000	52	0
200,000	56	8.3	20,000	75	4.1
400,000	69	8.3	30,000	81	10.4
600,000	75	12.6	50,000	86	16.6
800,000	81	16.7	80,000		100
1,000,000	88	25.2			
			100	2	0
2,000	3	0	500	8	0
6,000	10	0	2,000	39	0
10,000	11	0	14,650	73	0
40,000	21	4.1	15,000	74	0
70,000	35	6.3	20,000	79	4.1
100,000	49	8.3	30,000	90	8.3
300,000	64	10.4	50,000	97	12.5
400,000	69	18.75	100,000	104	25.0
600,000	70	23	150,000	110	27.0
800,000	74	29	153,850		100
1,000,000	81	54			
			100	16	0
6,000	1	0	600	29	0
10,000	4	0	2,000	53	4
50,000	42	0	6,000	64	6.3
80,000	46	0	10,000	70	10
100,000	49	0	15,000	75	18.8
200,000	50	10.4	25,000	86	27
400,000	74	20.8			
410,000	75	20.8			
600,000	76	20.8			
800,000	79	22			
1,000,000	82	25.2			

TABLE C-4 CYCLE-DAMAGE DATA FOR $(+25/90)_2$ - (continued)

Maximum Stress $\sigma_f = 31$ ksi		
<u>Cycles</u>	<u>Number of Transverse Cracks</u>	<u>% Delamination</u>
1	12	0
10	24	0
100	42	0
600	56	0
2,000	68	8.3
4,600	90	23
7,000	92	29
8,500	100	33.3
10,000	113	37.5
1	6	0
10	8	0
100	20	0
1,000	53	0
3,000	81	11.3
5,000	85	21.3
7,910		100
1	17	0
10	21	0
100	34	6.0
1,000	56	8.3
2,000	65	12.5
5,000	91	12.5
8,000	96	29.1
10,000	98	31.25
15,000	101	42.6

TABLE C-5 CYCLE-DAMAGE DATA FOR $(+25/90_3)_s$

Maximum Stress $\sigma_f = 19$ ksi			Maximum Stress $\sigma_f = 22$ ksi		
Cycles	Number of Transverse Cracks	% Delamination	Cycles	Number of Transverse Cracks	% Delamination
1,000	1	0	1,000	2	0
5,000	2	0	6,000	11	0
8,000	4	0	30,000	33	4.2
10,000	7	0	100,000	45	10.4
30,000	17	0	174,480		100
60,000	27	6.3			
			2,000	2	0
500	1	0	8,000	8	0
2,000	1	0	40,000	35	4.1
5,000	4	0	80,000	44	8.3
8,000	6	0	174,770		100
10,000	7	0			
50,000	16	4.1			
100,000	22	6.3	60	1	0
400,000	32	14.5	400	1	0
1,149,000	53	25	1,000	2	0
			5,000	12	0
2,000	1	0	20,000	18	4.1
4,000	2	0	150,000	50	12.5
8,000	3	0	200,000	73	18.8
10,000	3	0	250,000	75	27
60,000	8	2.1	280,000	75	62.5
100,000	8	6.3	280,010		100
1,320,120	34	16.6			
1,851,520	44	37.5			

TABLE C-5 CYCLE-DAMAGE DATA FOR $(+25/90_3)_s$ - (continued)

Maximum Stress $f = 25$ ksi		
<u>Cycles</u>	<u>Number of Transverse Cracks</u>	<u>% Delamination</u>
1	12	0
10	12	0
100	16	0
1,000	44	4.1
4,000	52	4.1
11,000	64	12.5
1	1	0
10	1	0
100	2	0
800	20	0
6,100	44	0
20,000	60	8.3
40,000	63	10.4
50,000	84	25
60,000	87	29.1
67,530		100
1	4	0
10	4	0
100	8	0
1,000	29	0
5,000	51	0
10,000	58	6.25
20,000	74	12.5
40,000	87	31.25
41,570		100

TABLE C-6 CUMULATIVE DAMAGE TEST DATA

Laminate	Maximum Fatigue Stress, ksi	Cycles @ Load	Number of Transverse Cracks
(0 ₂ /90 ₃) _s	26	10,000	6
	30	15,000	35
		30,000	42
	26	100,000	47
	26	10,000	6
	30	30,000	34
	26	100,000	39
	26	10,000	6
	30	30,000	36
	26	100,000	37
	26	10,000	7
	30	100	7
		1,000	8
		5,000	20
		10,000	23
		15,000	23
		20,000	24
		25,000	27
		30,000	28
	26	100,000	31
	15	100,000	0
	50	1	26
		10	44
		100	63
		1,000	94
		10,000	115
		100,000	121
		500,000	121
		1,000,000	124
	15	100,000	1
	50	1	36
		10	48
		100	69
		1,000	88
		10,000	108
		100,000	122
		1,000,000	124
Laminate	Maximum Fatigue Stress, ksi	Cycles @ Load	% Delamination
(±25/90) _s	20	100,000	0
	50	1	9.3
		5	9.3
		10	9.3
		20	10.7
		100	13.3
		182	100

C-)

TABLE C-6 CUMULATIVE DAMAGE TEST DATA (cont'd)

Laminate	Maximum Fatigue Stress ksi	Cycles @ Load	Number of Transverse Cracks
(±25/90) _s	20	100,000	0
	30	50,000	5.3
		80,000	8.0
		200,000	17.3
		300,000	21.3
	40	1,000	5.3
	50	1	8.0
		10	9.3
		30	12.0
		50	13.3
		70	13.3
		90	14.7
		100	16.0
	40	1,000	9.3
	50	1	12.0
		10	12.0
		30	14.7
	20	100,000	0
	50	1	8.0
		10	10.7
		40	13.3
		100	14.7
		150	17.3
		200	20.0
		300	29.3
	20	300,000	0
	40	50	0
		100	1.3
		500	4.0
	30	100,000	25.3
		200,000	33.3
	50	1	10.7
		10	12.0
	30	100	12.0
		1,000	12.7
		10,000	13.3
		100,000	16.0
		200,000	22.7
		300,000	29.3

TABLE C-6 CUMULATIVE DAMAGE TEST DATA (cont'd)

Laminate	Maximum Fatigue Stress ksi	Cycles @ Load	Number of Transverse Cracks
(±25/90) _s	40	1,000	14.7
	50	1	18.7
		11	20.0
		30	21.3
		50	24.0
<hr/>			
	50	1	5.3
		10	6.7
	30	100	6.7
		1,000	6.7
		10,000	8.0
		100,000	16.0
		200,000	20.0
		300,000	22.7
<hr/>			
	50	10	6.7
	30	200	6.7
		1,000	6.7
		10,000	6.7
		100,000	12.0
		200,000	17.3
<hr/>			

TABLE C-6 CUMULATIVE DAMAGE TEST DATA (cont'd)

Laminate	Maximum Fatigue Stress ksi	Cycles @ Load	Number of Transverse Cracks
(0 ₂ /90 ₂) _s	60	1	36
		100	72
		1,000	96
		10,000	126
		100,000	150
	80	1	150
		100	153
		1,000	153
		10,000	161
		100,000	162
	50	1,000	84
		1,000	138
		100,000	144
	80	1	113
		10	120
		100	133
	60	10	138
		100	139
		1,000	140
		10,000	149
		100,000	162
	60	1	36
		100	81
		1,000	107
		10,000	139
		100,000	154
	80	1	154
		100	155
		1,000	157
		10,000	161
		100,000	162
	80	1	95
		10	111
		100	129
	60	10	129
		100	129
		1,000	131
		10,000	139
		100,000	150

TABLE C-6 CUMULATIVE DAMAGE TEST DATA (cont'd)

<u>Laminate</u>	<u>Maximum Fatigue Stress ksi</u>	<u>Cycles @ Load</u>	<u>Number of Transverse Cracks</u>
(0 ₂ /90 ₂) _s	60	1	51
		100	95
		1,000	117
		10,000	138
		100,000	155
	80	1	156
		100	157
		1,000	157
		10,000	161
		100,000	166
	80	1	107
		10	112
		100	138
	60	10	139
		100	139
		1,000	139
		10,000	146
		100,000	158
		400,000	166
	50	1,000	50
	70	1,000	127
	50	100,000	135
	50	1,000	61
	70	1,000	128
	50	100,000	135

TABLE C-6 CUMULATIVE DAMAGE TEST DATA (cont'd)

<u>Laminate</u>	<u>Maximum Fatigue Stress ksi</u>	<u>Cycles @ Load</u>	<u>Number of Transverse Cracks</u>
(0 ₂ /90 ₃) _s	80	1	128
		10	136
	40	1	136
		10	136
		100	136
		10,000	136
		100,000	138
		1,000,000	138
	26	100,000	19
	30	200,000	46
	80	1	123
		10	127
	40	1	129
		10	129
		100	129
		10,000	129
		20,000	129
		1,000,000	134

END

FILMED

2-83

DTIC